2020

Air Quality and Climate Impacts of Western U.S. Wildfires

Vanessa Selimovic
University of Montana, Missoula

AIR QUALITY AND CLIMATE IMPACTS OF WESTERN US WILDFIRES

By

VANESSA SELIMOVIC

B.A. Chemistry, Concordia University, Portland, OR, 2014

Dissertation

presented in partial fulfillment of the requirements
for the degree of

Doctorate of Philosophy
in Chemistry

The University of Montana
Missoula, MT

August 2020

Approved by:

Scott Whittenburg, Dean of The Graduate School
Graduate School

Dr. Robert Yokelson, Committee Chair
Department of Chemistry and Biochemistry

Dr. Lu Hu, Committee Member
Department of Chemistry and Biochemistry

Dr. Mark Cracolice, Committee Member
Department of Chemistry and Biochemistry

Dr. Michael DeGrandpre, Committee Member
Department of Chemistry and Biochemistry

Dr. Philip Higuera, Committee Member
Department of Forestry

Selimovic, Vanessa, PhD, Summer 2020 Chemistry

Air quality and climate impacts of western US wildfires

Advisor: Dr. Robert Yokelson, Department of Chemistry

Abstract: Wildfire smoke impacts are important in the western US and projected to increase substantially in upcoming decades. It's impacts on regional and global scale atmospheric chemistry is dependent upon both physical and chemical changes that take place as biomass burning (BB) emissions are transported, diluted, and exposed to oxidation. In turn, evaluation of smoke modeling requires quality, long-term simultaneous measurements of wildfire smoke characteristics that provide both inert tracers to test production and transport (e.g. black carbon (BC) and CO) and reactive species to test chemical mechanisms (e.g. particulate matter (PM), O_3, brown carbon (BrC)). During the Fire Influence on Regional to Global Environments and Air Quality Experiment (FIREX-AQ) at the Missoula Fire Sciences Lab, we burned realistic fuel complexes for western wildfire ecosystems to better understand and assess their emissions profiles, and found that the average trace gas emissions were similar across the coniferous ecosystems tested and most of the variability observed in emissions could be attributed to differences in the consumption of components such as duff and litter, rather than the dominant tree species, which may have implications for land management strategies like prescribed burning. Further, our observations show that emissions of BC and BrC and its optical properties are strongly correlated with fuel type. Major findings of over 1000 hours of ambient smoke monitoring in a populated center downwind of multiple fires include a ~50% lower $\Delta PM_{2.5}/\Delta CO$ at Missoula than commonly observed in previously-published airborne studies of wildfire smoke suggesting that evaporation can dominate secondary organic aerosol (SOA) formation in aged smoke at surface altitudes. O_3 was enhanced by dilute smoke and suppressed by thick smoke, and O_3 and NO_2 were strongly anti-correlated, yielding high NO_3 production rates. On average, BrC accounted for about 50% of the aerosol absorption at 401 nm. Finally, in comparing our surface measurements of smoke to recent field campaign measurements, we find additional evidence for lower PM/CO ratios at the surface, compared to high elevation or airborne campaigns, suggesting temperature may play a critical role in the evolution of BB aerosol. These findings may have larger scale implications especially as it relates to land management and the increased implementation of prescribed fires.

ACKNOWLEDGEMENTS

My deepest gratitude extends to anyone and everyone who has supported me throughout my graduate studies and doctoral pursuits. Specifically, I am incredibly thankful to my advisor Bob Yokelson for the insight, patience, and time he devoted to me as my mentor. This work would be impossible without his support and guidance, and the support and guidance from my committee members: Lu Hu, Mark Cracolice, Michael DeGrandpre, and Philip Higuera. I also extend my thanks to Ted Christian and Chelsea Stockwell for their advice, encouragement, and friendship as group members. Although there are too many names to list here, I am incredibly grateful for those whom I worked alongside with and befriended during field campaigns—you made the long days not only bearable, but also enjoyable. In the same regard, I want to extend my gratitude to all those who provided data, advice, and meaningful considerations during my grad school career and in this work. Finally, thank you to my friends, family, and loved ones for their continued support, compassion, and words of encouragement, and to my dog Molly for her unconditional love (and fluffiness) throughout this journey.

TABLE OF CONTENTS

LIST OF FIGURES

LIST OF TABLES

ABBREVIATION INDEX

AAE	Absorption Ångström Exponent
AMS	Aerosol Mass Spectrometer
ARCTAS	Arctic Research of the Composition of the Troposphere from Aircraft and Satellites
BB	Biomass Burning
BBOA	Biomass Burning Organic Aerosol
BBOP	Biomass Burn Observation Project
BC	Black Carbon
BrC	Brown Carbon
CMB	Chemical Mass Balance
DEQ	Department of Environmental Quality
EC	Elemental Carbon
EFs	Emission Factors
ERs	Emission Ratios
FIREX-AQ	Fire Influence on Regional to Global Environments and Air Quality Experiment
FSL	Fire Sciences Laboratory
FTIR	Fourier Transform Infrared
HITRAN	High-resolution Transmission Molecular Absorption Database
LIDAR	Light Detection and Ranging
IR	InfraRed
MAC	Mass Absorption Coefficient
MCE	Modified Combustion Efficiency
MCT	Mercury-Cadmium-Telluride
MSC	Mass Scattering Coefficient
NMOGs	Non-Methane Organic Gases
OA	Organic Aerosol
OC	Organic Carbon
OP-FTIR	Open-Path Fourier Transform Infrared
PAS	Photoacoustic Aerosol Absorption Spectrometer
PAX	Photoacoustic Extinctiometer
PF	Prescribed Fire

PM	Particulate Matter
$PM_{1.0}$	Particulate Matter with Aerodynamic Diameter < 1.0 microns
$PM_{2.5}$	Particulate Matter with Aerodynamic Diameter < 2.5 microns
PNNL	Pacific Northwestern National Laboratories
POA	Primary Organic Aerosol
SAE	Scattering Ångström Exponent
$SEAC^4RS$	Studies of Emissions, Atmospheric Composition, Clouds and Climate Coupling by Regional Surveys
SOA	Secondary Organic Aerosols
SP2	Single Particle Soot Photometers
SSA	Single Scattering Albedo
SVOC	Semi-Volatile Organic Compound
USDA	U.S. Department of Agriculture
USFS	U.S Forest Service
VOC	Volatile Organic Compound
WE-CAN	Western Wildfire Experiment for Cloud Chemistry, Aerosol Absorption and Nitrogen
WF	Wildfire
WUI	Wildland Urban Interface

Chapter 1: Introduction

1.1 Western wildfire impacts and background

Biomass burning (BB) is a major source of trace gases, aerosols, and particulate matter (PM) that can significantly impact local, regional, and global atmospheric chemistry, air quality, climate forcing; visibility; and human health (Crutzen and Andreae, 1990; United States Environmental Protection Agency, 2016). BB is one of the largest global sources of fine organic aerosol (OA), black carbon (BC, aka "soot"), brown carbon (BrC, a subset of OA that absorbs UV light) (Bond et al., 2004; 2013; Akagi et al., 2011; Hecobian et al., 2010), greenhouse gases, and non-methane organic gases (NMOG) (Yokelson et al., 2008; 2009), which are precursors for the formation of ozone (O_3) and OA. Further, of the six criteria pollutants classified by the Environmental Protection Agency (EPA), BB can be a direct and indirect source of five of them (O_3, NO_2, CO, SO_2, PM). While the majority of BB occurs in the tropics, the small fraction of the global BB in the western US is responsible for a significant portion of US air quality impacts (Park et al., 2007; Liu et al., 2017; Wilkins et al., 2018; Zhou et al., 2018) and contributes to increasing health concerns. Wildfire smoke has been shown to have adverse respiratory and cardiovascular health effects, is associated with mortality and morbidity, and exhibits lung toxicity and mutagenicity (Le et al., 2014; Liu et al., 2015; Reid et al., 2016; Adetona et al., 2016; Kim et al., 2018). In some cases, long-range transport of BB emissions can cause air quality standards to be exceeded hundreds or thousands of kilometers downwind of the fire source (Jaffe et al., 2013; Wigder et al., 2013). In addition to health concerns, particulate matter from wildfires can reduce visibility, which can have impacts on safety and transportation (United States Environmental Protection Agency, 2019), and is a concern in protected visual environments such as national parks and wilderness areas, most of which are in the western US, where a majority of wildfires

occur. Wildfires are understood to be a key component of forest ecosystems, but climate change, the build-up of fuels due to fire suppression, and the expansion of the wildland-urban interface (WUI) have led to increased fire risk and fire behavior that is more difficult to control (Turner et al., 2019; Schoennagel et al., 2017; Stevens et al., 2014; Shvidenko and Schepascheko, 2013). While globally, the length of fire season has increased by ~19% from 1979 to 2013, the increase in fire season has been even greater in the western US (Jolly et al., 2015), and has been closely tied to temperature, drought, and anthropogenic climate change (Abatzoglou and Williams 2016; Marlon et al., 2012; Westerling et al., 2006). The expansion of the WUI increases wildfire threats to people, homes, and infrastructure and fundamentally changes the tactics and cost of fire suppression; these issues can account for as much as 95% of fire suppression costs (US Department of Agriculture, Forest Service, 2015). Aggressive fire suppression techniques have also led to an accumulation of fuels in drier forests previously adapted to frequent low-severity fires that reduced less fire-resistant vegetation. Prescribed fires, and reducing aggressive fire suppression techniques are options to remedy the situation, as prescribed fires can reduce hazardous fuels under safe conditions when smoke is largely directed away from most populated areas and they are a major, successful component of land management in the southeast US. However, recent research suggests that in the western US more prescribed fire can reduce air pollution from wildfires and benefit safety in the WUI, but it is unlikely that enough prescribed burning can be done to eliminate future increases in wildfire activity and subsequent air pollution (Schoennagel et al., 2017). Due to these expected increases in pollution, and to guide the recommended increased implementation of prescribed fires, robust models of smoke production, transport, and evolution are increasingly needed to understand the impacts of all fires on air quality, visibility, health, and climate.

To date, most of the research on the emissions and evolution of smoke from US fires has targeted prescribed fires (Burling et al., 2011; Akagi et al., 2013; Yokelson et al., 2013; May et al., 2014; Müller et al., 2016). However, wildfires account for the majority of area burned across the West, and they burn a different mix of fuels under environmental conditions with more intense photochemistry and different smoke dispersion scenarios, and they typically consume more fuel per unit area than prescribed fires and can have different emission factors (EFs, grams of compound emitted per kilogram of fuel burned) (Campbell et al., 2007; Yokelson et al., 2013; Urbanski, 2013; Liu et al., 2017). The chemical composition of freshly emitted smoke is complex and subject to change as fuels and combustion conditions change, and smoke evolution depends on both initial composition and fluctuating atmospheric processing scenarios (Jen et al., 2019; Hatch et al., 2019; Hatch et al., 2018; Ahern et al., 2019; Akagi et al., 2012). Wildfires in particular, may burn day and night for months in various fuel types, emitting smoke from multiple, rapidly changing locations with variable injection altitudes (Bertschi et al., 2003; Herron-Thorpe el at., 2014; Fromm et al., 2000; Stocks et al., 1996), which can then be subjected to a wide range of dispersion scenarios (Peterson et al., 2017; Chen et al., 2017). Important smoke evolution issues include the net result of competition between OA evaporation and secondary organic aerosol (SOA) formation, which affects the amount of PM, as well as the impact of smoke on criteria pollutants like O_3 and NO_2. Simulating wildfire smoke is complicated, with high diversity among models in large part due to inadequate representation of a multitude of variables (Shrivastava et al., 2017; Souri et al., 2017; Kinne et al., 2006). Further, characterizing and assessing model diversity is of limited value without quality reference observations, but reference data are only available for a handful of properties, and even then with severe restrictions in spatial and temporal nature (Shrivastava et al., 2017). While there are

studies that probe trace gas and aerosol optical property emissions of wildfire smoke sampled in the field (Liu et al., 2017; Lindaas et al., 2017; Landis et al., 2017; Collier et al., 2016; Eck et al., 2013; Sahu et al., 2012; Lack et al., 2012), much of the information is limited in temporal extent or incomplete chemically and fails to assess important issues, including the aging and evolution of smoke over time (e.g., hours to days), nighttime evolution and oxidation, or the contribution of constituents of increasingly recognized importance such as BrC (UV-absorbing OA).

1.2 Motivation and Goals

The overarching goal of this dissertation is to obtain temporally and spatially extensive in-situ reference data on biomass burning smoke in the western US using an extensive suite of instrumentation, in order to ultimately inform both smoke pollution model development and current and future land management strategies. The first phase was focused on investigating the emissions profiles of common western US forest-fire fuels in a managed laboratory setting to better understand the factors influencing the initial composition of smoke from real-world fires.

The next major phase characterized authentic ambient smoke in a populated center downwind of numerous typical wildfire sources. This provides a much-needed, extensive measurement of regional surface impacts and provides data useful for evaluating multiple assumptions and mechanisms in smoke models including: (1) ratios between tracers such as $\Delta BC/\Delta CO$, sensitive to the flaming/smoldering ratio at the source, (2) ratios including evolving species $\Delta O_3/\Delta CO$, $\Delta PM/\Delta CO$, $\Delta BrC/\Delta CO$, sensitive to secondary O_3 formation and aerosol evolution, (3) optical property measurements that can be normalized to aerosol mass data to probe multi-step, bottom up calculations of climate-relevant aerosol parameters and (4) time series or hourly-average values for inert tracers (e.g. BC, CO), which can be used to directly evaluate model assumptions

regarding emissions production, diurnal profiles of fuel consumption, and meteorology. The nature of typical aerosol optical properties and long-term aerosol trends or changes is also addressed in this phase. In conjunction with this, it is also useful to investigate smoke impacts on O_3 formation, and nighttime chemistry of smoke to probe the potential NO_3 contribution to in-situ nighttime formation of BrC or SOA. Additionally, the interaction of smoke with important non-fire sources, such as urban emissions, can be assessed.

Finally, the third goal was to extract insights from the comparison and synthesis of data from recent lab and airborne field measurements of smoke with our ambient smoke measurements downwind of the source. Exploring similarities and differences in the results from different sampling vantage points is another way to generate more robust model input and better understand the transitions from initial conditions to typical outcomes for model mechanism validation. More specifically, potential biases in the flaming/smoldering ratio of air or ground-based sampling can be explored and used to validate or improve emissions inventories. Investigation into the controls on how smoke evolves from the source to real world smoke evolution outcomes in population centers can inform how models should treat BrC persistence, SOA formation, and impacts on O_3. Lessons learned can also be used to optimize future campaigns in order to circumvent additional gaps or uncertainty in observational data associated with initial emissions and subsequent evolution of wildfire smoke.

1.3 Thesis Outline

Section 1.4 provides a brief synopsis of the main atmospheric processes relevant to this thesis that are influenced by BB emissions, an overview regarding BB aerosol dynamics in the atmosphere, and a description of sampling considerations for smoke.

Chapter 2 contains background information on common BB terms and calculations used to quantify emissions, including emission ratios (ERs), emission factors (EFs), modified combustion efficiency (MCE), single scattering albedo (SSA), absorption/scattering Ångström exponents (SAE/AAE), mass scattering coefficient (MSC) and mass absorption coefficient (MAC).

Chapter 3 introduces and provides a brief overview of the Fire Influence on Regional to Global Environments and Air Quality Experiment (FIREX-AQ) laboratory component that took place in fall 2016 at the Missoula Fire Science Laboratory (FSL). In addition to detailing laboratory configurations, fuels burned, and the suite of instrumentation deployed, this chapter covers major findings of trace gas measurements by the open-path Fourier transform infrared (OP-FTIR) spectrometer OP-FTIR and aerosol optical measurements by photoacoustic extinctiometer (PAX). The results are then compared to relevant field studies, to inform the use of the emissions data produced.

Chapter 4 presents an overview of the ambient monitoring done during the 2017 Missoula fire season and focuses on the results of trace gases measured by a Fourier transform infrared (FTIR) spectrometer, aerosol optical measurements by PAX, and $PM_{2.5}$ measurements produced by the Missoula Department of Environmental Quality. Major findings for over 500 hours of smoke-impacted data are presented in order to document the net combined effect of numerous fires on a heavily impacted surface site embedded in the west. This chapter characterizes the smoke impacts on a population center and documents real-world regional significance of BrC.

Chapter 5 is a follow-up to the 2017 measurements, and focuses on the ambient monitoring done during the 2018 Missoula fire season to bring a collective ambient monitoring time of over 1000

hours. This chapter expands upon the measurement techniques in 2017 by including an O_3 and NO_x monitor to calculate the production of NO_3 and probe the potential NO_3 contribution to in-situ nighttime formation of BrC. Chapter 5 further assesses the relevance of lab and airborne field measurements, the representativeness of emissions inventories, and interprets the interannual variability of wildfire pollution by comparing 2018 to 2017 measurements.

Chapter 6 presents a detailed comparison of our previous studies of ambient smoke pollution in Missoula, to recent near-source airborne and ground-based campaigns with a focus on FIREX (https://www.esrl.noaa.gov/csl/projects/firex-aq/) and Western Wildfire Experiment for Cloud Chemistry, Aerosol Absorption and Nitrogen (WE-CAN) (https://www.eol.ucar.edu/field_projects/we-can) data, primarily, but includes additional field campaigns as well. This chapter covers similarities and differences in measurements and results, addresses sampling biases, and investigates causes for the differences among sampling platforms, particularly as they relate to smoke evolution.

1.4 Literature Review

1.4.1 Atmospheric processes and biomass burning emissions

Smoke evolution is complex and highly dependent on variable atmospheric processing scenarios, but several smoke species and atmospheric processes are linked by a connection to UV light. The absorption of UV light by molecules drives many critical chemical reactions in the atmosphere and can lead to formation of new compounds or free radicals that drive various important oxidation cycles which ultimately influence the overall composition of the atmosphere. Hydroxyl radical (OH) is the primary atmospheric oxidant and is produced during the day when UV light from the sun photolyzes nitrous acid (HONO), or formaldehyde (HCHO) or photolyzes O_3 in the

presence of water vapor. The oxidation of compounds by OH contributes to the formation of O_3 (the major nighttime oxidant) via associated UV photolysis of NO_2. NO_2 in smoke plumes is from flaming combustion of biomass or can be from mixing with local, non-BB sources downwind of the fire source, while O_3 is abundant in background air and made during the daytime in smoke plumes (Akagi et al., 2012; Akagi et al., 2013). NO_2 and O_3 react to form nitrate radical (NO_3), which is stable enough at night in the absence of visible light, to be an important additional nighttime oxidant, which may then react with NMOG to form BrC and SOA (Figure 1.1).

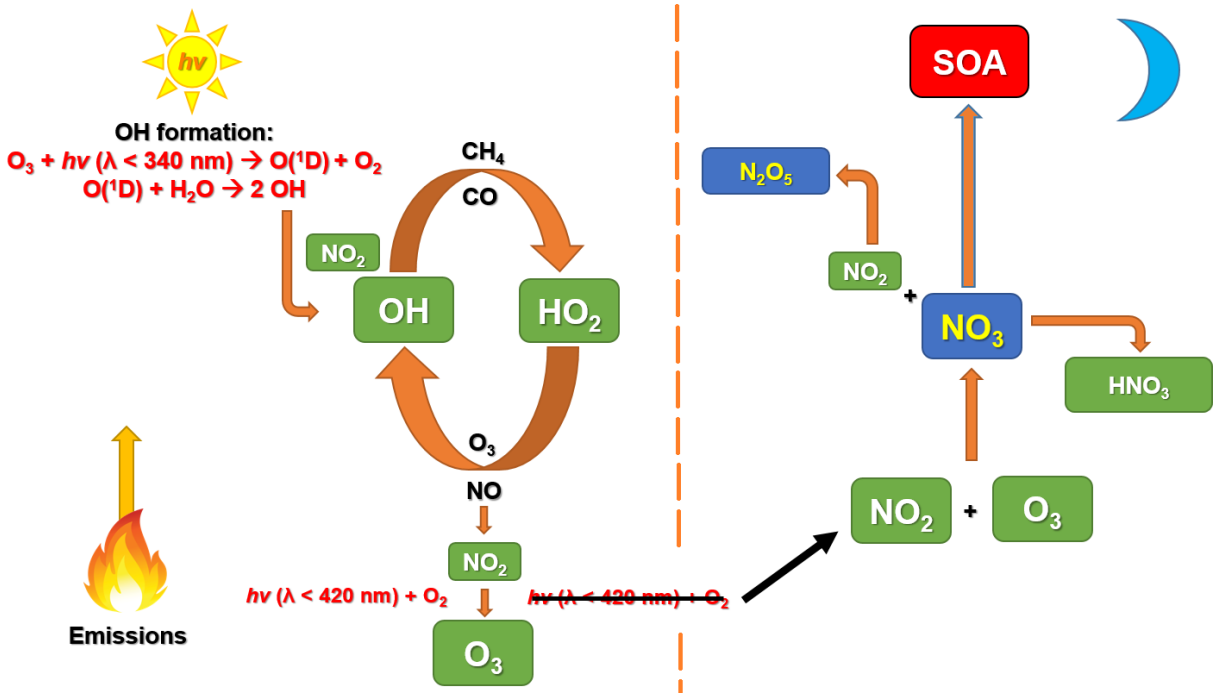

Figure 0.1 Simplified schematic of the atmospheric oxidants and daytime/nighttime atmospheric chemistry. Compounds shown in blue are only made at night. SOA = Secondary organic aerosol.

The amount of NMOG precursors and SOA is impacted by gas-particle partitioning, which depends on dilution and temperature (Robinson et al., 2007; May et al., 2013) and the emissions of NMOG are higher when the smoldering/flaming ratio increases (Burling et al., 2011), with

one study suggesting that the smoldering/flaming ratio is higher at night than during the day (Benedict et al., 2017). Stockwell et al., (2015) showed that smoldering combustion of biomass releases large amounts of monoterpenes, furans, cresol, etc., all of which can react quickly with NO_3 and form UV-absorbing organic nitrates that have potential to become condensed phase chromophores (BrC) as eventual products (Brown et al., 2013). Observations of nighttime smoke impacting the Colorado Front Range also showed high levels of these same precursors (Gilman et al., 2015), and OA in BB plumes intercepted at Mt. Bachelor Observatory was more oxidized after nighttime aging (Zhou et al., 2017). Thus, secondary nighttime formation of BrC from reactions of fire-emitted NMOGs with NO_3, and potentially O_3 or other pathways is likely, and may alter next-day photochemistry since BrC competes for UV photons with gases like HONO and NO_2. Although nighttime environmental conditions tend to favor smoldering combustion, which is more enriched in reduced nitrogen compounds that may be chromophores, the extent of this effect is un-probed by traditional day-time sampling. The SOA yields via nighttime oxidation of other reactive NMOGs present in smoke plumes are essentially unknown. With "stagnant" conditions, and especially stable source emissions, a BrC/CO ratio increase might be assigned to oxidation as opposed to changes in source emissions. Influences causing any observed nighttime changes in BrC could be difficult to separate, but nonetheless, nighttime smoke chemistry is so far nearly unstudied and requires more attention. Even if no mechanistic breakthroughs on BrC formation are made, good documentation of the characteristics of nighttime smoke is valuable.

1.4.2 Aerosol Absorption and Scattering

The term “aerosols” is used here to indicate particles suspended in the atmosphere. Aerosols have direct and indirect atmospheric effects, which alter Earth’s overall radiative budget and the thermal profile of the atmosphere chiefly by impacting the amount of solar radiation being reflected or absorbed. As a direct effect, aerosols both absorb some sunlight (heating) and scatter some sunlight back into space (cooling) with the balance depending mainly on particle chemistry and morphology. Indirectly, aerosols change how clouds reflect and absorb sunlight by acting as cloud condensation nuclei, by modifying the size (and optical properties) of cloud droplets, and changing cloud lifetimes via their size distribution and thermal impacts. Currently, global estimates of the radiative forcing due to BB aerosols vary significantly due to large uncertainty in their amount, size, optical properties, and chemical composition (Figure 1.2) Assumptions are made about the wavelength dependent ratio between absorption and scattering. Assumptions are also made regarding the strength of absorption and scattering per unit aerosol mass and the emissions and distribution of aerosol mass with different chemical, optical, and size characteristics. These difficult-to-validate assumptions are used to calculate (estimate) aerosol absorption and scattering in models and satellite retrievals (Ramanathan et al., 2001; Jiang and Feingold, 2006; McComiskey et al., 2008). One of the largest sources of uncertainty is the relative amount of absorption and scattering. Some models and satellite (e.g., MODIS) retrievals assume a constant value for fire aerosol throughout the BB season and the entire year, which may be an inaccurate approach, as it has been shown it can change over the course of the fire season (Eck et al., 2013). As mentioned in the Introduction, BB is a significant source of aerosols, notably in the form of BC and BrC, but is also an indirect producer of additional aerosol through formation of SOA, which affects total aerosol mass and optical properties.

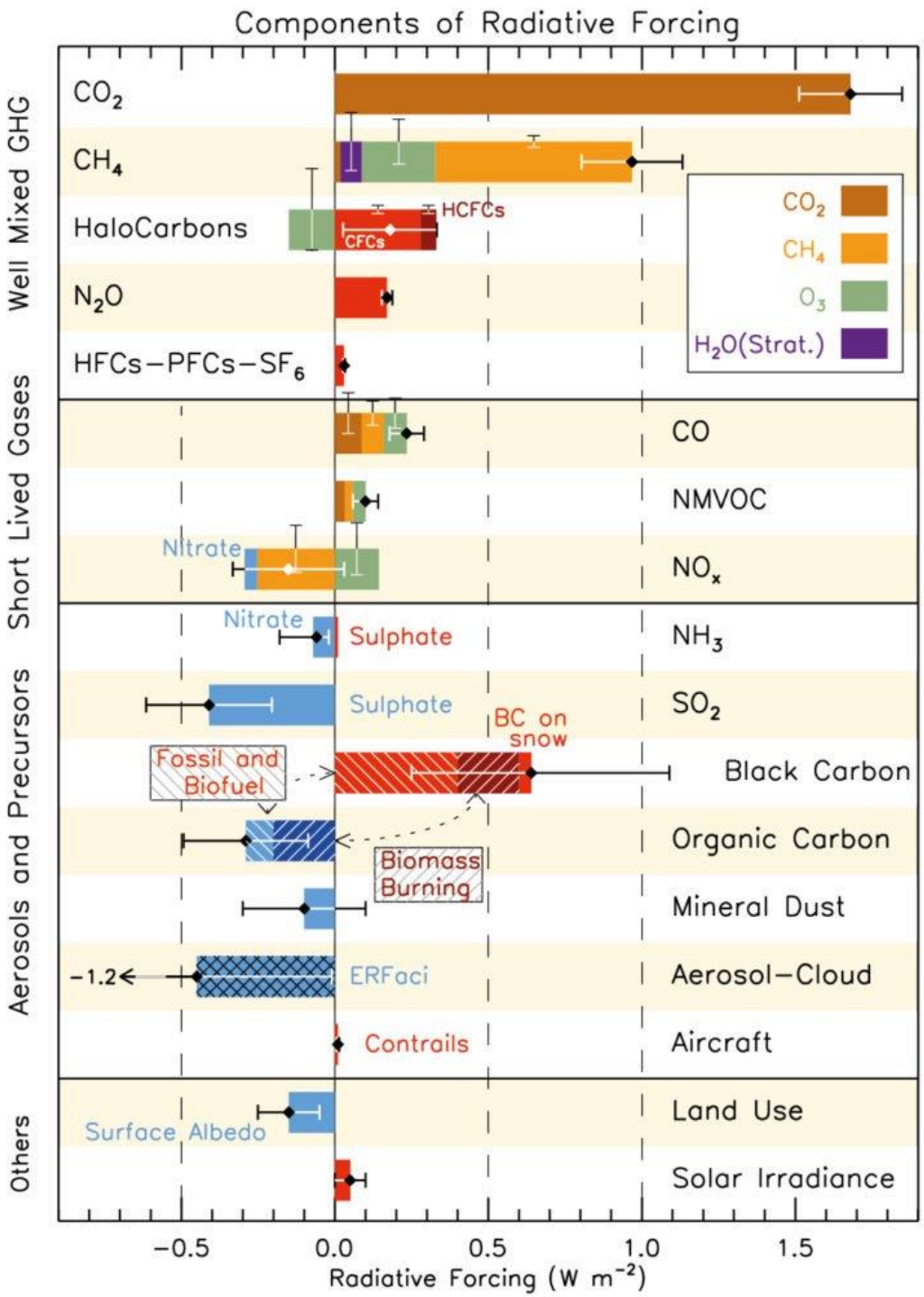

Figure 0.2 Bar chart of radiative forcing showing the high uncertainty in radiative forcing due to aerosols and aerosol precursors. Figure taken from the Intergovernmental Panel on Climate Change (IPCC), 2014.

BB is the largest global source of BC, an inorganic aerosol often referred to as 'soot'. BC absorbs light strongly at all wavelengths and is the second most positive global radiative forcing agent after CO_2. While BC is not well-mixed throughout the atmosphere like long-lived greenhouse gases, it is thought to have a major role in the climate system due to its ability to absorb solar radiation and its interactions with clouds (Hansen et al., 2000, Jacobson et al., 2000). Models try to calculate BC loading starting with either the BC emissions inventories or PM inventories and assumed BC/PM ratios, then disperse the emissions, but currently large uncertainties exist in BC EFs (Li et al., 2019). These uncertainties can be grouped into two different categories, which are related to either instrument differences or natural variability. Differences in instrumentation used to measure BC introduce uncertainty that can be especially problematic when attempting to compile emissions inventories due to inconsistencies among various techniques used. Natural fire-to-fire variability further complicates the situation due to the real differences in BC EF caused by MCE, fuel type, etc. In addition, the instrument-specific artifacts are impacted by the variable aerosol composition such as the relative amount of BrC/BC (Li and Shiraiwa, 2019; Subramanian et al., 2010). BC is made only by flaming combustion at the fire source, but its emissions are mixed with co-emitted BrC and non-absorbing OA. Thus, BC mass measurements can often be difficult, but ultimately aerosol absorption is the critical parameter climate models need. BC typically dominates aerosol absorption, but absorption by BrC and mineral dust also contributes to aerosol absorption, and absorption by BC can further be enhanced by coatings, which are common in wildfire plumes.

BB is also the largest global source of BrC. A significant amount of uncertainty in isolating and evaluating the optical properties of BrC and its overall radiative impact remains difficult to accurately assess. Nonetheless, several studies have found that including BrC in climate models

suggests that net radiative forcing of biomass burning would move in a positive direction. (Graber and Rudich, 2006; Ervens et al., 2011; Wang et al., 2014; Laskin et al., 2015; Wang et al., 2017; Feng et al., 2013; Jacobsen, 2014; Saleh et al., 2014; Forrister et al., 2015; Zhang et al., 2020). This has important climate implications, especially in association with warming-induced increases in fire activity (Westerling et al., 2006; 2016; Feng et al., 2013; Doerr and Santín, 2016; Bowman et al., 2017). Competition between destruction and formation of BrC is important for climate and BC measurement uncertainties, especially as they relate to the mixing state of BC. While the attribution of BrC is not exact and varies across studies (Pokhrel et al., 2017), BrC absorption will offset the climate cooling calculated for purely scattering OA depending on the amount emitted, its absorption cross-section, and its lifetime (Feng et al., 2013). One field study of BrC lifetime suggests a significant decrease of BrC over the course of a day but a prolonged persistence of BrC nonetheless (~ 6 % above background even 50 h after emission) (Forrister et al., 2015), and studies of relevant chemical mechanisms involving BrC have shown both increases and decreases (Lin et al., 2015; Liu et al., 2016; Xu et al., 2018). Satellite retrievals employing reasonable a priori aerosol layer heights indicate that BrC can have a strong impact in fresh BB plumes and a persistent significant impact in downwind regional haze (Jethva and Torres, 2011; Hammer et al., 2016). Optical properties are important during the day, and field smoke is likely to have high BrC at sunrise, especially if nighttime formation of BrC is prevalent. Measurements of the lifetime of BrC range from tens of minutes based on lab studies of surrogate compounds (Zhao et al., 2015) to much longer lifetimes (up to 40 days) suggested by lab studies of authentic BB-OA (Fleming et al., 2019) and in one field study (Forrister et al., 2015). Despite these important issues, in-situ data of the optical properties of BrC and BrC persistence were almost non-existent when this research began.

1.4.3 Sampling Considerations

Several different sampling approaches are useful for characterizing initial emissions of wildfires and subsequent aging, but each come with their own set of limitations. Airborne measurements of wildfires are optimal for representative near-source sampling of lofted smoke from fires and also the first few hours of plume evolution at higher altitudes in lofted plumes, but the contribution of nighttime smoke or unlofted smoke over the course of a fire is variable and largely un-sampled, which could cause these emissions to be under-estimated or remain uncharacterized (Yokelson et al., 2009; 2008). Ground based measurements at the source can sample the initial emissions of nighttime and unlofted smoke, but may under-sample smoke that is aggressively lofted or otherwise inaccessible. Further, ground-based measurements at the source seldom capture the downwind smoke impacts and the interactions of smoke with local, non-fire emissions in populated areas. As a result, airborne campaigns and ground-based source measurements normally do not provide much information on the specific or typical properties of smoke in heavily-impacted surface locations, which is critically necessary to evaluate model predictions of surface air quality (Shrivastava et al., 2017).

Ground-based sampling downwind of fires can characterize both aged and relatively fresh daytime or nighttime smoke (Benedict et al., 2017; Collier et al., 2016; Gilman et al., 2015). When continuous measurements are collected downwind of many fires burning at all stages over a long period of time, a large amount of data are collected that can help characterize overall regional fire emissions (Wiggins et al., 2020). When this approach is implemented in populated locations it can also provide extensive documentation of specific and typical smoke air quality impacts on the population, and insight into the interaction of regional smoke with non-fire sources on longer temporal scales. Unfortunately, extended detailed smoke measurements in

population centers are still relatively rare, and downwind ground-based sampling is subject to limitations as well. Surface stations are generally fixed and the amount of data collected can depend heavily on chance and the intensity of the regional fire season. Further, determining a smoke age or source for impacts measured by surface stations is not always trivial, and can be especially difficult in situations with multiple mixed sources; thus, surface-stations may lack specificity on fuels and fire behavior. In addition, in-situ surface data needs to be supplemented with vertical profiles or column data to probe upper level smoke, which may have larger relative impacts on climate.

Finally, laboratory-based measurements of simulated fires can lead to highly accurate emissions characterization in general, and can also provide extensive information on fuels and fire behavior. However, "lab fires" can differ significantly from real world fires on a larger scale. In particular, laboratory fires often tend to burn at higher average modified combustion efficiency (MCE) than observed in the field (Selimovic et al., 2018; Stockwell et al., 2015a; 2015b; Yokelson et al., 2008), and lab experiments can only simulate smoke aging and the interaction of smoke with non-fire sources. Each approach to post-emission smoke aging in the lab has limitations (e.g., wall losses, duration), and although chamber studies and experiments with oxidative flow reactors have been carried out extensively, these experiments have so far provided diverse outcomes without clarifying the controlling factors or establishing a typical "real world outcome" (Tcacik et al., 2017; Ahern et al., 2019; Coggon et al., 2019). A way forward that optimizes the strengths and minimizes the shortcomings of the above strategies should involve comparing and synthesizing observations from all available approaches.

Chapter 2: Biomass burning general information and useful ratios

2.1 Emission Inventories

Bottom-up, or source-based models and top-down, or receptor-based models are two techniques used to evaluate BB pollution and assess its impacts. For instance, in BB models, the mass of fuel burned (activity data) can be multiplied by EFs to generate estimates of initial emissions, which are then combined with models of dispersion, transport, and chemistry, in order to predict eventual concentrations of pollutants in the air. Sampling smoke before photochemical processing occurs is critical in these models since they are initial values, and is where laboratory sampling of realistically recreated western-wildfire ecosystems can be useful. However, knowledge gaps in initial conditions and sub-grid processes introduce uncertainty in bottom-up modeling approaches that are propagated throughout model predictions, thus accurate knowledge of BB EFs is critical to smoke forecasting.

Top-down modeling is complementary to bottom-up modeling and requires real-world measurements and knowledge of potential sources. It can be applied in several ways. One is to measure the products of a pollution source (in-situ or by satellite) and then use modeled meteorology and known EFs to constrain activity data. Another approach, is to divide the observed amount of products from a source by signals generated at the source to empirically calculate "emission coefficients" that can be applied to future observations of the source signals. Often for BB, meteorology is used to assign an amount of aerosol optical depth (AOD) observed by satellite to an amount of heat detected by satellite at the fire source. Then the emission coefficient is quickly applied to future heat observations to generate near real time emissions estimates. Top-down approaches typically start with a limited number of species measured by satellite (MODIS) or global networks (AERONET) and use literature ratios to generate estimates

for species not measured by satellite. Their results are an independent check on bottom-up approaches and the emission coefficients can be rapidly updated in some cases using "data assimilation" to update emissions inventories.

2.2 Emission ratios and emission factors

Time series are useful to characterize impacts and evaluate models, but using the time series of mixing ratios or concentrations for each analyte measured to derive other values such as the emission ratio or emission factor, puts them into a form that is broadly useful for study comparisons and implementation in local to global chemistry and climate models. The process starts by calculating excess mixing ratios (denoted ΔX for each species "X") by subtracting the relatively small average background mixing ratio measured before each fire (or smoke impact on longer time scales, see Chapter 4) from all the mixing ratios observed during a burn. The emission ratios to CO_2 are then used to derive EFs calculated by the carbon mass balance method via the following equation:

$$EF(X)\left(g\,kg^{-1}\right) = F_C \times 1000 \times \frac{MM_x}{AM_C} \times \frac{\frac{\Delta X}{\Delta CO_2}}{\sum_{j=1}^{n}\left(NC_j \times \frac{\Delta C_j}{\Delta CO_2}\right)} \quad (1)$$

where F_c is the measured carbon mass fraction of the fuel; MM_x is the molar mass of species X; AM_C is the atomic mass of carbon (12 g mol^{-1}); NC_j is the number of carbon atoms in each species j; C_j or ΔX referenced to ΔCO_2 are the source-average molar emission ratios for the respective species. The denominator of the last term in Eq. (1) estimates total carbon. Based on many BB

combustion sources measured in the past, the species CO_2, CO, and CH_4 usually comprise 97-99% of the total carbon emissions (Akagi et al., 2011; Stockwell et al., 2015).

2.3 Modified Combustion Efficiency

Two major combustion processes are often recognized for open burning of biomass: flaming and smoldering; where "smoldering" is an approximate term for all non-flaming processes (e.g. glowing and pyrolysis) as explored in more detail elsewhere (Yokelson et al., 1996, Koss et al., 2017; Sekimoto et al., 2018). Combustion efficiency is the fraction of fuel carbon converted to carbon as CO_2, which is maximized by flaming combustion, but the modified combustion efficiency (MCE) is also a useful approach for characterizing the relative amount of smoldering and flaming combustion by comparing the fuel carbon converted to CO_2 versus CO_2 + CO. Although the two processes often occur simultaneously throughout a fire, a high MCE (near 0.99) is an indication of nearly pure flaming, while a lower MCE (~0.8) is an indication of nearly pure smoldering (Akagi et al., 2011) and an MCE of 0.9 would indicate roughly equal amounts of flaming and smoldering (i.e. a flaming/smoldering ratio of ~1):

$$MCE = \frac{\Delta CO_2}{\Delta CO + \Delta CO_2} \quad (2)$$

2.4 Single scattering albedo and absorption Ångström Exponent

Scattering and absorption values can be combined directly to calculate the single scattering albedo (SSA, the ratio of scattering to total extinction). SSA is a useful input for climate models, whereby an SSA closer to 1 indicates a more "cooling" highly-scattering aerosol:

$$SSA = \frac{Scattering\ (\lambda)}{Scattering\ (\lambda) + Absorption\ (\lambda)} \quad (3)$$

The absorption Ångström exponent is useful as an indicator of BrC/BC, but in addition, the full aerosol absorption spectrum is often approximated with a power law function (absorption = $C \times \lambda^{-AAE}$) and thus the AAE determined with any wavelength pair can be used to approximately calculate the shape of absorption across the UV-VIS range (Reid et al., 2005) using the following equation, where the AAE of pure BC is close to one and larger values are indicative of smoke absorption more dominated by BrC emissions:

$$AAE = -\frac{\log(\frac{Absorption_{\lambda 1}}{Absorption_{\lambda 2}})}{\log\frac{\lambda_1}{\lambda_2}} \quad (4)$$

2.5 Mass Scattering and Mass Absorption Coefficients

Mass scattering coefficients (MSC) and mass absorption coefficients (MAC), allow the input of absorption and scattering of aerosols, based on mass measured, in a way that's useful to climate models. MSC and MAC directly relate the amount or mass of an aerosol to its interaction with light, by probing how strongly light is absorbed or scattered on a per mass basis.

$$MSC = \frac{Scattering\ (Mm^{-1})}{PM\ Mass\ (\mu g\ m^{-3})} \quad (5)$$

$$MAC = \frac{Absorption\ (Mm^{-1})}{PM\ Mass\ (\mu g\ m^{-3})} \quad (6)$$

Chapter 3: The Fire Influence on Regional and Global Environments Experiment (FIREX) Missoula Fire Sciences Lab Experiment

3.1 FIREX Lab Introduction:

The Fire Influence on Regional and Global Environments Experiment (FIREX) (https://www.esrl.noaa.gov/csd/projects/firex/) multiyear campaign led by the National Oceanic and Atmospheric Administration (NOAA) aimed to answer research questions and critical unknowns about BB that can be addressed with existing or new technologies, laboratory and field studies, and interpretive efforts in order to understand and predict the impact of North American fires on the atmosphere and ultimately support land management. The first phase of this multiyear campaign took place at the US Forest Service Fire Sciences Laboratory (FSL) in Missoula, Montana, in the fall of 2016. We deployed a comprehensive suite of standard instrumentation as well as newer measurement techniques and analysis methods to better assess BB emissions. Each approach has its strengths and weaknesses and many uncertainties are difficult to quantify based on data from a single instrument. Thus, combining results from many techniques to develop a larger data set is critical to achieving the fullest understanding of the capabilities of each method and to better comprehend the full diversity of the emissions and their impacts. We simulated the fuel and combustion conditions of real wildfires to the extent possible in hopes of obtaining the most relevant emissions measurements. As part of the first (laboratory) phase of FIREX we deployed an open-path Fourier transform infrared spectrometer (OP-FTIR) and two photoacoustic extinctiometers (PAXs) operating at 401 and 870 nm. After the first 31 fires, our 401 nm PAX was moved and sampled from a barrel as part of an intercomparison, while the 870 nm PAX stayed sampling the remaining stack fires. After all the stack fires were finished, the 870 nm PAX moved

to participate in an additional intercomparison of aerosol optical property measurement techniques carried out in BB aerosol.

3.2 FIREX Lab configurations

3.2.1: US Forest Service Fire Sciences Laboratory

The FSL has a large indoor combustion room described in more detail elsewhere (Christian et al., 2003; Burling et al., 2010). Briefly, the room is 12.5 m × 12.5 m × 22 m high with a 1.6 m diameter exhaust stack and a 3.6 m inverted funnel opening approximately 2 m above a continuously weighed fuel bed. The room can be pressurized to create a large constant flow that dilutes and completely entrains the fire emissions while venting through the stack. A sampling platform that can accommodate up to 1820 kg and sampling ports surround the stack 17 m above the fuel bed. Other instrumentation can be placed in adjacent rooms with sample lines pulling from ports at the sampling platform. Previous studies concluded that the temperature and mixing ratios are consistent across the width of the stack at the height of the platform, confirming well-mixed emissions that can be monitored by a number of different sample lines throughout the fire (Christian et al., 2004). Our simulated fires used two configurations, and are described in more detail in the following sections.

3.2.2: Stack burn configuration

In the first configuration, termed "stack burns", fires were ignited below the stack and they burned for a few minutes to half an hour. As the fire evolved, the emissions, partially diluted and cooled by outside air, traveled up through the stack at a constant flow rate (~ 3.3 m s^{-1}). At the platform

height, the well-mixed emissions were near ambient temperature, about 5 s old, and monitored by a large range of instruments in real time.

3.2.3: Room burn configuration

In the second scenario, referred to as "room burns", most of the instruments were relocated to rooms adjacent to the combustion chamber and used sample lines that extended well within the combustion room. The stack was raised, the combustion room was sealed, and the fuels were burned for several minutes. After about 15–20 min, the smoke from the whole fire was well mixed vertically in the combustion room and was monitored under approximately steady-state, lowlight conditions for up to several hours, though some infiltration and losses of gases and particles for some species occurred (Stockwell et al., 2014). Despite the losses, the configuration is useful for measurements requiring longer times. The OP-FTIR remained on the sampling platform during room burns, which helped to document the initial rise of flaming emissions and verified the overall mixing processes.

3.3 Fuels overview

Lab-based EFs are most accurate when they result from burning realistically re-created fuels from complex flammable ecosystems that produce emissions representative of field fires. Thus, we simulated the fuel and combustion conditions of real wildfires to the extent possible in hopes of obtaining the most relevant emissions measurements. A team of experts collected fuels that represent fire-prone western US ecosystems primarily from the Clearwater Wildlife Management Area (http://fwp.mt.gov/fishAndWildlife/wma/siteDetail.html? id=39754079) and the Lubrecht Experimental Forest (https://www.cfc.umt.edu/lubrecht/), which are managed by the state of Montana and University of Montana, respectively. Chaparral fuels and fuels for the Fire and

Smoke Model Evaluation Experiment (FASMEE, https://www.fasmee.net/) were sampled by forest fire experts at locations in California and Utah, respectively, and shipped overnight to the FSL. A few fuels representative of prescribed fires were sampled by foresters at SE US military bases and burned for comparison purposes and for the FASMEE project. Sagebrush and juniper were sampled locally. Indonesian peat, aspen shavings (also known as "excelsior"), and dung were sampled and burned because of their global importance and/or to investigate the impact of fuel chemistry (e.g., N content) on emissions. Fuel components for the forest ecosystems included duff; litter; dead and down woody debris in different size classes; herbaceous, shrub, and canopy fuels; and rotten logs from two of the above ecosystems (ponderosa pine and Douglas fir). These fuel components were burned both on their own and in realistic three-dimensional mixtures to mimic the different fuel complexes for various ecosystems. The first-order fire effects model (FOFEM) (Reinhardt et al., 1997) was used to calculate the relative amount of each component that typically burns in coniferous ecosystems, while pure components were burned to probe how they affected the total emissions. The coniferous ecosystems modeled and burned included ponderosa pine (Pinus ponderosa), lodgepole pine (Pinus contorta), Engelmann spruce (Picea engelmanii), Douglas fir (Pseudotsuga menziesii), and subalpine fir (Abies lasiocarpa). Chaparral was represented by manzanita (Arctostaphylos) and chamise (Adenostoma fasciculatum). A full description of the fuels for each fire, including collection location; C, H, N, S, and Cl content; dry weight of each component is included in Table S1.

3.4 Instrument overview

Extensive instrumentation that monitored both the gas-phase and particle-phase emissions from BB was deployed during the FIREX laboratory study. A table of all the instruments and their measurement capabilities can be found at the following URL

(https://www.esrl.noaa.gov/csl/projects/firex/firelab/instruments.html). For the first 31 stack fires the two PAXs were the only instruments measuring aerosol optical properties on the platform and only the 870 nm PAX measured optical properties on the sampling platform for the next 44 fires, which accounts for all the stack burns. The 401 nm PAX was deployed with a BC intercomparison that measured subsamples of smoke in a mixing barrel for fires 32–107. The 870 nm PAX was deployed with a large group of aerosol instruments that characterized aerosol subsamples from the room burns (fires 76– 107). Other aerosol measurements on the platform during the stack burns included filter sampling with off-line analysis of non-methane organic compounds and AMS characterization of diluted smoke.

3.4.1 OP-FTIR introduction

The OP-FTIR consisted of a Bruker MATRIX-M IR Cube spectrometer with a mercury cadmium telluride (MCT) liquid-nitrogen-cooled detector interfaced with a 1.6 m base open-path White cell. The optical path length was 58 m and IR spectra were collected at a resolution of 0.67 cm^{-1} from 600-4000 cm^{-1}. During stack burns, the OP-FTIR was positioned on the sampling platform so that the open path fully spanned the width of the stack. This allowed continuous direct measurements across the rising emissions. A pressure transducer and two temperature sensors were located directly adjacent to the White cell optical path and were used for spectrum fitting and to calculate mixing ratios from the IR spectra. For stack burns the time resolution was approximately 1.37 s and the duty cycle was > 95%. For the room burns, where concentrations changed more slowly,

we increased the sensitivity by co-adding scans (time resolution of approximately 5.48 s) and moved the OP-FTIR to the edge of the sample platform closest to the fires.

3.4.2 OP-FTIR data collection

Mixing ratios were determined for carbon dioxide (CO_2) carbon monoxide (CO), methane (CH_4), acetylene (C_2H_2), ethylene (C_2H_4), propylene (C_3H_6), 1,3-butadiene (C_4H_6), formaldehyde (HCHO), formic acid (HCOOH), methanol (CH_3OH), acetic acid (CH_3COOH), glycolaldehyde (C_2H_4O2), furan (C_4H_4O), furaldehyde (C_5H_4O), phenol (C_6H_6O), hydroxyacetone ($C_3H_6O_2$), water (H_2O), nitric oxide (NO), nitrogen dioxide (NO_2), nitrous acid (HONO), ammonia (NH_3), hydrogen cyanide (HCN), hydrogen chloride (HCl), and sulfur dioxide (SO_2). Mixing ratios were based on retrievals utilizing multicomponent fits to specific sections of mid-IR transmission spectra with a synthetic calibration nonlinear least-squares method (Griffith, 1996; Yokelson et al., 2007) applying both the HITRAN spectral database and reference spectra recorded at the Pacific Northwest National Laboratory (Rothman et al., 2009; Sharpe et al., 2004; Johnson et al., 2010, 2013). The above species were usually enhanced in the smoke well above the real-time detection limits, but some species such as 1,3-butadiene, furaldehyde, phenol, and HCl were frequently not enhanced to more than 2–3 times the real-time detection limit and are not reported in those cases. The uncertainties in the individual mixing ratios varied by spectrum and molecule and were influenced by uncertainty in the reference spectra (1–5 %) or the real-time detection limit

(0.5–20 ppb), whichever was larger. Typical stack concentrations ranged from hundreds of parts per billion to thousands of parts per million depending on the analyte (Fig. 3.1)

3.4.3 FTIR Measurement Strategy

We sampled a total of 75 stack burns and 32 room burns at the FSL combustion facility during October and November 2016. Figure 3.1 shows temporal profiles for the excess mixing ratios of 21 gas-phase compounds (not including water) measured with the OP-FTIR for a complete juniper canopy fire (fire 75). Immediately after ignition, the fire is characterized by a large increase in CO_2, corresponding to flaming, followed by a slower increase in CO from smoldering combustion. As is common to most fires, there is no clear distinction between flaming and smoldering but rather an evolving mix of the two processes. Fire-integrated ERs to CO_2 and EFs were determined for all 75 stack fires based on the whole fire. For room burns, we calculated EF based on integrating the ΔX only up to the point at which emissions were well mixed to capture the whole fire but also minimize the effect of wall losses and infiltration (see Fig. 3 in Stockwell et al., 2014).

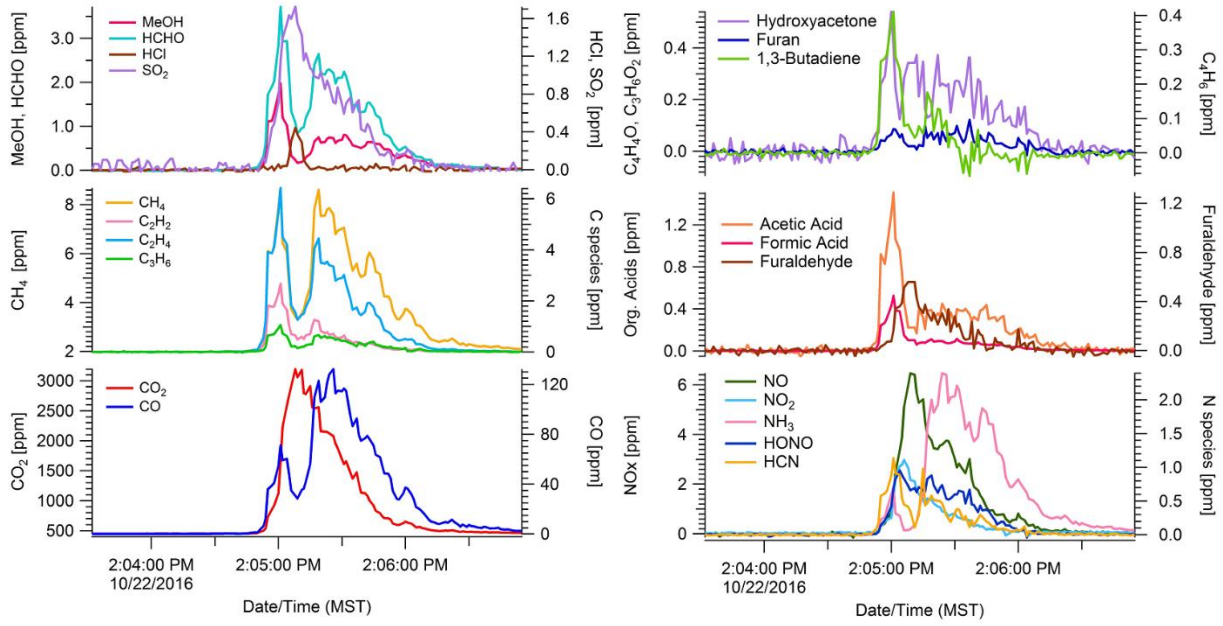

Figure 0.1 Excess mixing ratios of 21 trace gases vs time for a complete juniper canopy "stack" burn (#75) as measured by OP-FTIR. CO_2 denotes flaming, CO denotes smoldering. 1,3-butadiene is shown as an example of lower signal to noise data, but retained since there is no evidence of bias.

3.4.4 Emission ratio and emission factor determination

Excess mixing ratios were calculated for all 23-gas phase species measured using the OP-FTIR by subtracting the relatively small average background mixing ratio measured before each fire from all the mixing ratios observed during the burn. The molar ER for each species "X" relative to CO_2 ($\Delta X/\Delta CO_2$) is the ratio between the sum of ΔX over the entire fire relative to the sum of ΔCO_2 over the entire fire. A comparison of the sums is valid because the large entrainment flow ensures a constant total flow. Molar ERs to CO_2 were calculated for all the species measured using OP-FTIR for all 75 stack burns and the two most important room burns. For the other room burns, OP-FTIR data were generated only for CO_2, CO, CH_4, C_2H_4, C_2H_2, and H_2O as losses in the room add uncertainty to the mixing ratios for many NMOGs, NH_3, etc. The ERs to CO_2 were then used to derive EFs calculated with the carbon mass balance (CMB) method, which assumes all of the

burned carbon is volatilized and that all of the major carbon-containing species have been measured (Ward and Radke, 1993; Yokelson et al., 1996, 1999; Burling et al., 2010, Stockwell et al., 2014). Our estimate of total carbon includes CO_2, CO, and CH_4 (which usually comprise 97-99% of the total carbon emissions), and all the rest of the C-containing gases measured by OP-FTIR as well as the C in the particles (i.e. BC and OC) based on PAX data. Samples of each fuel component were analyzed for moisture content by weighing until dry and for C, H, N, S, and Cl by a commercial (ALS, Tucson) and an academic laboratory, whose results agreed well with each other on several overlapping fuel samples. The fire-average carbon mass fractions for mixed fuel beds were calculated from the average of the relevant fuel component analyses weighted by dry mass (Tab. S1). The usually small error in the CMB caused by neglecting char formation (Bertschi et al 2003) tends to be canceled by more complete combustion of the higher-C components (Santín et al., 2015) and both these effects are ignored here.

3.4.5 Photoacoustic extinctiometers (PAX) at 870 and 401 nm

Particle absorption and scattering ($B_{abs,}$ Mm^{-1}, $B_{scat,}$ Mm^{-1}) were measured directly at 1 s time resolution using two photoacoustic extinctiometers (PAX, Droplet Measurement Technologies, Inc., Longmont, CO; Lewis et al., 2008), and SSA at 401 (sensitive to BrC) and 870 nm (sensitive to BC), and the AAE were derived using those measurements. A 1L min^{-1} aerosol sample flow was drawn through each PAX using a downstream pump and split internally between a nephelometer and photoacoustic resonator for simultaneous measurement of light scattering and absorption. Scattering of the PAX laser was measured using a wide-angle reciprocal nephelometer that responds to all particle types regardless of chemical makeup, mixing state, or morphology. For absorption measurements, the laser beam was directed through the aerosol stream and modulated at a resonant frequency of the acoustic chamber. Absorbing particles transferred heat

to the surrounding air, inducing pressure waves that were detected via a sensitive microphone. We sampled stack burns through ~2 m of 0.638 cm (o.d.) Cu tubing that ran from the stack to a splitter that connected the two instruments. From the splitter, each separate sample line encountered a scrubber to remove absorbing gases (Purafil-SP Media, minimum removal efficiency 99.5%) and then a diffusion drier (Silica Gel 4-10 mesh) to remove water, with this order ensuring that both instruments were sampling at the same relative humidity (varying between 13 and 30%). The scrubber and drier were refreshed before any signs of deterioration were observed (e.g. color change) and the diffusion-based designs should incur minimal particle losses, but losses were not explicitly measured. After the drier, each sample line featured a 1.0 μm size-cutoff cyclone and two acoustic notch filters that reduced noise. Both PAX instruments were calibrated before and after the experiment using the manufacturer-recommended scattering and absorption calibration procedures utilizing ammonium sulfate particles and a propane torch to generate pure scattering and strongly absorbing aerosols, respectively. The estimated uncertainty in PAX absorption and scattering measurements has been estimated as ~4–11% (Nakayama et al., 2015).

3.4.6. PAX data collection

Advantages of the PAX include direct in-situ measurements, a fast response time, continuous autonomous operation, and eliminating the need for filter collection and the uncertainties that come with filter artifacts (Subramanian et al., 2007). In the PAX, the 870 nm laser is absorbed by in-situ black carbon containing particles only without filter or filter-loading effects that can be difficult to correct. We used the literature-recommended mass absorption coefficient (MAC) (4.74 ± 0.63 $m^2\ g^{-1}$ at 870 nm) to calculate the BC concentration ($\mu g\ m^{-3}$) (Bond and Bergstrom, 2006), but the BC mass can be adjusted using different MAC values if supported by future work. To a good approximation, sp^2-hybridized carbon (including BC) absorbs light proportional to frequency

(Bond and Bergstrom, 2006). Thus, the B_{abs} contribution from BC at 401 nm can be calculated from 2.17 times B_{abs} at 870, and any additional B_{abs} at 401 can be assigned to BrC subject to limitations due to "lensing" by coatings discussed elsewhere (Pokhrel et al., 2016; 2017; Lack and Langridge,2013; Lack and Cappa, 2010). Pokhrel et al. (2017) found that coatings typically accounted for much less than 30% of absorption in room burn smoke 1-2 hours old and coatings are likely much less important in 5 s old stack burn smoke (Akagi et al., 2012). Coating effects are very difficult to deconvolve from BrC effects even with additional instruments that were not available during the stack burns (Pokhrel et al., 2017). This adds some uncertainty to the BrC attribution (±25%), but not to the absorption measurements themselves. Absorption by the BrC component of OA means that an approximate mass of OA can be calculated using an OA MAC of 0.98 m^2/g (Lack and Langridge, 2013), but the MAC for OA is variable because BrC chemistry and BrC/OA vary and the OA MAC is also highly dependent on the BC/OA ratio as described elsewhere (Saleh et al., 2014). We use the qualitative OA to calculate a small term in our CMB that helps account for unmeasured C-species (assuming OA/OC of 1.6), but we do not report OA or OC in the tables as quantitative species. Critically though, we do report the OA absorption due mainly to BrC at 401 nm, a poorly characterized term that needs to be improved in climate models to better estimate the radiative forcing of BB aerosol (Feng et al., 2013). The mass ratio of BC to the simultaneous co-located CO_2, measured by the FTIR, was multiplied by EF for CO_2 to determine mass EFs for BC (g kg^{-1}). The EFs for scattering and absorption optical cross-sections at 870 and 401 nm (EF B_{abs}, EF B_{scat}) were calculated from the measured ratios of B_{abs} and B_{scat} to CO_2 and reported in units of m^2 per kg of dry fuel burned. We also report the portion of B_{abs} at 401 nm due to BrC.

3.5 OP-FTIR Results

3.5.1 Overview of wildfire trace gas emissions

The fire-integrated EFs for some of the most common western US ecosystem fuel complexes sampled in this study are summarized in Table 3.1. These are averages of the replicate fires (three to four replicate measurements for each fuel type). Table 3.1 does not reveal a strong ecosystem dependence across the coniferous ecosystems but does indicate lower EFs for many pollutants emitted by the chaparral fires. However, large wildfires often burn in multiple fuel types simultaneously. For instance, the Rim Fire burned in pine, pine–oak, and chaparral fuels simultaneously (Liu et al., 2017). These factors justify using a single set of EFs for all wildfires, unless detailed fuel data are available that warrant more precise EF estimates. The derivation of the best wildfire EFs is explored in more detail in the next section. A summary of all the EFs we measured with OP-FTIR and PAX for each individual fire can be found in Table S2, with the averages of specific fuel components and complexes found in Table S3. Numerous additional NMOGs that were measured using other instruments (e.g., $H3O^+$ chemical ionization mass spectrometer (CIMS) and I− CIMS) will be presented elsewhere (Koss et al., 2017). These additional species are often reactive and very important in plume chemistry even though they have only a small effect on the carbon mass balance. A few species were measured with both OP-FTIR and MS and the preferred values depend on several issues such as signal to noise (often better on MS), interference (often worse on MS), "stickiness", fragmentation, and proton affinity that are discussed in more detail elsewhere (Koss et al., 2017).

Table 0.1 Average emission factors (g kg^{-1}) of common Western U.S. ecosystems measured in the Missoula FSL.

Compound	Douglas Fir	Engelmann Spruce	Lodgepole Pine	Ponderosa Pine	Subalpine Fir	Chaparral - Chamise	Chaparral - Manzanita
CO_2	1685.99 (23.68)	1644.61 (55.81)	1688.52 (22.26)	1699.05 (23.11)	1659.79 (10.91)	1714.70 (14.78)	1698.45 (15.79)
CO	65.87 (12.66)	69.42 (18.47)	70.52 (9.67)	78.52 (10.90)	72.80 (5.07)	55.82 (4.96)	40.62 (0.72)
CH_4	2.31 (0.39)	3.02 (1.38)	2.61 (0.32)	2.76 (0.85)	3.86 (1.34)	1.26 (0.10)	1.14 (0.07)
Methanol (CH_3OH)	0.73 (0.14)	1.34 (0.70)	0.86 (0.20)	1.31 (0.59)	1.28 (0.55)	0.40 (0.04)	0.53 (0.07)
Formaldehyde (HCHO)	1.53 (0.40)	1.56 (0.26)	1.67 (0.50)	1.79 (0.46)	1.92 (0.32)	0.55 (0.002)	0.46 (0.14)
Hydrochloric Acid (HCl)	--	0.05	--	--	--	--	--
Acetylene (C_2H_2)	0.40 (0.11)	0.32 (0.07)	0.55(0.11)	0.47 (0.15)	0.50 (0.05)	0.31 (0.08)	0.22 (0.09)
Ethylene (C_2H_4)	1.33 (0.31)	1.18 (0.21)	1.85 (0.35)	1.61 (0.47)	1.86 (0.53)	0.48 (0.05)	0.57 (0.18)
Propene (C_3H_6)	0.35 (0.05)	0.45 (0.20)	0.71 (0.42)	0.52 (0.14)	0.68 (0.36)	0.11 (0.01)	0.17 (0.05)
Ammonia (NH_3)	0.47 (0.07)	1.13 (0.70)	0.62 (0.13)	0.69 (0.22)	0.85 (0.57)	0.56 (0.02)	0.52 (0.03)
1,3-Butadiene	0.01	0.02	0.06 (0.04)	0.04 (0.02)	0.09 (0.03)	--	--
Acetic Acid (CH_3COOH)	1.14 (0.20)	1.71 (0.46)	1.12 (0.46)	1.64 (1.03)	1.99 (1.36)	0.74 (0.05)	1.75 (1.39)
Formic Acid (CH_2O_2)	0.25 (0.07)	0.23 (0.02)	0.21 (0.05)	0.28 (0.09)	0.26 (0.06)	0.05 (0.002)	0.18 (0.16)
Furan (C_4H_4O)	0.14 (0.05)	0.15 (0.11)	0.18 (0.04)	0.30 (0.10)	0.16 (0.03)	0.06 (0.03)	0.46 (0.59)
Hydroxyacetone	0.58 (0.07)	0.75 (0.16)	0.53 (0.29)	0.97 (0.29)	0.72 (0.09)	0.36 (0.07)	0.31 (0.08)
Phenol	0.46 (0.41)	0.62 (0.09)	0.42 (0.18)	0.89 (0.20)	0.61 (0.27)	0.49 (0.07)	0.31 (0.09)
Furaldehyde	0.68	0.72 (0.17)	0.73 (0.06)	0.95 (0.26)	0.58 (0.37)	0.53 (0.25)	0.72 (0.11)
NO	1.83 (0.24)	1.71 (0.11)	1.84 (0.14)	1.25 (0.40)	1.85 (0.12)	2.39 (0.05)	1.89 (0.01)
NO_2	1.57 (0.32)	2.03 (0.44)	1.13 (0.32)	1.53 (0.70)	1.37 (0.19)	0.49 (0.11)	0.81 (0.10)
HONO	0.65 (0.18)	0.42 (0.16)	0.68 (0.05)	0.60 (0.19)	0.71 (0.05)	0.48 (0.11)	0.44 (0.01)
Glycolaldehyde	0.53 (0.06)	0.63 (0.06)	0.63 (0.10)	0.69 (0.17)	0.76 (0.14)	0.12	0.18
HCN	0.20 (0.02)	0.27 (0.05)	0.24 (0.05)	0.29 (0.08)	0.25 (0.05)	0.10 (0.03)	0.07
SO_2	1.18 (0.06)	1.32 (0.19)	1.31 (0.15)	1.49 (0.50)	1.67 (0.48)	0.82 (0.05)	0.90
MCE	0.94 (0.01)	0.94 (0.02)	0.94 (0.01)	0.93 (0.01)	0.94 (0.01)	0.95 (0.01)	0.96 (0.001)

[a]Values in brackets are (1σ) standard deviation.

3.5.2 Comparison of laboratory EF to wildfire-field based EF

It is important to compare our FIREX laboratory fire emissions data to field measurements of real wildfires to assess how representative and useful the lab-based data are, especially for the many species measured in the laboratory but not in the field. We assess representativeness by comparing the EF results for species measured in both the field and our laboratory fires. EF measurements on real wildfires are rare, but Liu et al. (2017) report recent EFs for three wildfires sampled during the 2013 Studies of Emissions and Atmospheric Composition, Clouds, and Climate Coupling by Regional Surveys (SEAC4RS, https://espo.nasa.gov/missions/seac4rs) (Toon et al., 2016) campaign, and the Biomass Burning Observation Project (BBOP, https://www.arm.gov/research/campaigns/aaf2013bbop) campaign. We compare our results from the FSL combustion studies to those reported by Liu et al. in two ways. In method one, we plot the lab-measured EFs against their corresponding MCEs for all the fires and we fit the data with a linear regression relationship for each compound. Using the slope and y-intercept of the linear regression, and the field-average MCE from Liu et al. of 0.912, we calculate a lab-based prediction of EF at the field-average MCE for each compound measured with the OP-FTIR. Figure 3.2 shows an example of the procedure for CH_4, comparing the lab-predicted EF at the field average MCE (4.76 g kg^{-1}) to the average field-measured wildfire EF (4.90 g kg^{-1}).

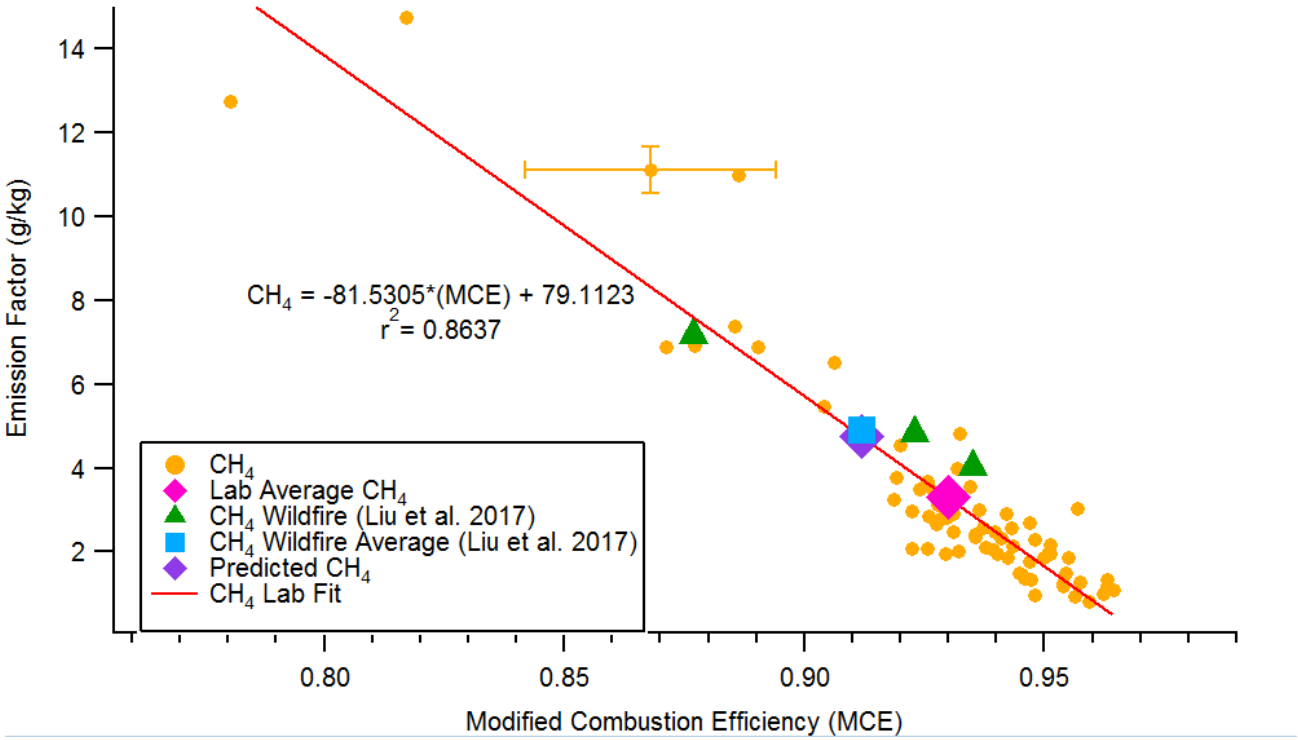

Figure 0.2 Methane emissions from 75 stack fires plotted against corresponding MCE and wildfire field methane emissions plotted against corresponding wildfire field MCE. Also included are the field average methane emissions (blue) and the predicted methane emissions (purple) using the linear regression shown and a field average MCE of 0.912.

In method 2, we compared the simple lab-average EF to the average field-measured wildfire EF. The results of these two methods are shown in Table 3.2 and Figure 3.2. Method 1 is generally preferred because the laboratory fires had a higher average MCE (i.e., a higher fire-integrated flaming / smoldering ratio) than the real wildfires sampled to date, most likely due to some unavoidable drying of the fuels during storage and some underrepresentation of the largest diameter fuels. The differences between the laboratory prediction at the field-average MCE and the field-average emissions are probably mostly due to the relative age of the smoke and the reactivity of compounds. The field study included smoke samples up to 2 h old and elevated OH, HO_2, H_2O_2, O_3, etc. have been observed in fresh smoke plumes (Hobbs et al., 2003; Yokelson et al., 2009).

Table 0.2 Summary of the comparison of emission factors (g kg^{-1}) measured in the lab and field (Liu et al., 2017).

Compound	Lab avg EF	Lab eqn slope	Lab eqn intercept	Lab-based Prediction	*Liu et al., 2017* EF	Predicted/ Field	Lab avg/ Field avg
CO_2	1646.90	2804.2418	-960.4016	1599.87	1454.00	1.10	1.13
CO	78.16	-1049.2971	1053.7505	95.74	89.30	1.07	0.88
CH_4	3.31	-81.5305	79.1123	4.67	4.90	0.95	0.68
NOx as NO	2.98	22.6627	-18.2162	2.47	0.49	5.04	6.08
Acetic Acid	1.88	-32.3429	31.9418	2.41	--	--	--
NO	1.81	12.6048	-9.9742	1.53	0.11	13.91	16.45
Formaldehyde	1.68	-30.4300	29.9621	2.18	2.29	0.95	0.73
Ethylene	1.63	-16.6799	17.1354	1.91	0.91	2.10	1.79
SO_2	1.37	-7.9297	8.7467	1.51	0.32	4.72	4.29
Methanol	1.32	-36.3839	35.1443	1.93	2.45	0.79	0.54
NO_2	1.20	-4.9035	5.7873	1.31	0.58	2.26	2.07
Ammonia	1.10	-31.3876	30.2792	1.62	--	--	--
Furaldehyde	0.82	-13.9054	13.7561	1.06	--	--	--
Hydroxyacetone	0.80	-15.9636	15.6891	1.11	1.13	0.98	0.71
Glycolaldehyde	0.73	-11.4308	11.3395	0.90	--	--	--
Phenol	0.70	-15.0074	14.7376	1.03	--	--	--
Propene	0.61	-10.0850	9.9817	0.77	0.35	2.20	1.74
HONO	0.56	-2.4751	2.8703	0.61	--	--	--
Acetylene	0.45	-2.4893	2.7722	0.50	0.24	2.08	1.89
HCN	0.36	-7.3943	7.2227	0.47	0.34	1.38	1.06
Formic Acid	0.27	-5.3701	5.2629	0.36	--	--	--
Furan	0.23	-5.3695	5.2244	0.32	0.51	0.63	0.45
1,3-Butadiene	0.17	-9.8599	9.3401	0.34	0.06	5.67	2.83
HCl	0.11	-2.5126	2.4661	0.17	0.004	35	27.5
Average Ratio Smoldering Compounds[a]						0.96	0.76
StDev Ratio						0.29	0.23
Fractional Uncertainty						0.30	0.30

[a]Average of less reactive/moderately reactive species: includes formaldehyde, methanol, hydroxyacetone and HCN. Reactive smoldering compounds were left out.

Thus the more reactive species (e.g., SO_2, HCl, NO_x , and some NMOGs) have lower EFs in the field data. For example, the lab/field ratio increases going from ethylene to propene to 1,3-butadiene in accordance with, though not directly proportional to, their increasing OH rate constants, and other chemistry, instrumental, and sampling challenges are relevant for some species (e.g., Finlayson-Pitts and Pitts, 2000; Apel et al., 2003; Fig. 7 in Hornbrook et al., 2011;

Burkholder et al., 2015). A few reactive species were measured in two older airborne studies of fresh western US wildfire smoke and they agree significantly better with our lab-based predictions (Radke et al., 1991; Hobbs et al., 1996). For instance, Radke et al. (1991) report EFs for NO_x as NO (2.0 g kg^{-1}), NH_3 (2.0 g kg^{-1}), and C_3H_6 (0.70 g kg^{-1}) for the Myrtle–Fall Creek wildfire that are all within 20% of our lab-predicted EFs. Hobbs et al. (1996) report an EF for SO_2 (0.79 g kg^{-1}) that is closer to our value than the Liu et al. 2017 value is despite the much lower MCE (0.81). Figure 3.3 shows the comparison for method one from Table 3.2 graphically. From Figure 3.3 it is clear that for the main relatively stable compounds, including formaldehyde, methanol, and hydroxyacetone; the lab-predicted EF falls within 20% of the measured wildfire EF and all the emissions except NO_x and SO_2 overlap within the observed variability. Also highlighted in Figure 3.3, many compounds such as HONO, acetic acid, ammonia, phenol, glycolaldehyde, formic acid, etc. were measured only for our laboratory fires. The lab-measured EFs for these OP-FTIR species and the data for many NMOG species measured by MS and FIREX data in general can thus be used to generate representative EFs or other data for real wildfires. Many of these EFs are critically important to represent wildfire emissions well: e.g. NH_3 (Benedict et al., 2017) and SOA or PAN precursors (Alvarado et al., 2015; Müller et al., 2016). Other approaches to generate representative data that are not explored in detail here, but should work well include reporting the average for the laboratory fires clustered around the field average MCE (Fires 8, 39, 45, 51, 59, and 66) or reporting ER to CO (e.g. Koss et al., 2017), where the latter can also be converted to EF by coupling with the field average EFCO. For example, if we take the average of six fires clustered around the field average MCE in the CH_4 plot shown in Figure 3.2, we get an average EF for CH_4 of 4.67, which is close to the Liu et al., reported value of 4.90. Alternatively, we can calculate a

molar ER for CH_4 to CO for all the laboratory fires (0.071), then utilize the wildfire average EF CO reported by Liu et al (89.3 g kg^{-1}) to calculate a new EF.

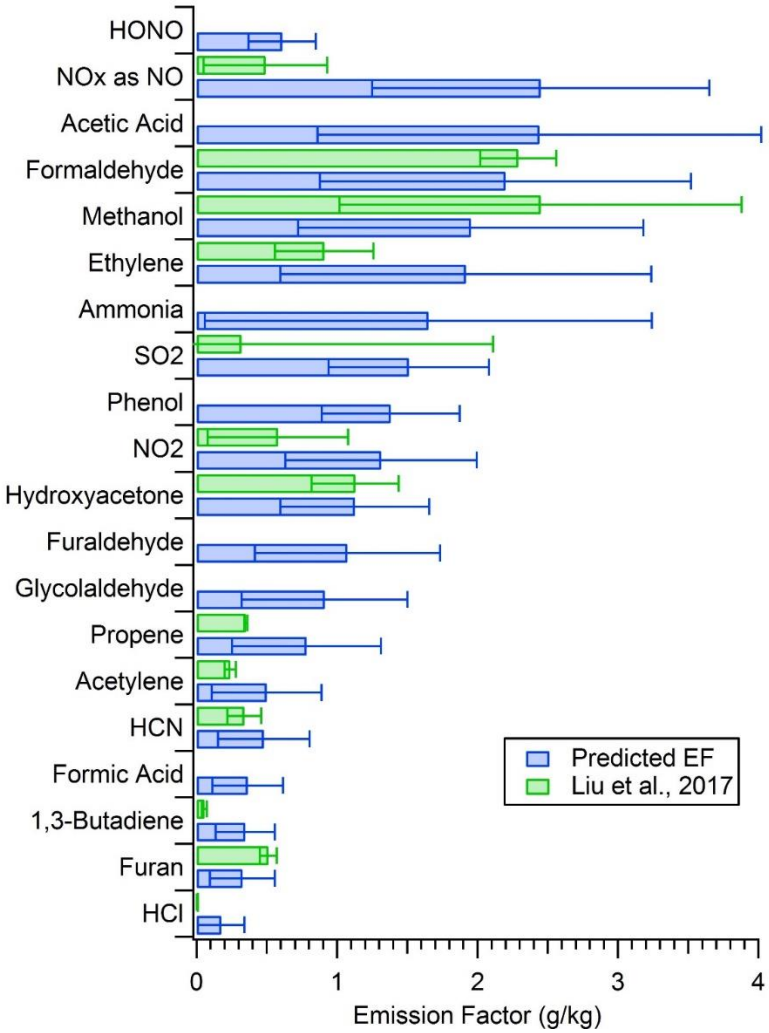

Figure 0.3. Comparison of the lab-predicted EFs at the field average MCE to average field-measured EFs reported by Liu et al. (2017).

Using this method, we get an EF for CH_4 of 3.78, which is within 20% of the field average value. Either of these methods should help reflect the field average flaming/smoldering ratio. In addition, positive matrix factorization was found to be a very useful method to predict field EF from the

laboratory data for NMOG as discussed elsewhere (Sekimoto et al., 2018). Given the small amount of field sampling, more field work is clearly needed.

3.5.3 EF dependence on fuel

We burned individual fuel components (duff, litter, canopy, etc.) in addition to mixtures of major components found in widespread Western US coniferous ecosystems for insights into fuel effects on emissions and to what degree specific emissions were enhanced by a certain component. For example, Figure 3.4 shows the EFs of 21 trace gases from the Douglas fir ecosystem fuel mixture burns side by side with the EFs from burning pure Douglas fir components in separate fires.

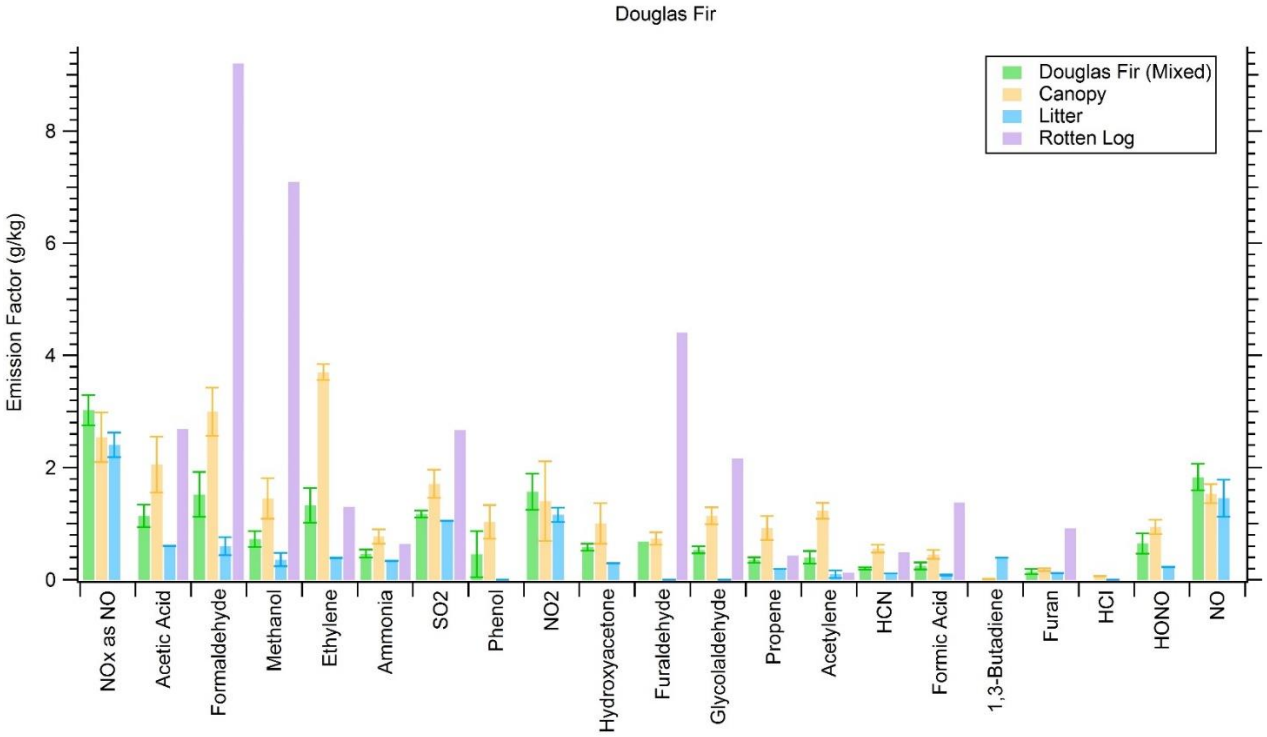

Figure 0.4 Trace gas emissions from mixed Douglas fir ecosystem (including sound, dead wood, but rotten log not included) and pure components. Sound dead wood was not burned separately except as untreated lumber.

Emissions of furaldehyde, formaldehyde and methanol were enhanced when burning a pure rotten log component; while acetylene, ethylene, and propene, as well as other non-methane hydrocarbons (NMHC), were more prevalent in emissions from Douglas fir canopy. We did the same analysis for a Ponderosa pine ecosystem (Figure 3.5).

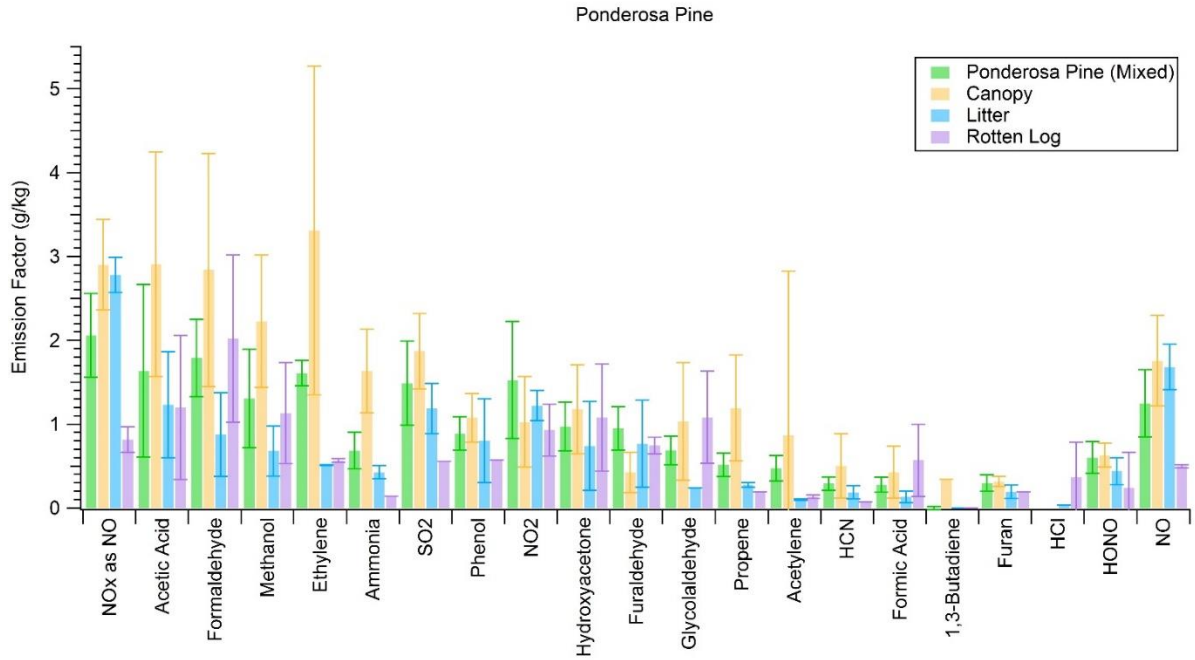

Figure 0.5. Trace gas emissions from mix Ponderosa pine ecosystem (including sound dead wood, rotten log not included) and pure components.

While the canopy component in Ponderosa pine produced enhanced emissions of NMHC, the rotten log did not contribute to the same level of enhancement in furaldehyde, formaldehyde and methanol because of a transition to flaming combustion during the second half of the fire. Additionally, we observed an enhancement in NO_x emissions from the litter and canopy components in Ponderosa Pine. Mixed coniferous ecosystem values are fairly similar for both fuels and agree within 30% for the majority of compounds, excluding methanol, furan, and NO_x. We also note that while the mixed Douglas fir and Ponderosa pine ecosystems that we burned

contained canopy, litter, and woody components in varying diameter classes, they did not contain a rotten log since the latter component is not included in FOFEM. We further investigate fuel variability by taking pure components from several ecosystems and comparing them to one another. Figure 3.6 shows species emitted by duff from three different coniferous ecosystems. Acetic acid and methanol are strongly emitted by all three duff fuels, but ammonia enhancement occurs in only Engelmann spruce and Subalpine fir fuels. Jeffrey pine duff had a lower EF for NH_3 despite similar fuel N. This could possibly be due to the age of the fuel as it was contained in storage longer than other fuels and not fresh. Additional results for other fuel components (rotten log, canopy, litter) are shown in Figures 3.6, 3.7, and 3.8 respectively.

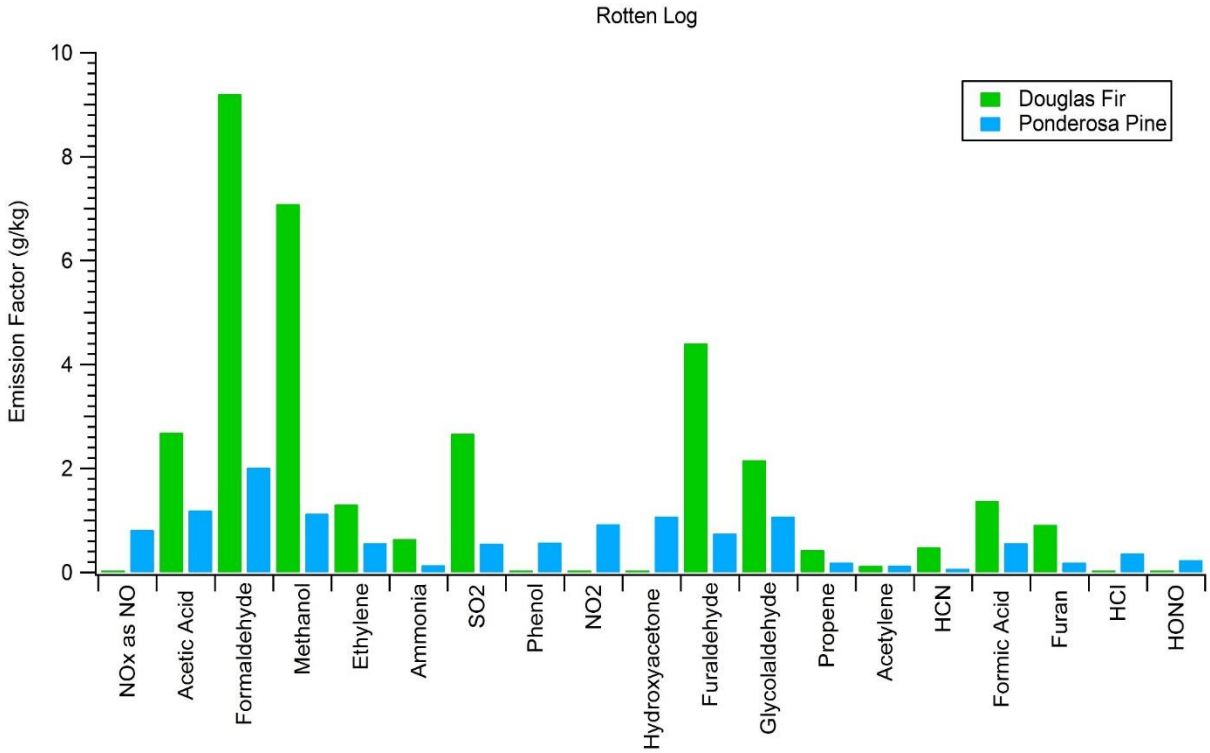

Figure 0.6. Trace gas emissions of a pure rotten log from two unique fuel types.

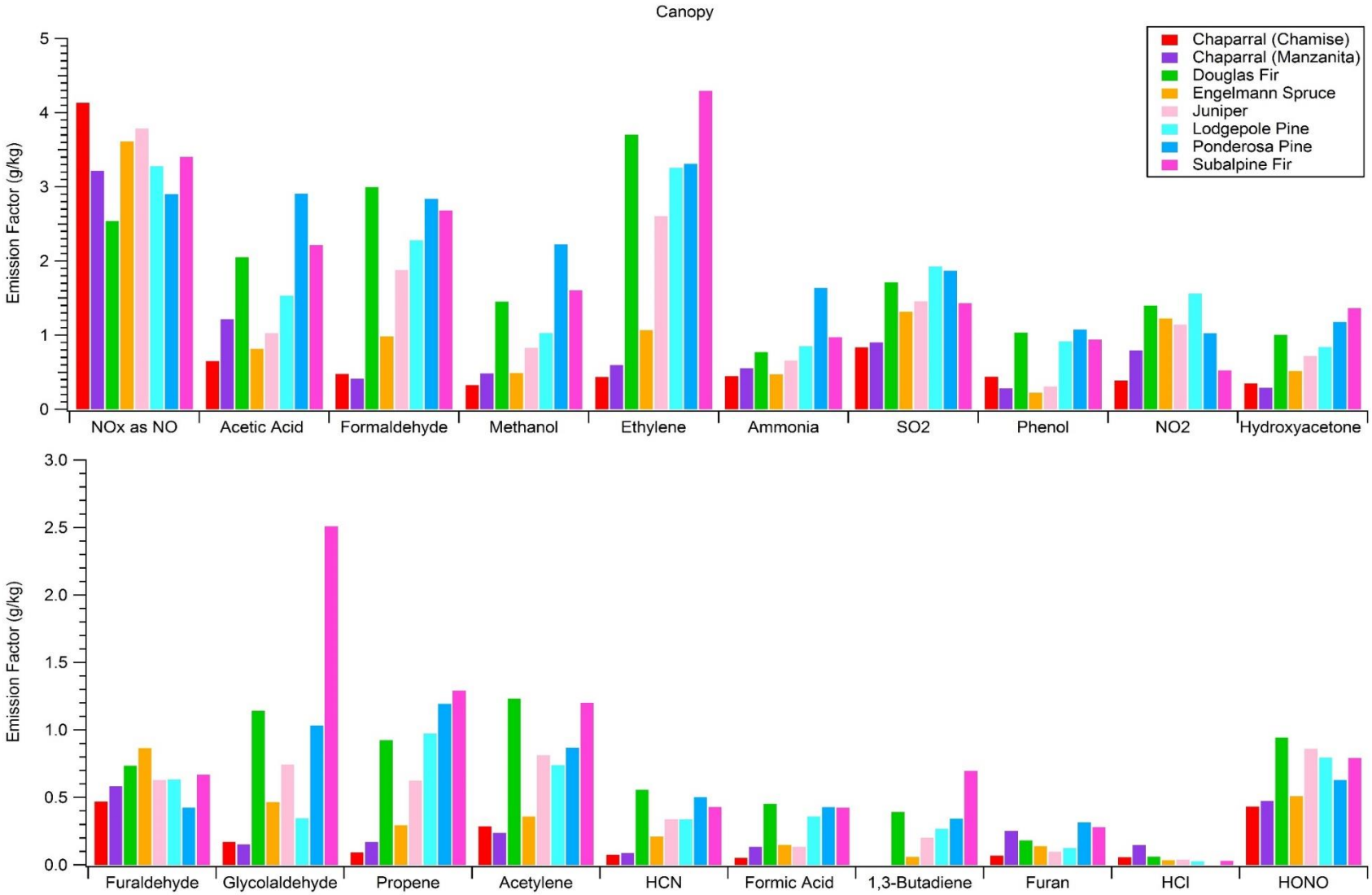

Figure 0.7 Trace gas emissions from the canopy of eight unique fuel types.

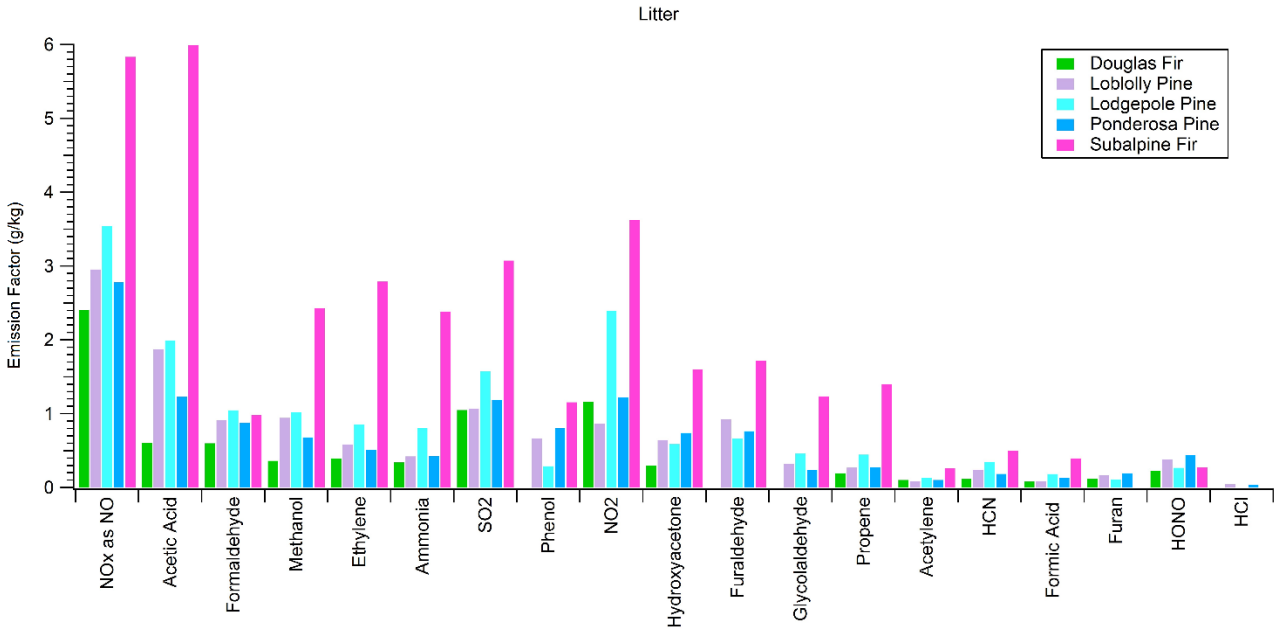

Figure 0.8. Trace gas emissions of litter from five unique fuel types.

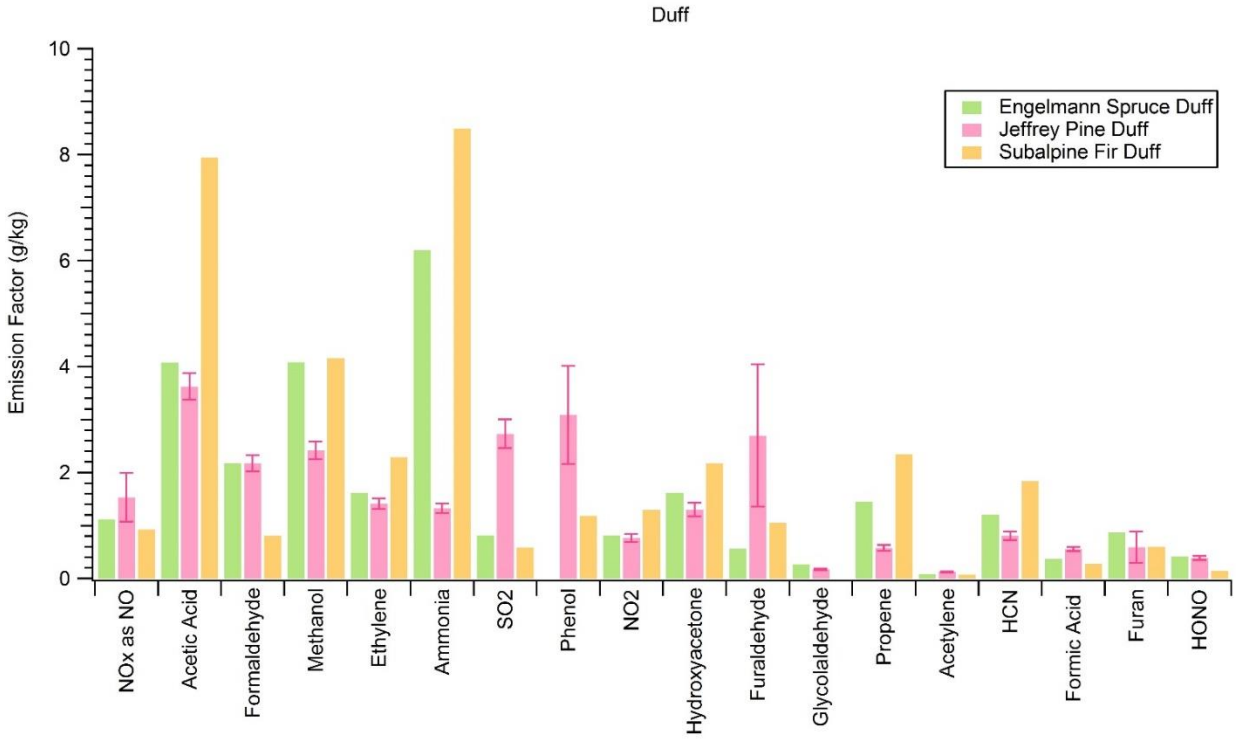

Figure 0.9. Trace gas emissions from pure duff of three different ecosystem types.

3.6 PAX results

3.6.1 Overview of optical properties

As mentioned previously, we measured absorption and scattering coefficients directly at 401 and 870 nm. For the first 31 stack fires, which includes most of the studied fuel types, we have both 401 and 870 nm data. For the remaining 44 stack fires, we only report data at 870 nm as we used our 401 nm PAX for intercomparison studies that will be reported elsewhere. Figure 3.10 plots the AAE and SSA at both wavelengths of 31 stack fires as a function of MCE. High AAE is an indicator of BrC and relates to smoldering, which is denoted by low MCE and high SSA values. Smoldering is also associated with higher EFs for OA, most NMOG, and other gases such as NH_3.

Low AAE, along with low SSA and high MCE values, indicates more flaming combustion, which is also generally associated with higher EF for BC and "flaming compounds" such as CO_2, NO_x, and SO_2.. The lab-based average fire-integrated optical properties for some of the most common Western U.S ecosystems are listed in Table 3.3. Table 3.3 does not reveal a strong ecosystem dependence among coniferous ecosystems tested for optical properties, but does indicate that chaparral fire aerosol has consistently lower SSA than coniferous fire aerosol and that there are significant contributions of absorption by BrC at 401 nm among all ecosystems. The absorption by BrC is responsible for at least half and up to two thirds of the absorption at 401 nm even at higher MCE. The laboratory average AAE of 2.80 ± 1.57 across all 31 fires confirms a role for BrC, while the lab-average SSA at both wavelengths indicates the fresh aerosol has a net warming influence in the atmosphere (SSA < 0.9, Praveen et al., 2012); although SSA can increase with smoke age (Yokelson et al., 2009). The absorption of BrC at 401 nm has several implications in atmospheric chemistry, including impacts on UV-driven photochemical reactions producing ozone, and the lifetime of NO_x and HONO. Furthermore, because of its absorbing nature, factoring in the BrC could mean the net radiative forcing of biomass burning is not cooling or neutral as often assumed, but warming if the BrC is sufficiently long-lived as probed in other FIREX studies and previous papers (e.g. Feng et al., 2013; Forrister et al., 2015).

Table 0.3 Lab-average emission factors (m^2 kg^{-1}) and fire-integrated optical properties for common Western U.S ecosystems.

Species	Douglas Fir	Engelmann Spruce	Lodgepole Pine	Ponderosa Pine	Chaparral - Chamise	Chaparral - Manzanita
Black Carbon (g kg^{-1})	0.23 (0.06)	0.12 (0.07)	0.34 (0.14)	0.48 (0.25)	0.45 (0.16)	0.32 (0.04)
EF B_{abs} 870	1.07 (0.29)	0.58 (0.32)	1.59 (0.67)	2.28 (1.20)	2.00 (0.68)	1.32 (0.15)
EF B_{abs} 401	7.63 (1.11)	6.22 (0.19)	10.20 (1.12)	12.06 (1.08)	10.40	8.65
EF B_{abs} 401 (BrC)	5.05 (0.70)	4.41 (0.27)	5.79 (0.77)	5.56 (0.76)	5.57	5.55
EF B_{scat} 870	3.01 (1.34)	3.36 (2.66)	2.79 (1.40)	4.55 (1.50)	0.52 (0.16)	0.90 (0.51)
EF B_{scat} 401	48.42 (7.27)	62.56 (7.40)	44.23 (7.03)	50.28 (9.92)	12.02	23.76
SSA 401	0.86 (0.01)	0.91 (0.01)	0.81 (0.02)	0.80 (0.04)	0.54	0.72
SSA 870	0.72 (0.08)	0.82 (0.09)	0.64 (0.07)	0.67 (0.11)	0.21	0.39
AAE	2.43 (0.09)	2.65 (0.30)	2.12 (0.19)	1.84 (0.18)	2.02	2.36
MCE	0.94 (0.01)	0.94 (0.02)	0.94 (0.01)	0.93 (0.01)	0.95 (0.01)	0.96 (0.001)

[a]Values in brackets are (1σ) standard deviation.

3.6.2 Comparison of laboratory optical properties to field optical properties

There are very few field measurements of the optical properties of smoke from US wildfires, but we can compare our results from the laboratory studies to the initial aerosol optical properties for one wildfire (the Rim Fire) reported by Liu et al. (2017) and Forrister et al. (2015). An AAE of 3.75 at an MCE of 0.923 for the Rim Fire is reported between these two studies. With the linear regression of the laboratory data shown in Figure 3.10, we can predict an AAE of 3.31 at the wildfire field average MCE (0.912) and an AAE of 2.91 at the Rim Fire MCE (0.923) using prediction method one described in Section 3.5.2.

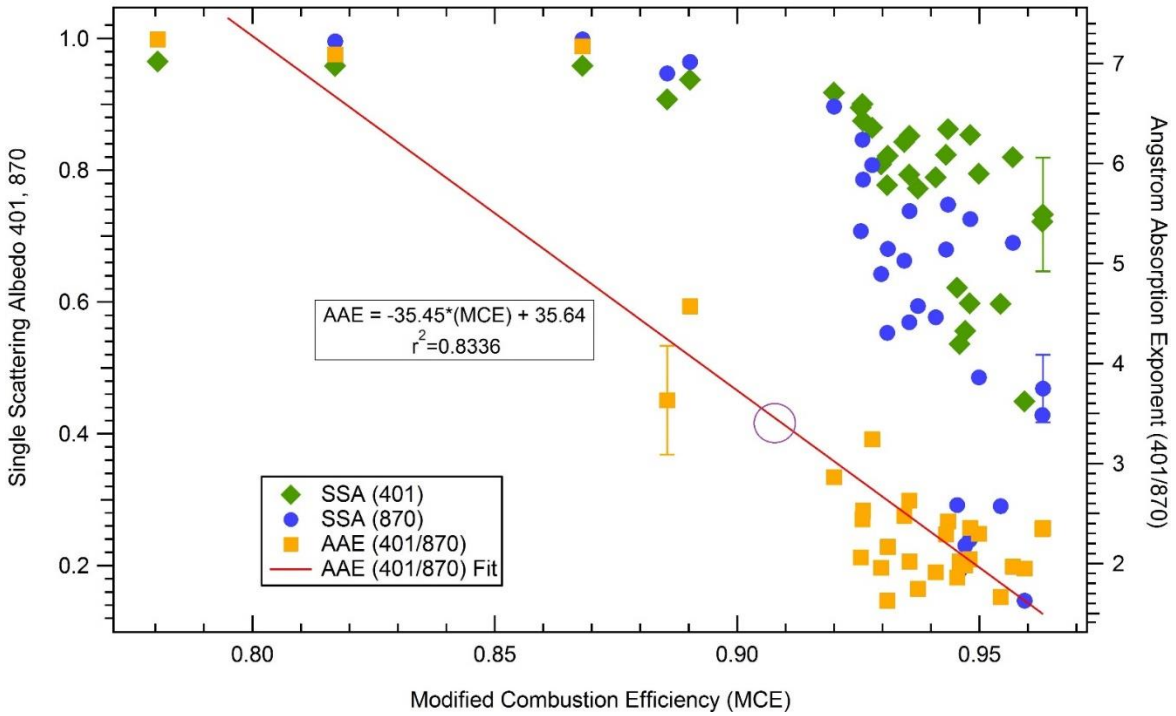

Figure 0.10 SSA at both wavelengths (401, 870 nm) and AAE (401/870) against MCE for 31 stack fires where both 401 and 870 nm data was available. The circle on the fit line represents the lab-predicted AAE using the wildfire field average MCE of 0.912. SSA is difficult to fit to MCE and fits better to EC and OC data, which were not available (Liu et al., 2014; Pokhrel et al., 2016).

At the wildfire field average MCE, our calculated AAE represents 88% of the reported Rim Fire AAE, while at the Rim Fire MCE, our calculated AAE represents 78% of the reported Rim Fire AAE. Although our calculated values are relatively close to the reported value, a small change in AAE implies a big change in the BrC/BC absorption ratio, but only a small change in the % absorption by BrC. Our AAE values imply that BrC accounts for 77 to 82% of the absorption at 401. The average of the AAE from the single Rim Fire measurement (3.75) and the AAE predicted from the more extensive laboratory fires (3.31) is ~3.5, which may be a reasonable best guess at the AAE of fresh US wildfire smoke and implies that ~86% of absorption at 401 nm is due to BrC. In Figure 3.11, we plot the initial % absorption by BrC at 401 nm for the Rim Fire measured AAE and for our lab-estimated AAE at the field average MCE. Figure 8 also shows the lab-measured

total $EF_{abs}401$ and the BrC contribution to $EF_{abs}401$ for 31 laboratory fires. BrC dominates absorption at 401 nm at low MCE values and as MCE increases, BrC absorption remains a significant but variable component of overall absorption. The variability is likely due to realistic "natural" fire-to-fire variability in fuels, moisture content, etc.

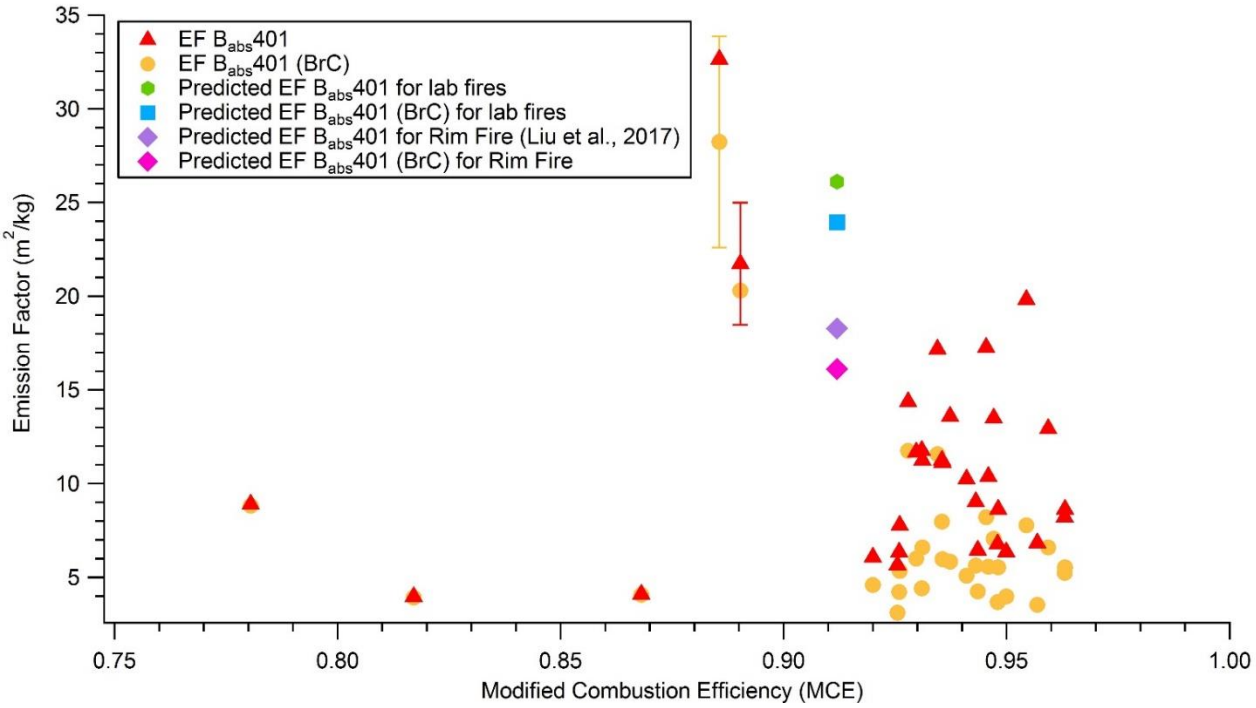

Figure 0.11. Absorption emission factors measured at 401 nm for "BC plus BrC" and for "BrC only" for 31 lab fires, Also shown are the fractional contributions of BrC to total absorption at 401 predicted from the lab AAE data at the field average MCE (green), the Rim Fire MCE (blue) and the field measured AAE (purple) (Forrister et al., 2015; Liu et al., 2017).

In Table 3.4 we report the study-averages for BC mass EF, absorption and scattering EFs, SSA, and AAE. The quantities that require 401 nm data are averages for the 31 stack fires where 401 and 870 nm data were obtained, while the quantities that need just 870 nm data are averages for all 75 stack fires. We also show the comparison of our lab-average and lab-predicted AAEs to the AAE in Forrister et al. (2015) and our lab-average and lab-predicted BC EF to the unpublished BC EF calculated as part of Liu et al., (2017). Table 3.4 also presents a set of equations that can be

used to fit lab-measured optical properties and make predictions at any MCE. However, more measurements of wildfires in the field and the laboratory (including aging) are needed to assess wildfire aerosol optical properties.

Table 0.4 Summary of the comparison of optical properties and emission factors (m^2 kg^{-1}) measured in lab to the Rim Fire.

Species	Lab avg	Lab eqn	r^2	Lab-based prediction using field average MCE	Rim Fire	Predicted/Field	Lab avg/Rim Fire
Black Carbon[b] (g kg^{-1})	0.68 (1.09)	$y = 1.7926x^{25.655}$	0.3237	0.174	0.187[e]	0.93	3.64
EF B_{abs} 870[b]	3.21 (5.16)	$y = 8.497x^{25.655}$	0.3237	0.49	--	--	--
EF B_{abs} 401[c]	11.16 (6.00)	$y = 11.385x^{1.7374}$	0.028	9.71	--	--	--
EF B_{abs} 401 (BrC)[c]	7.15 (5.20)	y = -32.81x + 37.53	0.0648	7.57	--	--	--
EF B_{scat} 870[b]	10.15 (22.64)	$y = 0.9868x^{-17.48}$	0.2404	4.84	--	--	--
EF B_{scat} 401[c]	70.37 (81.25)	y = -1343.6x+1314.7	0.4462	87.99	--	--	--
SSA (401)[c]	0.79 (0.13)	--		0.90[d]	--	--	--
SSA (870)[b]	0.64 (0.26)	--		0.91[d]	--	--	--
AAE[c]	2.80 (1.57)	y = -35.45x + 35.64	0.8335	3.31	3.75[f]	0.78	0.75

[a]Values in brackets are (1σ) standard deviation.
[b]Average for all 75 stack fires where 870 nm data is available.
[c]Average for 31 fires where both 401 and 870 nm is available.
[d]SSA values calculated from B_{abs} and B_{scat} EF
[e]Value not published (X. Liu private communication, https://www.nasa.gov/mission_pages/seac4rs/index.html)
[f]From Forrister et al.
[g]The low r^2 equations return reasonable values at the field average MCE.

3.6.3 Fuel dependence of aerosol optical properties

Burning individual fuel components in addition to mixtures found in typical, widespread western U.S ecosystems allows us to investigate the extent to which optical properties are either enhanced or diminished by certain components. Table 3.5 lists the study-average BC EF and optical properties for all the coniferous ecosystems shown in Table 3.3 and the study-average BC EF and optical properties for the individual fuel components averaged across all the coniferous ecosystems. The averages and standard deviations for each reported quantity indicate that there is

large variation among specific components and a large coefficient of variation for the coniferous ecosystem average. The variability could potentially depend on ecosystem type, fuel components, fuel moisture, or other things as discussed for trace gases in section 3.5.3. While there is considerable variation within each ecosystem type, the individual ecosystem averages in Table 3.3 all agree within 38% of the study-average for all the coniferous ecosystems shown in Table 3.5 and the AAEs are all within 20%.

Table 0.5 Optical properties and emission factors (m^2 kg^{-1}) for mixed coniferous ecosystems and ecosystem components.

Species	Mixed Coniferous Ecosystem[a]	Canopy[b]	Litter[c]	Duff[d]	Rotten Log[f]
Black Carbon (g kg^{-1})	0.43 (0.33)	0.46 (0.37)	0.68 (0.53)	0.50 (0.79)	0.43 (0.59)
EF B_{abs} 870	2.03 (1.58)	2.18 (1.77)	3.22 (2.51)	0.02 (0.007)	2.04 (2.84)
EF B_{abs} 401	9.02 (2.61)	14.53 (6.37)	14.29 (7.58)	4.08[e] (0.09)	7.86 (1.46)
EF B_{abs} 401 (BrC)	5.20 (0.61)	10.65 (5.14)	6.39 (2.84)	4.04[e] (0.10)	6.18 (3.73)
EF B_{scat} 870	4.51 (2.51)	10.00 (7.80)	2.28 (1.12)	6.73 (1.85)	22.21 (5.86)
EF B_{scat} 401	51.37 (7.87)	84.03 (55.92)	35.39 (11.14)	94.37[e] (2.45)	139.47 (153.27)
SSA 401	0.85 (0.05)	0.81 (0.05)	0.70 (0.17)	0.96[e] (<0.01)	0.89 (0.10)
SSA 870	0.71 (0.08)	0.71 (0.13)	0.48 (0.27)	0.99[e] (<0.01)	0.89 (0.15)
AAE	2.26 (0.36)	2.69 (0.36)	1.86 (0.20)	7.13[e] (0.06)	4.60 (3.73)
MCE	0.94 (<0.01)	0.92 (0.0.1)	0.93 (0.02)	0.87 (0.02)	0.86 (0.12)

[a]Douglas fir, Engelmann spruce, Lodgepole pine, Ponderosa pine, Subalpine fir
[b]Douglas fir, Engelmann spruce, Lodgepole pine, Ponderosa pine, Juniper, Subalpine fir
[c]Douglas fir, Loblolly pine, Lodgepole pine, Ponderosa pine, Subalpine fir
[d] Engelmann spruce, Jeffrey pine, Ponderosa pine, Subalpine fir
[e]Engelmann spruce
[f]Douglas fir, Ponderosa pine

However, Table 3.5 also shows that the average AAE for some ecosystem components is very different from the average AAE for all the coniferous ecosystems (2.26). For instance, the largest contribution to a high AAE per fuel component consumed comes from duff, where BrC accounts for almost all of the absorption at 401 nm (AAE 7.13). The rotten log component also contributes an anomalously high average AAE of 4.60. Thus, these components contribute more BrC relative to BC in proportion to their fuel consumption to the mixed ecosystem results where AAE is 2.26 and BrC accounts for just over half of the absorption at 401 nm. Conversely, litter consumption

would tend to lower a fuel mixture's AAE. However, AAE is a measure of the shape of the aerosol absorption cross-section and the absorption EFs are a measure of total emissions of absorbing material. In this respect, litter produces more BC absorption and more BrC absorption per unit mass than duff though at a lower BrC/BC ratio than duff. This is consistent with the lower SSA for litter. We conclude that the variability in mixed ecosystem optical properties was likely due to variable consumption of pure components, with a weaker dependence on the dominant tree species. For example, much of the variability in ecosystem average AAEs and the study average AAE is linked to the varying amount of duff consumed in the mixed fuel beds (Tab. S1). (The variability in actual duff consumption is likely larger than the variability in duff loading shown as the amount of residual material also varied.) Duff consumption in the field is increased by drought conditions, which would contribute variability on real fires (Davies et al., 2013). We can compare our duff results to previous measurements of optical properties of duff-fire aerosol by Chakrabarty et al (2010). These authors identified tarballs as a major BrC species produced by duff combustion and they measured an AAE of 4.2 (405 and 532 nm wavelength pair) for a Ponderosa Pine duff sample from MT. Including their other duff sample (AK feather moss duff), they obtained a study-average duff-combustion AAE of 5.3. We measured AAE on two much larger burns (~4 times more fuel mass, Fires # 12 and 26) in Engelmann Spruce duff, with different wavelengths, and at much lower MCE (0.843 ± 0.036 versus ~0.91). We obtained a study-average duff combustion AAE of 7.13 (0.057). Both studies observed a high AAE for duff combustion. Their lower AAE values could be related to different wavelengths used, the possibility of some BrC abs at 532 nm (Bluvshtein et al., 2017), the different duff type, and/or their higher MCE, which they attributed to sampling some flaming combustion during the ignition process. The AAE calculated from our AAE versus MCE fit (for all fuels) at their MCE of 0.91 is relatively closer to their value. In summary, the results

presented indicate that, in all cases, the overall ecosystem and mixture of components produces a significant amount of BrC. As mentioned previously, this has several implications in regional atmospheric chemistry and radiative forcing. Additional instruments were deployed on room burn experiments, where the fuels were also purposely changed to investigate the effect on optical properties and will be reported elsewhere.

3.6.4 Trace gas and BC emissions of peat, dung, and rice straw combustion

We also measured emissions from several fires of peat, rice straw, and dung, due to their widespread burning in Asia and their value as extreme examples of fuel impacts (e.g. high smoldering/flaming or high N or Cl content). Peat, which is especially important in Southeast Asia (Stockwell et al., 2016a) is similar to duff found in the western U.S in that it is often consumed by pure smoldering combustion and has a high AAE (Pokhrel et al., 2016), high HCN emissions, and low BC emissions. Although we did not measure AAE for peat, we do report an MCE of 0.83, where a low MCE likely indicates a high AAE. We also report EF's for CH_4 (10.39 g kg^{-1}), HCN (3.97 g kg^{-1}), acetic acid (4.44 g kg^{-1}) and BC (0.003 g kg^{-1}). We compare these values to the field measurements reported in Stockwell et al. (2016a): CH_4 (9.51 ± 4.74 g kg^{-1}), HCN (5.75 ± 1.60 g kg^{-1}), acetic acid (3.89 ± 1.65 g kg^{-1}) and BC (0.006 ± 0.002 g kg^{-1}) and find that our values agree well (EF BC extremely small compared to most biomass burning (Akagi et al., 2011) and gases within 31%) between peat measured in the laboratory and peat measured in the field. (A more detailed comparison will follow planned field measurements.) Additionally, we compare our dung MCE value (0.90), CH_4 (6.63 g kg^{-1}), HCN (1.96 g kg^{-1}), acetic acid (6.36 g kg^{-1}), and BC (0.01 g kg^{-1}) values to those based on field work in Nepal reported in Stockwell et al. (2016b): MCE (0.90), CH_4 (6.65 ± 0.46 g kg^{-1}), HCN (2.01 ± 1.25 g kg^{-1}), acetic acid (7.32 ± 6.59 g kg^{-1}), and BC (0.004 ± 0.003 g kg^{-1}). We find excellent agreement between our values (15% for trace gases and EF BC

very small) and those reported from field measurements in Nepal. Rice straw was burned because of its global importance in agricultural waste burning and to probe the extremes of fuel chemistry (Akagi et al., 2011). Grasses are usually very high in chlorine content (0.61%, Tab. S1; Lobert et al., 1996) and our EF for HCl of 0.65 g kg^{-1} for rice straw was the highest of any fuel measured during the FIREX campaign. Furthermore, our rice straw EF for HCl is comparable to Stockwell et al. 2015 (0.43 ± 0.29). The findings briefly summarized in this section further suggest and reinforce the idea that simulated laboratory fires can probe fuel effects and provide an accurate representation of measurements in the field, even outside the scope of Western U.S. wildfires. More comprehensive, recent discussions of these fuels can be found elsewhere (Stockwell et al., 2016a, b; Jayarathne et al., 2017a, b).

3.7 Conclusions

We measured trace gas and aerosol emissions from 107 simulated western wildfires during the FIREX campaign in the fall of 2016 using OP-FTIR and PAX. For 31 stack fires, we report aerosol measurements based on both 401 and 870 nm, and for the remaining 44 stack fires we report aerosol characteristics based on only 870 nm data. We provide the MCE and the mass EF (g kg^{-1}) for 23 different trace gases (not including water) and BC. We also provide the scattering and absorption EF (m^2 kg^{-1}) at 870 and 401 nm along with the $EF_{abs}401$ due to brown carbon only, SSA, and AAE. We burned canopy, litter, duff, dead wood, and other fuels in combinations using FOFEM to represent relevant ecosystems and as pure components to investigate the effects of individual fuels. Full trace gas data are reported for all 75 stack burns and two room burns, and CO_2, CO, CH_4, C_2H_4, C_2H_2, and MCE were archived for the remaining room burns. We found little variability in average trace gas EFs across coniferous ecosystems, but the average EFs for two chaparral species were similar to each other and lower than in coniferous ecosystems for most

pollutants, including CH_4 (1.20 ± 0.09 g kg^{-1}), formaldehyde (0.50 ± 0.06 g kg^{-1}), glycolaldehyde (0.15 g kg^{-1}) and HCN (0.09 g kg^{-1}) to name a few. Additionally, there was considerable variability in the average trace gas EF for certain fuel components. For instance, emissions of some NMOG were enhanced from a Douglas Fir rotten log and emissions of NO_x were enhanced from Ponderosa Pine litter and canopy components.

In similar fashion, there was little variation in the average optical properties for the different mixed coniferous ecosystems, but individual fuel components like duff and rotten logs contributed significantly on a per mass basis to the relative importance of BrC and BC, with BrC accounting for nearly 100% and 94% of the absorption at 401, respectively, for these fuel components (using data only from fires with measurements at two wavelengths).The lab-average AAE for all 31 fires, including those burning components like chaparral and coniferous canopy, which tend to burn more by flaming, was 2.8 (Tab. 3.6) indicating that BrC absorption contributed to over half (64%) of the absorption at 401 nm for the laboratory fires on average.

We compared the trace gas and aerosol emissions from the fires in our laboratory-simulated Western U.S ecosystems to those from real Western U.S wildfires measured in slightly-aged smoke in the field as reported by Liu et al. (2017) and Forrister et al. (2015). Despite some underrepresentation of the largest diameter fuel class we were able to use a simple procedure to account for the flaming to smoldering ratio and generate EF values from the laboratory data that were in agreement with the field data for most "stable" trace gases, including CH_4 (within 3%), formaldehyde (within 4%), methanol (within 20%), and hydroxyacetone (within 1% agreement). Most of the EF discrepancies were due to the field smoke being more aged. The excellent agreement suggests that FIREX data can be confidently used in general to represent real fires; especially for species not measured yet in the field. For instance, important compounds rarely, or

not previously measured in the field for western wildfires, but measured in this study include ammonia (1.65 g kg^{-1}), acetic acid (2.44 g kg^{-1}), HONO, and others (Fig. 3.3). Optical properties were not compared as extensively because limited field data are available, which highlights the need for more field measurements on true wildfires. However, a preliminary best guess for a fresh wildfire smoke AAE of ~3.5 is supported by averaging the lab-based predictions and more limited field data. Impacts on photochemical reactions producing ozone, and the lifetime of NO_x and HONO are likely as a result of the strong abundance of BrC. In addition, recognizing the presence of absorbing BrC in biomass burning plumes could alter the modeled contribution of biomass burning to net radiative forcing in a more positive direction (Saleh et al., 2014; Jacobsen, 2014, Feng et al., 2013). Finally, to investigate fuel chemistry impacts and due to their widespread global importance, we also measured EFs for fires in peat, dung, and rice straw and compared to field values reported by Stockwell et al. (2015, 2016a, 2016b). Our lab-based EFs for all three of these fuels were in good agreement with the field studies. Overall, our lab-simulated fires can provide important emissions data that is fairly representative of real fires and used to accurately assess BB impacts.

Chapter 4: Measurements of ambient smoke in Missoula, 2017

4.1 Overview of 2017 ground-based monitoring

Most of the western US, including the Rocky Mountains, constitutes a large fire prone-region. Missoula, Montana is the largest city completely surrounded by the Rocky Mountains. Missoula is also located within a large region of the inland Pacific Northwest where wildfires have caused air quality trends to deviate from the pattern in the rest of the US (McClure and Jaffe, 2018). Missoula frequently experiences smoke impacts typical of much of the urban and rural west due to local and regional western fires. In this study, we measured the wildfire smoke characteristics for 500 smoke-impacted hours during August-September of 2017, which constituted a prolonged period of record-breaking AQ impacts in Missoula. This very large sample of wildfire smoke helps address some of the afore-mentioned observational gaps in current wildfire field data. The main goals of this work are to document the net, combined effect of numerous fires on a heavily impacted surface site embedded in the region and thus, also help assess the representativeness of field measurements, emissions inventories, and models. In more detail, we characterize the smoke impacts on a population center and we document the real-world regional significance of BrC. Comparisons are possible to our time series of BC, CO, PM, etc or diurnal cycles for these species for a more relaxed test. Our real-time through study-average ratios for "inert" tracers such as ΔBC/ΔCO are compared with ΔBC/ΔCO in the field measurements that are available to build emissions inventories that serve as model input. The time-resolved and study-average values of dynamic ratios (e.g. ΔPM/ΔCO) help elucidate the net effect of secondary aerosol formation and evaporation. Our measurements provide real-world aerosol optical properties (e.g., SSA, AAE, etc.) and can be used with the aerosol mass data at real-time through study-average resolution to

probe multi-step, bottom-up calculations of climate-relevant aerosol optical properties. We present our results and compare them to those previously reported for wildfire field measurements and prescribed fire field measurements.

4.1.1 Site Description

Trace gases and particles were measured through co-located inlets at the University of Montana (UM), ~12.5 m above the ground through the window of our laboratory on the fourth (top) floor of the Charles H. Clapp building (CHCB). The UM campus encompasses an area of ~0.89 km^2 and is located on the eastern edge of Missoula, with the CHCB located in the southeastern corner of campus. The CHCB is ~ 1.1 km from the nearest road that gets appreciable traffic during the summer, thus our measurements were not significantly influenced by automobile emissions (see Sect 4.1.4). $PM_{2.5}$ measurements were made by the Montana Department of Environmental Quality via a stationary $PM_{2.5}$ monitor located in Boyd Park, Missoula, which is ~3.2 km southwest of our UM laboratory, with both sites being located in the Missoula valley proper.

4.1.2 Investigating smoke origin and back trajectory calculations

To investigate the sources contributing to smoke events we used a combination of back trajectory calculations, satellite imagery, and local meteorological data that provided insights into mixing and smoke origin. Back trajectories were calculated utilizing the National Oceanic and Atmospheric Administration (NOAA) Air Resources Laboratory Hybrid Single Particle Lagrangian Integrated Trajectory (HYSPLIT; Stein et al., 2015; Draxler et al., 1999; Draxler et al., 1998; Draxler et al., 1997) initialized from UM (46.8601º N, 113.9852º W) at 500, 1200, and 3000 m above ground level during the hour at which enhancements for that particular smoke event were at a maximum. Back trajectories were run using the High Resolution Rapid Refresh (HRRR)

operational model, which uses the Weather Research and Forecasting (WRF) modeling system combined with observational data assimilation and is run over the contiguous US at 3km × 3km resolution (Benjamin et al., 2016). For events that spanned multiple days, multiple back trajectories were initialized during the hour(s) at which enhancements for the sub-events were at a maximum. Because of the complex local topography and micrometeorology, the combination of back trajectories, satellite imagery (GOES "loops") and other evidence can only suggest a most likely smoke origin and cannot provide an exact smoke age. Our best guess at the smoke origin for each event is listed in Table S4 and Table S5.

4.1.3 Brief description of 2017 regional and selected local fires

Missoula experienced smoke impacts from local (western MT) and regional fires with regional fires including fires in California, Idaho, Oregon, Washington, and British Columbia. Over ~1.2 million ha burned in British Columbia in 2017(BC Wildfire Service, 2017). More than 4 million ha burned in the US during the 2017 fire season, making it one of the largest to date. Idaho, Oregon, and Washington had burned areas over 263,000 ha, 283,000 ha, and 161,000 ha, respectively. California and Montana experienced their largest burned areas to date, with both states experiencing close to 526,000 ha burned each (National Interagency Fire Center, 2017). Although the complicated meteorology and topography of the Missoula valley makes attributing smoke sources somewhat difficult (as noted above), we can say with some degree of certainty that the majority of the fresh smoke impacting Missoula came from two local fires, the Lolo Peak fire and the Rice Ridge fire (Table. 4.1). The Lolo Peak fire started at high elevation ~15 km SW of Missoula (46.674º N, 114.268º W) on 15 July 2017 and burned continuously (mostly at lower and lower elevations) until it eventually grew to over 20,000 ha. The fuel description as given by Inciweb (https://inciweb.nwcg.gov/incident/5375/) is summarized as containing generally sparse

or patchy subalpine fir (*Abies lasiocarpa*) with dead Whitebark pine (*Pinus albicaulis*) above ~2100 m. Below 2100 m, fuels were mainly typical of a variety of coniferous-dominated ecosystems with major tree species such as ponderosa pine (*Pinus ponderosa),* sub-alpine fir (*Abies lasiocarpa),* and lodgepole pine (*Pinus contorta).* Lower elevations near containment lines were dominated by ponderosa pine with grassy understory. The Rice Ridge fire started 24 July 2017 ~52 km NE of Missoula (47.268º N, 113.485º W). The fire eventually burned over 64,000 ha, with a notable run on 3 September 2017, where it doubled in size from ~20,000 ha to ~40,000 ha. Fuels involved were timber (litter and understory), and brush (https://inciweb.nwcg.gov/incident/5414/).

4.1.4 Overview of smoke impacts in Missoula

Figure 4.1 shows the hourly average mixing ratios of CO, BC, and $PM_{2.5}$ observed from 11 August to 10 September 2017, which includes nearly all of the 2017 Missoula smoke impacts. There were more than 20 distinct periods of major smoke-impacts that are readily identified by large simultaneous enhancements in CO, BC, and $PM_{2.5}$. Sustained periods when $PM_{2.5}$ was elevated well above the 12.5 μg m^{-3} EPA standard for "good" air quality were designated as events and assigned a letter in Fig. 4.1 and Tab. S4. The highest hourly values were observed on 4 September 2017, the morning after the Rice Ridge fire doubled in size ($PM_{2.5,}$ 471 μg m^{-3}, CO 2.78 ppm, BC 3.62 μg m^{-3}). This event is discussed in more depth as a case study in a later section (4.5). Numerous other $PM_{2.5}$ peaks exceeded e.g. levels of 100 μg m^{-3}. "Cleaner" periods between smoke peaks became less extensive as the regional atmosphere became increasingly polluted until widespread clearing on 10 September 2017. Overall high correlation of CO and BC to $PM_{2.5}$ suggest that the smoke was normally well mixed on the spatial scale that separated the $PM_{2.5}$ and UM monitors. Many of the longer smoke impacts that spanned several days were necessarily

integrated as a single event for calculating ratios between species, but we also initialized back trajectories from local maxima to further explore the source region of the smoke, which was probably always mixed to some extent (Tab. S4)

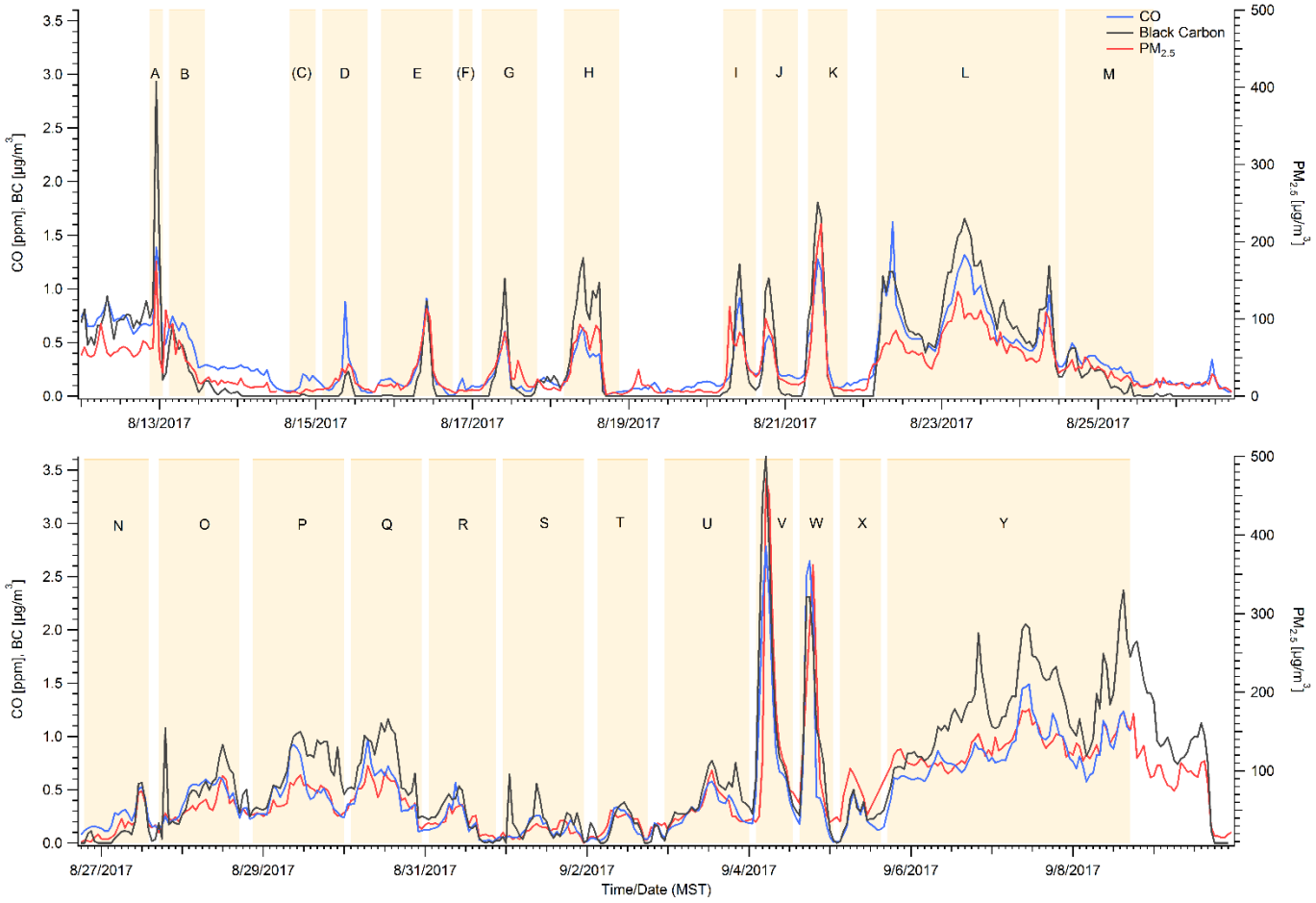

Figure 0.1. Time series of hourly CO, BC, and $PM_{2.5}$ measurements from Missoula. Sections highlighted in yellow indicated smoke-impacted periods. Peaks labeled with a parentheses indicated events that could not be attributed to biomass burning sources, and were excluded from analysis.

4.2 Instrument Descriptions

4.2.1 Fourier transform infrared spectrometer

Trace gas measurements were made using an FTIR (Midac, Corp., Westfield, MA) with a Stirling cycle cooled mercury-cadmium-telluride (MCT) detector (Infrared Associates, Stuart, FL; Ricor USA Inc., Salem, NH) interfaced with a 17.22 m path closed multipass White cell (Infrared Analysis, Inc., Anaheim, CA) that is coated with a halocarbon wax (1500 Grade, Halocarbon Products Corp., Norcross, GA) to minimize surface losses (Yokelson et al., 2003). Although the system was designed for source measurements, and is described elsewhere in more detail (Akagi et al., 2013; Stockwell et al., 2016a, Stockwell et al., 2016b), the FTIR is convenient for ambient monitoring because the Stirling cooled detector does not require refilling of liquid nitrogen and thus allows for mostly autonomous operation. Ambient air was drawn through the 2.47 liter White cell at ~6 liters per minute via a downstream IDP-3 dry scroll vacuum pump (Agilent Technologies) using a 0.635 cm o.d. corrugated Teflon inlet that was positioned outside the window (~12.5 m above ground level). Cell temperature and pressure were also logged on the system computer (Minco TT176 TRD MKS Baratron 722A). Spectra were collected at a resolution of 0.50 cm^{-1} covering a frequency range of 600-4200 cm^{-1}. A time resolution of approximately 5 minutes was more than adequate and sensitivity was increased by co-adding scans at this frequency. Gas phase species (with their respective detection limits in parentheses), including carbon monoxide (CO, 20 ppb), methane (CH_4, 20 ppb), acetylene (C_2H_2, 2 ppb), ethylene (C_2H_4, 2 ppb), methanol (CH_3OH, 3 ppb), and ammonia (NH_3, 2 ppb) were quantified by fitting selected regions of the mid-IR transmission spectra with a synthetic calibration nonlinear least-squares method (Griffith, 1996; Yokelson et al., 2007). The uncertainties in the individual mixing ratios

(ppmv) varied by spectrum and molecule and were influenced by uncertainty in the reference spectra (1-5%) or the real time detection limit, whichever was larger. The procedure used to correct for gases outside of the spectrometer cell raised the uncertainty to ~20 ppb for background CO and CH_4, but did not affect the measured enhancements above background during smoke episodes. Calibrations with NIST-traceable standards indicate that peak CO values had an uncertainty of less than 5%. The FTIR system was designed for source sampling and the sensitivity was adequate to measure a significant amount of usable trace gas data, but not every species on every event. In addition, an FTIR system problem caused the trace gas data to terminate about one day before the smoke cleared.

4.2.2 PAX configurations for ambient sampling

Particle absorption and scattering coefficients (B_{abs}, Mm^{-1}, B_{scat}, Mm^{-1}) were measured directly at 1 s time resolution using two photoacoustic extinctiometers (PAX, Droplet Measurement Technologies, Inc., Longmont, CO; Lewis et al., 2008; Nakayama et al., 2015). SSA at 401 (nominally a 405 nm system) and 870 nm, and AAE were derived using those measurements. Although the PAXs measured every second, data was averaged to 5 minutes, which was deemed adequate for the final analysis and matched the time resolution used by the FTIR for the same reason. A 1L min^{-1} aerosol sample flow was drawn through each PAX using a downstream IDP-3 dry scroll vacuum pump (Agilent Technologies) and split internally between a nephelometer and photoacoustic resonator for simultaneous measurement of light scattering and absorption. Both PAX instruments contain an internal pump, however these internal pumps were bypassed to improve measurement sensitivity, as the pumps can contribute an amount of acoustic noise that is noticeable in clean-air ambient measurements. Scattering of the PAX laser light was measured using the wide-angle (6º-174º) reciprocal nephelometer that responds to all particle types

regardless of chemical makeup, mixing state, or morphology. For absorption measurements, the laser beam was directed through the aerosol stream and modulated at a resonant frequency of the acoustic chamber. Absorbing particles transferred heat to the surrounding air, inducing pressure waves that were detected via a sensitive microphone.

The PAX sample line was ~4.7 m of 0.483 cm o.d. conductive silicon tubing positioned outside the window ~12.5 m above ground level and co-located with the FTIR inlet. The tubing transferred outside air to a scrubber to remove light-absorbing gases (Purafil-SP Media, minimum removal efficiency 99.5%) and then a diffusion drier (Silica Gel 4-10 mesh) to remove water, with post-drier relative humidity varying between 13 and 30%. The scrubber and drier were refreshed before any signs of deterioration were observed (e.g. color change). The diffusion based designs will cause small particle losses, but losses were not explicitly measured. After the drier, a splitter connected to the two instruments. After the splitter, each sample line featured a 1.0 μm size-cutoff cyclone and two acoustic notch filters that reduced noise. Both PAX instruments were calibrated before, during, and after the experiment using the manufacturer-recommended scattering and absorption calibration procedures utilizing ammonium sulfate particles and a propane torch to generate purely scattering and strongly absorbing aerosols, respectively. The 401 nm data was only used after August 27 because of frequent clogging of the $PM_{1.0}$ cyclone before that date.

The estimated uncertainty in PAX absorption and scattering measurements has been estimated to be ~4-11% (Nakayama et al., 2015). A few other sources of uncertainty in the measurements and/or calculations are poorly characterized; MAC increases due to coatings, potential particle losses in the drier or scrubber, and truncation error in the nephelometer. Mie calculations provided by the manufacturer suggest the scattering could be underestimated by about 1% at 870 nm and 2.5% at 401 nm due to truncation error (J. Walker, private communication). This would reduce the mass

scattering coefficients (Sect. 4.4.2) and typically a 1% reduction in scattering would imply approximately a tenth of a percent of value underestimate of SSA. Miyakawa et al. (2017) reported a size-independent particle transmission up to 400 nm of 84±5% in their diffusion drier. Larger particles may be transmitted more efficiently. We did not measure size distribution or transmission efficiency in this study and thus, we did not adjust the data. Size-independent particle losses would reduce scattering, absorption, and derived BC, but should have only a small impact on SSA or AAE. Unlike particle losses, an increased MAC due to "lensing" via coatings could inflate BC values by up to ~30% (Pokhrel et al., 2017).

4.2.3 Montana Department of Environmental Quality $PM_{2.5}$ Monitor

The Montana DEQ uses beta attenuation monitors (Met One Instruments, Model BAM-1020) in accordance with US EPA Federal Equivalent Methods (FEM) for continuous $PM_{2.5}$ monitoring. At the beginning of each sample hour, a constant ^{14}C source emits beta rays though a spot of clean glass fiber filter tape. The beta rays are measured by a photomultiplier tube to determine a zero reading. The BAM-1020 then advances this spot of tape to the sample nozzle, where it filters a measured amount of outside air at 16.7 L min^{-1}. At the end of the sample hour, the attenuation of the beta ray signal by the filter spot is used to determine the mass (and concentration µg m^{-3} at ambient temperature and pressure) of the particulate matter. Hourly detection limits for the BAM-1020 are <2.4 µg m^{-3} (1σ). Current and archived air quality data for the state of Montana can be accessed using the following link: http://svc.mt.gov/deq/todaysair/. More information on the BAM-1020 can be found at http://metone.com/air-quality-particulate-measurement/regulatory/bam-1020/. Note PAX size cutoff was 1.0 micron and the PM size cutoff is 2.5 µm. The mass in the 1.0-2.5 µm range is thought to be a small part of the total mass (e.g. 10-

20% in Fig. 2 in Reid et al., 2005a), but the size range difference does affect data interpretation as detailed later.

4.2.4 Emission ratios and downwind enhancement ratios

Time series are useful to characterize impacts and evaluate models, but we also used the time series of mixing ratios or concentrations for each analyte measured to derive other values that are broadly useful for study comparisons and implementation in local to global chemistry and climate models. As part of this, we produced emission ratios (ERs) and enhancement ratios. The calculation of these two types of ratios is the same, but an emission ratio is only the appropriate term for a ratio measured directly at a source or further downwind for relatively inert species such as BC or CO. First, an excess mixing ratio (denoted by "ΔX" for each species X) is calculated for all species measured by subtracting the relatively small background mixing ratio based on a sloping baseline from before to after a smoke impact. For example, the ratio for each species relative to CO (ΔX/ΔCO) is the ratio between the sum of ΔX over the entire smoke impacted period relative to the sum of ΔCO over the entire smoke impacted period. Mass or molar ratios to CO were calculated for BC, PM, and all the gases measured by the FTIR that exhibited enhancement above background levels for each smoke impacted period. Emission factors (EF), which can be derived by including the molar ER to CO_2 in the carbon mass balance method were not calculated (Section 2.1 and Selimovic et al. 2018). The diurnal variation for CO_2 is considerable, and the smoke was mainly aged (not reflecting initial emissions for most species) in Missoula. The prolonged "small" ΔCO_2 peaks that persist for times similar to the natural, substantial variation that CO_2 has have uncertain values. E.g., for CO_2, the wildfire smoke impacts in Missoula are largely diluted and protracted enough to not completely dominate background variability as is the case for the other gases and for source sampling (Stockwell et al., 2016a, Stockwell et al., 2016b, Akagi et al., 2011, Akagi et

al., 2012). Since ΔCO_2 are not as reflective of fire impacts, then by extension, the modified combustion efficiency (MCE) which is defined as $\Delta CO_2/(\Delta CO_2 + \Delta CO)$, is not as useful as an index of the combustion flaming to smoldering ratio in this study as in measurements closer to the source (Yokelson et al., 2013b). Other approximate indicators of the relative amount of flaming to smoldering such as $\Delta BC/\Delta CO$ or $\Delta CH_4/\Delta CO$ can still be used.

4.3 Trace gas measurements

4.3.1 Trace gas ratios

Table 4.1 reports study average ratios weighted by event duration (time-weighted) to CO for gases measured by the FTIR. These measurements are representative of moderately aged regional wildfire smoke. We interpret our results by comparing them to emission ratios measured in the lab (Selimovic et al., 2018) and other field studies mostly in fresher smoke (Liu et al., 2017; Landis et al., 2017; Radke et al., 1991). CO is a major pollutant in the atmosphere with BB as a main source. In Missoula, especially in the summer, the CO background is not strongly influenced by non-fire sources. CH_4 on the other hand has more background variability, but at these smoke levels the ratio of CH_4 to CO, while variable, yields a study average (0.166 ± 0.088) that mostly reflects the real average $\Delta CH_4/\Delta CO$ fire emission ratio.

Table 0.1 Time-weighted study average enhancement ratios (ratioed to CO) compared to emission ratios reported in other studies. Values in parenthesis are 1σ.

Compounds	This Work	Selimovic et al., 2018[a]	Selimovic et al., 2018[b]	Liu et al., 2017	Landis et al., 2017	Radke et al., 1991[c]	Urbanski et al., 2013
Methane (CH_4)	0.1661 (0.0884)	0.0741 (0.0698)	0.0870	0.0960 (0.0425)	0.104 (0.001)	0.0503 (0.0420)	0.0946 (0.0108)
Acetylene (C_2H_2)	0.0014 (0.0004)	0.0062 (0.0607)	0.0056	0.0028 (0.0022)	--	0.0023 (0.0018)	--
Ethylene (C_2H_4)	0.0114 (0.0022)	0.0209 (0.0193)	0.0199	0.0102 (0.0033)	--	--	--
Methanol (CH_3OH)	0.0199 (0.0013)	0.0148 (0.0152)	0.0176	0.0240 (0.0160)	--	--	--
Ammonia (NH_3)	0.0133 (0.0064)	0.0232 (0.0350)	0.0279	--	--	0.0219 (0.0099)	--

[a] Measured lab values at lab fire MCE
[b] Calculated from EF vs MCE fit based on average wildfire MCE reported in Liu et al.
[c] Averages of Myrtle Fall Creek and Silver Fire

Yates et al. (2016) reported a smoldering stage $\Delta CH_4/\Delta CO$ ER of 0.095 (±0.023) for the Rim Fire, which is lower than our study average ER, but the ratio reported in Yates et al. (2016) comes from airborne measurements closer to the source and from a single fire source. Our higher study average ER of CH_4 is indicative of smoldering (Reisen et al., 2018; Yokelson et al., 1997). Because the measurement was not in a direct downslope flow of smoke into Missoula, this ratio suggests that smoldering emissions from regional fires can be and were frequently transported to the Missoula valley. This may be why our study average is higher than observed in airborne studies. In a consistent observation, we find that ERs for $\Delta CH_4/\Delta CO$ are lower when the $\Delta BC/\Delta CO$ ERs are higher (Fig. 4.2), which is indicative of a flaming to smoldering ratio dependence (Christian et al., 2003).

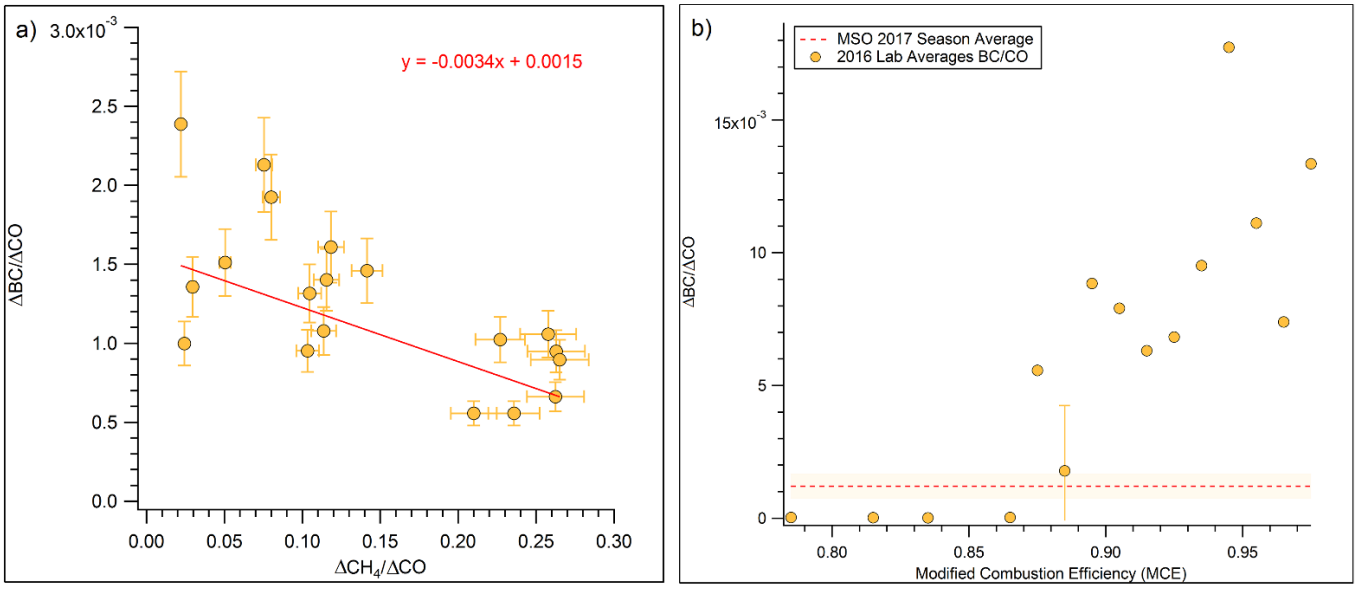

Figure 0.2 a) Methane emission ratio versus black carbon emission ratio. Point shown are for events that have both a CH_4/CO ratio and a BC/CO ratio. b) Lab average (Selimovic et al., 2018) BC/CO ratio versus modified combustion efficiency (MCE), separated into bins by 0.01 of MCE.

This is a useful result, because our two metrics for combustion characteristics at the fire source are consistent and it indicates that the variability in ratios between species observed at Missoula was partly due to variable combustion types at the regional fire sources along with the expected effects of variable aging that are discussed next. Next, we compare other measured trace gas ratios, including some more reactive VOC, to the limited amount of data available from previous airborne and lab studies. Liu et al. (2017) sampled smoke between 1-2 h old on average, and did not report an ER value for NH_3. However, Liu et al. (2017) reported an average wildfire MCE that Selimovic et al. (2018) used with measurements of very fresh lab fire smoke to calculate an ER value for $\Delta NH_3/\Delta CO$ based on the average wildfire MCE reported in Liu et al. (2017). The predicted NH_3 value (0.0279) for wildfires based on an average wildfire MCE (0.91), is about twice our observed average $\Delta NH_3/\Delta CO$ (0.0133). Radke et al. (1991), measured an $\Delta NH_3/\Delta CO$ range from 0.037 for fresh smoke to 0.011 when including samples up to 48 h old. Our 2017 individual ratios span a range (Tab. S4). Near the high end we see $\Delta NH_3/\Delta CO$ of 0.0196 for relatively fresh smoke assigned to the nearby Lolo Peak Fire and 0.0216 for event "S" where the origin is unclear. Our lowest ratios are about ¼ of our highest ratios (0.0044) (Tab. S4). Akagi et al. (2012) measured a mid-day $\Delta NH_3/\Delta CO$ half-life of ~5h, which suggests that our average sample age is roughly equivalent to ~5h of mid-day processing and our oldest samples (with NH_3 data) are aged equivalent to about 10 hours of "mid-day processing" (Tab. S4). However, the "time since emission" is potentially longer than indicated by a "photochemical age" since, according to the GOES satellite, a lot of smoke was produced in the evening and OH processing may not have started fully until the next day. In addition, we note that the true processing ages have potential to be even longer, since the true initial $\Delta NH_3/\Delta CO$ may have been higher than our highest observed

ratios as we were not immediately adjacent to sources. This possibility is supported by the fact that NH_3 and CH_4 emissions have been shown to be linked (Yokelson et al., 1997), and our "high" $\Delta CH_4/\Delta CO$ value for event "S" (~0.14) could indicate that the real initial $\Delta NH_3/\Delta CO$ was higher than ~0.022. Finally, the $\Delta NH_3/\Delta CO$ ratio is also related to the size and age of particles as is discussed in section 4.4.1.

C_2H_4 has been observed to decay in isolated plumes with a similar half-life to ammonia (Akagi et al., 2012; Hobbs et al., 2003), and our study average $\Delta C_2H_4/\Delta CO$ ratio (0.011) is again about half that in the other wildfire studies in younger smoke reported in Tab. 4.1 (~0.02) or listed elsewhere (Akagi et al., 2011). Our lower $\Delta C_2H_4/\Delta CO$ ratios tended to occur when the $\Delta NH_3/\Delta CO$ ratio was also lower (Tab. S4), but unfortunately there are only two events with data for both gases and not enough measured values to warrant a detailed analysis. Methanol and acetylene react at least an order of magnitude more slowly with OH than C_2H_4. Our average methanol enhancement ratio (0.019) thus falls in the middle of the other wildfire values (0.0148 – 0.024) as might be expected when any aging effects are smaller than the natural high variability in initial emissions (Akagi et al., 2011). In fact $\Delta CH_3OH/\Delta CO$ has been observed to increase or decrease slightly or stay the same for several hours of aging (Akagi et al., 2012, Akagi et al., 2013, Müller et al., 2016). We have only a few data points for $\Delta C_2H_2/\Delta CO$, but their average is significantly lower than the other wildfire studies. Since C_2H_2 is associated with flaming combustion (Lobert et al., 1991; Yokelson et al., 2013a) this could be due to the prevalence of smoldering that was also indicated by the high average $\Delta CH_4/\Delta CO$ ratios as noted above. Another point about our trace gas data is that our mixing ratios for CO are valuable as an inert tracer for wildfire emissions for comparison to models and they can be useful for inferring the initial emissions of other gases if those gases emission ratios to CO have been measured elsewhere (Selimovic et al., 2018; Koss et al., 2018; Liu et al., 2017).

CO can also be used as a scaling/normalizing factor for particle emissions, which is discussed in the next section.

4.3.2 ΔBC/ΔPM$_{2.5}$, ΔBC/ΔCO, ΔPM$_{2.5}$/ΔCO

BC is estimated to be the second strongest global climate warming agent and BB is the main BC source (Bond et al., 2004). Accurate BC measurements are challenging and aerosol absorption remains poorly understood in atmospheric models (Bond et al., 2013). In contrast, CO is measured reliably at a network of surface sites and in aircraft campaigns, and can also be retrieved by satellite (MOPITT, IASI, AIRS, etc.). As a result, CO emissions estimates are available for most sources, including fires, and the estimates are in reasonable agreement for western wildfires (Liu et al., 2017). BC and ΔBC/ΔCO measurements by modern methods for wildfires are rare, thus, our BC, CO, and ΔBC/ΔCO measurements from a large sample of wildfire smoke can be used with CO emissions to update BC emissions estimates from wildfires (see below). BC is made only by flaming combustion at a fire source and despite the fact that its production rate can vary strongly with flame turbulence, the ΔBC/ΔCO ratio can serve as a rough indicator of the fire's flaming to smoldering ratio (Vakkari et a., 2018; Christian et al., 2003; Yokelson et al., 2009; Shaddix et al., 1994) as exploited earlier in Fig. 4.2b. Table 4.2 reports our study average ratios (time weighted) of ΔBC/ΔCO, ΔBC/ΔPM$_{2.5}$, and ΔPM$_{2.5}$/ΔCO and compares them to the limited measurements of wildfire smoke available in the lab (Selimovic et al., 2018) and in the field (Liu et al., 2017; Sahu et al., 2012; Hobbs et al., 1996). Our ΔBC/ΔCO ratio (0.0012) is a bit lower than the aircraft measured averages of Sahu et al. (2012) (0.0014), and Liu et al. (2017) (0.0016), and the Selimovic et al. (2018) estimate at the field average MCE for wildfires from Liu et al. 2017 (0.0018). The Hobbs et al. (1996) average value for their two fires specifically identified as wildfires is notably

higher than the other values and is actually an ΔEC/ΔCO (elemental carbon to CO) measurement that could be biased high. The Selimovic et al. 2018 lab average is also higher, but obtained at the higher lab-average MCE. The uncertainty in our value is likely asymmetric because coatings in aged PM could inflate absorption and our BC value by a small amount.

Table 0.2. Time-weighted study average enhancement ratios (g g^{-1} ratioed to CO) compared to emission ratios reported in other studies.

Ratios	This Work	Selimovic et al., 2018[a]	Selimovic et al., 2018[b]	Liu et al., 2017[c,d]	Sahu et al., 2012	Hobbs et al., 1996[e]
BC/CO	0.0012 (0.0005)	0.0087	0.0018	0.0016 (0.0018)	0.0014	0.0103
$BC/PM_{2.5}$	0.0095 (0.0003)	--	--	0.0060 (0.0054)	--	--
$PM_{2.5}/CO$	0.1263 (0.0015)	--	--	0.2661 (0.1342)	--	0.4923

[a] Measured lab values at lab fire MCE
[b] Calculated from EF vs MCE fit based on average wildfire MCE reported in Liu et al.
[c] Average of Rim Fire and Big Windy Complex. BC data was analyzed for Liu et al. (2017) study, but not reported.
[d] PM values reported are $PM_{1.0}$
[e] PM values reported are $PM_{3.5}$

Taken together, this suite of observations is roughly consistent with our ground-based site being impacted by relatively more smoldering combustion (MCE ~ 0.87±0.02, based on Fig. 4.2b) than airborne studies (MCE 0.91 Liu et al., 2017; 0.90 Sahu et al., 2012). Liu et al. (2017) calculated an average annual CO production from western US wildfires for 2011-2015 of 5240 ± 2240 Gg, which they reported was in good agreement with an EPA estimate based on a similar burned area in the 2011 National Emissions Inventory (4894 Gg). Ratioing to the Liu et al. estimate with the average field study ΔBC/ΔCO in Tab. 4.2 (0.0014 ± 0.0002) suggests that western US wildfires emit 7.3 ± 3.3 Gg of BC per year. This is significantly lower than a previous estimate, but the other estimate is not strictly comparable since it is based on elemental carbon (EC) measurements and for a different year (2006) (Mao et al., 2015).

Changes in the ΔPM/ΔCO ratio as a plume ages can be used as a metric for the net effect of secondary formation or evaporation of organic and inorganic aerosol (Yokelson et al., 2009; Akagi

et al., 2012; Jolleys et al., 2012; Vakkari et al., 2014; Vakkari et al., 2018). Table 4.2 indicates that our ground-based $\Delta PM_{2.5}/\Delta CO$ (0.126 ± 0.002) is about half that obtained at aircraft altitudes in fresher wildfire smoke (0.266 ± 0.134) as reported by Liu et al. (2017) and ~4 times less than that reported for very fresh smoke by Hobbs et al., (1996) (0.492). Further our lower $\Delta BC/\Delta CO$ ratio suggests enhanced smoldering, which should preclude a large drop in $\Delta PM/\Delta CO$ (Reisen et al., 2018). Liu et al. (2017) and Forrister et al. (2015) measured smoke aging for the Rim Fire (a large California wildfire) as the plume aged and found that the $\Delta OA/\Delta CO$ ratio started high and then dropped to a value (0.125 ± 0.025) similar to our $\Delta PM_{2.5}/\Delta CO$. However, Collier et al. (2016) found no age dependence for $\Delta OA/\Delta CO$ for plumes intercepted at Mount Bachelor or on the G-1 aircraft and obtained a value for $\Delta OA/\Delta CO$ (0.25 ± 0.07) close to both the $\Delta OA/\Delta CO$ and $\Delta PM_{1.0}/\Delta CO$ of Liu et al. (2017) in fresh Rim Fire smoke. Taken together, these observations suggest that, on time scales up to ~1-2 days for the wildfire smoke studied to date, aging and/or higher average ambient temperatures at lower elevations may encourage some OA evaporation and reduce downwind PM impacts, Some studies in other fire types have found secondary formation to dominate at low elevation (Yokelson et al., 2009; Vakkari et al., 2014) so it is premature to generalize this observation to all BB and more study is needed. However, both of the latter studies measured smoke within a few hours of the source, and our lower $\Delta PM_{2.5}/\Delta CO$ indicates that evaporation of PM dominated over formation of PM as smoke was transported to the Missoula valley in smoke that was between several hours and several days old.

The climate impacts of smoke are strongly related to the $\Delta BC/\Delta PM$ ratio and also the SSA and BrC, which are described in more detail in other sections. The $\Delta BC/\Delta PM$ ratio also allows for a rough estimate of ambient BC from ambient PM data when BC isn't measured, but caution is

needed since PM may not be conserved as long as BC, and ΔBC/ΔPM is also variable at the source. Our study average $\Delta BC/\Delta PM_{2.5}$ ratio (0.0095, Fig. 4.3) is higher than the study average $\Delta BC/\Delta PM_{1.0}$ in Liu et al. 2017 (0.006) but falls within the range observed for two wildfires measured in Liu et al. (2017), despite the differences in measurement techniques ($PM_{2.5}$ vs. $PM_{1.0}$, etc.).

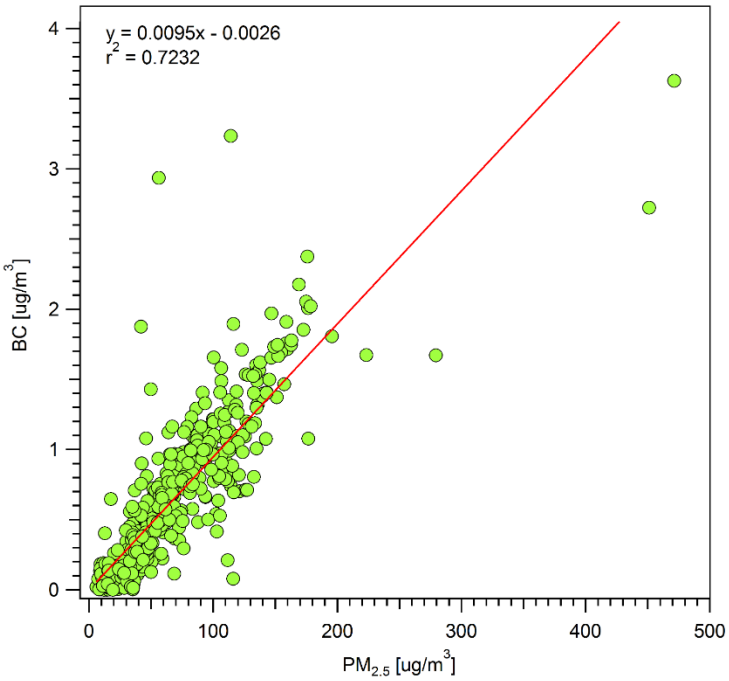

Figure 0.3 ΔBC/ΔPM ratio based on linear regression of 1-hour data.

It's possible that the ΔBC/ΔPM ratio reported in this study is up to ~30% too high if we consider the effects of coating on BC and lensing as a positive error (Pokhrel et al., 2017). Previous studies found that smoldering combustion emits anywhere between 2-49 times more PM than flaming combustion (Jen et al., 2019; Kim et al., 2018; Reisen et al., 2018; Yokelson et al., 2013a), so the combination of our ΔBC/ΔCO ratio that is indicative of more smoldering combustion and a BC/PM ratio that is similar to or slightly above measurements closer to fire sources (Liu et al., 2017) again

suggests that some net evaporation of PM is occurring at lower, warmer altitudes during transport between the wildfire sources and our surface site. Again, this is worth more study since this could modify air quality and health effects. OA is the main component of PM and the ΔBC/ΔPM ratio is likely similar to the ΔBC/ΔOA ratio. Our ΔBC/ΔPM ratio (~1%) then suggests that the aerosol measured was overwhelmingly organic, and thus strongly cooling, especially if the impact of BrC or lensing was small. Further, the mass-absorption coefficient (MAC) for OA scales with the ΔBC/ΔOA ratio (Saleh et al., 2014) so we anticipate a low MAC, which is explored more in section 4.4.2.

4.4 Aerosol optical properties

4.4.1 UV-absorption by brown carbon

While the attribution of BrC is not exact and varies across studies (Pokhrel et al., 2017), BrC absorption will offset the climate cooling calculated for purely-scattering OA depending on the amount emitted, its MAC, and its lifetime (Feng et al., 2013). One field study of BrC lifetime suggests a significant decrease of BrC over the course of a day, but a prolonged persistence of BrC nonetheless (~6% above background even after 50h following emission) (Forrister et al., 2015), and studies of relevant chemical mechanisms involving BrC have shown both increases and decreases **(**Lin et al., 2015; Liu et al., 2016; Xu et al., 2018). Satellite retrievals employing reasonable a-priori aerosol layer heights indicate that BrC can have a strong impact in fresh BB plumes and a persistent significant impact in downwind regional haze (Jethva et al., 2011; Hammer et al., 2016). Here we present in-situ data showing persistent widespread regional impacts of BrC. Table 4.3 lists the study-average AAE and percent contribution to absorption at 401 nm by BrC. We interpret our results by comparing them to the limited measurements of wildfire smoke in the

lab and field and measurements for "flaming dominated" savanna fires (Selimovic et al., 2018; Forrister et al., 2015; Eck et al., 2013). Theoretically, aerosol absorption that is dominated by black carbon would have an AAE close to 1.0 (Bergstrom et al., 2002; Bond and Bergstrom, 2006; Bergstrom et al., 2007), which is the case in Eck et al., 2013 where they report an average AAE of 1.20 for measurements of savannah fires in southern Africa. On the other hand, Selimovic et al. (2018) and Forrister et al. (2015) calculated AAEs for fresh smoke of 3.31 and 3.75, respectively, for various mixed coniferous fuels burned in a laboratory and in the field.

Table 0.3 Time-weighted study average AAE & %BrC contribution compared to other studies.

	This Work	Selimovic et al., 2018a	Selimovic et al., 2018b	Forrister et al., 2015	Eck et al., 2013
AAE	1.96 (0.38)	2.80 (1.57)	3.31	3.75	1.20
%BrC	50.72 (12.78)	64.19 (17.20)	78.00	--	--

[a] Measured lab values at lab fire MCE
[b] Calculated from average wildfire MCE reported in Forrister et al., 2015.

Our study average AAE (1.96 ± 0.38) is almost 2 times lower than the average value recommended for fresh wildfire smoke (~3.5) in Selimovic et al. (2018), but higher than that reported in Eck et al. (2013). This is also the case for the percent contribution to absorption at 401 nm by BrC, where a lower AAE corresponds to lower BrC absorption. The AAE recommended for fresh wildfire smoke implies the %-absorption by BrC at 401 nm is close to 86%, but we still see significant (~50%) absorption by BrC at 401 nm, on average, despite some aging of the smoke at our site.

Although we cannot determine precise smoke ages in this study, we can construct an analysis of our data that probes the trend in AAE and % absorption by BrC with aging. We start by noting that Mie scattering calculations (J. Walker, personal communication, 2017) imply that the ratio of $B_{scat}401/B_{scat}870$ should decrease as average particle size increases (e.g. Schuster et al., 2006; Eck et al., 1999; Kaufman et al., 1994) and average particle size is well-known to increase with particle

age (Akagi et al., 2012; Eck et al., 2013; Carrico et al., 2016). We also show in Fig. 4.4a that the $\Delta NH_3/\Delta CO$ ratio decreases with $B_{scat}401/B_{scat}870$ and we know NH_3/CO decreased with aging with a ~5 hour half-life in the fall and under slower photochemical conditions in Tab. 2 in Akagi et al. (2012). Thus, the range in $B_{scat}401/B_{scat}870$ shown in Fig. 4a represents about 10 hours of day-time aging. We also see a weak trend, but significant decrease in AAE over a similar range of our size/age parameter in Fig. 4.4b. Our data for AAE versus a proxy for average age of mixed-age smoke is more variable than the AAE versus known transport time for a single plume in Forrister et al. (2015), but still supports a similar conclusion: that the net effect of BrC aging is a substantial decrease in AAE over the course of ~10 hours of aging.

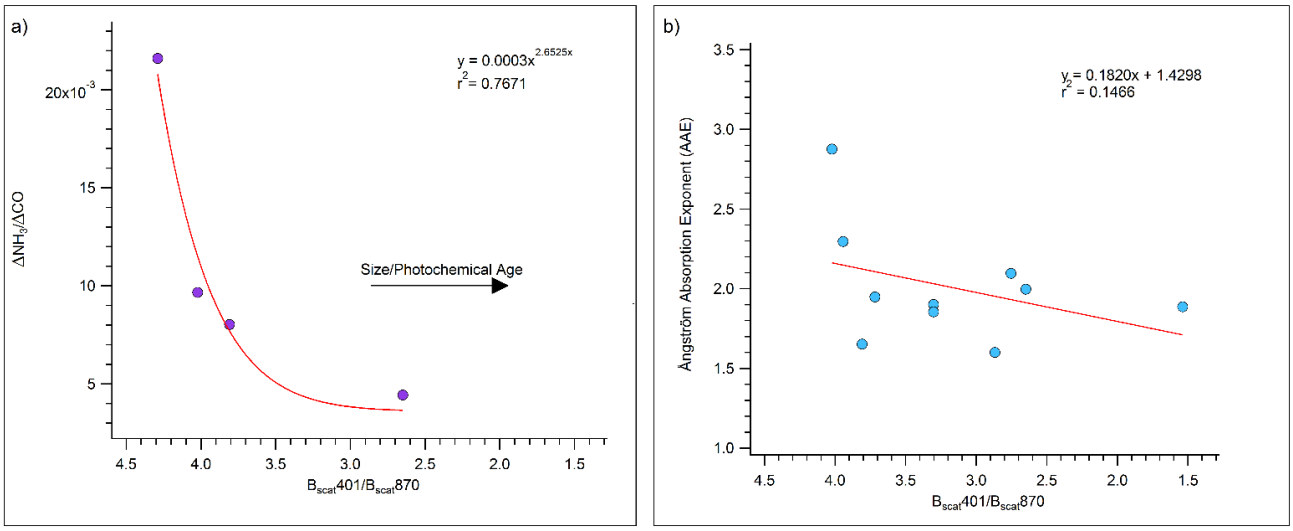

Figure 0.4 a) Plot of the peak-integrated $\Delta NH_3/\Delta CO$ ratio versus our size proxy (401 Scattering/870 Scattering) for smoke impacts that have an $\Delta NH_3/\Delta CO$ ratio. b) Plot of the peak-integrated absorption Angstrom exponent versus our size proxy (401 Scattering/870 Scattering) when both PAXs were operational.

We also speculate that, in addition to aging, the time of day that smoke is formed may impact BrC and AAE. We motivate that hypothesis next and then explore the issue in subsequent sections. Selimovic et al. (2018) showed that BrC accounted for most of the absorption at 401 nm when

MCEs were in a low range associated with dominant smoldering combustion. Benedict et al. (2017) further observed that smoke impacts from a nearby wildfire had a much higher smoldering/flaming ratio at night than during the day, which then suggests the potential for increased BrC formation at night. It is also known that smoldering combustion of biomass emits many precursors, including monoterpenes, furans, cresol, etc. (Stockwell et al., 2015); that can react quickly with the major night time oxidant, NO_3, and ostensibly form UV-absorbing organic nitrates that could augment BrC. In fact, estimates using current data strongly suggest that a substantial nighttime secondary BrC source could exist. The EF for primary organic aerosol (POA) produced by BB typically ranges from 3 to 30 g kg^{-1} (May et al., 2014; Liu et al., 2016, 2017). The EF for known plus unidentified non-methane organic gases (NMOGs) with intermediate to low volatility ranges from 3 to 100 g kg^{-1}. Converting even a small percentage of the co-emitted NMOGs that are known to react quickly with NO_3 could yield substantial amounts of BrC and build up a reservoir of BrC during dark hours. Once daytime commences, other studies show that some types of BrC, depending on the precursor, can experience rapid photochemical degradation or formation via both direct photolysis and oxidation (Zhao et al., 2015; Lee et al., 2014, Zhong and Jang et al., 2014; Sareen et al., 2013). In summary, our extensive in-situ measurements show that even after 1-2 days of aging, BrC remains a significant component of ambient smoke, and that the climate properties of the regional haze have a non-BC absorption contribution. However, the details of the formation and lifetime of BrC are complicated and probably vary diurnally.

4.4.2 Single scattering albedo, mass absorption coefficient, and mass scattering coefficient

This section starts with an important reminder/caveat. Our scattering and absorption data is measured for particles up to 1.0 μm, but the PM mass reported by the Missoula DEQ site includes particles up to 2.5 μm. Thus, using our data to calculate mass absorption coefficients (MAC) and

mass scattering coefficients (MSC) will produce lower limit values that are not directly comparable to those obtained when the range for both optical and mass measurements goes up to 2.5 µm. Nevertheless it is potentially useful to link $PM_{1.0}$ and $PM_{2.5}$ measurements since measurements at 1 µm cutoffs are common in field campaigns, but $PM_{2.5}$ still remains the common measurement in regional networks.

Table 4.4 lists our time-weighted study average of MAC, MSC, and SSA at multiple wavelengths and compares them to similar works. Our MAC and MSC values were calculated by plotting 1-hr averages of $B_{scat}401$, $B_{abs}401$, and $B_{scat}870$, $B_{abs}870$ versus the 1-hr $PM_{2.5}$ values to calculate an MSC(401), MAC(401), MSC(870), MAC(870), respectively (Fig. 4.5). Values at other wavelengths were calculated with a power law fit using the calculated averages. Our ($\Delta PM_{1.0}/\Delta PM_{2.5}$) MSC values are lower than those reported for $PM_{2.5}/PM_{2.5}$, but still potentially useful. For instance, the $\Delta PM_{1.0}/\Delta PM_{2.5}$ MSC at 870 nm is one to a good approximation, which suggests a convenient way to estimate $PM_{2.5}$ directly from PAX-870 scattering data. Using a 1-micron cut-off probably isolated the combustion-generated OA and BC pretty well, but dust, ash and biological particles can be physically entrained in wildfire plumes (Formenti et al., 2003; Gaudichet et al., 1995; Hungershoefer et al., 2008). The particles in the 1.0-2.5 micron range are a small part of the total mass in smoke emissions (Reid et al., 2005a) but they contribute disproportionately to the scattering. The additional absorption that we might have measured with a 2.5 micron cutoff may be less significant. Our study average MAC at 401 nm is only 0.19 ± 0.08 $m^2\ g^{-1}$, consistent with a low BC/OA ratio (Saleh et al., 2014).

Table 0.4 Time-weighted study average SSA, MAC, and MSC compared to other work.

Parameter	λ (nm)	This Work	Selimovic et al., 2018[b]	Selimovic et al., 2018[c]	Eck et al., 2013	McMeeking et al., 2005	Reid et al., 2005b
SSA	401	0.93 (0.01)	0.79 (0.13)	0.9	--	--	--
	540	0.937[a]	--	--	--	--	0.85 (0.03)
	550	0.938[a]	--	--	0.81-0.88	0.92 (0.02)[d]	0.86-0.90
	870	0.94 (0.02)	0.64 (0.26)	0.92	--	--	--
MAC	401	0.23 (0.01)	--	--	--	--	--
	530	0.143	--	--	--	0.37 (0.05)[e]	--
	540	0.138					0.7 (0.4)
	550	0.132	--	--	--	--	0.7-0.8
	870	0.04 (<0.01)	--	--	--	--	--
MSC	401	3.23 (0.06)	--	--	--	--	--
	530	2.13	--	--	--	5.5 (0.5)[e]	--
	540	2.07	--	--	--	--	3.2-4.2
	550	2.02	--	--	--	--	3.6-3.8
	870	1.01 (0.02)	--	--	--	--	--

[a] Calculated values using fit based on 401 and 870 nm values.
[b] Measured values at lab fire MCE.
[c] Calculated from EF versus MCE fit based on average wildfire MCE reported in Liu et al., 2017.
[d] McMeeking et al., 2005b.
[e] McMeeking et al., 2005a.

SSA, AAE, and SAE are commonly used to calculate aerosol absorption and scattering in models and satellite retrievals. (Ramanathan et al., 2001; McComiskey et al., 2008). Uncertainty in the SSA is one of the largest sources of uncertainty in estimating the radiative effect of aerosols (Jiang and Feingold, 2006; McComiskey et al., 2008). Some models and satellite (e.g. MODIS) retrievals assume a constant value of SSA for fire aerosol throughout the biomass burning season and the entire year, which may be an inaccurate approach. Eck et al. (2013) found an increase in SSA at 550 nm from 0.81 in July to 0.88 in October in southern Africa.

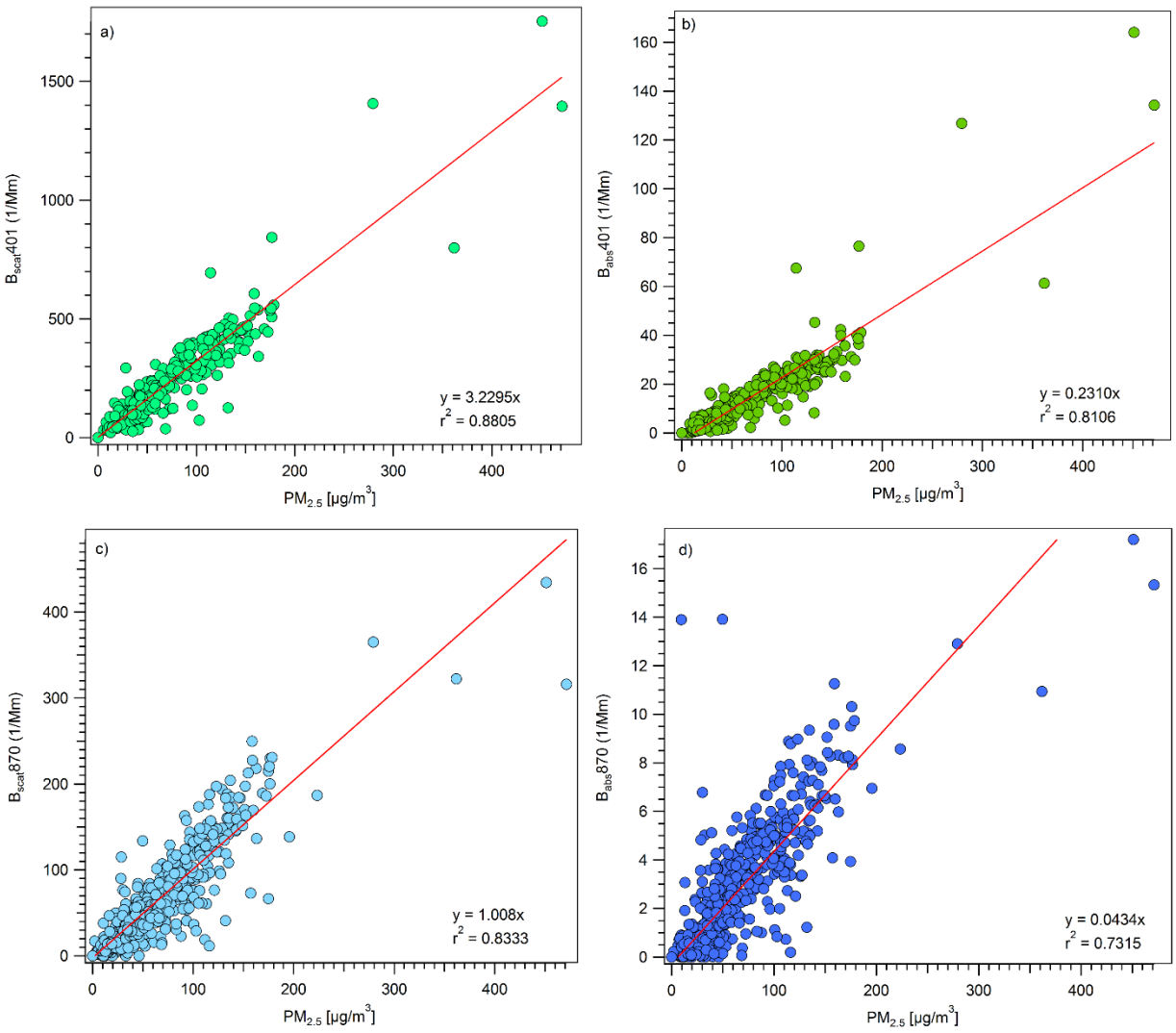

Figure 0.5 Mass absorption and mass scattering coefficient data at 401 and 870 nm.

In Fig. 4.6 we present evidence for an increase in the SSA for moderately aged wildfire smoke over a prolonged period of biomass burning. While we did not directly measure SSA at 550 nm, we did measure SSA at 870 nm for the duration of the sampling period and SSA at 401 nm for the duration that the PAX 401 was operational. Figure 4.6 shows a moderate increasing trend in the SSA at 870 nm (change in SSA), but no significant trend in the SSA at 401 nm. It could be that

because the sampling period of the PAX 401 nm only covers ~2 weeks, any trend that may be present is not apparent within this time frame.

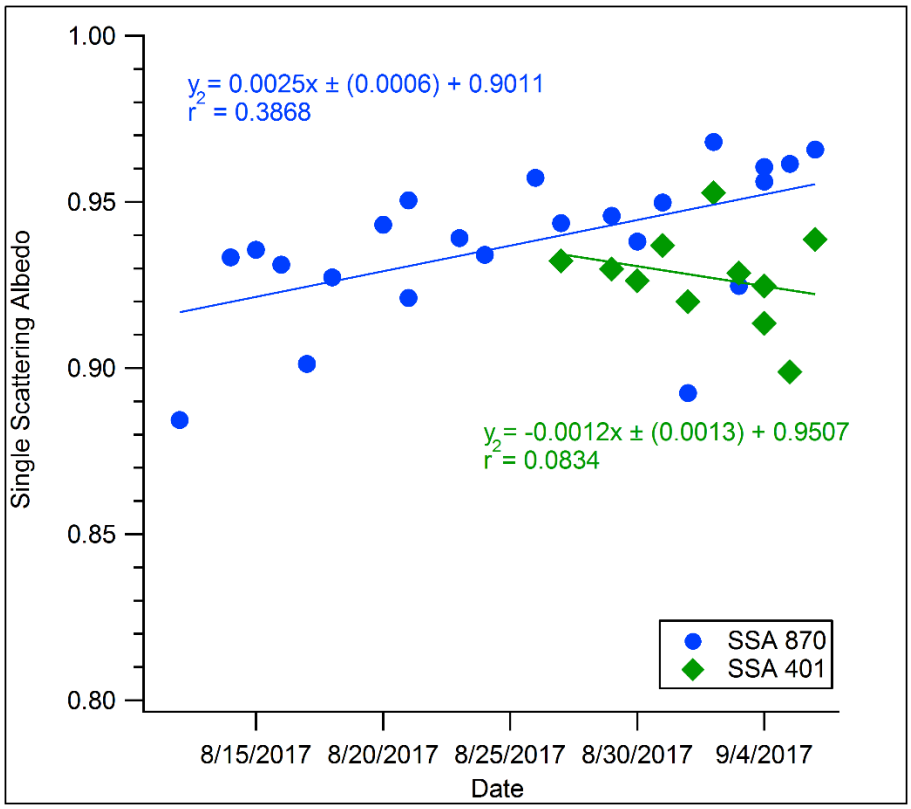

Figure 0.6 Plot of single scattering albedo over the course of the ambient smoke-monitoring period. Points represent SSA absorption and scattering integrated over smoke-impacted events.

Table 4.4 shows our study average SSA at 870 nm and 401 nm, which are ~0.94 and 0.93 respectively, and are similar to the SSA reported at 550 nm in McMeeking et al. (2005b) of 0.92. Our SSA and the SSA reported in McMeeking et al. (2005b) are higher than the sometimes quoted typical surface SSA of the earth (~0.9, Praveen et al., 2012) which suggests that the wildfire $PM_{1.0}$ in regional haze would contribute to regional cooling (Thornhill et al., 2018; Kolusu et al., 2015). Conversely, an SSA range like that reported in Eck et al. (2013) could contribute to warming,

which could potentially contribute to a positive-feedback cycle associated with biomass burning (Jacobsen, 2014).

4.5 Case study: Labor Day weekend

Figure 4.7 highlights our data for Labor Day weekend (LDW), spanning ~50 hours from 4 September 2017 to 5 September 2017. We focus on this time period because it includes the largest impacts in Missoula, a regional smoke-production episode detected as far downwind as Europe (https://earthobservatory.nasa.gov/images/90980/an-american-aerosol-in-paris) (Ansmann et al., 2018), and an opportunity to compare what is likely smoke from one fire, subjected to different processing scenarios. Peak "V" is smoke that was likely primarily produced at night and transported to Missoula at night before subsequent photochemistry and dilution in the Missoula Valley. In contrast, peak "W" is smoke that was likely produced and transported during the day before aging in Missoula. Surface winds observed coming from the east, our back trajectory calculations, and satellite observations along with the high concentration values of peak V all imply that the smoke was mostly sourced from a local fire (Rice Ridge) and about 2-4 hours old. Our peak-integrated proxy for particle size (4.02, smaller particle size) and the peak-integrated $\Delta NH_3/\Delta CO$ ratio (9.66×10^{-3}) for peak "V" suggest that the smoke retained fairly fresh characteristics even factoring in the daytime tail on the peak (Tab. S4). The peak integrated AAE (2.88) is the highest observed value for AAE from this study for any peak where an AAE could be derived. The same is true for the %401-absorption by BrC (~77%). The UV absorption results are within the range observed for fresh smoke reported in Selimovic et al., 2018 and reiterated again earlier in Tab. 4.3, which lists average AAE values for fresh smoke between 2.80 and 3.75 (Forrister et al., 2015). Average values for %401-absorption by BrC in fresh smoke ranged between 64 and 86% (Selimovic et al., 2018), and again our integrated result for peak V falls in

this range. In summary, the moderately-aged, strongly night-influenced peak has properties not inconsistent with significant amounts of BrC due to smoldering combustion or substantial nighttime BrC formation via reactions with NO_3 or O_3.

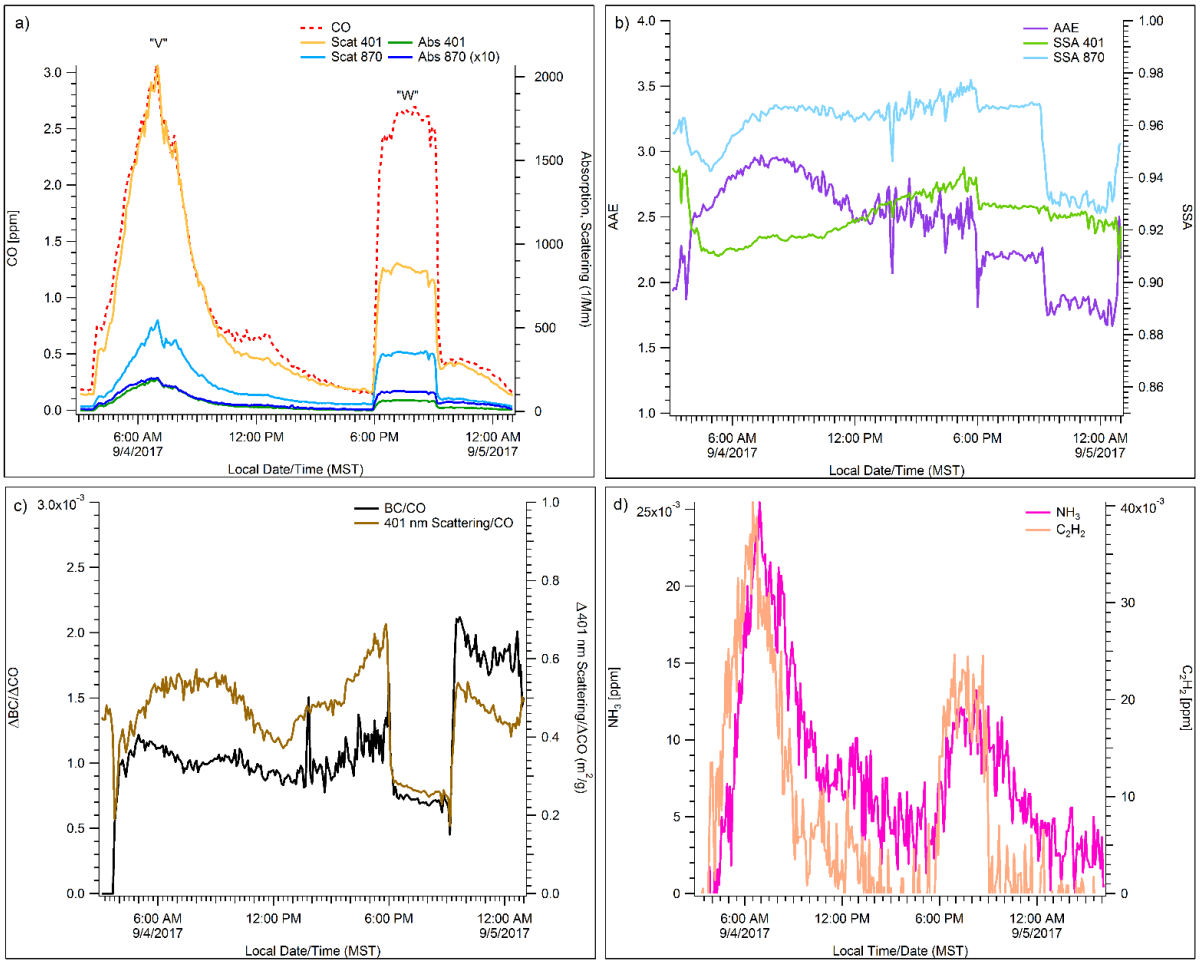

Figure 0.7 High resolution (5-minute) time series of smoke-impacts measured in Missoula over Labor Day weekend (see Sect.4.5).

While not readily apparent via satellite observations due to stacked smoke layers, our back trajectory calculations, a similar peak shape on an upwind monitor, visual observations of a wall of smoke arriving from the northeast, and high concentrations of PM at the Missoula measuring site strongly suggest that peak "W", with an onset in the early evening, also mostly came from the

Rice Ridge Fire as daytime produced/processed smoke. Peak "W" has a 401/870 scattering ratio (2.65) that implies larger particle sizes and an $\Delta NH_3/\Delta CO$ ratio (0.0044) that is ~50% that of Peak "V". The ratio of $\Delta C_2H_4/\Delta CO$ decreases by ~30% from peak V to peak W. The AAE for peak "W" is 2.00, which is ~30% less than the AAE for Peak "V", and corresponds to a lower %401-absorption by BrC for the evening-onset peak (~54%). Taken together, these values imply larger particles and more photochemically aged smoke. Interestingly, the ratio of $\Delta CH_4/\Delta CO$ and $\Delta BC/\Delta CO$ are essentially similar for peaks V and W. This implies the flaming/smoldering ratio at the source for these events was similar (NO_3 chemistry could still have been more important for peak V). While nighttime wildland fire combustion may be normally more smoldering dominated, LDW was marked by an unusual lack of nighttime RH recovery and an aggressive doubling of the fire size. Thus data from a different, more typical period is likely needed to probe diurnal differences in fresh smoke.

4.6 Diurnal cycles

Diurnal cycles of smoke measured in Missoula provide some insight into regional meteorological effects and have some potential to further probe the day versus night flaming/smoldering issues raised in the previous section (4.5). There is, however, a variable delay from production to receptor. Figure 4.8 shows the diurnal cycle of CO and the average hourly $PM_{2.5}$ measured across the entirety of the smoke sampling period. Levels of CO and $PM_{2.5}$ peak together from about 5 to 11AM, which is consistent with increased smoldering at night, but would also reflect the mixed layer height. Figure 4.9 shows the diurnal cycles of $PM_{2.5,}$ hourly average BC, and hourly average %401-absorption by BrC (8 August 2017 to 10 September 2017). In this case we see that "potential" BrC absorption peaks in the early AM while BC peaks in the evening. One possible

explanation for this is that despite variation in mixed layer height there is “typically” an increase in the flaming to smoldering ratio that produces more black carbon and less brown carbon during the day.

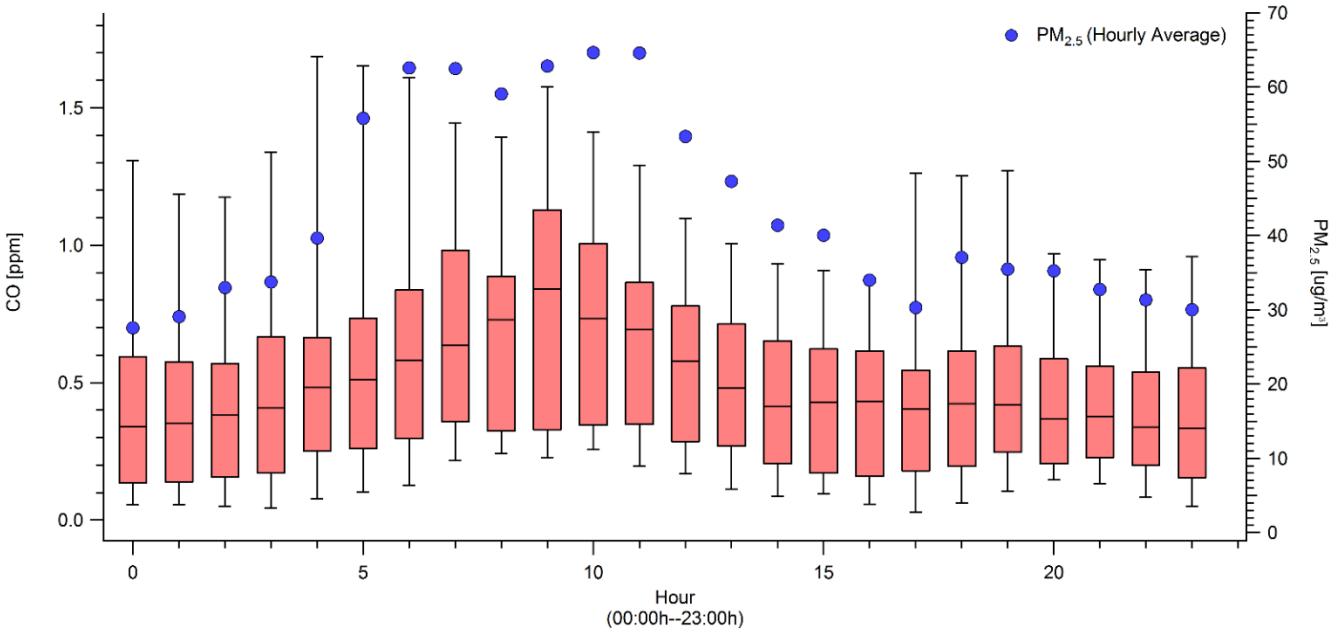

Figure 0.8 Diurnal plot of CO and $PM_{2.5}$, shown for the entirety of the monitoring period.

If nearby (less diluted) fires with shorter transport times strongly influence the peak times a signal of diurnal variation at the source could be partially evident at our site. However, we can’t rule out that an increase in photo-bleaching throughout the middle of the day impacts the peak position for absorption by BrC, but even then, the absorption by BrC remains about half of the absorption at 401 nm on average.

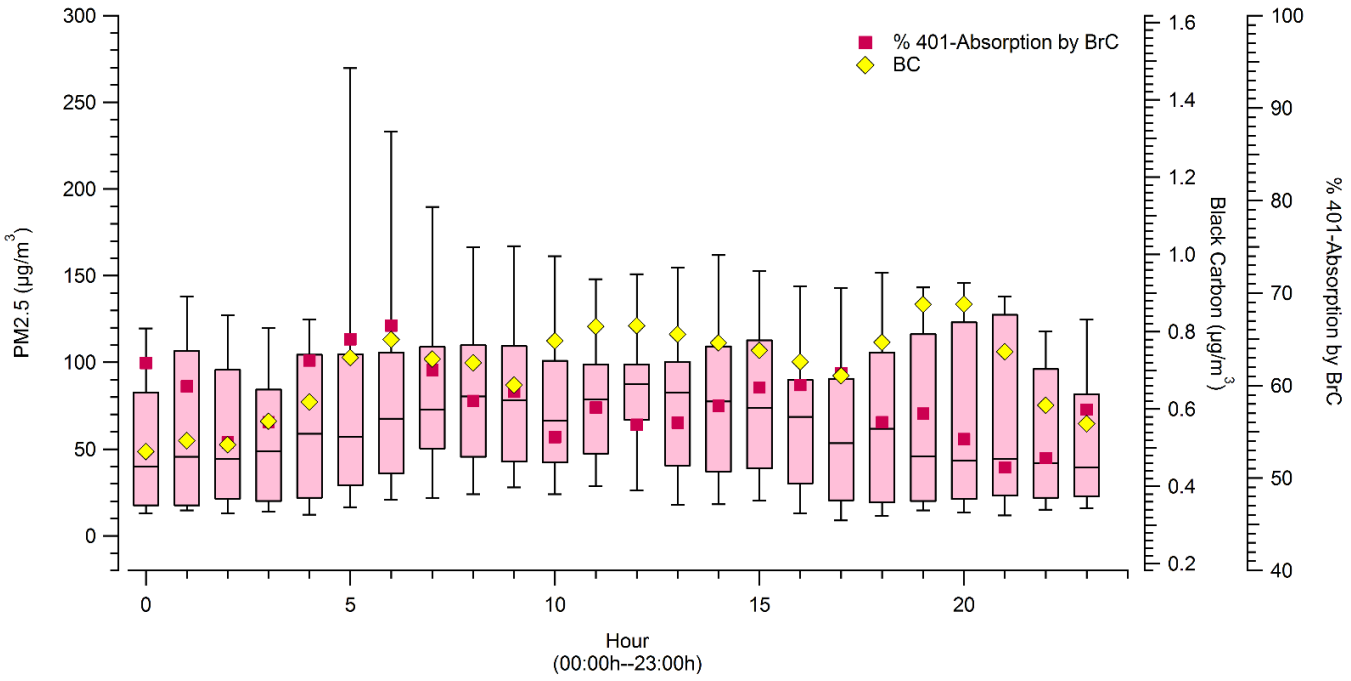

Figure 0.9 Diurnal plot of average $PM_{2.5}$, hourly average % 401-Absorption by BrC, and hourly average BC. BC and PM shown for the entirety of the monitoring period, but %401-Absorption by BrC only shown for when the PAX 401 was operational.

4.7 Brief comparison to prescribed fire data

Of the 718 hours we sampled during August and September 2017, 500.5 hours were part of a smoke event, which is close to three quarters (~70%) of the total monitoring time period. Of the total 718 hours of monitoring, over half (56%) violated the National Ambient Air Quality Standards (NAAQS) for allowable $PM_{2.5}$ averaged over 24 hours (35 µg m^{-3}). The hourly average for the entire sampling period of ~54 µg m^{-3} of $PM_{2.5,}$ is an average exceedance of the 24-hour NAAQS standard by 42%. One possible approach to minimizing wildfire AQ impacts is pre-emptive prescribed burning. Prescribed fires reduce hazardous fuels, burn less fuel per unit area, make less smoke per unit fuel consumption, and can be ignited when conditions are favorable for minimizing air quality impacts (Liu et al., 2017).

It is of interest to compare our large sample of ambient wildfire data to the comparatively rare data from airborne wildfire studies and prescribed fire data to see if our large sample size supports the earlier (Liu et al., 2017) conclusions regarding the nature of the smoke and emissions. More strongly supported conclusions can reinforce the land management implications. Table 4.5 lists the ΔBC/ΔCO, ΔBC/ΔPM, and ΔPM/ΔCO ratios for our ambient wildfire study, the airborne wildfire study from Liu et al., (2017), and prescribed fire values reported in May et al., (2014). The ΔPM/ΔCO values for fresh wildfire smoke in Liu et al. (2017) and aged wildfire smoke (this study) are about three and 1.5 times higher than ΔPM/ΔCO for fresh smoke from prescribed fires in May et al. (2014) when comparing to all their US prescribed fires (Tab. 4.5). For only prescribed fires in western US mountain coniferous ecosystems (last column Tab. 4.5), the ΔPM/ΔCO for fresh smoke is close to our value for aged wildfire smoke. However, May et al. (2015) noted that ΔPM/ΔCO decreased by about a factor of two after several hours of aging on at least one prescribed fire.

Table 0.5 Comparison of wildfire emission/ enhancement ratios to prescribed fire emission ratios (g g^{-1})

Ratios	This Work	Liu et al., 2017[a, b]	May et al., 2014[b]	May et al., 2014[b,c]
BC/CO	0.0012 (0.0005)	0.0016 (0.0018)	0.013 (0.007)	0.006
BC/PM2.5	0.0095 (0.0003)	0.0060 (0.0054)	0.163 (0.019)	0.048
PM2.5/CO	0.1263 (0.0015)	0.2661 (0.1342)	0.080 (0.030)	0.11 (0.01)

[a] Average of Rim Fire and Big Windy Complex. BC data was analyzed for Liu et al. (2017) study, but not reported.
[b] PM values reported are PM1.0
[c] Values for the Shaver and Turtle fires (prescribed burns).

The ΔBC/ΔCO for prescribed fires is higher than the wildfire average by a factor of ~9 (all prescribed fires) or ~4 (last column), roughly suggesting a higher MCE for prescribed fires. Ignoring smoke age, the ΔBC/ΔPM for prescribed fires is higher than the wildfire average by a factor of ~20 (all prescribed fires) or ~6 (last column). The ΔBC/ΔPM observations suggest that

wildfire smoke is overwhelmingly more organic, which is important partly because many optical properties scale with the BC/OA ratio (Saleh et al., 2014). In general, our ground-based wildfire study confirms the earlier airborne indications that prescribed fires are less smoky but also less cooling than wildfires. Differences in smoke production and chemistry between wild and prescribed fires should be researched more and have air quality and land management implications.

4.8 Conclusions

A major, prolonged wildfire smoke/haze episode impacted the NW U.S. and SW Canada during August through September of 2017. During this episode, we collected over 500 hours of data characterizing smoke/haze properties with FTIR and PAXs at 870 and 401 nm at a ground-based site in Missoula, MT. This is probably the most extensive real-time data on wildfire smoke properties to date. Our low $\Delta BC/\Delta PM$ (0.0095 ± 0.0005) ratio confirmed the overwhelmingly organic nature of the smoke observed in the airborne studies of wildfire smoke to date. Our $\Delta BC/\Delta CO$ ratio (0.0012 ± 0.0005) for our ground site was moderately lower than observed in aircraft studies suggesting a relatively larger contribution from smoldering combustion. Despite our lower $\Delta BC/\Delta CO$ ratio our $\Delta PM/\Delta CO$ ratio was about half that measured in fresh smoke from aircraft. Taken together with aircraft measurements in aged wildfire smoke, this suggests that OA evaporation, at higher ambient temperatures nearer the surface may typically reduce PM air quality impacts on the time scale of several hours to days. $B_{scat}401/B_{scat}870$ was used as a proxy for size and age of the smoke particles with this interpretation being supported by the trace gas data. The size/age proxy implied that AAE decreased significantly after about ten hours of smoke aging, consistent with the single BrC lifetime measurement in an isolated plume. The results clearly show that non-BC absorption can be important in "typical" regional haze/moderately-aged smoke with

BrC accounting for about half the absorption at 401 nm on average for the entire data set. The diurnal trends show BrC, PM, and CO peaking in early morning and BC peaking in early evening. Over the course of one month, the SSA at 870 nm increased from ~0.9 to ~0.96.

Chapter 5: Measurements of ambient smoke in Missoula, 2018

5.1 Overview of 2018 Measurements

In August-September of 2017, we began measurements of wildfire smoke impacting the Missoula valley (a western urban center downwind of numerous wildfires), eventually obtaining 500 hours of data of smoke-impacted time as a result. In this study we continued the measurements, with an expanded suite of instruments, for another 517 hours of smoke impacts during August-September 2018. Two PAXs, an FTIR, and, added in 2018, an O_3 monitor, a NO_x monitor, and a second FTIR were used to characterize smoke that entered the valley. A Montana Department of Environmental Quality (DEQ) BAM 1020 measured $PM_{2.5}$ (particulate matter ≤ 2.5 μm in diameter). The PAXs provided measurements of scattering and absorption at two wavelengths (401 nm, 870 nm), BC mass, contributions to UV absorption nominally due to BrC, and derivations of the SSA and AAE. The optical property measurements can be normalized to the aerosol mass data to probe multi-step, bottom-up calculations of climate-relevant aerosol optical properties that start with aerosol mass. Further, combining CO measured by our FTIRs with the other species measured (BC, $PM_{2.5}$) produced ratios relevant to models, as mentioned above. Finally, we measured smoke impacts on O_3 and combining our NO_2 and O_3 measurements allowed us to calculate the NO_3 production rate and probe the potential NO_3 contribution to in-situ nighttime BrC formation. The main goals of this study were to assess the relevance of lab and airborne field measurements, the representativeness of emissions inventories, and guide model development by documenting actual surface level characteristics of aged/transported wildfire smoke in a representative, regional population center. Results are also

interpreted to assess the interannual variability of our results by comparing 2018 to our previous (2017) measurements of ambient smoke in the Missoula valley.

5.2 Site Descriptions

Our smoke monitoring sites in Missoula, MT remained unchanged between 2017 and 2018, and they are described in more detail in Selimovic et al. (2019). A few key details are reiterated here. Trace gases and particles were measured through co-located inlets at the University of Montana (UM), ~12.5 m above the ground through the window of our laboratory on the top floor of the Charles H. Clapp building (CHCB), which is ~1.1 km from the nearest road that gets significant traffic during summer recess (http://map.umt.edu/#17/46.85920/-113.98335). $PM_{2.5}$ measurements were made by the Montana DEQ via a stationary $PM_{2.5}$ monitor located in Boyd Park, Missoula ~3.2 km southwest of the CHCB, with both sites being located in the Missoula valley proper. Missoula is located ~800 km from the nearest large cities deep within an extensive, lightly-populated to unpopulated region containing few anthropogenic sources. Missoula and the surrounding region are occasionally impacted by prescribed fires and more frequently by summer wildfires, which can be numerous (https://www.nifc.gov/fireInfo/fireInfo_statistics.html).

5.3 Instrument Details

5.3.1 FTIR

Measurements of CO were made using two co-located FTIRs. The first FTIR (Midac Corp., Westfield, MA), used during the 2017 smoke measurements is described in detail elsewhere (Selimovic et al., 2019). The second FTIR, added during the 2018 monitoring period, consists of

a Bruker Matrix-M IR Cube spectrometer with an MCT Stirling cycle cooled detector interfaced to a permanently aligned 78 m closed uncoated multipass White cell (IR Analysis, Inc.) that is more sensitive due to the longer path length. Ambient air was drawn into both systems at ~6 L min^{-1} via a downstream IDP-3 dry scroll vacuum (Agilent Technologies) pump using two respective 0.635 o.d. corrugated Teflon inlets co-located with the other inlets. Spectra for both FTIRs were collected at a resolution of 0.50 cm^{-1}. A time resolution of approximately 5 minutes was more than adequate for both systems and sensitivity was increased by co-adding scans at their respective frequencies. Although the systems were designed for source measurements, and are described elsewhere in more detail (Akagi et al., 2013; Stockwell et al., 2016a, b, Selimovic et al., 2019), both FTIRs are convenient for ambient monitoring because the Stirling cooled detectors do not require refilling of liquid nitrogen allowing mostly autonomous operation. Additionally, the use of two FTIRs allowed for intercomparison of trace gas measurements, and served to supplement data in instances where it might have been missing from the other system (i.e. if one system shut down unexpectedly). Although both FTIRs can measure an extensive range of trace gases from sources, in the relatively dilute smoke impacting Missoula during 2018, most gases were retrieved with insufficient signal to noise or influenced by too many sources (e.g. CH_4, CO_2) to be readily interpretable, thus, only CO is reported. To summarize in context; in 2017 many of the wildfires were close to Missoula, CO levels reached almost 3000 ppb, and a number of gases (such as ethylene, ammonia, methanol, etc.) were often above the FTIR detection limits of several ppb. In 2018, the wildfires were further from Missoula, CO levels remained below ~800 ppb, and only excess CO was measured with sufficient signal to noise to clearly dominate background variability. CO mixing ratios were quantified by fitting a region of the mid-IR transmission spectra with a synthetic calibration nonlinear least squares

method (Griffith, 1996; Yokelson et al., 2007) applying the HITRAN spectral database (Rothman et al., 2009). Excess CO was virtually identical on the two systems. Uncertainties in excess CO mixing ratios in smoke (ppmv) varied by spectrum and were dominated by uncertainty in the reference data (<5%) and the background (~5-20 ppb).

5.3.2 Ozone Monitor

The 2B Technologies (Boulder, CO) model 211 O_3 monitor is a dual-beamed 254 nm photometer that uses the reaction between ambient O_3 and NO generated in situ by upstream photolysis of added nitrous oxide (N_2O) to quantify ozone by conventional UV photometry without the issues affecting conventional O_3 scrubbers. Light intensity measurements are made with O_3 present (I) and with O_3 selectively removed by NO (I_0), and the O_3 concentration is then calculated using the Beer-Lambert Law. O_3 calibrations were run using a model 306 O_3 calibrator (Birks et al., 2018a, 2B Technologies). Some UV-absorption O_3 monitors remove O_3 by passing the sample air flow through a solid scrubber, which ideally would destroy O_3 but pass mercury and any UV-absorbing compounds. In practice, however, mercury and aromatic compounds such as benzene, toluene, xylene, etc., can adsorb or react at the solid-phase scrubber surface. As a result, traditional O_3 monitors may report erroneously high O_3 values by up to a few ppb in some cases (2B Technologies, https://twobtech.com/docs/tech_notes/TN040.pdf). A 2 L min^{-1} sample flow of ambient air was drawn into the instrument through a 0.638 cm o.d. FEP inlet (~12.5 m above ground level) and a Teflon filter (Savillex, 47 mm 5-6 micron) to remove particles, which was replaced every 2 weeks or when visual signs of filter loading were apparent. O_3 was sampled at 1 minute intervals, but the data were averaged to 5 min for final analysis to match the time resolution of the FTIRs. Resolution of the 211 O_3 monitor is 0.1 ppb, with a limit of detection (2σ) of 1.0 ppb for a 10s average.

5.3.3 NOx Monitor

The 2B Technologies model 405 nm NO_x monitor measures nitrogen dioxide (NO_2) directly by absorbance at 405 nm and nitric oxide (NO) after conversion to NO_2 with ~100% efficiency using the reaction of NO with O_3. Because NO_2 has a lower absorption cross-section than O_3, a folded cell with corner mirrors is used to produce a long absorbance path of ~2 m to achieve approximately similar sensitives for NO_2 as for ozone (Birks et al., 2018b). Sample air is continuously drawn through the instrument by an internal pump at a flow rate of ~1.5 L min^{-1} through 0.638 cm o.d. FEP tubing co-located with the other inlets and a Teflon filter (Savillex, 47 mm 5-6 micron) to remove particles. The filter was replaced every ~2 weeks or when visual signs of filter loading were apparent. The instrument was "zeroed" on multiple occasions using zero air that was humidified to match ambient RH with nafion tubing. This ensures the refractive index in the cell and the path length do not change. The measurement of light intensity in the absence (I_0) and presence (I) of NO_2, allows the NO_2 concentration to be calculated using the Beer-Lambert Law. NO is quantified by measuring the decrease in light intensity while adding O_3 to convert NO to NO_2. A small, ~1-2%, loss of 405 nm absorbance from the reaction of NO_2 with O_3 is corrected in the firmware (Birks et al., 2018b). NO_2, NO, and NO_x were measured/logged at 1 minute time resolution, but the data were averaged to 5 min for final analysis to match the time resolution of the FTIRs and NO and NO_2 were corrected for small zero offsets (~2 ppb average). NO_x was recalculated from corrected NO and NO_2. Accuracy of the NO_x monitor was limited primarily by the drift in manual zeros of 0.75 ppb with total uncertainty in 5-minute NO_x data being ~2 ppb (1σ).

5.3.4 Photoacoustic extinctiometers (PAX) at 870 and 401 nm

Particle absorption and scattering coefficients (B_{abs}, Mm^{-1}, B_{scat}, Mm^{-1}) were measured directly at 1 s time resolution using two photoacoustic extinctiometers (PAX, Droplet Measurement Technologies, Inc., Longmont, CO; Lewis et al., 2008; Nakayama et al., 2015), which were then used to derive the single scattering albedo (SSA) at 401 and 870 nm and the absorption and scattering Ångström exponents (AAE, SAE). Details for calculating SSA and AAE, as well as operation and limitations of the PAX instrumentation are described in detail elsewhere (Selimovic et al., 2019), but we reiterate a few key points for the 2018 monitoring period. The main PAX sample line was 0.638 cm (o.d.) Cu tubing co-located with the other inlets. A 1L min^{-1} aerosol sample flow was drawn through each PAX using a downstream IDP-3 scroll vacuum pump (Agilent Technologies). A scrubber and dryer removed absorbing gases and kept relative humidity below 30%, as described in detail by Selimovic et al., 2019. The 1 Hz PAX data were averaged to 5 minutes and matched the time resolution used by the other instruments. In 2018, we switched from a 1.0µm cutoff cyclone to 2.5µm cyclone.

We directly measured aerosol absorption (B_{abs}, Mm^{-1}) and calculated BC concentration (µg m^{-3}) at ambient temperature and pressure using the literature and manufacturer-recommended mass absorption coefficient (MAC) for pure BC (4.74 ± 0.63 m^2 g^{-1} at 870 nm) (Bond and Bergstrom, 2006), but note that the BC mass can be adjusted using a different MAC value. To a good approximation, sp^2-hybridized carbon (including BC) absorbs light proportional to frequency (Bond and Bergstrom, 2006). Thus, the B_{abs} contribution from BC at 401 nm can be derived from ~2.17 times B_{abs} at 870 nm (assuming an AAE of one, negligible BrC absorption at 870 nm, and minimal lensing effects). Any additional B_{abs} at 401 nm can be assigned to BrC (B_{abs}, BrC) with this attribution subject to limitations discussed elsewhere (Pokhrel et al., 2016; 2017; Lack and Langridge, 2013; Lack and Cappa, 2010).

Uncertainty in PAX absorption and scattering measurements has been estimated to be ~4-11% (Nakayama et al., 2015), and 5 minute noise in scattering and absorption for the 870 nm instrument were 5 Mm^{-1} and <1 Mm^{-1}, respectively, while 5 minute noise in scattering and absorption for the 401 nm instrument were 20 Mm^{-1} and <1 Mm^{-1}, respectively. However, a few sources of uncertainty, for instance, MAC increases due to coatings, particle losses in the dryer or scrubber, and truncation error in the nephelometer may all contribute. Mie calculations suggest scattering could be underestimated by 1% at 870 nm and 2.5% at 401 nm due to truncation error. This would reduce mass scattering coefficients (MSCs, $m^2\ g^{-1}$) (Section 4.6) and typically a 1% reduction in scattering would imply approximately a tenth of a percent of value underestimation in SSA. Particle losses would reduce scattering, absorption, and derived BC, but have no impact on SSA, SAE, or AAE. We found that adding an extra scrubber reduced scattering and absorption at both wavelengths by 7±5% on average and adjusted the data upwards by 13% to account for both the dryer and scrubber (Selimovic et al., 2019). Unlike particle losses, an increased MAC due to "lensing", mentioned above, could inflate BC values by up to ~30% (Pokhrel et al., 2017).

5.3.5 Montana Department of Environmental Quality $PM_{2.5}$

The Montana DEQ uses beta attenuation monitors (Met One Instruments, Model BAM-1020) in accordance with US EPA Federal Equivalent Methods (FEM) for continuous $PM_{2.5}$ monitoring, which is described in more detail in Selimovic et al., 2019. Critically, however, combining $PM_{2.5}$ measurements with our scattering and absorption measurements from the PAX allows us to derive values for MAC and MSC at both wavelengths, which is discussed more in Section 4.6. Current and archived air quality data for the state of Montana can be accessed using the following link: http://svc.mt.gov/deq/todaysair/. We attempted to be precise about $PM_{1.0}$ and

$PM_{2.5}$ when comparing measurements, but also note that $PM_{1.0}$ is usually about 80% of $PM_{2.5}$ (Reid et al., 2005a, Fig. 2), and so in some cases when a statement is true for both sizes, we may indicate that by using the general term PM (particular matter).

5.4 Emission ratios (ERs) and downwind enhancement ratios

We used the time series of our mixing ratios or concentrations for each analyte measured to derive other values that are broadly useful for both study comparisons and integration in local to global chemistry and climate models. In order to do this, we produced emission ratios (ERs) and enhancement ratios. The calculation of these two types of ratios is identical, but an emission ratio is only the appropriate term for a ratio measured directly at a source or further downwind for a relatively inert species such as BC or CO. An excess amount, denoted by "ΔX" for each species X is calculated for all species measured by subtracting the comparatively small background based on a sloping baseline from the first to the last point of a smoke impact. Then, for example, the ratio for each species relative to CO (ΔX/ΔCO) is the ratio between the sum of ΔX over the entire smoke impacted period relative to the sum of ΔCO over the entire smoke impacted period. Mass ratios to CO were calculated for BC and $PM_{2.5}$ with enhancement of hourly $PM_{2.5}$ above 12.5 μg/m^3 used to define the time limits for each smoke impacted period as discussed further in sections 5.6 and 5.6.1.

5.6 Overview of smoke impacts

Figure 5.1 shows the hourly average concentrations for $PM_{2.5}$, AAE derived from 5-minute averages of B_{abs} at 401 and 870 nm, and 5-minute average concentrations or mixing ratios of BC, CO, NO_x and O_3 from 7 August to 10 September 2018. Most of the summer was characterized by air quality (AQ) classified as "good" by the US EPA (< 12.5 μg/m^3 of $PM_{2.5}$) and clear

visibility of mountains up to 80 km distant. As shown in more detail in Figures 5.2 to 5.6, smoke from wildfires and one prescribed fire contributed to episodes lasting for ~1-4 days during which hourly $PM_{2.5}$ ranged as high as 120 µg/m^3 ("unhealthy", US EPA), distant mountains "disappeared," and nearby mountains were partially obscured (Fig 5.7). In Fig. 5.1, wildfire smoke episodes are represented by the yellow shaded area and were identified by sustained periods (≥ 6 hours) when hourly $PM_{2.5}$ was elevated above the 12.5 µg m^{-3} EPA standard for "good" air quality and smoke was visibly present. Episodes started at the first point elevated above the cutoff and ended at the last elevated point before a sustained clean period or a wind shift bringing smoke from a new direction started a new event. Wildfire smoke episodes also had large simultaneous enhancements in CO and BC. High correlation of CO and BC to $PM_{2.5}$ suggests that the smoke was well mixed on the spatial scale that separated the $PM_{2.5}$ and UM equipment. In contrast, anthropogenic pollution (26-Aug – 5 Sept) is confidently identified and differentiated from smoke because it presents as much briefer spikes in CO or NO_x without sustained impacts on both regional visibility or the $PM_{2.5}$ monitor several km distant.

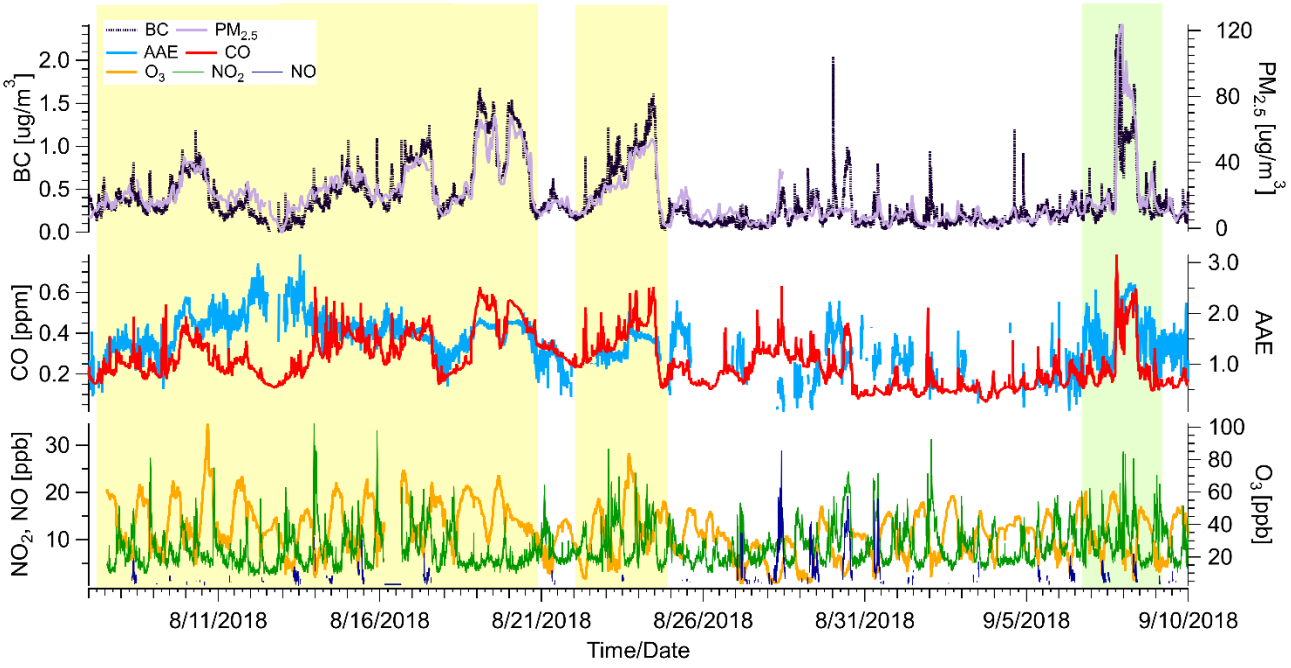

Figure 0.1. Time series of hourly PM, hourly derived AAE, 5-minute BC, CO, NO_x, O_3 measurements from Missoula. Sections shaded in yellow represent wildfire smoke impacted periods. Sections shaded in green represent prescribed fire smoke impacted periods. Unshaded areas represent anthropogenic impacts and were not included in the analysis.

To investigate the wildfire sources contributing to each episode we used a combination of meteorological observations, geostationary satellite observations, near-surface smoke according to the High Resolution Rapid Refresh (HRRR) model (https://rapidrefresh.noaa.gov/hrrr/), and back trajectory calculations utilizing the National Oceanic and Atmospheric Administration (NOAA) Air Resources Laboratory Hybrid Single Particle Lagrangian Integrated Trajectory (HYSPLIT; Stein et al., 2015; Draxler, 1999; Draxler and Hess, 1997, 1998). For wildfires, the fact that multiple fires at different distances upwind (~150-800 km) could simultaneously impact Missoula, the long duration of the impacts, variable winds over the duration, and complex topography and micrometeorology made precise smoke ages difficult to assign or even inappropriate. An "age spectrum" may be a more fitting concept. We characterize the wildfire

smoke as “up to several days old” with 20 ± 10 hours being a rough best guess at average age in 2018. Supplemental figures S1-S5 provide our best guess at the source region for each smoke episode. The situation in 2017 was similarly complex, but much more of the Missoula smoke in 2017 was from wildfires < 100 km distant (see map at https://www.atmos-chem-phys-discuss.net/acp-2018-1063/acp-2018-1063-AC3-supplement.pdf). Thus, an age characterizing most of the smoke could sometimes be estimated in 2017 and the 2017 smoke was clearly younger and more concentrated on average in 2017 (hourly $PM_{2.5}$ up to 471 µg/m^3) than 2018 (Selimovic et al., 2019).

We also present measurements for one 2018 “summer” prescribed fire impact (shaded in green). The prescribed fire was a well-documented, isolated event and the exact location was known allowing a reliable estimate of smoke age as ~3 hours old. The prescribed fire burned over 100 hectares, in a Lodgepole pine dominated ecosystem, and was a stand-replacing fire, producing smoke likely more similar to that from naturally occurring wildfires than is the case for the more common lower-intensity spring or fall prescribed fires that focus on clearing out understory fuels while preserving overstory trees.

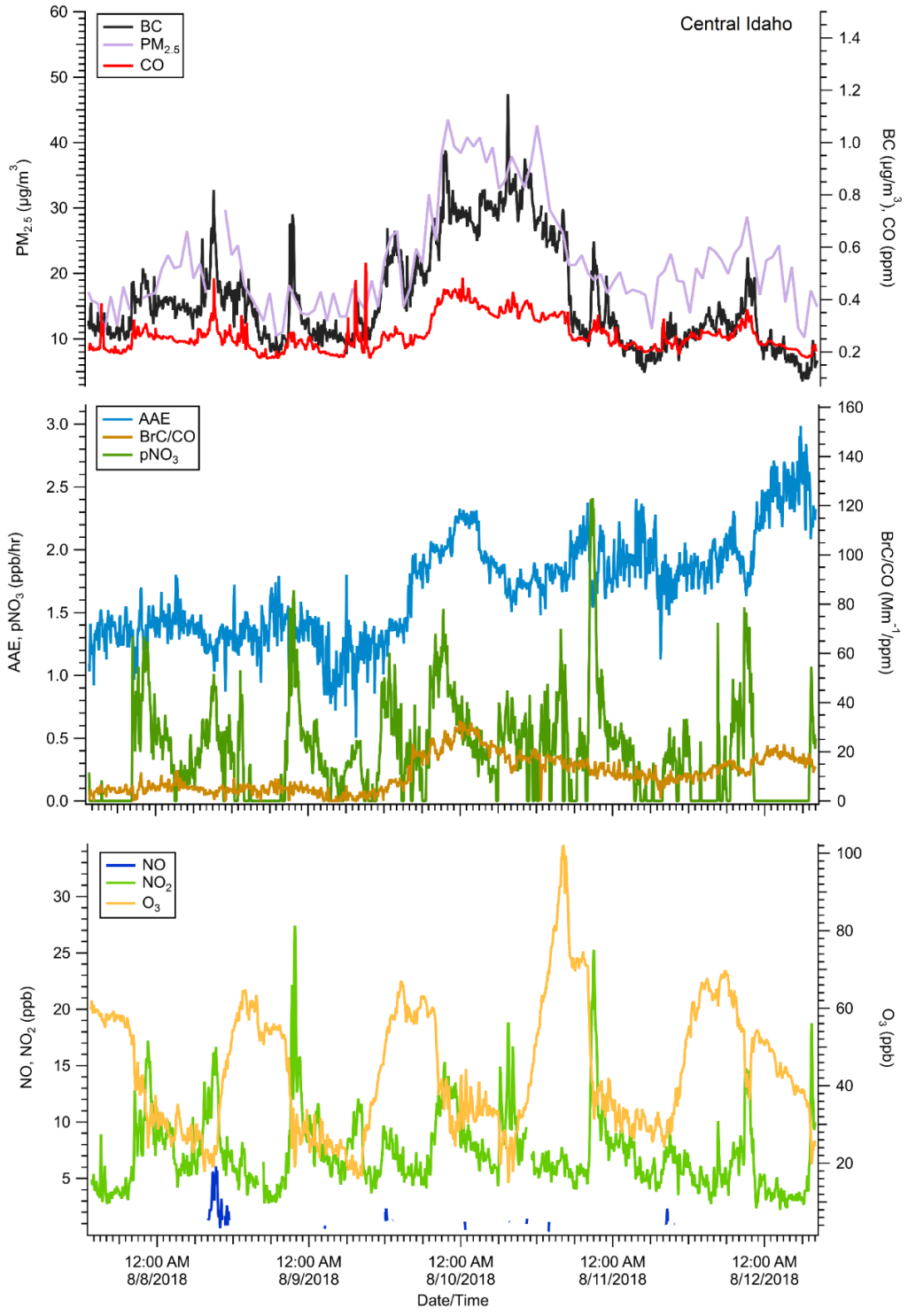

Figure 0.2 Time series of hourly $PM_{2.5}$, 5-minute BC, CO, NO_x, and O_3 measurements from Missoula. Hourly derived AAE and calculated p(NO_3) using 5-minute measurements of NO_2 and O_3 are also shown. Graph label (Central Idaho) represents our best guess at smoke source location based on satellite observations and back trajectory calculations.

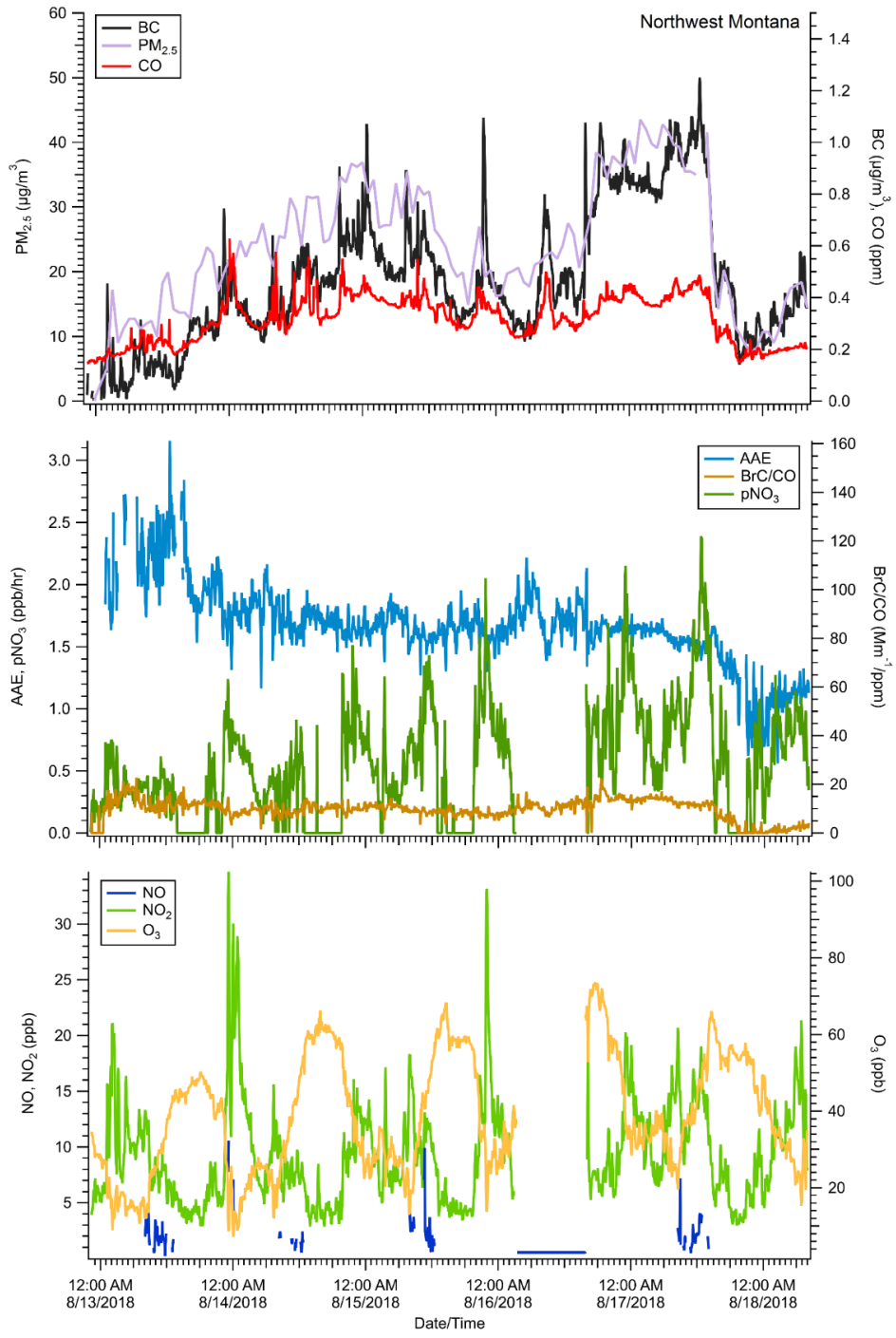

Figure 0.3 Time series of hourly $PM_{2.5}$, 5-minute BC, CO, NO_x, and O_3 measurements from Missoula. Hourly derived AAE and calculated p(NO_3) using 5-minute measurements of NO_2 and O_3 are also shown. Graph label (Northwest Montana) represents our best guess at smoke source location based on satellite observations and back trajectory calculations.

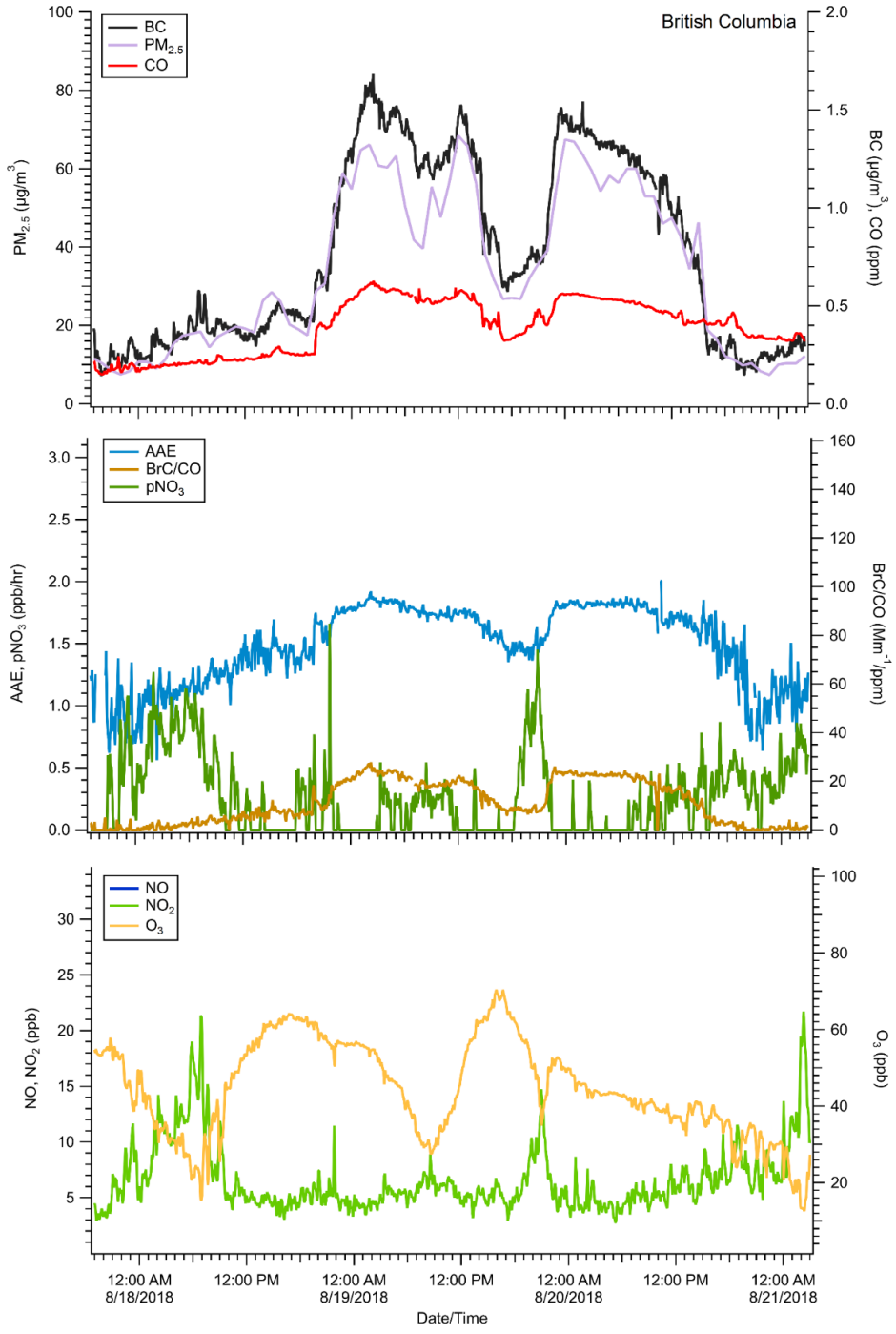

Figure 0.4 Time series of hourly $PM_{2.5}$, 5-minute BC, CO, NO_x, and O_3 measurements from Missoula. Hourly derived AAE and calculated p(NO_3) using 5-minute measurements of NO_2 and O_3 are also shown. Graph label (British Columbia) represents our best guess at smoke source location based on satellite observations and back trajectory calculations.

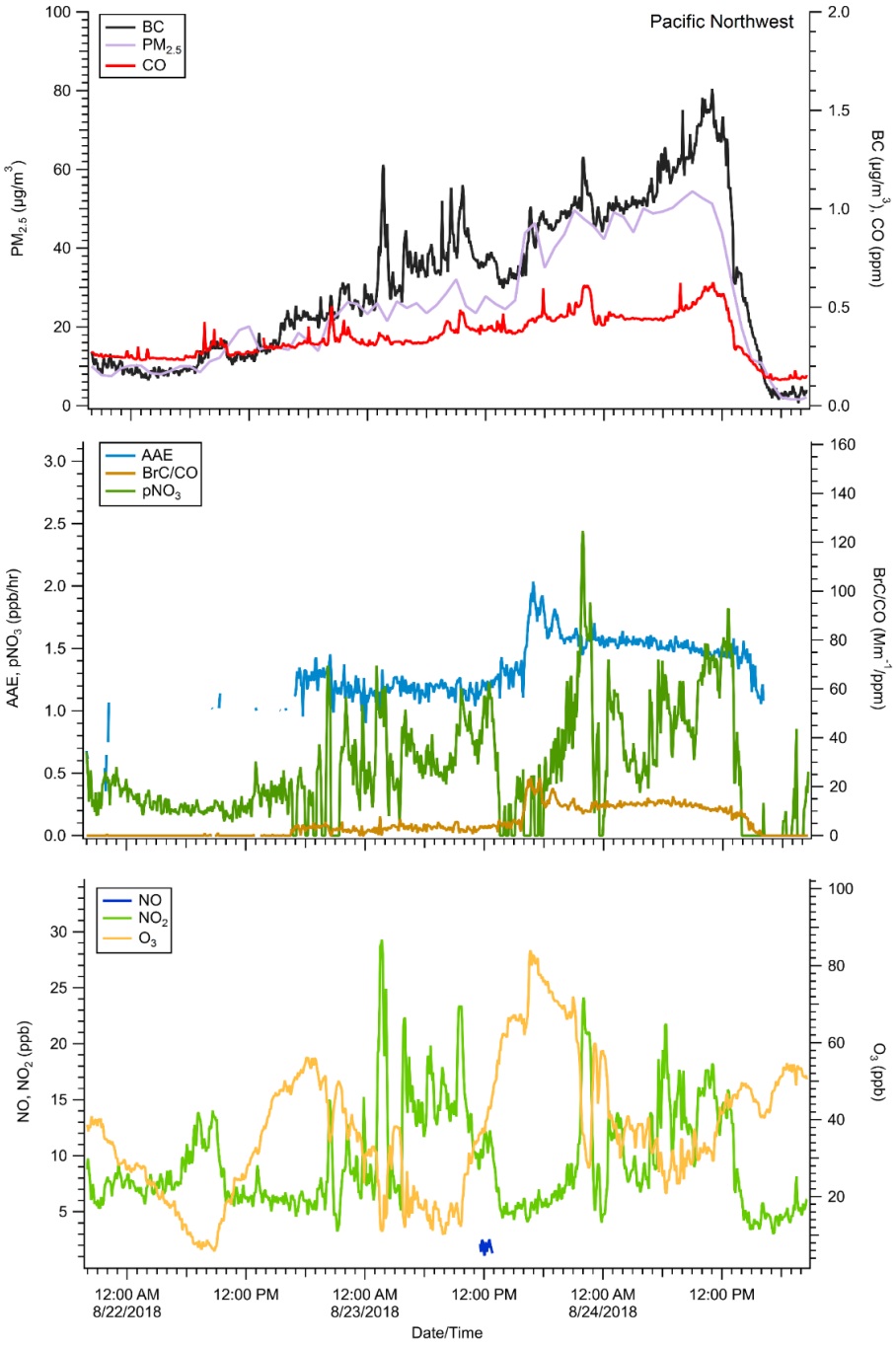

Figure 0.5 Time series of hourly $PM_{2.5}$, 5-minute BC, CO, NO_x, and O_3 measurements from Missoula. Hourly derived AAE and calculated p(NO_3) using 5-minute measurements of NO_2 and O_3 are also shown. Graph label (Pacific Northwest) represents our best guess at smoke source location based on satellite observations and back trajectory calculations.

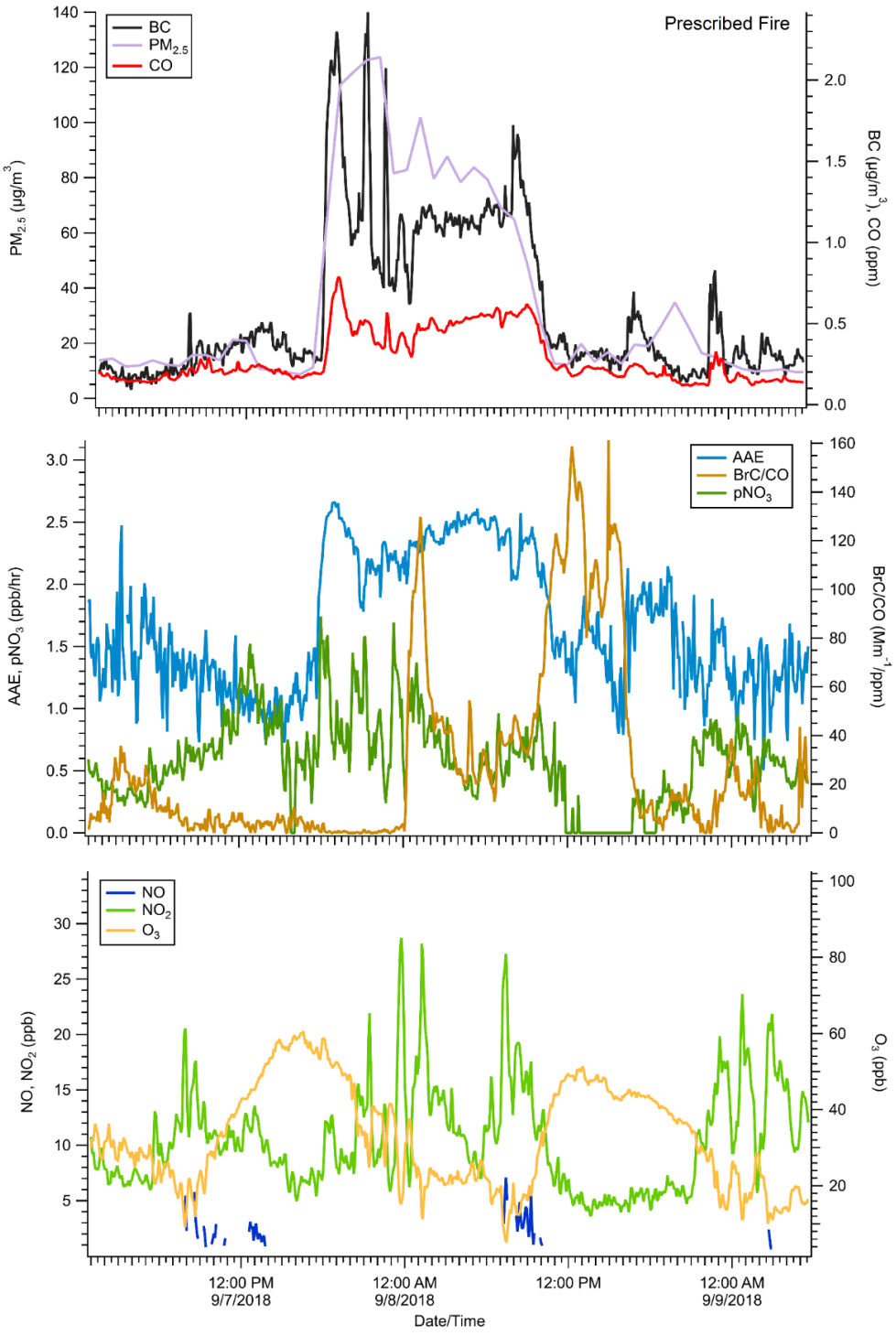

Figure 0.6 Time series of hourly $PM_{2.5}$, 5-minute BC, CO, NO_x, and O_3 measurements from Missoula for the one prescribed fire measured. Hourly derived AAE and calculated p(NO_3) using 5-minute measurements of NO_2 and O_3 are also shown.

Figure 0.7 Comparison of "cut-off" conditions (top photo), to typical "smoke impacted conditions" shown in the bottom photo.

5.7 Results and discussion

5.7.1 O_3

Numerous airborne studies have documented O_3 formation in smoke plumes (Akagi et al., 2013; Liu et al., 2016) and several studies have suggested that wildfires can also lead to an increase in the amount of ground-level O_3 (Brey and Fischer, 2016; Liu et al., 2016; Morris et al., 2006). For instance, wildfire emissions enhanced average summertime monthly mean O_3 by 2-8 ppb in the Intermountain West (Jaffe et al., 2018). In another study boundary layer O_3 showed more influence from local, continental or marine sources, while observations at high elevation sites (1.5—3.0 km above sea level) showed greater influence from large-scale downward mixing of free tropospheric air and from transport of photochemically aged plumes from wildfires (Ambrose et al., 2011). In general, the total amount of O_3 in an area is a complex combination of the relative amounts of NMOGs and NO_x, meteorological conditions supporting local production, and the amount of O_3 present in background/transported air (Lindaas et al., 2017). In this section we investigate the effect of both dilute, aged (up to several days) wildfire smoke and thicker, moderately fresh (~3 hour old) prescribed fire smoke on O_3 levels in Missoula by comparing the amount of O_3 present in typical conditions during clear sky to smoke impacted days.

The two largest mixing ratios in our five-minute O_3 data are associated with aged smoke from Idaho (102 ppb, Fig, 5.2) and Washington (82 ppb, Fig. 5.5). O_3 values associated with aged smoke from Idaho occurred during higher than normal daily maximum temperatures (38ºC), but the O_3 values associated with aged Washington smoke were in cooler air in comparison (25ºC). Although higher temperatures are associated with higher O_3 values, the fact that these peaks are

about 45 and 25 ppb higher, respectively, than the typical summertime 5-min O_3 maximum in clean air suggests that aged smoke (and the meteorological conditions that favor smoke production) can be associated with significant enhancements in O_3 exposure. To explore this systematically, we used hourly average O_3 data. Diurnal cycles for O_3 in each case are plotted in Figure 5.8a, and were compiled by computing hourly averages from five minute O_3 data, for each hour of the day over the duration of the study.

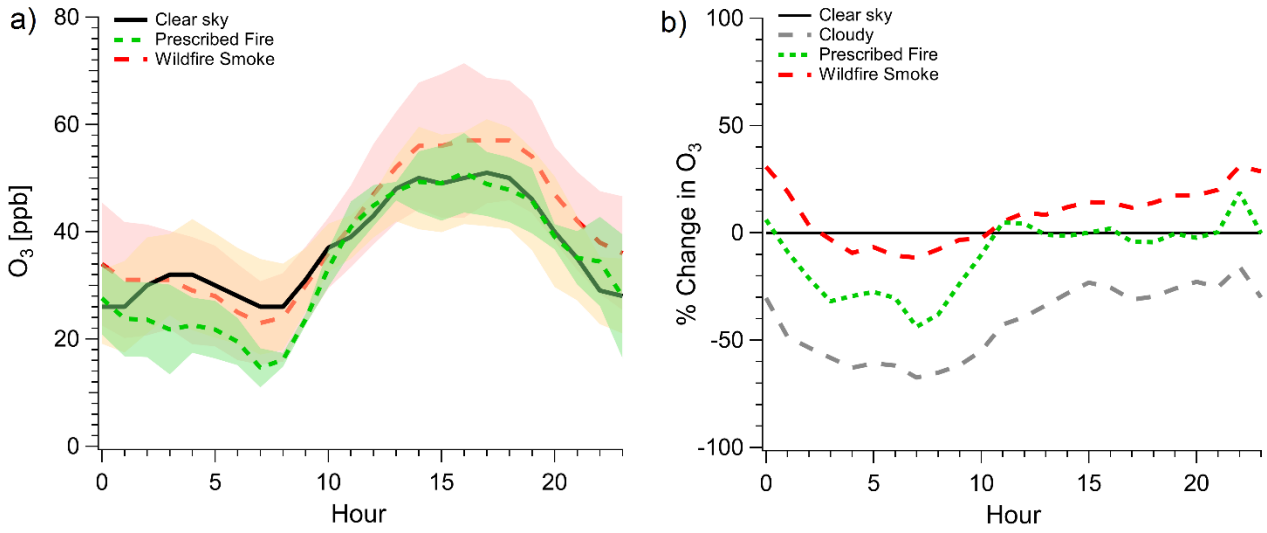

Figure 0.8 Panel (a): A comparison of the 2018 average diurnal cycle of O_3 during clear-sky, wildfire (aged, up to several days) smoke impacted periods, and prescribed (3 hours old) smoke impacted periods. Shaded area in yellow represents ±1σ for clear-sky background values. Shaded area in green represents ±1σ for prescribed fire smoke values. Shaded area in red represents ±1σ for wildfire smoke values. Panel (b): Percent change relative to the average diurnal cycle of O_3 during wildfire smoke impacted, prescribed fire smoke impacted, and cloudy days.

To facilitate discussion, we divided the study data into 4 categories with the average daily $PM_{2.5}$ and temperature given for each category in parentheses. "Clear" days (6.8±1.9 μg m^{-3}, 19±3.6 ºC) and "cloudy" days (7.2±2.2 μg m^{-3}, 14±2.3 ºC) were verified using historical weather data (https://www.wunderground.com/history/) and satellite retrievals (http://rammb-slider.cira.colostate.edu/) and had good AQ with $PM_{2.5} \leq 12.5$ μg m^{-3}. "Wildfire" (26±16.5 μg m^{-}

^{3}, 21±3.3 ºC) and "prescribed fire" days (87 µg/m^3, 20 ºC) had $PM_{2.5}$ > 12.5 µg/m^3 due to these fire types respectively. Although we acknowledge that O_3 exhibits a temperature dependence and typical concentrations vary seasonally, on clear days hourly-average O_3 mixing ratios remained fairly consistent around 50 ± 5 ppb during the afternoon and 30 ± 5 ppb at night throughout the monitoring period. Figure 5.8 shows increases in O_3 diurnal cycle mixing ratios throughout most periods of the day during wildfire smoke-impacted times, compared to the average clear sky diurnal cycle. The O_3 mixing ratio averaged over the whole of the diurnal cycle was, on average, ~6 ppb (15%) higher during wildfire smoke-impacted periods than during clear sky periods. Conversely, the O_3 mixing ratio averaged over the whole of the diurnal cycle was on average ~4% lower during the prescribed fire (thick smoke) impacted period than clear sky conditions; most likely due to reduced photochemical production associated with high $PM_{2.5}$ and BrC levels (Baylon et al., 2018). McClure and Jaffe (2018) observed a consistent pattern in Boise, ID in summer 2017 where smoke enhanced O_3 up to 60-70 µg/m^3 $PM_{2.5}$, but reduced O_3 at higher $PM_{2.5}$ levels. In Missoula in 2018, we observe the largest relative enhancements of O_3 during aged, wildfire smoke impacted periods after sunset and persisting for several hours after midnight with the mixing ratio of O_3 on average, ~9 ppb (23%) higher than corresponding average clear sky periods. This suggests that aged smoke could prolong the O_3 lifetime in the dark or that wildfire smoke enhanced daytime O_3 formation upwind of Missoula more than in Missoula, and these air masses arrived in Missoula after dark, with the latter case implying substantial regional enhancement in O_3 due to wildfire smoke.

Smoke evolution was studied in isolated BB plumes by combining field observations during the Southeast Nexus (SENEX) campaign with chemical box modeling using laboratory derived BB emission factors (EFs) measured as part of the Fire Influence on Global and Regional

Environments (FIREX) campaign (Selimovic et al., 2018; Koss et al., 2018). The model of Decker et al., (2019) showed that although a change in the ambient concentration of O_3 has little effect on the relative reactivity of nighttime oxidants such as NO_3 and O_3, including night-time O_3 oxidation in photochemical models should still be critical, as it has potential to affect next day photochemistry. For instance, Decker et al., (2019) reported that while the nighttime oxidation of NMOGs produced by BB for some fuels is dominated by NO_3, in some cases, oxidation by O_3 remains significant (e.g. 43% for ponderosa pine fires). An important note however is that these model results are lower limits that are applicable to the center of a young BB plume and do not include later dispersion, where non-BB sources of NO_x mixed with O_3 downwind generate NO_3 and lead to additional depletion of BB-NMOGs. This mixing effect is likely most significant in urban areas impacted by BB plumes. Urban sources of NO_x mixed with ambient background O_3 and elevated O_3 formed in aged plumes can contribute to additional oxidation and depletion of BB produced NMOGs.

5.7.2 NO_x

NO_x is effectively a precursor to two main atmospheric oxidants (O_3 and NO_3) and its chemistry is related to BrC as noted earlier. We note that for the majority of our sampling period, (≥ 95% of the time), our NO values were below detection limits. Further, when we did briefly measure NO during smoke impacted periods, the NO/NO_2 ratio was about ~0.23. Thus, our NO_x measurement is mostly a measurement of NO_2. NO_x/CO is usually about 1-2% in fresh forest fire plumes and after 2-3 hours NO_x is converted chiefly to PAN and particle nitrate in roughly equal amounts with ΔPAN/ΔCO observed as ~0.3% in aged wildfire smoke impacting Boise, ID (Akagi et al., 2011, 2012, Liu et al., 2016, 2017; McClure and Jaffe, 2018). During 2018 impacts in Missoula from smoke aged ~20 hours our 5-minute data shows NO_2 as peaks that are ~20-30

ppb (about 10-15% of CO) and poorly correlated with CO confirming a mostly local source (Figs 5.2—5.6). Some of the largest NO_x peaks occur after dark before midnight, and NO_2 peaks are dramatically anti-correlated with O_3, which is consistent with high NO_3 production rates (Figs 5.2—5.6) We investigate the interaction with both wildfire and prescribed fire smoke in an analysis identical to the analysis done for O_3, whereby diurnal cycles of NO_x were plotted by computing hourly averages from 5-minute NO_x data, for each hour of the day over the duration of the study. Figure 5.9 shows that were no significant changes to the diurnal cycle of typical "clear-sky" concentrations of NO_x during either aged wildfire-smoke impacted periods or moderately fresh prescribed fire impacts. For the duration of the study, NO_x for both of the latter periods remained within the range of typical ambient concentrations, again suggesting our measured NO_x is likely the result of local emissions.

The trend in the hourly average diurnal cycle loosely resembles a traffic source peaking during morning traffic and afterwards diluting. Plume dilution and rapid loss of NO_x as smoke is transported away from a fire suggests slowing of O_3 formation downwind. However, several studies show that urban sources of NO_x mixed with biomass burning plumes can lead to an increase in O_3 (Jacob et al., 2010; Lee et al., 2009), and the highest O_3 formation rates in smoke plumes sampled by Akagi et al., (2013) occurred when a plume was mixed with urban emissions. Thus, our measurements of urban NO_x are likely critical to explaining some portion of the daytime O_3 enhancements discussed in the previous section.

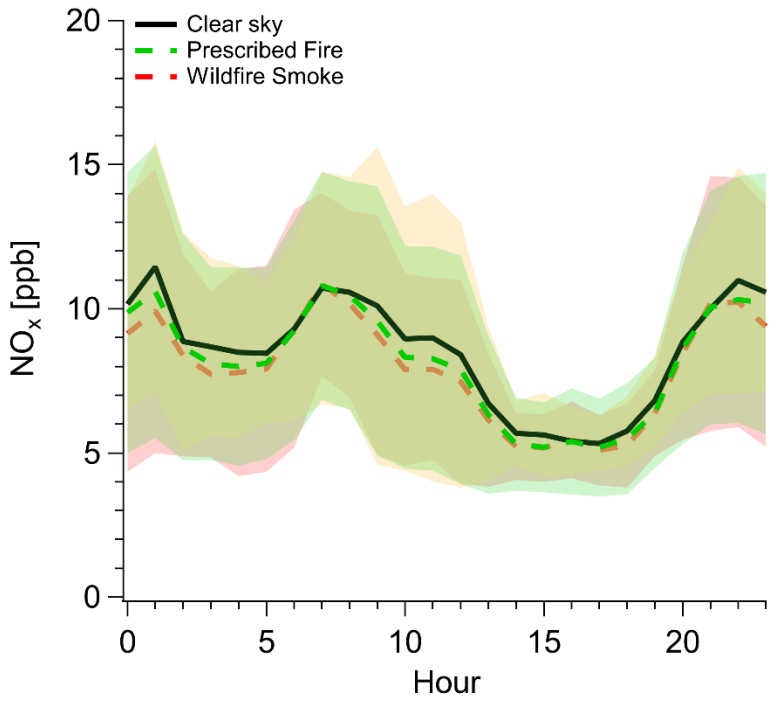

Figure 0.9 Average hourly diurnal cycles of NO_x measured in the Missoula valley calculated from 1 hour averages of 5-minute data. Shaded area in yellow represents ±1σ for background values. Shaded area in green represents ±1σ for prescribed fire smoke values. Shaded area in red represents ±1σ for wildfire smoke values.

5.7.3 NO_3 Production

$P(NO_3)$ is the instantaneous formation rate of NO_3 through reaction of NO_2 and O_3 calculated via the following: $P(NO_3) = K_{NO3}[NO_2][O_3]$ ($k=3.2 \times 10^{-17}$ cm^3 $molec^{-1}$ s^{-1} at 298 K; Burkholder et al., 2015). Reactions of NO_3 with many NMOGs are efficient and can lead to the production of organic nitrates and secondary organic aerosol (Brown et al., 2012), altering nighttime oxidative budgets. Several studies show NO_3 leading to formation of secondary BrC aerosol, suggesting that nighttime oxidation may be a significant source of BB derived BrC, which has potential to affect next-day photochemistry (Palm et al., 2017; Laskin et al., 2015; Mohr et al., 2013; Iinuma et al., 2010). Using laboratory emission factors measured at the Missoula Fire Sciences Lab in

2016 (Selimovic et al., 2018; Koss et al., 2018), Decker et al. (2019) modeled an NO_3 production rate ($P(NO_3)$) of 1 ppbv hr^{-1} in fresh plumes, and here we present complementary evidence of high $P(NO_3)$ occurring in aged smoke. Although NO_3 is rapidly photolyzed during the day, we calculate $P(NO_3)$ during night and day, because high NMOG concentrations and suppression of photolysis in thick smoke might make reactions of NO_3 competitive with photolysis. Figs. 5.2—5.6 show numerous $P(NO_3)$ peaks above 1 ppb/hr and some above 2 ppb/hr. Figure 5.10 plots high resolution (5 minute) data of O_3 and NO_2 as a function of calculated $P(NO_3)$. Although the highest instances of $P(NO_3)$ were observed during wildfire smoke impacted periods (2.44 ppbv hr^{-1}) (Fig. 5.10d), on average, $P(NO_3)$ was highest during prescribed fire impacts (Fig 5.10c).

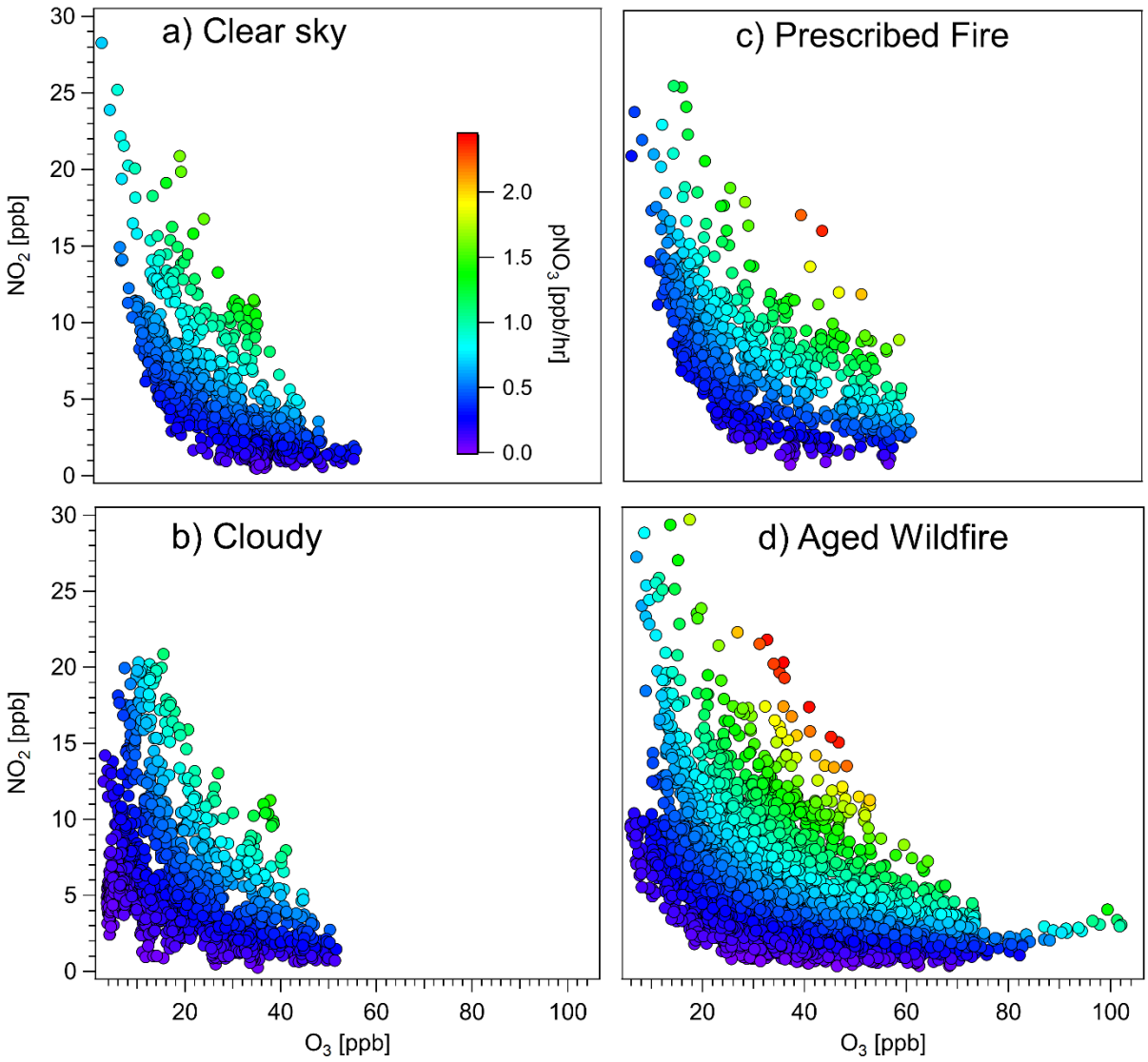

Figure 0.10 NO_2/O_3 plots colored by pNO_3. Panel (a) represents typical clear sky conditions, panel (b) represents cloudy and clean conditions, panel (c) represents prescribed-fire (3 hours old) smoke conditions, panel (d) represents aged (up to several days) wildfire smoke impacted conditions.

The average $P(NO_3)$ for wildfire impacts was 0.57 ± 0.36 ppbv hr^{-1}, and the average for prescribed fire impacts was 0.66 ± 0.32 ppbv hr^{-1}. In both cases, $P(NO_3)$ is higher than when compared with clear, smoke-free $P(NO_3)$ (0.47 ± 0.26 ppbv hr^{-1}) and during cloudy periods (0.35 ± 0.25 ppbv hr^{-1}). In Figure 5.11, we investigate diurnal trends in $P(NO_3)$ by calculating hourly

averages from 5-minute data of O_3 and NO_2 and then plotting them as a function of the hour of day. A weak trend shows that high $P(NO_3)$ is driven by large percentage increases in NO_2, which has implications for when/where NO_3 is formed. For example, at the plume source, where BB-NO_2 is abundant, NO_3 production is likely high, as shown in Decker et al. (2019). In addition, our data confirms that formation of NO_3 in smoke downwind of fires due to "added" NO_2 is also important, and was most important after sunset. This is likely due to non-fire sources of NO_2 (urban) or, to a lesser degree, lightning and NO_2 from the thermal decomposition of fire-generated PAN mixing with enhanced levels of O_3 in aged plumes driving NO_3 production.

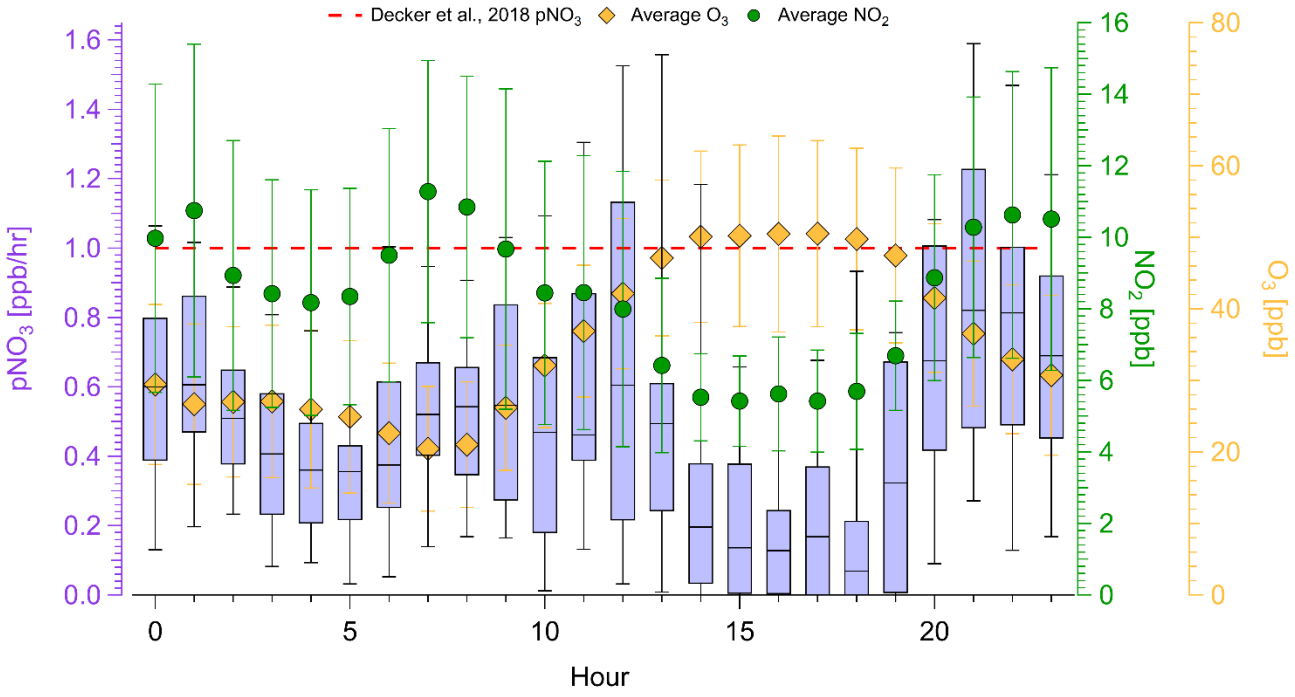

Figure 0.11. Hourly diurnal box and whisker plot of pNO_3 plotted with hourly diurnal plots of O_3 and NO_2. Values were derived from hourly averages of 5-minute wildfire smoke impacted data. Error bars on O_3 and NO_2 represent 1σ.

5.7.4 $\Delta BC/\Delta PM_{2.5}$, $\Delta BC/\Delta CO$, $\Delta PM_{2.5}/\Delta CO$

We begin this section with a summary of the importance of the $\Delta BC/\Delta CO$, $\Delta BC/\Delta PM_{2.5}$ and $\Delta PM_{2.5}/\Delta CO$ ratios. Although BC is estimated to be the second strongest global climate warming agent, accurate measurements of ambient BC and BC EFs remains challenging, and aerosol absorption remains a large contributor to uncertainty in models (Bond et al., 2013; Li et al., 2019). CO emissions estimates are in reasonable agreement for western wildfires (Liu et al., 2017), and can be used to derive BC emissions estimates. For example, combining the measurements of these two "inert" tracers into a $\Delta BC/\Delta CO$ ratio can be used with CO emissions to update BC emissions estimates from wildfires, which could improve model input and further assist in validating current models. In addition, BC is only made by flaming combustion at the fire source, and although its production can differ vary with flame turbulence (Shaddix et al., 1994), the $\Delta BC/\Delta CO$ ratio can be used as a rough indicator of the fire flaming to smoldering ratio, as demonstrated in Selimovic et al. (2019) Figure 2b. Turning to reactive species, a rough metric for the net effect of secondary formation and evaporation of organic and inorganic aerosol is provided by changes in the $\Delta PM/\Delta CO$ ratio as smoke ages. However, as referenced in the Introduction, there remains much ambiguity about the factors controlling the evolution of this ratio as smoke is transported downwind, and, in addition, few studies provide this ratio in heavily-impacted surface locations which is critical in assessing model predictions of surface air quality, especially as it relates to impacts on populated areas (Bian et al., 2017; Lim et al., 2019; Ahern et al., 2019; Morgan et al., 2019). BC/PM can also indicate PM evolution and roughly indicate climate impacts.

Table 5.1 reports our 2018 $\Delta BC/\Delta CO$, $\Delta PM_{2.5}/\Delta CO$, and $\Delta BC/\Delta PM_{2.5}$ mass ratios for aged wildfire smoke impacts and for the one fresher prescribed fire smoke impact. $\Delta BC/\Delta PM_{2.5}$ ratios were calculated by computing 1 hour averages of 5 minute BC derived from PAX 870 absorption data and then plotted against 1 hour $PM_{2.5}$ data (Fig. 5.12). In Fig. 5.12 we plotted all the wildfire points together to show good overall correlation and illustrate one method of obtaining an time-weighted average. The individual $\Delta BC/\Delta PM_{2.5}$ ratios for the four 2018 wildfire-smoke events are 0.0183, 0.020, 0.0225, and 0.0242 (average 0.0213 ± 0.002 g/g) (Table S6). The variability is only about 10% of the mean and the average computed this way is ~12% lower than plotting all points together. $\Delta BC/\Delta CO$ ratios were calculated as described in the methods section using integrated 5-minute data to account for, and maintain the high time resolution. $\Delta PM_{2.5}/\Delta CO$ was solved for using the two ratios calculated above.

Table 0.1 Study average enhancement ratios (g g^{-1}) ratioed to CO, compared to ratios reported in other studies.

Study	Fire Type[a]	Age (h)	ΔBC/ΔCO	$\Delta PM_{2.5}/\Delta CO$	$\Delta BC/\Delta PM_{2.5}$
This work	WF	20 (10)	0.0026 (0.0007)	0.107 (0.0278)	0.0243 (0.0002)
	PF	~ 3	0.0026	0.165	0.0157 (0.0011)
Selimovic et al., 2019[b,c]	WF	4—20	0.0014 (0.0006)	0.1263 (0.0015)	0.0107 (0.0003)
Garofalo et al., 2019[d, e]	WF	0—6	--	0.201 (0.045)	--
McClure and Jaffe, 2018	WF	--	--	0.119 (0.01)	--
Liu et al., 2017[d,e, f]	WF	0—2	0.0016 (0.0018)	0.2661 (0.1342)	0.0060 (0.0054)
Collier et al., 2016[d, e]	WF	0—48	--	0.237 (0.082)	--
May et al., 2014[d, g]	PF	0—2	--	0.11 (0.01)	--
Sahu et al., 2012	PF	--	--	--	0.048

[a] WF stands for wildfire, PF stands for prescribed fire.
[b] BC measurements at 1.0 micron cutoff
[c] BC values reported from 2017 have been adjusted 13% to account for dryer losses in the PAX instrumentation.
[d] PM values reported are $PM_{1.0}$.
[e] High altitude samples.
[f] Average of Rim Fire and Big Windy Complex. BC data were analyzed for Liu et al., 2017, but not reported.
[g] Values for the Shaver and Turtle fires (prescribed burns in coniferous ecosystem in Sierra Nevada mountains)

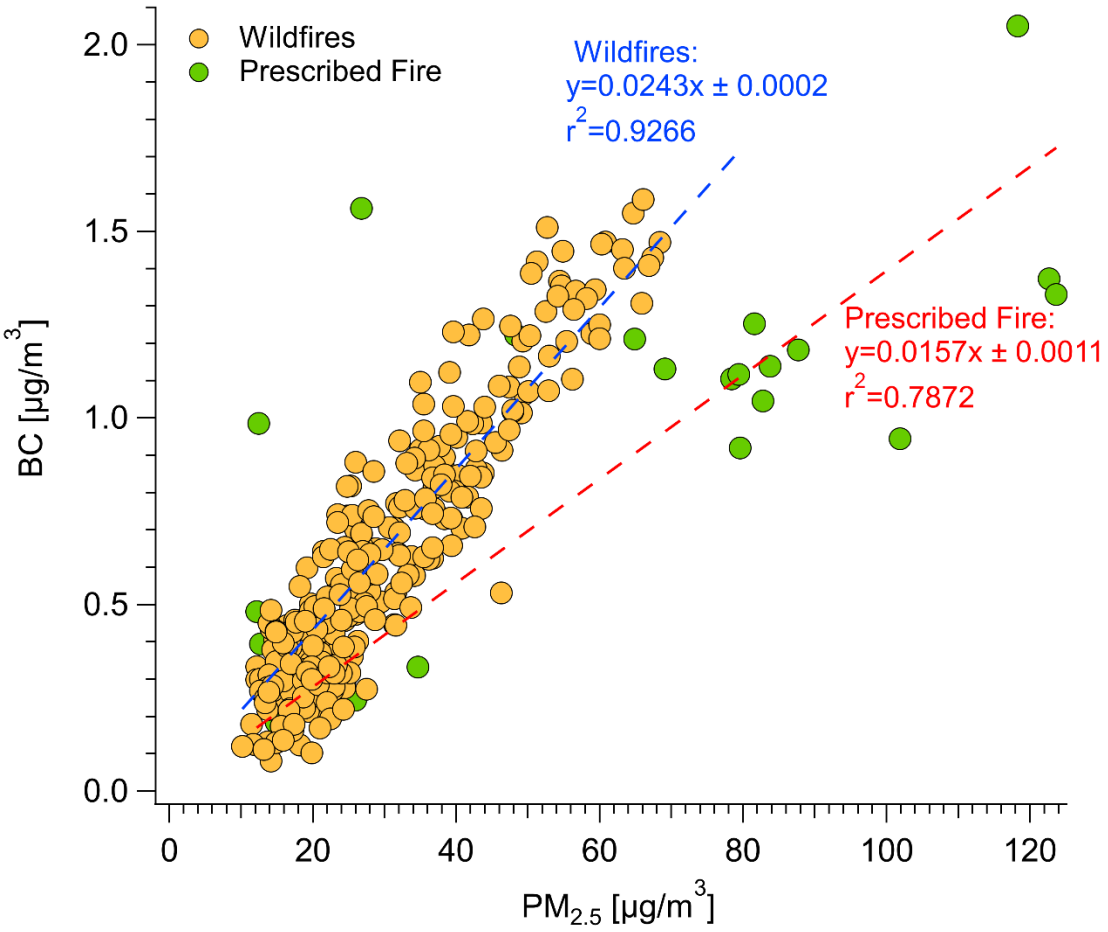

Figure 0.12. Hourly BC versus hourly $PM_{2.5}$. Slopes represent the corresponding BC/PM ratio.

We assess our results by comparing them in Table 5.1 to the previous 2017 measurements of ambient smoke in the Missoula valley (Selimovic et al., 2019) and to airborne measurements (Liu et al., 2017; May et al., 2014; Sahu et al 2012). Our 2018 wildfire ΔBC/ΔCO ratio (0.0026 ± 0.0007) is roughly two times higher than in the 2017 wildfire smoke (0.0014 ± 0.0006) measured by Selimovic et al., (2019). While it's difficult to assess the exact reason for the 2017 to 2018 differences, a likely combination of several factors exist to potentially explain them. First, the wildfire smoke impacting Missoula in 2017 was from closer fires, which could enhance impacts of smoke more dominated by smoldering combustion and with lower BC/CO, as shown in

Selimovic et al., (2019). Equivalently, assuming BC and CO remain inert during transport, our higher ΔBC/ΔCO ratio in 2018 could be indicative of fire emissions more dominated by flaming combustion, which were lofted by convection and then transported to the Missoula valley. Additionally, the PAX 870, which we use to derive our BC measurements, does not discriminate against any coating effects, so it is possible that our 2018 BC values are more inflated by lensing effects than in the younger 2017 smoke. Switching from a 1.0 μm to a 2.5 μm cyclone would add additional mass and could potentially lead to larger values in PAX 870 absorption. Even though BB-BC is nearly all sub-micron, other super micron components (micro-char, dust) may absorb weakly and cause larger calculated values of BC (Han et al., 2009; Clarke et al., 2004). Although the mass in the 1.0-2.5 μm range is thought to be a small part of the total mass (Reid et al., 2005a Fig. 2), the size range difference does affect data interpretation. Overall, despite the above caveats, in summary, it's significant that our ground-based, downwind 2-yr average ΔBC/ΔCO (0.0020 ± 0.0007) is just 33% higher than the average of the airborne studies of western wildfires (0.0015 ± 0.0018) by Liu et al., (2017) and Sahu et al., (2012) as this is consistent with low bias of either platform towards flaming or smoldering combustion.

Selimovic et al. (2019) coupled the average annual CO emissions by wildfires for 2011-2015 (5240±2240 Gg) from Liu et al., (2017) with their field average ΔBC/ΔCO (0.0014 ±0.0002) to estimate that western US wildfires emit 7.3 ± 3.3 Gg of BC a year. Using the same method described in that study, but now with two years of Missoula ΔBC/ΔCO data included in the field average (0.0018±0.0006), we update that value to 9.4 ± 4.0 Gg of BC produced by wildfires per year. In addition, our ΔBC/ΔCO average across two years times the EF CO for wildfires measured in Liu et al., (2017) (89.3), suggests an EF BC for wildfires of 0.18 g kg^{-1}. Our ΔBC/ΔCO for the summer-time prescribed fire in coniferous fuels in this study (0.0026) is ~2.3

times less than the ΔBC/ΔCO ratio for fall (November) prescribed fire measurements in western US montane fuels reported in May et al., 2014 (0.006); likely reflecting more smoldering consumption of duff and dead/down fuels in the summer prescribed fire.

Our surface $\Delta PM_{2.5}/\Delta CO$ ratios for aged wildfire smoke across both years (0.1167 ± 0.0136) are consistently about half that of fresh wildfire smoke samples acquired at higher altitudes in airborne or mountain-top studies (0.2348 ± 0.0326) (Collier et al., 2016; Liu et al., 2017; Garofalo et al., 2019). Deposition is not a likely cause of our lower surface $\Delta PM_{2.5}/\Delta CO$ since our surface ΔBC/ΔCO is not lower and we see evidence of super-micron aerosol in the plumes (Sect 5.7.6). In addition, our lower $\Delta PM_{2.5}/\Delta CO$ ratios at the surface are consistent with some aircraft samples acquired at relatively lower elevations and latitudes and likely warmer temperatures (Forrister et al., 2015; Capes et al., 2008). Other ground-based observations of wildfire smoke have seen $PM_{2.5}$/CO ratios similar to our Missoula ratio (0.119 ± 0.01, McClure and Jaffe, 2018). This reinforces the observation from Selimovic et al., (2019) that on timescales up to ~1-2 days, aging and/or higher ambient temperatures at the surface may lead to substantial net OA evaporation. This decrease with age may not occur at high altitude, but significantly reduce downwind surface PM impacts. Our $\Delta PM_{2.5}/\Delta CO$ value (0.165) for the fresher prescribed fire smoke (~3 hours old) is higher than both our 2017 and 2018 values for aged wildfire smoke, but still significantly lower than the airborne wildfire average from Liu at al. (2017). Our prescribed fire $\Delta PM_{2.5}/\Delta CO$ ratio is higher than our wildfire ratio, but has a similar ΔBC/ΔCO ratio (at least for 2018). One potential simple explanation is distance, in that the prescribed fire was closer to the Missoula valley than the wildfires impacting the valley during that same year, and thus experienced less dilution-driven evaporation. Additionally, lower surface temperatures (8ºC —29ºC) during the time of the prescribed fire impact, in comparison to temperatures during

some of the wildfire impacts may have been less conducive to PM evaporation (Li and Shiraiwa, 2019). The ~15% higher $\Delta PM_{2.5}/\Delta CO$ ratio for 2017 wildfire smoke in Missoula may reflect younger average smoke age (Selimovic et al., 2019). Our summer prescribed fire $\Delta PM_{2.5}/\Delta CO$ ratio is 50% higher than the ratio reported for fresh smoke from the fall prescribed fires in western montane fuels in May et al., (2014) (0.11), but May et al., (2015) also note that their $\Delta PM_{1.0}/\Delta CO$ decreased by about a factor of 2 after several hours of aging on at least one prescribed fire. Fuel and measurement differences (additional mass in the 1.0-2.5 μm range) mentioned earlier could also both potentially account for some of the higher PM/CO produced by the summer prescribed fire.

We stress that there is now more than 1000 hours of ground-based data from Missoula suggesting that a typical $PM_{2.5}/CO$ value for aged wildfire smoke at the surface is about half the value in fresh to moderately-aged well-lofted wildfire plumes (Liu et al., 2017; Garafalo et al., 2019; Collier et al., 2016). One airborne wildfire study by Forrister et al., (2015) at lower latitudes and sampling elevations than the other airborne studies is consistent with the downwind net evaporation we apparently observe in Missoula. We also stress that, despite the evidence for PM evaporation during aging, there is strong data discussed next supporting the idea that wildfires produce more PM than spring or fall prescribed fires on a per fuel burned or per area burned basis. Liu et al., (2017) reported that emission factors for $PM_{1.0}$ ($gPM_{1.0}$/kg fuel burned) burned) are almost 4 times higher in wildfires (27.1 ± 6.1) than spring and fall prescribed fires (7.3 ± 4.2, May et al., 2014). Our 2-year average $\Delta PM_{2.5}/\Delta CO$ ratio in aged wildfire smoke (~0.117) is ~1.7 times higher than implied for aged, fall western montane prescribed fire smoke (~0.07) based on May et al., (2014; 2015) suggesting that a signal of the difference in initial PM emissions can survive aging. Fuel consumption in spring/fall prescribed fires at the national level

is typically 7.2 ± 2.7 Mg ha^{-1} (Yokelson et al., 1997; 2013) as opposed to 34.6 ± 9.9 Mg ha^{-1} on wildfires (Campbell et al., 2007; Santín et al., 2015). Combining the emissions and fuel consumption differences implies that wildfires emit 18 ± 14 times more PM per area burned. Although prescribed fires cannot simply replace all wildfires (Turner et al., 2019; Schoennagel et al., 2017) their potential to reduce the level of wildfire impacts deserves more attention. In addition, incorporating higher wildfire initial emissions and temperature-dependent, post-emission OA evaporation may improve models of wildfire smoke impacts (Nergui et al., 2017).

Our study average $\Delta BC/\Delta PM_{2.5}$ ratio for wildfire smoke in 2018 is roughly double our $\Delta BC/\Delta PM_{2.5}$ ratio for 2017 wildfire smoke (Selimovic et al., 2019), and ~4 times higher than the aircraft average $\Delta BC/\Delta PM_{1.0}$ for 2013 wildfires (Liu et al. 2017; Selimovic et al. 2019). Likely reasons for the higher ratio in 2018 include the possible reasons for a higher BC/CO ratio in 2018 mentioned above: e.g., increased lensing in more aged smoke, transport of more flaming smoke, and (less likely) including other absorbers with the $PM_{2.5}$ cutoff. In addition, $BC/PM_{2.5}$ could be higher in 2018 aged wildfire smoke because of more time (on average) for PM evaporation. OA is the main component of wildfire PM (Liu et al., 2017; Schlosser et al., 2017), so the $\Delta BC/\Delta PM$ ratio should be similar to the $\Delta BC/\Delta OA$ ratio, which suggests a "low" MAC in the UV for the wildfire OA (Saleh et al., 2014; section 5.7.6). Our low $\Delta BC/\Delta PM_{2.5}$ ratios across both years (~1-2%), along with high SSA (Sect 5.7.6), further confirm that wildfire aerosol is overwhelmingly organic and strongly cooling. Our summer prescribed fire $\Delta BC/\Delta PM_{2.5}$ is ~3 times lower than the ratio reported for fall prescribed fires in similar fuels in May et al., (2014), which is likely (as noted above) because drier summer burning conditions enables consumption of fuels (e.g., dead/down, duff) that tend to burn by smoldering, but are too wet to burn as efficiently in spring/fall. While we indicate above that wildfires are likely smokier than

spring/fall prescribed fires, which has poor implications for air quality, they also appear to have less positive climate forcing. In any case, again, differences in smoke production and chemistry between wildfires and prescribed fires warrants further research, as more definite conclusions can reinforce land management implications.

5.7.5 UV-Absorption by BrC and AAE

The AAE is an important aerosol optical parameter used for characterization and apportionment studies. Further, the AAE can be used to separate BrC from BC absorption (Liu et al., 2018), and higher AAEs are correlated with absorption that is more dominated by BrC (Pokhrel et al., 2016; 2017; Selimovic et al., 2018; 2019). A lab study with wildfire fuels found that BrC accounted for ~86% of absorption by particles in the UV (401 nm) on average in fresh smoke (AAE of 3.50) which has implications for UV-driven photochemical reactions of O_3 and the lifetimes of e.g. NO_x and HONO (Selimovic et al., 2019). Satellite AAE retrievals and one airborne study indicate that BrC can have a strong impact in fresh wildfire plumes (AAE 2.8—3.75) and significant, persistent impacts in downwind regional haze/plumes (Hammer et al., 2016; Jethva and Torres, 2011; Forrister et al., 2015). There is variability in BrC attribution methods across studies (Forrister et al., 2015; Pokhrel et al., 2017), but despite this, BrC absorption would decrease the climate cooling calculated for purely scattering OA depending on its MAC, lifetime, and the amount emitted (Feng et al 2013; Forrister et al., 2015). Furthermore, sources of BrC not directly emitted from BB, including the photo-oxidation of NMOGs need to be considered. However, these complex processes produce BrC with optical properties and lifetime that are not yet comprehensively evaluated. Mixing state, combustion conditions, chemical transformation and photochemical aging are all factors that can influence the absorption of secondary BrC

(Tomaz et al., 2018; Wang et al., 2017; Laskin et al., 2015; Wang et al., 2014; Ervens et al., 2011; Graber and Rudich, 2006; Fleming et al., 2019).

In Table 5.2 we present two years of in situ smoke/haze data from Missoula showing persistent widespread regional impacts of BrC and the associated AAE values. Smoke age is a key factor. In 2017 the episode with the highest AAE (2.88, 77% BrC absorption at 401 nm) was due to smoke from a wildfire just ~2-4 hours upwind and the 2017 average AAE (for smoke 2-48 hours old) was 1.96 ± 0.38 (51% BrC absorption at 401 nm). The 2018 wildfire smoke was more aged on average (no nearby wildfires) and had a lower study-average AAE of 1.71 ± 0.04 (47% BrC absorption at 401 nm), but the one relatively fresh prescribed fire smoke episode in 2018 had a higher than average AAE of 2.49 (71% BrC absorption at 401 nm).

Table 0.2 Study average AAE and %BrC contribution to absorption at 401 nm compared to other studies.

Ratios	Fire Type	This Work	Selimovic et al., 2019	Selimovic et al., 2018[b]
AAE	WF	1.71 (0.04)	1.96 (0.38)	3.31
	PF	2.49 (0.04)	--	
%BrC	WF	46.55 (0.51)	50.72 (12.78)	78
	PF	70.79 (0.42)	--	--

[a] WF stands for wildfire, PF stands for prescribed fire. Wildfire smoke was more aged (up to several days) than prescribed fire smoke (~3 hours).
[b] Lab fires, calculated from the average of wildfire MCE reported in Forrister et al., 2015.

Remarkably, despite the large range in episode smoke ages across both years, BrC accounted for roughly 50% of the UV-absorption at 401 nm on average both years. The small ~4% difference in % BrC absorption at 401 nm year to year likely indicates that the decrease after emission in net BrC slows significantly after a few hours similar to the observations in the Rim Fire plume (Forrister et al., 2015). In any case obtaining the same average value for moderately aged smoke two years in a row suggests our regional smoke AAE value (~1.7 – 1.9) is a useful target for

model validation, which would be hard to demonstrate in lab studies or airborne studies of a single plume.

It is interesting to speculate about the impact of combustion conditions and nighttime effects on multiday aging of BrC. Selimovic et al., (2018) showed that higher AAE in the initial emissions is associated with more smoldering combustion. Relatively more smoldering as demonstrated by the lower ΔBC/ΔCO ratio in 2017 could have contributed to the higher AAE in 2017 (along with differences in smoke age). In addition, wildfires can produce much of their emissions at times of day shortly before or after photo-bleaching would stop (Saide et al., 2015) and wildfires can have a higher smoldering to flaming ratio at night than during the day (Benedict et al 2017), which would likely enhance emissions of both primary BrC (Selimovic et al., 2018) and BrC precursors. Precursors include monoterpenes, furans, etc., that can react with the major nighttime oxidant, NO_3 to form UV-absorbing organic nitrates. Estimates using current NMOG data strongly suggest that a substantial nighttime secondary BrC source could exist (Stockwell et al., 2015, Gilman et al., 2015, Hatch et al., 2017). Converting even a small fraction of co-emitted NMOGs that are known to react quickly with NO_3 could yield substantial amounts of BrC during dark hours and oxidation of NMOGs by O_3 could also be important, as mentioned previously. Our five-minute data shows a potential example of this in Fig. 5.13. Shortly before 12 AM on 12-August there is a spike in NO_3 production followed by a prominent increase in AAE (from ~1.6 to ~3.0) that lasts until sunrise. The increase in AAE is likely not due to arrival of fresher, usually more concentrated, smoke, which we also commonly see, since hourly $PM_{2.5}$ is simultaneously decreasing.

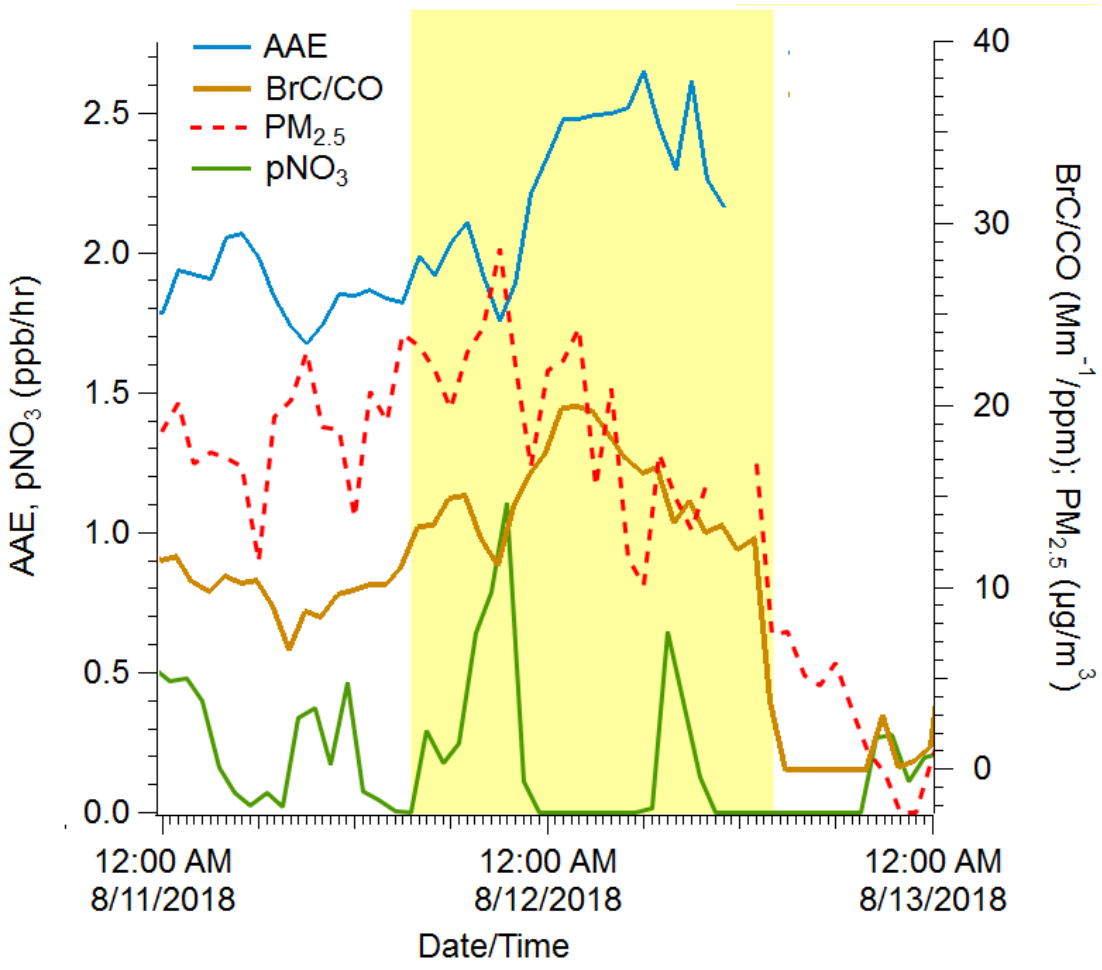

Figure 0.13 A likely example of nighttime, secondary BrC formation. Shortly before midnight a spike in pNO_3 occurs, followed by increases in AAE and BrC/CO as $PM_{2.5}$ decreases, which rules out an influx of fresh smoke. These changes are consistent with increasing BrC content of the aerosol driven by reactions of NO_3 with NMOG.

In Figure 5.14, we show the diurnal cycle of %-absorption by BrC at 401 nm, with night-time production of NO_3. The %-absorption by BrC at 401 nm is slightly enhanced at night (11%) and loosely follows the NO_3 production (enhanced by 29% at night) consistent with a role for the effects discussed above. However, with the data available, we can't completely separate the potential effects of nighttime NO_3 reactions, enhanced smoldering emissions, or transport/mixing. Nonetheless, the presence of NO_3 as a major nighttime oxidant in the

formation of BrC should be considered, as our high NO_3 production rates in an earlier section show.

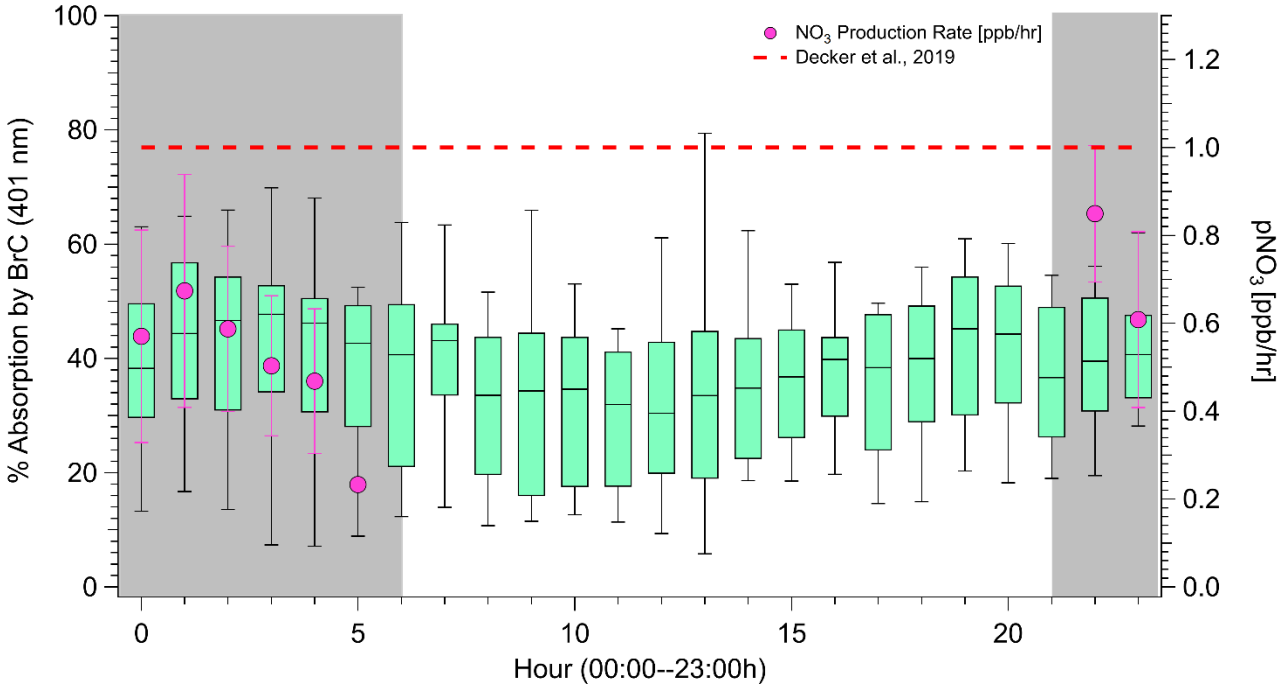

Figure 0.14 Hourly diurnal box and whisker plot of %-Absorption by BrC calculated from hourly averages of wildfire smoke impacted 5-minute data compared to the night-time (shaded area) hourly average pNO_3. Error bars on pNO_3 represent 1σ.

5.7.6 SSA, MAC, MSC

Table 5.3 lists our 2018 study average SSAs, MACs, and MSCs. MACs and MSCs can be coupled with $PM_{2.5}$ data to describe the optical properties of aerosol on a per mass basis. Our MAC and MSC values were obtained by plotting 1 hour averages of $B_{scat}401$, $B_{abs}401$, and $B_{scat}870$, $B_{abs}870$ versus the 1 hour $PM_{2.5}$ values in order to calculate an MSC(401), MAC(401), MSC(870), and MAC(870) (Fig. 5.15). In Selimovic et al. (2019), we produced MAC and MSC values by comparing our scattering and absorption measurements measured at a 1.0 μm cutoff to

$PM_{2.5}$ data that was available. These values were lower limits and are not directly comparable to the ones obtained in this study, where the range for both optical and mass measurements goes up to 2.5 μm. Nonetheless, it is useful to list the results from both studies as a range of values, since 1.0 μm cutoffs are common in field campaigns, but $PM_{2.5}$ still remains the default measurement in regional networks. We also note that going to a $PM_{2.5}$ cutoff may have added ash, micro-char and aerosol that is non-combustion generated, such as dust or primary biological aerosol particles, all of which can be physically entrained in wildfire plumes (Formenti et al., 2003; Gaudichet et al., 1995; Hungershoefer et al., 2008; Mardi et al., 2018; Schlosser et al., 2017; Maudlin et al., 2015; Shingler et al., 2016).

Table 0.3 Study average MAC and MSC compared to other works. United are m^2 g^{-1}.

Parameter	λ (nm)	This Work[a] (WF)	This Work[a] (PF)	Selimovic et al., 2019[b, c]
SSA	401	0.95 (<0.01)	0.95	0.93 (0.01)
	870	0.95 (<0.01)	0.94	0.94 (0.02)
MAC	401	0.43 (0.01)	0.46 (0.03)	0.26 (0.01)
	401 (BrC)	0.18	0.29	0.16
	870	0.12 (<0.01)	0.07 (0.01)	0.05 (<0.01)
MSC	401	7.37 (0.06)	5.88 (0.39)	3.65 (0.07)
	530	4.70	3.25	2.41
	870	2.12 (0.02)	1.13 (0.09)	1.14 (0.02)

[a] In this work MAC and MSC values are $PM_{2.5}$ absorption and scattering value divided by $PM_{2.5}$ mass, and values between 401 and 870 nm are obtained from power law fits

[b] In this work MAC and MSC values are $PM_{1.0}$ absorption and scattering value divided by $PM_{2.5}$ mass, and values between 401 and 870 nm are obtained from power law fits.

[c] MAC and MSC values have been adjusted 13% to account for dryer loss in the PAX instrumentation. SSA is unaffected by this loss.

Several things stand out comparing 2017 and 2018 data in Table 3. The SSA(401) is lower in 2017 (0.93) than 2018 (0.95), but SSA(870) is similar both years consistent with the 2017 smoke being fresher and with higher BrC content. MAC(401) and 870 almost doubled from 2017 to 2018. Since our $\Delta BC/\Delta PM_{2.5}$ also approximately doubled, this makes sense and is not inconsistent with the work of Saleh et al., (2014) who found that the MAC for OA increased with BC/OA (wildfire PM is mostly OA). A contribution to UV absorption from the increased cutoff

and thereby sampling more entrained micro-char or dust (Han et al., 2015; Russell et al., 2010) could also play a role. The latter is supported by the ~25% increase in calculated MSC(530). Although the particles in the 1.0-2.5 µm range contribute perhaps 20% of the total particle mass in BB emissions (Reid et al., 2005a), they contributed significantly to both the total absorption and scattering in 2017-18 smoke, but did not strongly affect the SSA.

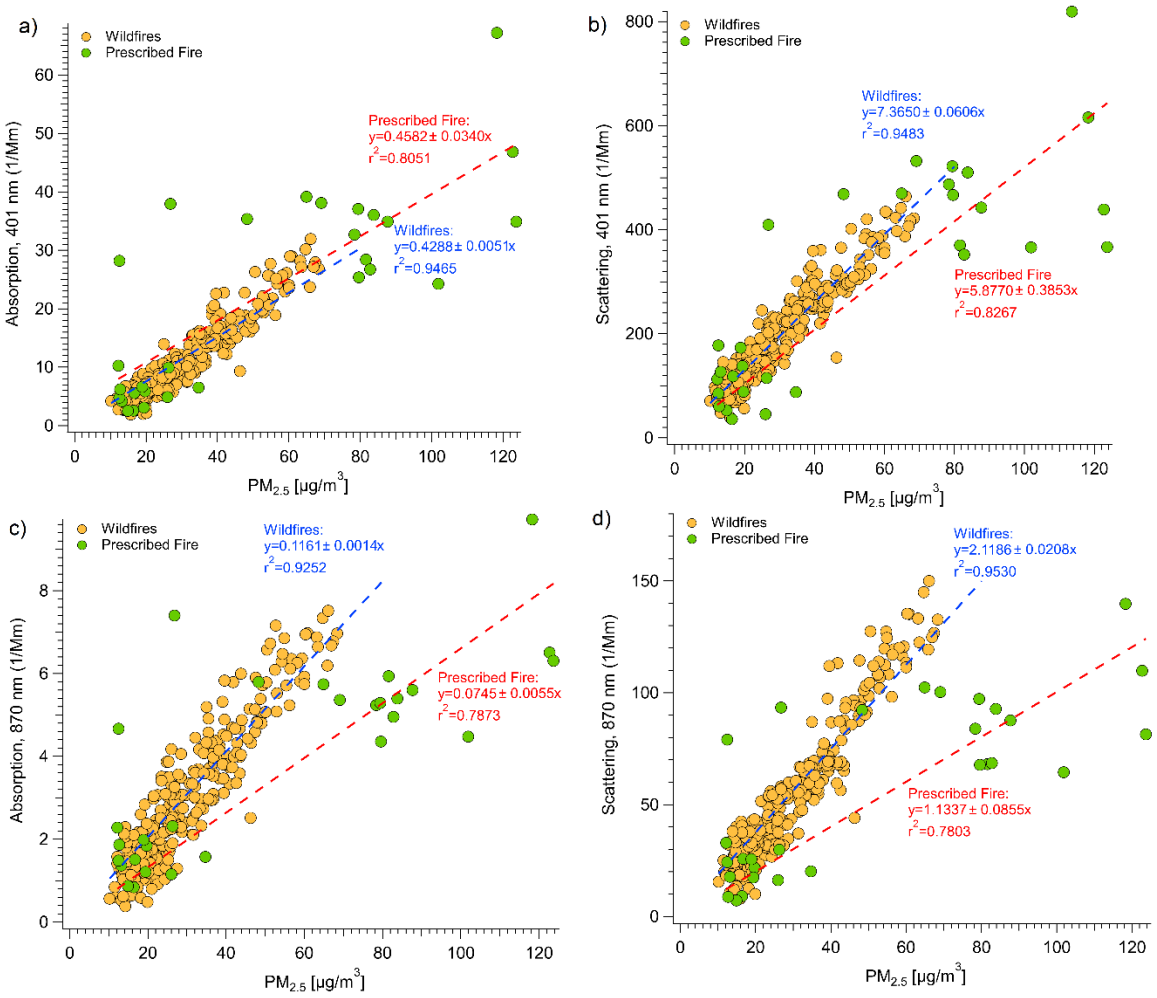

Figure 0.15 (a) Mass absorption coefficient at 401 nm calculated from 1-hr averages of absorption at 401 nm versus hourly average $PM_{2.5}$. (b) Mass scattering coefficient at 401 nm calculated from 1-hr averages of scattering at 401 nm versus hourly average $PM_{2.5}$. (c) Mass absorption coefficient at 801 nm calculated from 1-hr averages of absorption at 870 nm versus hourly average $PM_{2.5}$. (d) Mass scattering coefficient at 870 nm calculated from 1-hr averages of scattering at 870 nm versus hourly average $PM_{2.5}$.

The SSA is frequently used to calculate aerosol absorption and scattering in models and satellite retrievals. Uncertainty in the SSA is one of the main sources of uncertainty in estimating the radiative effect of aerosols (McComiskey et al., 2008; Jiang and Fiengold, 2006), and assuming constant values of SSA throughout the year may sometimes be inaccurate, as shown by Selimovic et al., (2019) in 2017 in Missoula, where the SSA at 870 nm in Missoula increased over a month, and Eck et al. (2013), where the SSA at 530 nm in Southern Africa increased by 0.07 between July and October. These increases are consistent with an increase in the smoldering/flaming ratio as regional fuels dry (Akagi et al., 2011; Liu et al., 2014; Pokhrel et al., 2016); Selimovic et al., 2019). Our study average wildfire SSA at 401 nm is slightly higher than the 2018 study average SSA observed in Selimovic et al. (2019), but falls within the observed variability for 870 nm. Our values at both wavelengths are higher than a typical surface SSA of the earth (~0.9, Praveen et al., 2012), which suggests that overall, the wildfire PM measured in this study would contribute to regional cooling (Thornhill et al., 2018; Kolusu et al., 2015). However, Figure 5.16 shows we do not find an increase in either the SSA at 870 nm or the SSA at 401 nm over the duration of our 2018 sampling period. SSA has been shown to increase as smoke ages (Haywood et al., 2003; Yokelson et al., 2009; Liu et al., 2014), and the additional aging in the 2018 smoke may have obscured any trend based on flaming or smoldering sources, as we received little impact from local sources in 2018, unlike in 2017 (Selimovic et al., 2019).

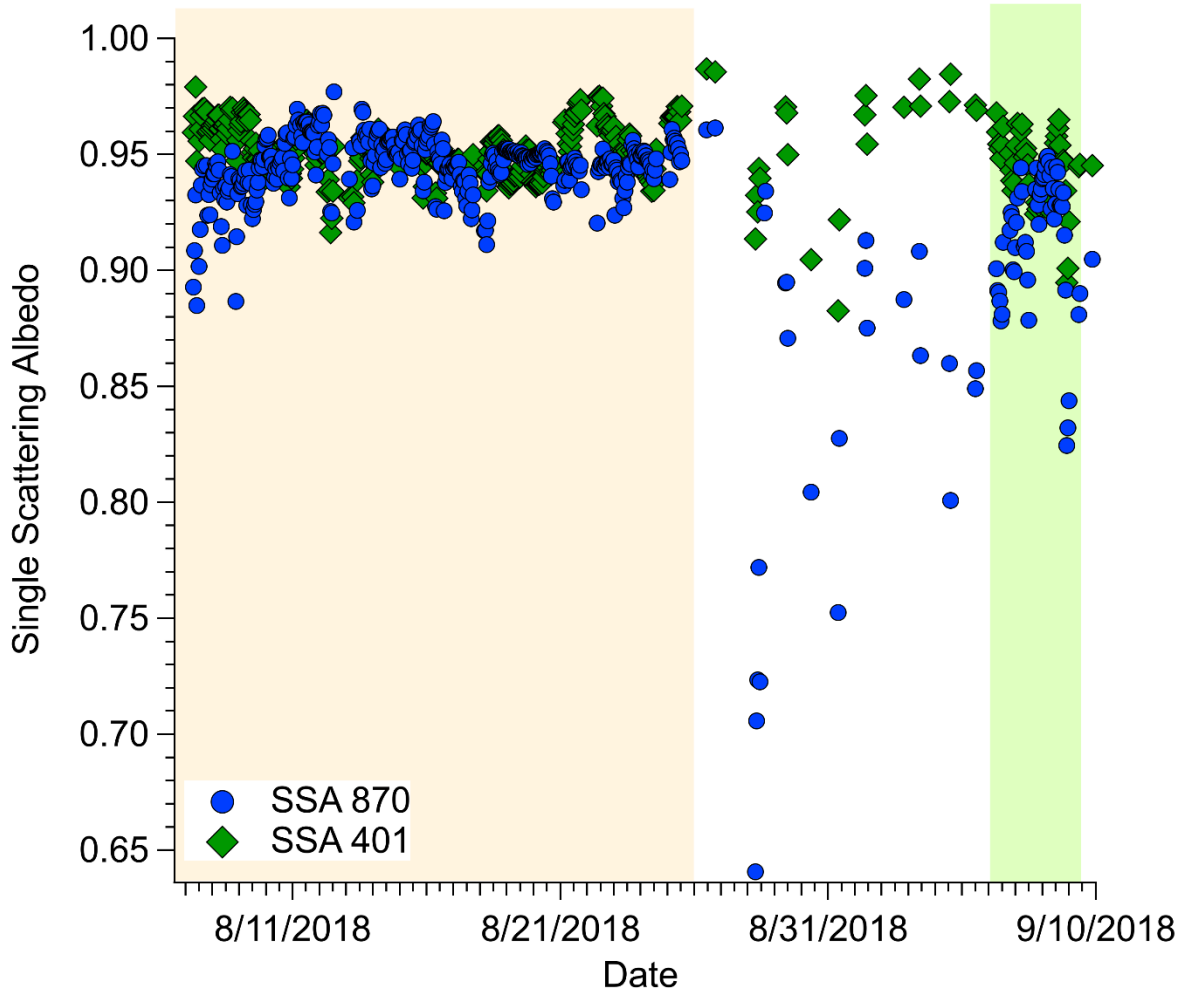

Figure 0.16. Plot of single scattering albedo at 401 and 870 nm versus the entirety of the sampling duration, calculated for each hour. Sections shaded in yellow represent wildfire smoke impacted periods. Sections shaded in green represent prescribed fire smoke impacted periods. Unshaded areas represent anthropogenic impacts.

5.8 Conclusions

In this study, we measured smoke properties in 2018 in Missoula, MT, a western urban center that was downwind of numerous wildfires and one prescribed fire. We sampled over 500 h of smoke impacts characterizing CO, aerosol optical properties, effects of wildfire and prescribed fire smoke on O_3 and NO_3 production, and explored how inert tracers and evolving ratios inform understanding of smoke production and evolution. By comparing and combining with our

measurements of less aged smoke in Missoula from 2017 we analyze data for over 1000 h of ambient smoke from western wildfire fuels, primarily coniferous forests. Our low two-year ΔBC/ΔPM average (0.0175 ± 0.0094) confirms the overwhelmingly organic and thus strongly cooling nature of wildfire smoke, and is in line with observations from other field studies. Our 2018 ΔBC/ΔCO ratio (0.0026 ± 0.0007) is almost double the ratio measured in 2017 in Missoula, and suggests a greater influence from lofted smoke produced by flaming combustion, but the average of our ΔBC/ΔCO ratio across two years (0.0020 ± 0.0007) is close to airborne field observations of wildfire smoke, implying low bias between platforms. Conversely, ΔPM/ΔCO measured at our surface site across both years was consistently ~50% lower than field studies conducted at higher elevations suggesting that OA evaporation at higher temperatures near the surface may reduce wildfire PM air quality impacts.

On average, O_3 was enhanced when wildfire smoke was present by ~15% (6 ppb) relative to typical clear-sky levels, with the largest percentage enhancements occurring after sunset and before midnight. The larger O_3 increase after dark likely implies widespread, regionally-enhanced O_3 production upwind, but the arrival of thick smoke just before dark during the prescribed fire impact may have suppressed morning O_3 formation. There appeared to be no smoke impacts on the diurnal cycle of NO_x, suggesting that for the duration of the study, NO_x was likely the result of local emissions. However, NO_3 production rates were significant and slightly elevated relative to background conditions when both wildfire and prescribed fire smoke were present.

On at least one occasion, a nighttime increase in AAE followed, and was likely due to, a spike in $P(NO_3)$. On average, the contribution to absorption at 401 nm by BrC was slightly enhanced at

night and loosely followed NO_3 production, but this warrants more study. Despite the large range in episodic smoke ages across both years, BrC accounted for roughly 50% of the UV-absorption at 401 on average, signifying wide-spread persistence of BrC even as smoke ages and is transported downwind. Obtaining similar AAE values for moderately aged smoke two years in a row implies that our regional smoke AAE value (1.7—2.0) is a useful target for model validation. The SSA at both wavelengths remained consistent over the course of the sampling period in 2018, but was higher than the SSA at both wavelengths for anthropogenic aerosol.

Chapter 6: Comparison of wildfire aerosol emissions and evolution among multiple in-situ platforms

6.1 Overview

A way forward that optimizes the strengths and minimizes the shortcomings of the sampling strategies discussed in the introduction involves comparing and synthesizing observations from all the valuable approaches. By exploring similarities and differences in the results from different techniques, preferred model input can be generated and typical outcomes can be documented for model validation. Quantification of OA amounts downwind of fire sources is a key parameter for global models, but differences among airborne, ground-based, laboratory, near source, and downwind measurements of wildfire OA need to be reconciled. Incorporating specificity on the variable chemical mechanisms controlling the evolution of secondary organic aerosol (SOA) and thus developing appropriate aging schemes in models is challenging, but combining field observations from multiple sampling platforms at the source, and downwind, provides an opportunity to assess both bottom-up and top-down models of wildfire OA, and address lingering ambiguity in the factors controlling evolution of wildfire aerosol, including quantification of emission sources, dispersion, and transport to name a few. In this chapter, I synthesize and compare measurements of BC/CO, PM/CO, and absorption by BrC from recent in-situ field studies of western wildfires. From there, I point out where the results are similar or different, and discuss the implications as they relate to the future of smoke modeling and forecasts.

6.2 Platforms and Instrumentation

Most of the data used in the analyses presented in this paper were part of two recent large-scale field campaigns with a focus on western U.S. wildfires. In situ measurements during the Western

Wildfire Experiment for Cloudy Chemistry, Aerosol Absorption and Nitrogen campaign (WE-CAN, https://www.eol.ucar.edu/field_projects/we-can) were conducted aboard the National Science Foundation (NSF) C-130 based in Boise, ID in summer 2018 and featured several mobile labs, including the Aerodyne Mobile Lab (AML) and ground sites. Additional in situ measurements were conducted during The Fire Influence on Regional to Global Environments and Air Quality campaign (FIREX-AQ, https://www.esrl.noaa.gov/csl/projects/firex-aq/) based in Boise in summer 2019, aboard the NASA DC-8. This campaign again featured the AML in addition to other mobile labs and ground sites. The remainder of the data compared to is mostly from recent studies of smoke impacts in Missoula (Selimovic et al., 2020; Selimovic et al., 2019) and Boise (McClure and Jaffe, 2018), the Studies of Emissions and Atmospheric Composition, Clouds and Climate Coupling by Regional Surveys campaign (SEAC^{4}RS, Toon et al., 2016), or the Biomass Burning Observation Project campaign (BBOP, https://www.arm.gov/research/campaigns/aaf2013bbop) to name a few, and referenced in the text when already published. Data from the WE-CAN and FIREX-AQ aircraft were 1 second time resolution, whereas data from the AML was 1-minute time resolution, and fixed ground site data were typically on a 5-minute to hourly basis. In Table 6.1, we list the instrument name, platform, sample interval, accuracies, and a technical reference for all the WE-CAN and FIREX-AQ instruments that supplied data for this study. Details regarding the instrumentation for the other studies we compare to are available in the references.

6.3 Overview of Sampling

During WE-CAN and FIREX-AQ, airborne smoke plume sampling normally attempted a pseudo-Lagrangian approach summarized next. The aircraft sampled initial emissions as close to the source as practical, before sampling aged emissions with transects perpendicular to the wind

direction at increasing distances downwind of the fire. Downwind distances were typically selected to give roughly one-hour increments of physical aging for up to 8 hours total. For stable source emissions and a well-mixed plume, the changes observed with distance should be due mainly to photochemical aging. Even for an evolving source, the downwind differences will mainly reflect photochemistry if the plume is well mixed and the sample-time increments are close to the physical age increments. In practice some limitations mean the data also reflect natural fire variability to a varying extent for each flight/fire. The Federal Aviation Administration (FAA) and air traffic control placed temporary flight restrictions on airspace above active fires, which determined the minimum distance to the fire and the altitude at which we sampled the plume. In some cases the plume was not yet well mixed and already slightly aged in the closest pass. In some flight plans, some downwind passes were associated with an earlier time of emission than the closest pass. The data that best reflect photochemical changes were readily identified based on the behavior of well-understood species, but some data moderately impacted by source evolution and poor mixing were still valuable to increase the overall representativeness of the sampling. (Garofalo et al., 2019). The sampling of fires in older studies sometimes involved long-axis sampling as described elsewhere (Liu et al., 2017).

Ground-based sampling at fixed locations in Missoula and Boise sampled "plumes of opportunity" typically aged a few hours to a few days as described in detail elsewhere (Selimovic et al., 2020; Selimovic et al., 2019; McClure and Jaffe, 2018). Ground-based with mobile labs typically involved driving as close to the fire sources as possible and often parking in designated safe, "smoky" locations. This gave access to fresher smoke than fixed sites and typically in more rural area less impacted by other sources than the fixed sites.

Table 0.1 Aircraft and ground-based measurement techniques used in this work, for newly reported data.

Measurement	Campaign	Method	Sample Interval	Calibration Accuracy	Reference
CO	FIREX	Differential absorption CO measurement	1 s		Sachse et al., [1987] and Sachse [1981], Diskin et al., [2001]
	WE-CAN	Cavity ring down spectroscopy	1 s		Yver Kwok et al., [2015]
	AML	Cavity ring down spectroscopy	1 min		Yver Kwok et al., [2015]
	MSO	Fourier transform infrared spectroscopy	5 min		Selimovic et al., [2020], [2019]
Black Carbon	FIREX	Single particle soot photometer	1 s		Schwarz et al., [2008], Perring et al., [2017]
	WE-CAN	Single particle soot photometer	1 s		Schwarz et al., [2010], Levin et al., [2014]
	AML	Single particle soot photometer	1 min		Schwarz et al., [2008]
	MSO	Photoacoustic Extinctiometer (PAX)	1 s		Selimovic et al., [2020], [2019]
Non-refractory submicron aerosol/ particulate matter	FIREX	Aerosol mass spectrometer	1 s		DeCarlo et al., [2006], Canagaratna et al., [2007]
	WE-CAN	Aerosol mass spectrometer	1 s		Garofalo et al., [2019]
	AML	High resolution aerosol mass spectrometer	1 min		Onasch et al., [2012]
	MSO	EBAM $PM_{2.5}$, Missoula DEQ	1 hr		Selimovic et al., [2020], [2019].
Brown Carbon	WE-CAN	Photoacoustic spectroscopy (PAS)	1 s		Pokhrel et al., [2016]
	MSO	Photoacoustic extinctiometers (PAX)	1 s		Selimovic et al., [2020], [2019]

6.4 Calculation of emission ratios and enhancement ratios

This work considers both fresh (near-source) and aged (downwind) smoke samples and derives values that are broadly useful for both study comparison and integration in local to global chemistry and climate models, in the form of emission ratios (ERs) and enhancement ratios. The calculation of these two types of ratios is identical, but an ER is only the appropriate term for a ratio measured directly at a single source, or further downwind for a relatively insert species such as BC or CO. Both types of ratios can be calculated using integrals or regression with the choice of approach having little impact as described in detail elsewhere (Selimovic et al., 2020; Selimovic et al., 2019; Garofalo et al., 2019). We used regression to compute ratios between species for the WE-CAN and FIREX airborne data newly presented here. The calculations of ERs and enhancement ratios for airborne and fixed ground site data that has already been published are described the references herein. A full analysis of all the data from a mobile lab moving through smoke and traffic is beyond the scope of this study. Here we combine measurements of HCN/CO (>0.002), a tracer for BB, to quickly select the readily apparent longer lasting BB plumes and examine their BC/CO and OA/CO characteristics also using regression.

6.5 Results and Discussion

6.5.1 ΔBC/ΔCO

BC and CO are both relatively inert in the atmosphere on short time scales and useful for evaluating model outputs of total emissions production, diurnal profiles of fuel consumption, and meteorology (Selimovic et al., 2019). In addition, the ratio ΔBC/ΔCO is useful a rough indicator of the flaming/smoldering ratio that produced a smoke sample (Selimovic et al., 2019). In this

study comparing multiple platforms, we use BC/CO ratios as a quick preliminary check for evidence that airborne or ground-based sampling are "biased" toward flaming or smoldering, respectively. While modified combustion efficiency (MCE) also reflects the flaming/smoldering ratio, in aged samples MCE can be distorted by mixing due to the large and variable CO_2 background (Yokelson et al., 2013b). Our BC/CO based probe of sampling bias also has a few caveats. BC production by flaming combustion is strongly affected by flame turbulence and therefore somewhat "noisy" (Selimovic et al., 2019; Shaddix et al., 1994). In addition, the BC data used here were obtained using an SP2 in all the studies except the Missoula ground site where photoacoustic absorption was used (Selimovic et al., 2019). The sources of error impacting these two approaches differ as a function of mixing state, which adds some uncertainty (Li et al., 2019).

Table 6.2 reports the emission (near source) and enhancement (downwind) ratios of ΔBC/ΔCO (g g^{-1}) from recent lab, ground, and airborne-based studies of western wild and prescribed fires. The airborne campaign wildfire average ΔBC/ΔCO is ~20% higher than the average at ground-based sites, but both averages fall within the observed variability of one another. In stark contrast, the lab-reported ΔBC/ΔCO average is almost four to five times higher than the average airborne or ground-site value, respectively. This discrepancy is likely the result of lab fires burning at a higher modified combustion efficiency (MCE), associated with more flaming combustion, higher BC emissions and thus a higher ΔBC/ΔCO ratio (Selimovic et al., 2018).

Table 0.2. Enhancement ratios (g g^{-1}) of BC/CO and PM/CO from various studies of western wildfires and prescribed fires.

Platform	Study	Fire Type	Approx. Age	ΔBC/ΔCO	ΔPM/ΔCO
LAB	FIREX Firelab (Selimovic et al., 2018)	Stack burns	<5 s	0.0087 (0.0026)	--
		Room burns	1-2 h	--	--
GROUND	MSO[1] 2017 (Selimovic et al., 2019)[4]	Wildfire	12 - 48 h	0.0014 (0.0006)	0.1263 (0.0015)
	MSO 2018 (Selimovic et al., 2020)[5]	Wildfire	24 - 72 h	0.0026 (0.0007)	0.1070 (0.0278)
		Prescribed Fire	3 h	0.0026	0.165
	MSO 2019[5]	Prescribed Fire	3 - 6 h	0.0019 (<0.0001)	0.1124 (0.0168)
	AML[2] 2019[4,6]	Wildfire	1 – 48 h	0.0014 (0.0002)	0.1179 (0.0272)
	AML 2018[4,6]	Wildfire	1 – 48 h	0.0018 (0.0007)	0.1268 (0.0412)
HIGH ELE. AIRBORNE	MBO[3] (Collier at el., 2016)[4,6]	Wildfire			0.3122 (0.0987)
	FIREX-AQ (2019) [4,6]	Wildfire	<1 - 3 h	0.0034 (0.0020)	0.2967 (0.0881)
	WE-CAN (2018) [4,6]	Wildfire	<1 – 8 h	0.0029 (0.0009)	0.2010 (0.0452)
	SEAC4RS/BBOP (Liu et al., 2017) [4,6]	Wildfires	< 2 h	0.0016 (0.0018)	0.2661 (0.1342)
	SEAC4RS/BBOP, G1 (Collier at el., 2016) [4,6]	Wildfires	Up to 48 h		0.2251 (0.0480)
	Rim Fire (Forrister et al., 2015) [4,6]	Wildfire	Fresh (1-2 h)		~0.41
	Rim Fire (Forrister et al., 2015) [4,6]	Wildfire	Old (9-50 h)		~0.15
	SLOBB (May et al., 2014) [4,6]	Prescribed Fire		0.006	0.11 (0.01)
	ARCTAS (Sahu et al., 2012)	Wildfires	1 - 3 h	0.0014 (0.0005)	--
Ground Site/Low Elevation Wildfire Average				0.0018 (0.0005)	0.1195 (0.0092)
Airborne/High Elevation Wildfire Average				0.0023 (0.0010)	0.2477 (0.0369)

[1]MSO stands for Missoula.
[2]AML stands for Aerodyne Mobile Lab.
[3]MBO stands for Mount Bachelor Observatory
[4]$PM_{1.0}$
[5]$PM_{2.5}$
[6]Organic Aerosol (OA)

With this perspective, assuming BC and CO truly remain inert during transport, the relatively small difference in ΔBC/ΔCO ratios among airborne and ground-based platforms shown in Fig. 6.1 suggests all platforms sampled smoke from a similar mix of flaming and smoldering. The box plots in Figure 6.1 show that a wider range of values exists among the ΔBC/ΔCO ratios derived from the airborne studies of wildfires (0.0020) compared to the ground-based studies (0.0012) (Table S8), but in both cases this range more likely reflects real fire-to-fire (fuel type, fuel moisture, loading, etc.) and year-to-year (seasonality, drought, snowmelt, etc.) variability rather than differences among measurement techniques, since most of the campaigns utilized similar methodologies. Thus we can proceed to the other comparisons without strong concerns that smoke generated by a fundamentally different mix of flaming and smoldering was sampled by the airborne and ground-based platforms.

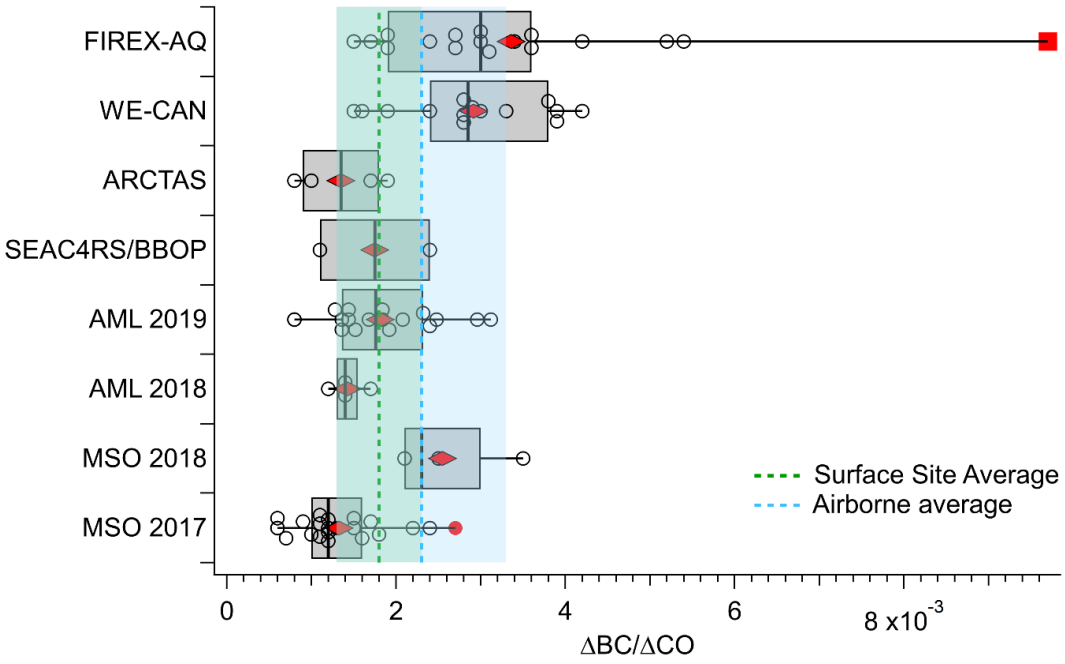

Figure 0.1. Box plot and whisker plot showing individual ΔBC/ΔCO (g g^{-1}) ratios (open circles) for each fire/plume or event respective to the wildfire campaign. Closed squares represent outlies. Diamonds reflect campaign averages. Shaded areas represent 1σ of the averages for each platform.

Before moving on we quickly update BC emissions estimates as explained next. Current emissions estimates for CO are in reasonable agreement for wildfires, and can thus be used to derive and update BC emissions estimates using BC/CO ratios (Selimovic et al., 2020; Liu et al., 2017). Liu et al., 2017 estimated that western US wildfires produced an annual average of 5240 ± 2240 Gg of CO between 2011-2015, which the study reports is in good agreement with an EPA estimate based on the 2011 National Emissions Inventory (4894 Gg). Combining the Liu et al estimate with the ground-based field average ΔBC/ΔCO suggests that western US wildfires emit 9.43 ± 4.03 Gg of BC per year, but using the airborne field average ΔBC/ΔCO suggests that western US wildfires emit 12.05 ± 5.15 Gg per year; thus the true value for wildfire emissions of BC is likely within this range.

6.5.2 ΔPM/ΔCO

During smoke plume evolution, the net result of competition between evaporation of primary and secondary aerosol and formation of SOA affects the total amount of PM, health impacts, visibility, climate, and air quality, but also the mixing state of BC and the resulting measurement challenges noted above. A metric for the net effect of secondary formation and evaporation of organic and inorganic aerosol is provided by changes in the PM/CO ratio as smoke ages. All evidence shows wildfire $PM_{1.0}$ is overwhelmingly composed of OA (85-99%) (Selimovic et al., 2020; Selimovic et al., 2019; Garofalo et al., 2019; Liu et al., 2017). In addition, $PM_{1.0}$ is about 80% or more of $PM_{2.5}$ in wildfire smoke (Reid et al., 2005). Because of these similarities, to increase the amount of relevant data considered, we henceforth compare $PM_{1.0}$, $PM_{2.5}$, and OA interchangeably in this section. In general, field and laboratory studies of BBOA evolution so far provide variable outcomes with no clear indication of the factors controlling the evolution (Hodshire et al., 2019; Garofalo et al., 2019; Vakkari et al., 2018; Tkacik et al., 2017; Forrister et

al., 2015; Cubison et al., 2011; Yokelson et al., 2009). Increasing oxidation of biomass burning organic aerosol (BBOA) with atmospheric aging is ubiquitous, which implies that SOA is being produced, but multiple studies have hypothesized that this production of SOA is balanced by the dilution-induced evaporation of primary organic aerosol (POA) to explain the overall changes observed in the field (Hodshire et al., 2019; Morgan et al., 2019; Zhou et al., 2017; May et al., 2015; Jolleys et al., 2012; Cubison et al., 2011; Capes et al., 2008).

Specifically for wildfires, Garofalo et al., (2019) observed no net change in OA/CO for smoke aged up to 8 hours during WE-CAN, and Collier et al., (2016) found the same for smoke aged up to almost 50 hours sampled at Mount Bachelor Observatory (MBO) or via the G-1 aircraft. However, Forrister et al., (2015) observed a significant drop in OA/CO in a wildfire plume when sampling at lower elevation. Although rare, long-term surface measurements of aged wildfire smoke have also consistently reported PM/CO ratios that are roughly half the value in fresh to moderately-aged well-lofted wildfire plumes (Selimovic et al., 2020; Selimovic et al., 2019; McClure and Jaffe, 2018). These different outcomes are potentially related to higher ambient temperatures closer to the surface leading to substantial net OA evaporation (Selimovic et al., 2020; Selimovic et al., 2019). To further investigate these trends, we compare the emission (near source) and enhancement (downwind) ratios of $\Delta PM/\Delta CO$ or $\Delta OA/\Delta CO$ ($g\ g^{-1}$) from the published studies mentioned above, along with these ratios from the productive new ground-based, and airborne studies of western wildfires in Table 6.2 and Figure 6.2. As seen in Fig. 6.2. all the studies show some fire to fire variability in observed ratios as would be expected for uncontrolled natural fires burning in complex fuels with emissions processed in diverse scenarios. However, the updated age-independent study-average $\Delta PM/\Delta CO$ ratios from high-elevation airborne and high elevation ground-based studies of wildfires (MBO) cluster distinctly

at roughly double the age-independent study-average ΔPM/ΔCO wildfire ratios reported at the surface. This confirms the pattern observed earlier.

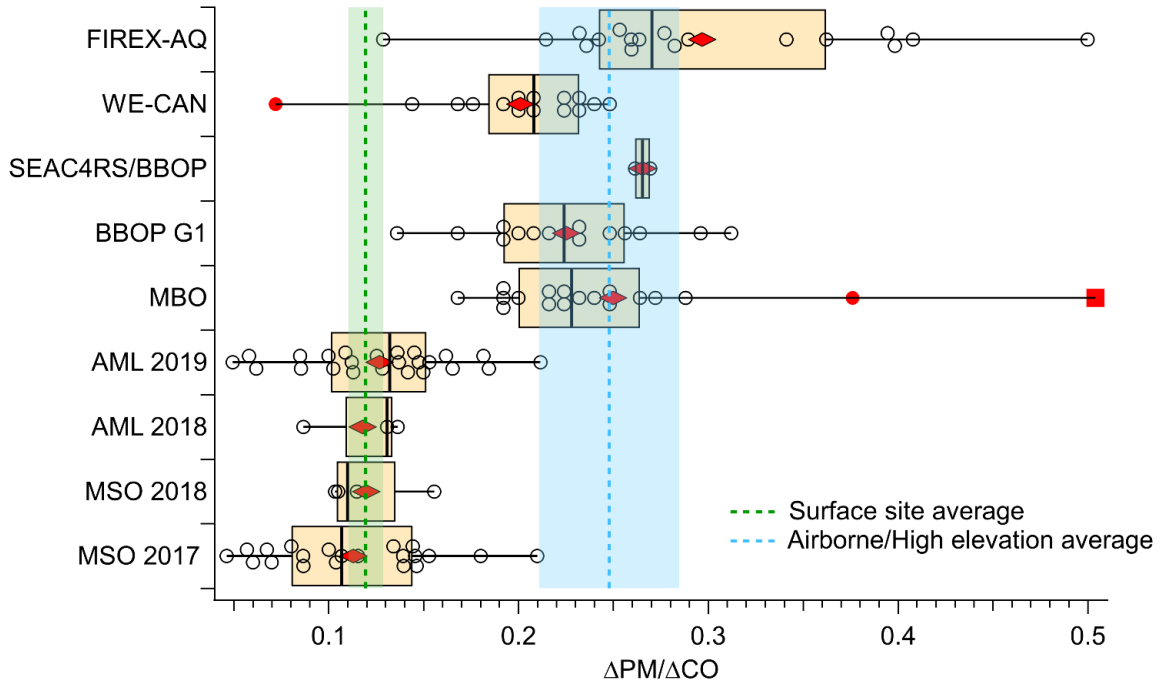

Figure 0.2. Box and whisker plot of age-independent ΔPM/ΔCO (g g^{-1}) ratios (open circles) for each fire/plume or event respective to the wildfire campaign. Closed circles and squares represent outliers. Diamonds reflect campaign averages. Shaded areas represent 1σ of the averages.

The narrow variability among study-average surface site ratios is remarkable, especially when considering the wider range in smoke age among individual measurements. As shown in Figure 6.2, smoke aged up to several days measured in Missoula has similar PM/CO ratios to smoke measured near the source by the AML for both years. Additionally, the PM/CO ratios from both of these studies are also in agreement with the PM/CO ratio measured in Boise (a populated urban center), by in McClure and Jaffe (2018) (0.119 ± 0.01 g g^{-1}). If variability in starting conditions, rapid photochemistry, and chemical evolution were truly completely responsible for changes or differences observed in PM/CO ratios across all sampling platforms, then we would not expect to see distinct grouping by elevation regime. Thus, although plume to plume

variability is important to consider, an apparent difference among surface and high elevation or airborne campaigns is also important and could be the effect of temperature, which we investigate next.

Temperature impacts the rates of chemical reactions, with plumes in colder environments likely undergoing slower rates for second order reactions, but possible increases for three body reaction. Temperature also affects the volatility distribution, which impacts the gas-particle partition rate, and is associated with an order of magnitude shift in effective saturation concentration (C*) for every 20 K change in temperature (Donahue et al., 2006). Temperature also impacts aerosol viscosity and equilibrium times with especially large changes in the latter near the glass transition temperature (Li and Shiraiwa, 2019). On average, the surface sites during wildfire season ranged from 17—37 ºC, whereas temperatures in aircraft or high elevation campaigns tended to be much cooler (-10ºC—10ºC). It is well known from thermodenuder studies that rapid heating evaporates substantial aerosol mass (Huffman et al., 2009), but the effects of long residence times at these specific temperatures has not been specifically targeted in a controlled study to our knowledge. Comparisons of BBOA volatility measured indoors in the Missoula Fire Sciences Lab (FSL) to that of BBOA volatility measured in an outdoor chamber suggested that aerosol from the chamber studies was less volatile than model predictions based on the measurements themselves (May et al., 2013). However, May et al., (2013) also report that the chamber was on average, 10ºC colder than the FSL, and accounting for this temperature difference greatly improved the model performance and brought predictions to within experimental uncertainty (May et al., 2013, Fig 6). Thus, evaporation of OA due to average warmer temperatures at the surface likely contributes systematically to the lower PM/CO ratios observed on the ground, rather than some other processing associated with aging of smoke since

the lower ratios agree well with one another in spite of several variables among the campaigns themselves. This generalization may be useful in simplifying models of surface smoke impacts, which could be particularly important in estimating impacts on urban or populated areas, and may have potential implications in land management, but additional observations and further study is necessary.

6.5.3 California Central Valley flight during WE-CAN

An outlier shown as part of the WE-CAN data set in Figure 6.2 shows an individual PM/CO ratio much closer to some of the individual ratios observed at ground sites (0.070 g g^{-1}). This data point is associated with a research flight conducted on 8 August 2018 (RF08) through the central valley of California, and presents an interesting case study on the effects of chemical aging and temperature on the evolution of OA. On this day, California's Central Valley was inundated with smoke from the Carr Fire and fires in Mendocino and Yosemite. Although a precise smoke age cannot be determined for the smoke sampled during this flight, it stands out in stark comparison to the other flights, as this was some of the only significantly (>8 h) aged smoke sampled during the WE-CAN campaign. Further, RF08 is unique in that missed approaches conducted at three airports during this research flight may provide a direct in-situ analysis into variability in OA/CO at different altitudes and subsequently, temperatures.

Figure 6.3a plots 1 Hz OA (µg sm^{-3}) versus CO (ppbv) data for the Central Valley flight as a function of altitude. Figure 6.3b plots these same variables as a function of temperature. A clear bifurcation in the OA/CO ratio (µg sm^{-3} $ppbv^{-1}$) is shown in both figures. The OA/CO ratio is half the value at warmer observed surface temperatures (300-310 K) compared to the value at temperatures hovering around or below freezing (273 K) at higher altitudes. An alternate

explanation for lower OA/CO near the surface could be mixing with air masses that contained non-BB CO and low OA. However, plots of two common BB tracers acetonitrile (Fig 6.3c.) and HCN (Fig 6.3d), do not exhibit the same large bifurcation. This argues strongly against the smoke having been diluted by non-BB CO near the surface, as we would expect both tracer ratios to CO to drop significantly with the addition of anthropogenic or other non-BB CO.

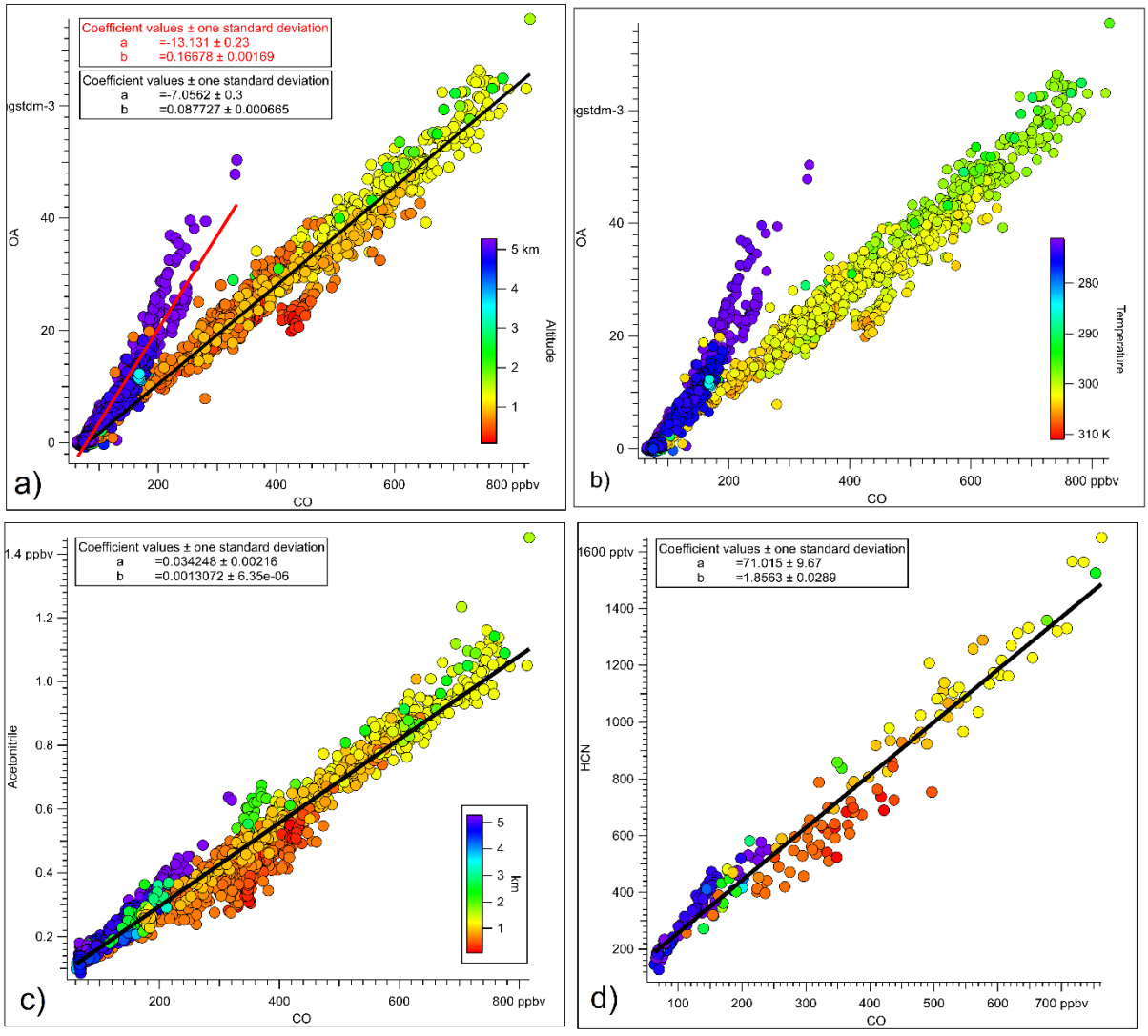

Figure 0.3. (a) Plot of 1Hz data of organic aerosol (OA, $PM_{1.0}$) versus CO, as a function of altitude (km above ground level). (b) Plot of 1Hz data of organic aerosol (OA, $PM_{1.0}$) versus CO, as a function of temperature (K). (c) Plot of 1Hz data of acetonitrile versus CO, colored as a function of altitude (km above ground level). (d) Plot of HCN versus CO, colored as a function of altitude (km above ground level).

The temperature dependence of the OA/CO ratios is consistent with our observations in section 6.5.2 and the general trend observed for platforms at or near the surface compared to those at high elevation or in the air. A vertical profile of the missed approaches may provide additional insight into the composition of the different layers of the atmosphere, but is beyond the scope of the study here. A marker for the extent of POA evaporation and SOA formation is f_{44}, which is the ratio of the integrated signal of the CO_2^+ ion detected by high resolution aerosol mass spectroscopy (HR-AMS) and has been used as a tracer for SOA and aged POA (Garofalo et al., 2019). Critically, f_{44} can probe the age of the smoke at different elevations, which we explore in Figure 6.4. In Fig 6.4, we find that f44 has about the same value for all the smoke points, but when these points are colored by temperature it reveals higher OA/CO at lower temperature, further aligning with the trends we observe in earlier sections.

Our observations of temperature effects on PM/CO have a few other general implications. One is that reporting temperature and OA concentration in conjunction with emission factor measurements could help account for study to study variability in measurements due to gas-particle partitioning. Also, higher temperatures and evaporation of BBOA during atmospheric transport near the surface may change the gas-phase photochemistry at the surface relative to high altitudes. This latter effect could be substantial. A preliminary estimate of the NMOG/CO ratio in airborne samples during WE-CAN is about 0.28 g g-1 (Permar et al., in prep). Adding another 0.12 g g-1 would be a 42% increase in total NMOG. The evaporation of BBOA may also explain the tendency to see higher total NMOG as a function of MCE in lab studies of BB emissions (Stockwell et al., 2015; Koss et al., 2018).

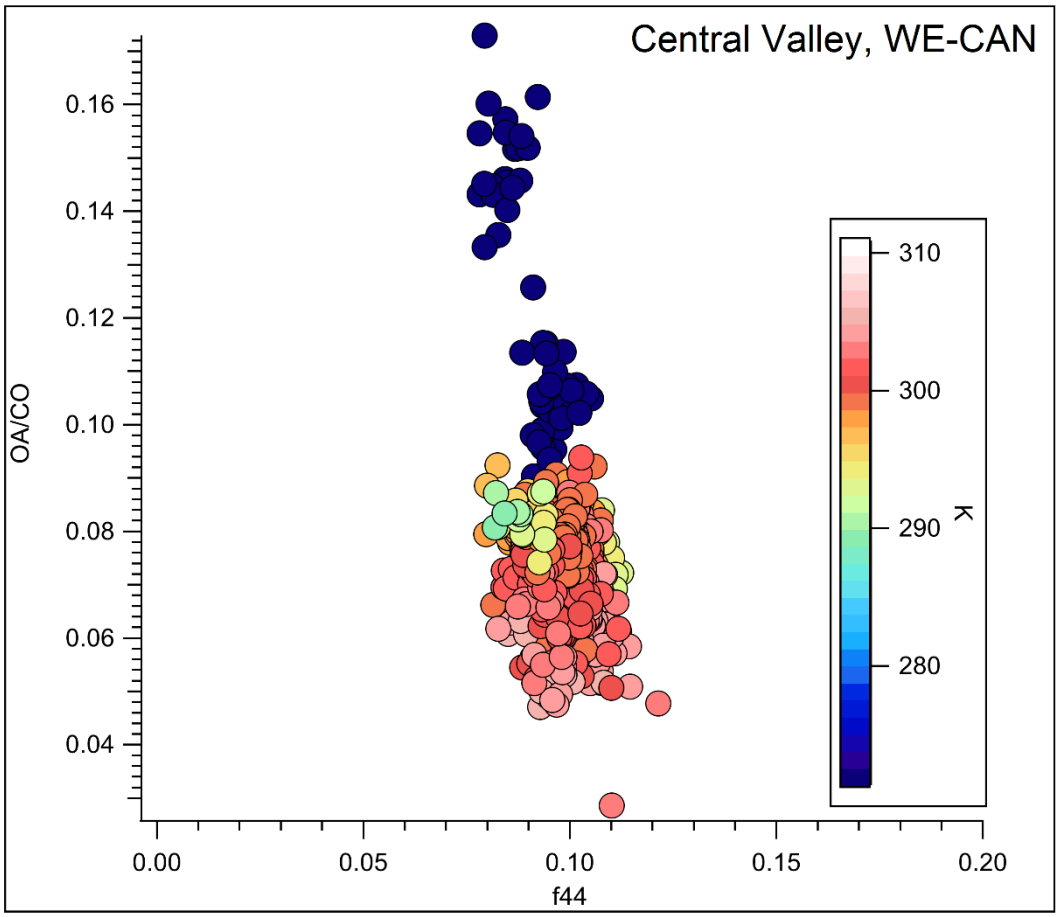

Figure 0.4. Figure of the OA/CO ratio versus f_{44}, a marker for POA evaporation and SOA formation, colored as a function of temperature.

6.5.4 BrC & Absorption Angstrom Exponent

UV-absorbing BBOA known as BrC is an important component of the radiative budget of smoke plumes, but the initial emissions of BrC and its lifetime are still not well constrained (Saleh et al., 2014; Jacobsen, 2014, Feng et al., 2013). Absorption by BrC decreases the climate cooling calculated for purely scattering OA depending on the amount emitted, its mass absorption coefficient (MAC), and lifetime (Feng et al., 2013). This is critical to understand especially in association with warming-induced increases in fire activity (Bowman et al., 2017; Wang et al.,

2017; Doerr and Santin 2016; Jacobsen et al., 2014; Saleh et al., 2014; Feng et al., 2013; Westerling et al., 2006). BrC can be quantified using BrC/CO ratios or absorption Ångström exponent (AAE) (Forrister et al., 2015) and we use the latter here. Until recently, only one airborne study had measured fresh BrC absorption in a wildfire plume (AAE ~3.75, Forrister et al., 2015). A laboratory study of simulated wildfires was in reasonable agreement in finding that BrC can account for about 86% of the absorption at 401 nm in fresh smoke (AAE ~3.5, Selimovic et al., 2019). The single previously-published airborne measurement of BrC lifetime and extensive ground-based monitoring in moderately aged smoke at Missoula are consistent in suggesting a half-life for BrC of about 10 daylight hours (Forrister et al., 2015; Selimovic et al., 2019). In the airborne study about 10% of BrC remained after two days, while smoke physically-aged < 1 day on average in Missoula had about 50% of the probable initial BrC remaining. In contrast, lab studies have suggested that secondary net formation and net destruction of BrC can both occur (Fleming et al., 2020; Tomaz et al., 2018; Wang et al., 2017; Laskin et al., 2015; Wang et al., 2014). Nighttime secondary formation of BrC due to wildfire smoke mixing with urban NOx was observed in Missoula and Israel (Selimovic et al., 2020; Bluvshtein et al., 2017) and nighttime SOA formation in smoke plumes was reported by Collier et al., (2016). Models have also suggested that nighttime SOA and BrC formation can occur (Decker et al., 2019), but the extent to which either impacts next-day photochemistry remains poorly understood. Nighttime mixing with urban NOx is likely more important for understanding impacts on populated areas than regional average behavior and many lab studies have relied on BrC surrogates and artificial light sources. The chemical processes that produce or destroy BrC are complicated, and can depend on mixing state, combustion conditions, chemical transformation, and photochemical aging, which makes modeling the UV optical properties somewhat

ambiguous (Fleming et al., 2020; Tomaz et al., 2018; Wang et al., 2017; Laskin et al., 2015; Wang et al., 2014). For all these reasons, additional BrC observations in real daytime regional smoke plumes are of great value. Here, we jointly examine the new WE-CAN BrC data from the 8 plumes sampled in the most Lagrangian fashion and BrC data from four precisely-aged smoke events in Missoula.

On the short aging time-scales from the WE-CAN plumes (2-8 hours) BrC can be seen to both increase slightly or decrease slightly, with mixing effects likely obscuring some of the photochemical trend (Fig. 6.5). Thus, to gain more statistics, in Figure 6.6, we plot the AAE values from all the individual plume transects from all 8 fires together as function of physical age along with AAEs for the four precisely aged smoke events in Missoula (including two previously unpublished events from 2019) and the lab average AAE reported in Selimovic et al., 2018. Note that in contrast to the brief airborne plume transects, the Missoula measurements benefit from hours of signal averaging at a single physical age. Figure 6.6 also shows the initial AAE is much higher in lab smoke about 5 seconds old. In Fig. 6.6, the Missoula-based points clearly indicate a decrease in AAE with a half-life of about 10 hours. Though the airborne points have more scatter, they generally support the ground-based trend. Thus our analysis supports the earlier conclusions of an initial AAE near 3.5 and a decay with a half-life near 10 hours. Although specificity on the factors controlling BrC evolution are difficult to ascertain, useful empirical generalizations about the persistence of BrC and its optical properties can still be made and implemented in models, by incorporating measurements from multiple platforms.

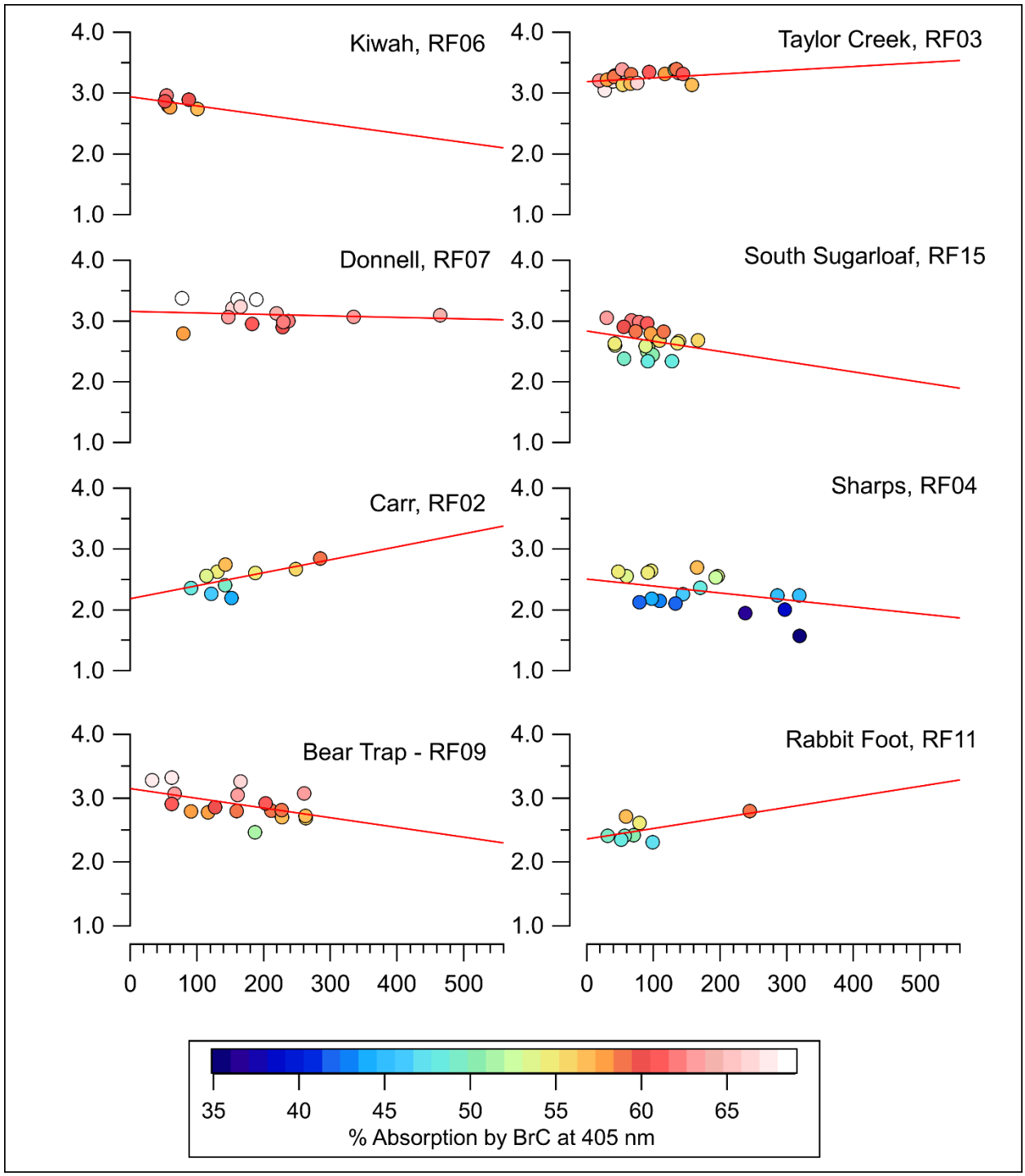

Figure 0.5. Individual plots of AAE versus physical age (in minutes) as a function of % absorption by BrC at 405 nm, for fires sampled during the WE-CAN campaign. Each point represents the integrated AAE and BrC for one plume pass during that specific fire.

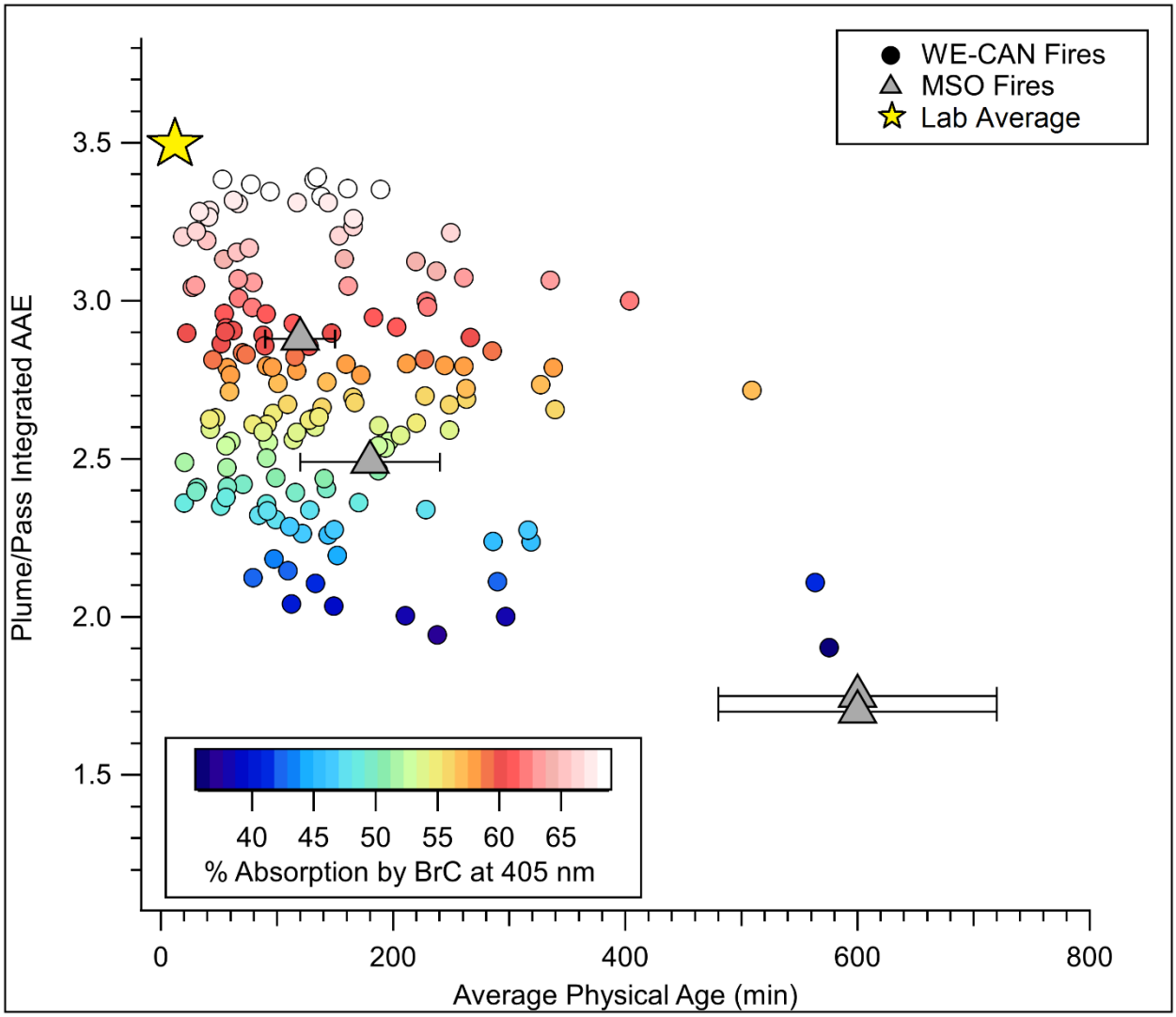

Figure 0.6. Plot of integrated AAE for each individual plume pass during WE-CAN, and integrated event average AAE (see Selimovic et al, 2020, 2019) for smoke measurements in Missoula (MSO) versus average physical age. For details on the lab average AAE, see Selimovic et al., 2018.

6.6 Conclusions

From 2017-2019 western US wildfires were intensively sampled using aircraft, fixed sites, and mobile labs. By comparing and synthesizing observations from all three platforms along with previously published work we arrive at two main conclusions about wildfire smoke. One is that the summertime evolution of wildfire PM/CO and wildfire NMOG/CO differs in the atmosphere by altitude and temperature. Specifically, PM/CO at the surface (0.12 g g-1) is typically about half the value in the upper atmosphere (0.248 g g-1). This implies that relatively more organic compounds are partitioned to the gas phase at the surface, which is supported by comparisons of total NMOG at typical aircraft altitudes with lab studies. The increased understanding of surface level smoke could improve air quality modeling while upper level (cold) smoke likely impacts climate more. The altitude/temperature effect on gas-particle partitioning is likely general and consistent with recent measurements in African smoke (Fig. 5, period 3 in Wu et al., 2020). In any case, the ratios found here present targets for model evaluation. A second climate-relevant conclusion is that fresh wildfire smoke has an AAE near 3.5 and a BrC half-life of about 10 daylight hours. This again provides an empirical target for model evaluation or use. The extent to which these findings apply to other fire types may differ. We find BrC persistence, but also note that BrC carbon initial values and lifetime may depend more on fuel chemistry and fire type.

Chapter 7: Broader Implications and Future Directions

The research presented here aims to address gaps associated with forecasting and modeling of smoke pollution, by providing high quality reference data on wildfire emissions of trace gases and aerosols, and aerosol optical properties. The results both on initial emissions and evolution of smoke can be an independent check on bottom-up and top-down modeling approaches, and can be used to quickly update emissions inventories and chemical processing scenarios. Further, exploring similarities and differences in the results from different sampling vantage points (lab, airborne, ground, near-source, downwind, etc.) of wildfire smoke is an efficient way to generate more robust model input on not only wildfire emissions, but also the transitions from initial conditions to typical outcomes of smoke downwind. This also helps assess model mechanism validation, and can ultimately help evaluate community exposure to smoke pollution on long-term scales.

Critically, our lab-based research of wildfire emissions showed that fire behavior and the ratio of flaming to smoldering (MCE) play a large role in determining the emissions of wildfires. Fire behavior can change based on temperature, relative humidity, wind, fuel type, fuel moisture, etc., and is integral to better understanding and estimating the uncertainties in reference data for model input, especially as it relates to night-time combustion and the massive under-representation of night-time fuel consumption and chemistry in models. Lab results also showed that there was little variability in emissions between the varying dominant tree types in coniferous ecosystems. However, coniferous ecosystems produced about twice the emissions of some common NMOGs per mass burned compared to chaparral fuels. Further, individual components of wildfire ecosystems (duff, rotten log, etc.,) had different emissions profiles and produced varying amounts of trace gases and aerosols per unit mass, depending on what was

being burned, which could have serious implications for land management strategies like prescribed burning. This is critical when consideration is given to the fact that prescribed fires and wildfires often burn different components of an ecosystem, with the former only generally burning surface fuels like grass, shrubs, duff and litter, while the latter may burn through all components, including canopy. In the same regard, individual components produced variable amounts of aerosol, with differing contributions of the UV-absorbing organic aerosol BrC accounting for the absorption at 401 nm, and BrC in some cases accounting for roughly the entirety (100%) of the absorption at 401 nm. Smoldering combustion (lower MCE) produced more BrC, and flaming combustion (higher MCE) produced less BrC.

Competition between destruction and formation of BrC is important for climate and BC measurement uncertainties, especially as they relate to the mixing state of BC, and BrC absorption will offset the climate cooling calculated for purely scattering OA depending on the amount emitted, its absorption cross-section, and its lifetime. The research presented here indicates that BrC initially accounts for a large percentage (>80%) of the absorption at 401 nm in fresh smoke and eventually decays to ~50% in ambient studies on longer time scales, thus suggesting that BrC absorption was persistent even after several days of smoke aging. Secondary nighttime formation of BrC from reactions of fire-emitted NMOGs with NO_3, and potentially O_3 or other pathways, is likely and may alter next-day photochemistry since BrC competes for UV photons with gases like HONO and NO_2, which alters the concentration of criteria pollutants and may have health impacts to local communities. Some evidence suggested that there was nighttime formation of BrC, but influences causing these observed changes are difficult to separate, and more research is needed in order to assess the cause, and commonality. Nighttime smoke chemistry is so far nearly unstudied even with the addition of the research above and

requires more attention. Even if no mechanistic breakthroughs on BrC formation are made, good documentation of the characteristics of nighttime smoke, and BrC is valuable.

Although there was a wide range of individual AAE values for wildfire smoke (~1.2—7), the average AAE values ranged from 3.5 for fresh lab smoke, to ~1.5 for smoke aged up to several days in Missoula, with higher values being associated with fresh smoke that had a higher BrC content, and more smoldering combustion (lower MCE). An analogous trend was observed for higher MCE values, fresh smoke with more flaming combustion had a higher MCE and higher BC content. Wildfire smoke measured in the lab produced SSAs at both wavelengths that were lower and suggestive of more warming aerosol (~0.70—0.80), but aged smoke measured in ambient studies, and on longer temporal scales suggested the aerosol was more cooling (SSA = >0.90, 0.93—0.96), potentially due to coating or growth of the aerosol as it ages. Further, the latter studies showed an increased in the SSA at 870 over the course of the fire season. These implications are critical to better comprehending the impact that wildfire produced aerosol has on radiative forcing, and suggests that fresh smoke contributes to localized warming, whereas the aerosol becomes more scattering, and thus cooling as it ages and is transported downwind. These phenomenon are critical for model inputs which may assume one single value for aerosol optical properties rather than a dynamic value that may change over the time, and can have an impact on predictions of air quality, climate, and critically, climate forcing.

Finally, comparing the results of several recent wildfire campaigns using inert and reactive tracers to test sampling bias, model smoke production, and model chemistry, suggested that there was minimal to no sampling bias among ground-based and airborne campaigns, and that variability in black carbon emissions from these platforms was likely due to interannual and fire to fire variability rather than sampling strategy or technique. However, comparison of the

reactive species across these campaigns (e.g. PM/CO ratio), showed that the airborne campaign values were twice the values on the ground, which again may have serious implications for smoke modeling and prediction, especially in relation to air quality and visibility as mentioned above, but also community exposure. Temperature is one potential reason for this observed difference, but more observations such as possible composition changes that would indicate volatility drive evolution are needed to either confirm this, or elucidate a new rationale. Further directions and studies of wildfire smoke should include more observations on night-time characteristics of smoke, particularly as it relates to nighttime oxidants O_3 and NO_3 and to the formation of BrC. Additional observations that are more temporally extensive are also needed in order to fully encapsulate and recognize trends and chemical changes in wildfire pollution, which becomes increasingly critical as more and more populations are predicted to become exposed to smoke in the coming decades.

REFERENCES

Abatzoglou, J. T., and Williams, A. P: Impact of anthropogenic climate change on wildfire across western US forests, P. Natl. Acad. Sci. USA, 113(42), 11770—11775, https://doi.org/10.1073/pnas.1607171113, 2016.

Adetona, O., Reinhardt, T. E., Domitrovich, J., Broyles, G., Adetona, A. M., Kleinman, M. T., Ottmar, R. D., and Naeher, L. P.: Review of the health effects of wildland fire smoke on wildland fire fights and the public, Inhal. Toxicol. 28(3), 95-139, doi: 10.3109/08958379.2016.1145771, 2016.

Ahern, A. T., Robinson, E. S., Tkacik, D. S., Saleh, R., Hatch, L. E., Barsanti, K. C., Stockwell, C. E., Yokelson, R. J., Presto, A. A., Robinson, A. L., Sullivan, R. C., and Donahue, N. M.: Production of secondary organic aerosol during aging of biomass-burning smoke from fresh fuels and its relationship to VOC precursors, J. Geophys. Res., 124, 3583–3606 https://doi.org/10.1029/2018JD029068, 2019.

Akagi, S. K., Craven, J. S., Taylor, J. W., McMeeking, G. R., Yokelson, R. J., Burling, I. R., Urbanski, S. P., Wold, C. E., Seinfeld, J. H., Coe, H., Alvarado, M. J., and Weise, D. R.: Evolution of trace gases and particles emitted by a chaparral fire in California, Atmos. Chem. Phys., 12, 1397-1421, doi:10.5194/acp-12-1397-2012, 2012.

Akagi, S. K., Yokelson, R. J., Burling, I. R., Meinardi, S., Simpson, I., Blake, D. R., McMeeking, G. R., Sullivan, A., Lee, T., Kreidenweis, S., Urbanski, S., Reardon, J., Griffith, D. W. T., Johnson, T. J., and Weise, D. R.: Measurements of reactive trace gases and variable O3 formation rates in some South Carolina biomass burning plumes, Atmos. Chem. Phys., 13, 1141–1165, doi:10.5194/acp-13-1141-2013, 2013.

Akagi, S. K., Yokelson, R. J., Wiedinmyer, C., Alvarado, M. J., Reid, J. S., Karl, T., Crounse, J. D., and Wennberg, P. O.: Emission factors for open and domestic biomass burning for use in atmospheric models, Atmos. Chem. Phys., 11, 4039–4072, doi:10.5194/acp-11-4039-2011, 2011.

Alvarado, M. J., Lonsdale, C. R., Yokelson, R. J., Akagi, S. K., Coe, H., Craven, J. S., Fischer, E. V., McMeeking, G. R., Seinfeld, J. H., Soni, T., Taylor, J. W., Weise, D. R., and Wold, C. E.:

Investigating the links between ozone and organic aerosol chemistry in a biomass burning plume from a prescribed fire in California chaparral, Atmos. Chem. Phys., 15, 6667-6688, https://doi.org/10.5194/acp-15-6667-2015, 2015.

Ambrose, J.L., Reidmiller, D.R. and Jaffe, D.A.: Causes of high O3 in the lower free troposphere over the Pacific Northwest as observed at the Mt. Bachelor Observatory. Atmos. Environ. 45: 5302–5315, 2011.

An American Aerosol in Paris: https://earthobservatory.nasa.gov/images/90980/an-american-aerosol-in-paris, last access: 14 February 2019.

Ansmann, A., Baars, H., Chudnovsky, A., Mattis, I., Veselovskii, I., Haarig, M., Seifert, P., Engelmann, R., and Wandinger, U.: Extreme levels of Canadian wildfire smoke in the stratosphere over central Europe on 21–22 August 2017, Atmos. Chem. Phys., 18, 11831-11845, https://doi.org/10.5194/acp-18-11831-2018, 2018.

Apel, E. C., Calvert, J. G., Gilpin, T. M., Fehsenfeld, F., and Lonneman, W. A.: Nonmethane hydrocarbon intercomparison experiment (NOMHICE): Task 4, ambient air, J. Geophys. Res., 108, D9, 4300, doi:10.1029/2002/JD002936, 2003.

Baylon, P., Jaffe, D. A., Hall, S. R., Ullmann, K., Alvarado, M. J., & Lefer, B. L: Impact of biomass burning plumes on photolysis rates and ozone formation at the mount bachelor observatory. *J. Geophys. Res. Atmos.*, 124(4), 2272—2284, doi:10.1002/2017JD027341, 2018.

Benedict, K. B., Prenni, A. J., Carrico, C. M., Sullivan, A. P., Schichtel, B. A., and Collett Jr., J. L.: Enhanced concentrations of reactive nitrogen species in wildfire smoke, Atmos. Environ., 148, 8–15, 2017.

Benjamin, S. G., Weygandt, S. S., Brown, J. M., Hu, M., Alexander, C., Smirnova, T. G., Olson, J. B., James, E., Dowell, D. C., Grell, G. A., Lin, H., Peckham, S. E., Smith, T. L., Moninger, W. R., Kenyon, J., and Manikin, G. S.: A North American Hourly Assimilation and Model Forecast Cycle: The Rapid Refresh, Monthly Weather Review, 144, 1669–1694, https://doi.org/10.1175/MWR-D-15-0242.1, 10 2016.

Bergstrom, R. W., Pilewskie, P., Russell, P. B., Redemann, J., Bond, T. C., Quinn, P. K., and Sierau, B.: Spectral absorption properties of atmospheric aerosols, Atmos. Chem. Phys., 7, 5937-5943, https://doi.org/10.5194/acp-7-5937-2007, 2007.

Bergstrom, R. W., Russell, P. B., and Hignett, P: Wavelength dependence of the absorption of black carbon particles: predictions and results from the TARFOX experiment and implications for aerosol single scattering albedo, J. Atmos. Sci., 59, 567-577, https://doi.org/10.1175/1520-0469(2002)059<0567:WDOTAO>2.0.CO;2, 2002.

Bertschi, I. T., Yokelson, R. J., Ward, D. E., Christian, T. J., and Hao, W. M.: Trace gas emissions from the production and use of domestic biofuels in Zambia measured by open-path Fourier transform infrared spectroscopy, J. Geophys. Res., 108, 8469, doi:10.1029/2002JD002158, 2003.

Bertschi, I.T., R.J. Yokelson, J. G. Goode, D.E. Ward, R.E. Babbitt, R. A. Susott, and W.M. Hao, Trace gas and particle emissions from fires in large diameter and belowground biomass fuels, J. Geophys. Res., 108, 8472, doi:10.1029/2002JD002100, 2003.

Bian, Q., Jathar, S. H., Kodros, J. K., Barsanti, K. C., Hatch, L. E., May, A. A., Kreidenweis, S. M., and Pierce, J. R.: Secondary organic aerosol formation in biomass-burning plumes: theoretical analysis of lab studies and ambient plumes, Atmos. Chem. Phys., 17, 5459–5475, https://doi.org/10.5194/acp-17-5459-2017, 2017.

Birks, J. W., Williford, C. J., Andersen, P. C., Turnipseed, A. A., Strunk, S., and Ennis, C. A.: Portable ozone calibration source independent of changes in temperature, pressure and humidity for research and regulatory applications, Atmos. Meas. Tech., 11, 4797–4807, https://doi.org/10.5194/amt-11-4797-2018, 2018a.

Birks, J. W., Andersen, P. C., Williford, C. J., Turnipseed, A. A., Strunk, S. E., Ennis, C. A., and Mattson, E.: Folded tubular photometer for atmospheric measurements of NO_2 and NO, Atmos. Meas. Tech., 11, 2821–2835, https://doi.org/10.5194/amt-11-2821-2018, 2018b.

Bluvshtein, N., P. Lin, J. M. Flores, L. Segev, Y. Minon, E. Tas, G. Snyder, C. Weagle, S. S. Brown, A. Laskin, and Y. Rudich, Broadband optical properties of biomass-burning aerosol and

identification of brown carbon chromophores, J. Geophys. Res., 122, doi:10.1002/2016JD026230, 2017.

Bond, T. C. and Bergstrom, R.: Light absorption by carbonaceous particles: An investigative review, Aerosol Sci. Tech., 40, 27–67, 2006.

Bond, T. C., Doherty, S. J., Fahey, D.W., Forster, P. M., Berntsen, T., DeAngelo, B. J., Flanner, M. G.,Ghan, S., Kärcher, B., Koch, D., Kinne, S., Kondo, Y., Quinn, P. K., Sarofim, M. C., Schultz, M. G., Schulz, M., Venkataraman, C., Zhang, H., Zhang, S., Bellouin, N., Guttikunda, S. K., Hopke, P. K., Jacobson, M. Z., Kaiser, J. W. , Klimont, Z., Lohmann, U., Schwarz, J. P., Shindell, D., Storelvmo, T., Warren, S. G., and Zender, C. S.: Bounding the role of black carbon in the climate system: A scientific assessment, J. Geophys. Res., 118, 5380-5552, doi:10.1002/jgrd.50171, 2013.

Bond, T. C., Streets, D. G., Yarber, K. F., Nelson, S. M., Woo, J.-H., and Klimont, Z.: A technology-based global inventory of black and organic carbon emissions from combustion, J. Geophys. Res., 109, D14203, doi:10.1029/2003JD003697, 2004.

Bowman, D. M. J. S., Williamson, G. J., Abatzoglou, J. T., Kolden, C. A., Cochrane, M. A., and Smith, A. M. S.: Human exposure and sensitivity to globally extreme wildfire events, Nature ecology and evolution, 1(0058), doi: 10.1038/s41559-016-0058, 2017.

Bowman, K. W., Liu, J., Bloom, A. A., Parazoo, N. C., Lee, M., Jiang, Z., Menemenlis, D., Gierach, M. M., Collatz, G. J., Gurney, K. R., and Wunch, D: Global and Brazilian Carbon Reponse to El Nino Modoki 2011—2010, Earth and Space Science, 4, 637—660, https://doi.org/10.1002/2016EA000204, 2017.

Braun, R. A., Dadashazar, H., MacDonald, A. B., Aldhaif, A M., Maudlin, L. C., Crosbie, E.: Impact of wildfire emissions on chloride and bromide depletion in marine aerosol particles. *Environ. Sci. & Tech.,* 51(16), 9013-9021, doi:10.1021/acs.est.7b02039., 2017.

Brey, S. J. and Fischer, E. V: Smoke in the City: How Often and Where Does Smoke Impact Summertime Ozone in the United States?, *Environ. Sci. Technol.,* 50, 1288–1294, https://doi.org/10.1021/acs.est.5b05218, 2016.

Brown, S. S., Dubé, W. P., Karamchandari, P., Yarwood, G., Peischl, J., Ryerson, T. B., Neuman, J. A., Nowak, J. B., Holloway, J. S., Washenfelder, R. A., Brock, C. A., Frost, G. J., Trainer, M., Parrish, D. D., Fehsenfeld, F. C., and Ravishankara, A. R.: The effects of NOx control and plume mixing on nighttime chemical processing of plumes from coal-fired power plants, J. Geophys. Res., 117, D07304, doi:10.1029/2011JD016954, 2012.

Brown, S. S.; Dubé, W. P.; Bahreini, R.; Middlebrook, A. M.; Brock, C. A.; Warneke, C.; deGouw, J. A.; Washenfelder, R. A.; Atlas, E.; Peischl, J.; Ryerson, T. B.; Holloway, J. S.; Schwarz, J. P.; Spackman, R.; Trainer, M.; Parrish, D. D.; Fehsenfeld, F. C.; Ravishankara, A.R., Biogenic VOC oxidation and organic aerosol formation in an urban nocturnal boundary layer: Aircraft vertical profiles in Houston, TX. Atmos. Chem. Phys., 13, 11317-11337, 2013.

Burkholder, J. B., Sander, S. P., Abbatt, J.., Barker, J. R., Huie, R. E., Kolb, C. E., Kurylo, M. J., Orkin, V. L., Wilmouth, D. M., and Wine, P. H: "Chemical Kinetics and Photochemical Data for Use in Atmospheric Studies, Evaluation No. 18", JPL Publication 15-10, Jet Propulsion Laboratory, Pasadena, http://jpldataeval.jpl.nasa.gov, 2015.

Burling, I. R., Yokelson, R. J., Griffith, D. W. T., Johnson, T. J., Veres, P., Roberts, J. M., Warneke, C., Urbanski, S. P., Reardon, J., Weise, D. R., Hao, W. M., and de Gouw, J.: Laboratory measurements of trace gas emissions from biomass burning of fuel types from the southeastern and southwestern United States, Atmos. Chem. Phys., 10, 11115–11130, doi:10.5194/acp- 10-11115-2010, 2010.

Burling, I. R., Yokelson, R. J., Akagi, S. K., Urbanski, S. P., Wold, C. E., Griffith, D. W. T., Johnson, T. J., Reardon, J., and Weise, D. R.: Airborne and ground-based measurements of the trace gases and particles emitted by prescribed fires in the United States, Atmos. Chem. Phys., 11, 12197–12216, doi:10.5194/acp-11-12197-2011, 2011.

Campbell, J., Donato, D., Azuma, D., and Law, B.: Pyrogenic carbon emission from a large wildfire in Oregon, United States, J. Geophys. Res., 112, G04014, doi:10.1029/2007JG000451, 2007.

Capes, G., Johnson, B., McFiggans, G., Williams, P. I., Haywood, J., and Coe, H.: Aging of biomass burning aerosols over West Africa: Aircraft measurements of chemical composition,

microphysical properties, and emission ratios, J. Geophys. Res., 113, D00C15, doi:10.1029/2008JD009845, 2008.

Carrico, C. M., Petters, M. D., Kreidenweis, S. M., Collett, J. L., Engling, G., Malm, and Malm, W. C: Aerosol hydroscopicity and cloud droplet activation of extracts of filters from biomass burning experiments, J. Geophys. Res. Atmos., 113(D23), https://doi.org/10.1029/2008JD009845, 2008.

Chakrabarty, R. K., H. Moosmuller, L.-W. A. Chen, K. Lewis, W. P. Arnott, C. Mazzoleni, M. Dubey, C. E. Wold, W. M. Hao, and S. M. Kreidenweis.: Brown carbon in tar balls from smoldering biomass combustion, Atmos. Chem. Phys., 10(13), 6363-6370, 2010.

Chen, J., Li, C., Ritovski, Z., Milic, A., Gu, Y., Islam, M., Wang, S., Hao, J., Zhang, H., He, C., Guo, H., Fu, H., Miljevic, B., Morawska, L., Thai, P., Lam, Y. F., Pereira, G., Ding, A., Huang, X., and Dumka, U. C: A review of biomass burning: Emissions and impacts on air quality, health, and climate in China, Sci. Total Environ., 579, 1000—1034, https://doi.org/10.1016/j.scitotenv.2016.11.025, 2017.

Christian, T., Kleiss, B., Yokelson, R. J., Holzinger, R., Crutzen, P. J., Hao, W. M., Saharjo, B. H., and Ward, D. E.: Comprehensive laboratory measurements of biomass-burning emissions: 1. Emissions from Indonesian, African, and other fuels, J. Geophys. Res., 108, 4719, doi:10.1029/2003JD003704, 2003.

Christian, T. J., Kleiss, B., Yokelson, R. J., Holzinger, R., Crutzen, P. J., Hao, W. M., Shirai, T., and Blake, D. R.: Comprehensive laboratory measurements of biomass-burning emissions: 2. First intercomparison of open path FTIR, PTR-MS, GC-MS/FID/ECD, J. Geophys. Res., 109, D02311, doi:10.1029/2003JD003874, 2004.

Clarke, A. D., Shinozuka, Y., Kapustin, V. N., Howell, S., Huebert, B., Doherty, S., Anderson, T., Covert, D., Anderson, J., Hua, X., Moore, K. G., II, McNaughton, C., Carmichael, G., and Weber, R.: Size distributions and mixtures of dust and black carbon aerosol in Asian outflow: Physiochemistry and optical properties, J. Geophys. Res., 109, D15S09, doi:10.1029/2003jd004378, 2004.

Collier, S., Zhou, S., Onasch, T.B., Jaffe, D. A., Kleinman, L., Sedlacek, A. J. 3rd., Briggs, N. L., Hee, J., Fortner, E., Shilling, J. E., Worsnop, D., Yokelson, R. J., Parworth, C., Ge, X., Xu, J., Butterfield, Z., Chand, D., Dubey, M. K., Pekour, M. S., Springston, S., and Zhang, Q.: Regional influence of aerosol emissions from wildfires driven by combustion efficiency: insights from the BBOP campaign, Environ. Sci. Technol., 50(16), 8513-22, doi:10.1021/acs.est.6b01617, 2016.

Crutzen, P. J. and Andreae, M. O.: Biomass burning in the tropics: Impact on atmospheric chemistry and biogeochemical cycles, Science, 250, 1669–1678, doi:10.1126/science.250.4988.1669, 1990.

Cubison, M. J., Ortega, A. M., Hayes, P. L., Farmer, D. K., Day, D., Lechner, M. J., Brune, W. H., Apel, E., Diskin, G. S., Fisher, J. A., Fuelberg, H. E., Hecobian, A., Knapp, D. J., Mikoviny, T., Riemer, D., Sachse, G. W., Sessions, W., Weber, R. J., Weinheimer, A. J., Wisthaler, A., and Jimenez, J. L.: Effects of aging on organic aerosol from open biomass burning smoke in aircraft and laboratory studies, Atmos. Chem. Phys., 11, 12049–12064, https://doi.org/10.5194/acp-11-12049-2011, 2011.

Davies, M. G., Gray, A., Rein, G., and Legg, C. J.: Peat consumption and carbon loss due to smouldering wildfire in a temperate peatland, Forest Ecology and Management, 308, 169-177, doi:10.1016/i.foreco.2013.07.051, 2013.

Decker, Z. C. J., Zarzana, K. J., Coggon, M., Min, K. E., Pollack, I., Ryerson, T. B., Peischl, J., Edwards, P., Dubé, W. P., Markovic, M. Z., Roberts, J. M., Veres, P. R., Graus, M., Warneke, C., de Gouw, J., Hatch, L. E., Barsanti, K. C., and Brown, S. S: Nighttime Chemical Transformation in Biomass Burning Plumes: A Box Model Analysis Initialized with Aircraft Observations, Environ. Sci. Technol., 53(5), 2529—2538, doi: 10.1021/acs.est.8b05359, 2019.

Doerr, S. H., and Santin, C: Global trends in wildfire and its impacts: perceptions versus realities in a changing world, Philos. T. Roy. Soc. B., 371(1696), https://doi.org/10.1098/rstb.2015.0345, 2016.

Draxler, R.R., and G.D. Hess: Description of the HYSPLIT_4 modeling system. NOAA Tech. Memo. ERL ARL-224, NOAA Air Resources Laboratory, Silver Spring, MD, 24 pp, 1997.

Draxler, R.R., and G.D. Hess: An overview of the HYSPLIT_4 modeling system of trajectories, dispersion, and deposition. *Aust. Meteor. Mag.*, 47, 295-308, 1998.

Draxler, R.R.: HYSPLIT4 user's guide. NOAA Tech. Memo. ERL ARL-230, NOAA Air Resources Laboratory, Silver Spring, MD, 1999.

Draxler, R.R.: HYSPLIT4 user's guide. NOAA Tech. Memo. ERL ARL-230, NOAA Air Resources Laboratory, Silver Spring, MD, 1999.

Eck, T., Holben, B. N, Reid, J., Dubovik, O., Smirnov, A., O'Neill, N, Slutsker, I., and Kinne, S: Wavelength dependence of the optical depth of biomass burning, urban, and desert dust aerosols, J. Geophys. Res., 104(D24), 31,333 – 31,349, 1999.

Eck, T. F., Holben B. N., Reid, J. S., Mukelabai, M. M., Piketh, S. J., Torres, O., Jethva, H. T., Hyer, E. J., Ward, D. E., Dubovik, O., Sinyuk, A., Schafer, J. S., Giles, D. M., Sorokin, M., Smirnov, A., and Slutsker, I.: A seasonal trend of single scattering albedo in southern African biomass-burning particles: implications for satellite products and estimates of emissions for the world's largest biomass burning source, J. Geophys. Res-Atmos, 118(1), 6414—6432, doi:10.1002/jgrd.50500, 2013.

Ervens, B., Turpin, B. J., and Weber, R. J.: Secondary organic aerosol formation in cloud droplets and aqueous particles (aqSOA): a review of laboratory, field and model studies, Atmos. Chem. Phys., 11, 11069-11102, https://doi.org/10.5194/acp-11-11069-2011, 2011.

Feng, Y., Ramanathan, V., and Kotamarthi, V. R.: Brown carbon: a significant atmospheric absorber of solar radiation?, Atmos. Chem. Phys., 13, 8607–8621, doi:10.5194/acp-13-8607-2013, 2013.

Finlayson-Pitts, B. J. and Pitts Jr., J. N.: Chemistry of the Upper and Lower Atmosphere, Academic Press., San Diego, USA, 969 pp., 2000.

Fleming, L. T., Lin, P., Roberts, J. M., Selimovic, V., Yokelson, R., Laskin, J., Laskin, A., and Nizkorodov, S. A.: Molecular composition and photochemical lifetimes of brown carbon chromophores in biomass burning organic aerosol, Atmos. Chem. Phys., https://doi.org/10.5194/acp-2019-523, 2019.

Formenti, P., Elbert, W., Maenhaut, W., Haywood, J., Osborne, S., and Andreae, M. O: Inorganic and carbonaceous aerosols during the Southern African Regional Science Initiative (SAFARI 2000) experiment: Chemical characteristics, physical properties, and emission data for smoke from African biomass burning. J. of Geophys. Res., 108, 8488. doi: 10.1029/2002JD002408, D13, 2003.

Forrister, H., Liu, J., Scheuer, E., Dibb, J., Ziemba, L., Thornhill, K. L., Anderson, B., Diskin, G., Perring, A. E., Schwarz, J. P., Campuzano-Jost, P., Day, D. A., Palm, B. B., Jimenez, J. L., Nenes, A., and Weber, R. J.: Evolution of brown carbon in wildfire plumes. Geophys. Res. Lett., 42, 4623-4630, doi:10.1002/2015GL063897, 2015.

Fromm, M., Alfred, J., Hoppel, K., Hornstein, J., Bevuilacqua, R., Shettle, E., Servranckx R., Li, Z., and Stocks, B: Observations of boreal forest fire smoke in the stratosphere by POAM III, SAGE II, and lidar in 1998, J. Geophys. Res., 27(9), 1407—1410, https://doi.org/10.1029/1999GL011200, 2000.

Garofalo, L. A., Pothier, M. A., Levin, E. J. T., Campos, T. Kreidenweis, S. M., and Farmer, D. K: Emission and Evolution of Submicron Organic Aerosol in Smoke from Wildfires in the Western United States, ACS Earth Space Chem., 3, 1237—1247, 2019.

Gaudichet, A., Echalar, F., Chatenet, B. Quisefit, J. P., Malingre, G., Cachier, H., Buat-Menard, P., Artaxo, P., and Maenhaut, W.: Trace elements in tropical African savanna biomass burning aerosols, J. Atmos. Chem., 22(1-2), 19—39, doi:10.1007/BF00708179, 1995.

Gilman, J. B., Lerner, B. M., Kuster, W. C., Goldan, P. D., Warneke, C., Veres, P. R., Roberts, J. M., de Gouw, J. A., Burling, I. R., and Yokelson, R. J.: Biomass burning emissions and potential air quality impacts of volatile organic compounds and other trace gases from fuels common in the US, Atmos. Chem. Phys., 15, 13915-13938, doi:10.5194/acp-15-13915-2015, 2015.

Graber, E. R. and Rudich, Y.: Atmospheric HULIS: How humic-like are they? A comprehensive and critical review, Atmos. Chem. Phys., 6, 729-753, https://doi.org/10.5194/acp-6-729-2006, 2006.

Griffith, D. W. T.: Synthetic calibration and quantitative analysis of gas phase infrared spectra, Appl. Spectrosc., 50, 59–70, 1996. Hardy, C. C., Conard, S. G., Regelbrugge, J. C., and Teesdale,

D. R.: Smoke emissions from prescribed burning of southern California chaparral, Res. Pap. PNW-RP-486, US Department of Agriculture, Forest Service, Pacific Northwest Research Station, Portland, OR, 1996.

Hammer, M. S., Martin, R. V., van Donkelaar, A., Buchard, V., Torres, O., Ridley, D. A., and Spurr, R. J. D.: Interpreting the ultraviolet aerosol index observed with the OMI satellite instrument to understand absorption by organic aerosols: implications for atmospheric oxidation and direct radiative effects, Atmos. Chem. Phys., 16, 2507–2523, https://doi.org/10.5194/acp16-2507-2016, 2016.

Han, Y., Wu, Y., Wang, T., Xie, C., Zhao, K., Zhuang, B., and Li, S: Characterizing a persistent Asian dust transport event: Optical properties and impact on air quality through the ground-based and satellite measurements over Nanjing, China, Atmos. Environ. 115, 304—316, https://doi.org/10.1016/j.atmosenv.2015.05.048, 2015.

Hardy, C. C., Regelbrugge, J. C., & Teesdale, D. R. (1996) Smoke emissions from prescribed burning of southern California chaparral, Res. Pap. PNW-RP-486, US Department of Agriculture, Forest Service, Pacific Northwest Research Station, Portland, OR. https://doi.org/10.2737/PNW-RP-486.

Hatch, L. E., Yokelson, R. J., Stockwell, C. E., Veres, P. R., Simpson, I. J., Blake, D. R., Orlando, J. J., and Barsanti, K. C.: Multi-instrument comparison and compilation of non-methane organic gas emissions from biomass burning and implications for smoke-derived secondary organic aerosol precursors, Atmos. Chem. Phys., 17, 1471–1489, https://doi.org/10.5194/acp-17-1471-2017, 2017.

Hatch, L. E., Rivas-Ubach, A., Jen, C. N., Lipton, M., Goldstein, A. H., and Barsanti, K. C.: Measurements of I/SVOCs in biomass-burning smoke using solid-phase extraction disks and two-dimensional gas chromatography, Atmos. Chem. Phys., 18, 17801–17817, https://doi.org/10.5194/acp-18-17801-2018, 2018.

Haywood, J. m., Osborne, S. R., Francis, P. N., Keil, A., Formenti, P., Andreae, M. O., and Kaye, P. H: The mean physical and optical properties of regional haze dominated by biomass burning aerosol measured from the C-130 aircraft during SAFARI 2000, J. Geophys. Res., 108(D13), https://doi.org/10.1029/2002JD002226, 2003.

Hecobian, A., Zhang, X., Zheng, M., Frank, N., Edgerton, E. S., and Weber, R. J.: Water-Soluble Organic Aerosol material and the light-absorption characteristics of aqueous extracts measured over the Southeastern United States, Atmos. Chem. Phys., 10, 5965-5977, https://doi.org/10.5194/acp-10-5965-2010, 2010.

Herron-Thorpe, F. L., Mount, G. H., Emmons, L. K., Lamb, B. K., Jaffe, D. A., Wigder, N. L., Chung, S. H., Zhang, R., Woelfle, M. D., and Vaughan, J. K.: Air quality simulations of wildfires in the Pacific Northwest evaluated with surface and satellite observations during the summers of 2007 and 2008, Atmos. Chem. Phys., 14, 12533-12551, doi:10.5194/acp-14-12533-2014, 2014.

Hobbs, P. V., Reid, J. S., Herring, J. A., Nance, J. D., Weiss, R. E., Ross, J. L., Hegg, D. A., Ottmar, R. D., and Liousse, C.: Particle and trace-gas measurements in smoke from prescribed burns of forest products in the Pacific Northwest, Biomass Burning and Global Change, vol. 1, New York, MIT Press, 1996.

Hobbs, P. V., Sinha, P., Yokelson, R. J., Christian, T. J., Blake, D. R., Gao, S., Kirchstetter, T. W., Novakov, T., and Pilewskie, P.: Evolution of gases and particles from a savanna fire in South Africa, J. Geophys. Res., 108(D13), 8485, doi:10.1029/2002JD002352, 2003.

Hornbrook, R. S., Blake, D. R., Diskin, G. S., Fried, A., Fuelberg, H. E., Meinardi, S., Mikoviny, T., Richter, D., Sachse, G. W., Vay, S. A., Walega, J., Weibring, P., Weinheimer, A. J., Wiedinmyer, C., Wisthaler, A., Hills, A., Riemer, D. D., and Apel, E. C.: Observations of nonmethane organic compounds during ARCTAS − Part 1: Biomass burning emissions and plume enhancements, Atmos. Chem. Phys., 11, 11103-11130, https://doi.org/10.5194/acp-11-11103-2011, 2011.

Hungershoefer, K., Zeromskiene, K., Iinuma, Y., Helas, G., Trentmann, J., Trautmann, T., Parmar, R. S., Wiedensohler, A., Andreae, M. O., and Schmid, O.: Modelling the optical properties of fresh biomass burning aerosol produced in a smoke chamber: results from the EFEU campaign, Atmos. Chem. Phys., 8, 3427-3439, https://doi.org/10.5194/acp-8-3427-2008, 2008.

Iinuma, Y., Böge, O., Gräfe, R., and Herrmann, H.: Methylnitrocatechols: atmospheric tracer compounds for biomass burning secondary organic aerosols, Environ. Sci. Technol., 44, 8453e8459,https://doi.org/10.1021/es102938a, 2010.

Jacob, D. J., Crawford, J. H., Maring, H., Clarke, A. D., Dibb, J. E., Emmons, L. K., Ferrare, R. A., Hostetler, C. A., Russell, P. B., Singh, H. B., Thompson, A. M., Shaw, G. E., McCauley, E., Pederson, J. R., and Fisher, J. A.: The Arctic Research of the Composition of the Troposphere from Aircraft and Satellites (ARCTAS) mission: design, execution, and first results, Atmos. Chem. Phys., 10, 5191-5212, https://doi.org/10.5194/acp-10-5191-2010, 2010.

Jacobson, M. Z.: Effects of biomass burning on climate, accounting for heat and moisture fluxes, black and brown carbon, and cloud absorption effects, J. Geophys. Res. Atmos., 119, 8980-9002, doi:10.1002/2015JD021861, 2014.

Jaffe, D. A., Cooper, O. R., Fiore, A. M., Henderson, B. H., Gail, S., Russell, A. G., Henze, D. K., Langford, A. O., Lin, M. and Moore, T.: Scientific assessment of background ozone over the U.S.: implications for air quality management, Elem. Sci. Anthr., 6, 56, https://doi.org/10.1525/elementa.309, 2018.

Jaffe, D. A., Wigder, N., Downey, N., Pfister, G., Boynard, A., and Reid, S. B: Impact of wildfires on ozone exceptional events in the western U.S., Environ. Sci. Technol., 47(19), 11065—11072, doi:10.1021/es402164f, 2013.

Jayarathne, T., Stockwell, C. E., Bhave, P. V., Praveen, P. S., Rathnayake, C. M., Islam, Md. R., Panday, A. K., Adhikari, S., Maharjan, R., Goetz, J. D., DeCarlo, P. F., Saikawa, E., Yokelson, R. J., and Stone, E. A.: Nepal Ambient Monitoring and Source Testing Experiment (NAMaSTE): Emissions of particulate matter from wood and dung cooking fires, garbage and crop residue burning, brick kilns, and other sources, Atmos. Chem. Phys. Discuss., https://doi.org/10.5194/acp-2017-510, in review, 2017a.

Jayarathne, T., Stockwell, C. E., Gilbert, A. A., Daugherty, K., Cochrane, M. A., Ryan, K. C., Putra, E. I., Saharjo, B. H., Nurhayati, A. D., Albar, I., Yokelson, R. J., and Stone, E. A.: Chemical characterization of fine particulate matter emitted by peat fires in Central Kalimantan, Indonesia,

during the 2015 El Niño, Atmos. Chem. Phys. Discuss., https://doi.org/10.5194/acp-2017-608, in review, 2017b.

Jen, C. N., Hatch, L. E., Selimovic, V., Yokelson, R. J., Weber, R., Fernandez, A. E., Kreisberg, N. M., Barsanti, K. C., and Goldstein, A. H.: Speciated and total emission factors of particulate organics from burning western US wildland fuels and their dependence on combustion efficiency, Atmos. Chem. Phys., 19, 1013-1026, https://doi.org/10.5194/acp-19-1013-2019, 2019.

Jethva, H. and Torres, O.: Satellite-based evidence of wavelength-dependent aerosol absorption in biomass burning smoke inferred from Ozone Monitoring Instrument, Atmos. Chem. Phys., 11, 10541-10551, https://doi.org/10.5194/acp-11-10541-2011, 2011.

Jiang, H., and Feingold, G.: Effect of aerosol on warm convective clouds: aerosol-cloud-surface flux feedbacks in a new coupled large eddy model, J. Geophys. Res. Atmos., 111(D1), https://doi.org/10.1029/2005JD006138, 2006.

Johnson, T. J., Profeta, L. T. M., Sams, R. L., Griffith, D. W. T., and Yokelson, R. J.: An infrared spectral database for detection of gases emitted by biomass burning, Vibrational Spectroscopy 53, 97-102, 2010.

Johnson, T. J., Sams, R. L., Profeta, L. T. M., Akagi, S. K., Burling, I. R., Yokelson, R. J., and Williams, S. D.: Quantitative IR spectrum and vibrational assignments for glycolaldehyde vapor: Glycolaldehyde measurements in biomass burning plumes, J. Phys. Chem. A, 117, 4096−4107, doi.org/10.1021/jp311945p, 2013.

Jolleys, M. D., Coe, H., McFiggans, G., Capes, G., Allan, J. D., Crosier, J., Williams, P. I., Allen, G., Bower, K. N., Jimenez, J. L., Russell., L. M., Grutter, M., and Baumgardner, D: Characterizing the aging of biomass buring organic aerosol by use of mixing ratios: a meta-analysis of four regions, Environ. Sci. Technol., 46(24), 13093-13102, https://doi.org/10.1021/es302386v, 2012.

Jolly, W. M., Cochrane, M. A., Freeborn, P. H., Holden, Z. A., Brown, T. J., Williamson, G. J., and Bowman, D. M. J. S: Climate-induced variations in global wildfire danger from 1979 to 2013, Nat. Commun., 6, 7537, doi:10.1038/ncomms8537.

Kaufman, Y., A. Gitelson, A. Karnieli, E. Ganor, R. Fraser, T. Nakajima, S. Mattoo, and Holben, B. N.: Size distribution and scattering phase function of aerosol particles retrieved from sky brightness measurements, J. Geophys. Res., 99(D5), 10,341 – 10,356, 1994.

Kinne, S., Schulz, M., Textor, C., Guibert, S., Balkanski, Y., Bauer, S. E., Berntsen, T., Berglen, T. F., Boucher, O., Chin, M., Collins, W., Dentener, F., Diehl, T., Easter, R., Feichter, J., Fillmore, D., Ghan, S., Ginoux, P., Gong, S., Grini, A., Hendricks, J., Herzog, M., Horowitz, L., Isaksen, I., Iversen, T., Kirkevåg, A., Kloster, S., Koch, D., Kristjansson, J. E., Krol, M., Lauer, A., Lamarque, J. F., Lesins, G., Liu, X., Lohmann, U., Montanaro, V., Myhre, G., Penner, J., Pitari, G., Reddy, S., Seland, O., Stier, P., Takemura, T., and Tie, X.: An AeroCom initial assessment – optical properties in aerosol component modules of global models, Atmos. Chem. Phys., 6, 1815–1834, https://doi.org/10.5194/acp-6-1815-2006, 2006.

Kim, Y. H., Warren, S., Krantz, Q. T., King, C., Jaskot, R., Preston, W. T., George, B. J., Hays, M. D., Landis, M. S., Higuchi, M., DeMarini, D., and Gilmour, M. R: Mutagenicity and lung toxicity of smoldering versus flaming emissions from various biomass fuels: implications for health effects from wildland fires, Environ. Health Perspect, 126(1), doi: 10.1289/EHP2200, 2018.

Kolusu, S. R., Marsham, J. H., Mulcahy, J., Johnson, B., Dunning, C., Bush, M., and Spracklen, D. V.: Impacts of Amazonia biomass burning aerosols assessed from short-range weather forecasts, Atmos. Chem. Phys., 15, 12251-12266, https://doi.org/10.5194/acp-15-12251-2015, 2015.

Koss, A. R., Sekimoto, K., Gilman, J. B., Selimovic, V., Coggon, M. M., Zarzana, K. J., Yuan, B., Lerner, B. M., Brown, S. S., Jimenez, J. L., Krechmer, J., Roberts, J. M., Warneke, C., Yokelson, R. J., and de Gouw, J.: Non-methane organic gas emissions from biomass burning: identification, quantification, and emission factors from PTR-ToF during the FIREX 2016 laboratory experiment, Atmos. Chem. Phys. Discuss., https://doi.org/10.5194/acp-2017-924, in review, 2017.

Koss, A. R., Sekimoto, K., Gilman, J. B., Selimovic, V., Coggon, M. M., Zarzana, K. J., Yuan, B., Lerner, B. M., Brown, S. S., Jimenez, J. L., Krechmer, J., Roberts, J. M., Warneke, C., Yokelson, R. J., and de Gouw, J.: Non-methane organic gas emissions from biomass burning: identification, quantification, and emission factors from PTR-ToF during the FIREX 2016 laboratory experiment, Atmos. Chem. Phys., 18, 3299-3319, https://doi.org/10.5194/acp-18-3299-2018, 2018.

Lack, D. A., Cappa, C. D., Covert, D. S., Baynard, T., Massoli, P., Sierau, B., Bates, T. S., Quinn, P. K., Lovejoy, E. R., and Ravishankara, A. R.: Bias in Filter Based Aerosol Light Absorption Measurements Due to Organic Aerosol Loading: Evidence from Ambient Measurements, Aerosol Sci. Tech., 42, 1033–1041, https://doi.org/10.1080/02786820802389285, 2008.

Lack, D. A. and Cappa, C. D.: Impact of brown and clear carbon on light absorption enhancement, single scatter albedo and absorption wavelength dependence of black carbon, Atmos. Chem. Phys., 10, 4207-4220, https://doi.org/10.5194/acp-10-4207-2010, 2010.

Lack, D. A. and Langridge, J. M.: On the attribution of black and brown carbon light absorption using the Ångström exponent, Atmos. Chem. Phys., 13, 10535-10543, https://doi.org/10.5194/acp-13-10535-2013, 2013.

Lack, D. A., Langridge, J. M, Bahreini, R., Cappa, C. D., Middlebrook, A. M., and Schwarz, J. P.: Brown carbon and internal mixing in biomass burning particles, PNAS, 109, 14802-14807, doi:10.1073/pnas.1206575109, 2012.

Landis, M. S., Edgerton, E. S., White, E. M., Wentworth, G. R., Sullivan, A. P., and Dillner, A. M: The impact of the 2016 Fort McMurray Horse River wildfire on ambient air pollution levels in the Athabasca Oil Sands Region, Alberta, Canada, Sci. Total. Environ., 618, 1665—1676, doi:10.1016/j.scitotenv.2017.10.008., 2017.

Laskin, A., Laskin, J., and Nizkorodov, S. A: Chemistry of atmospheric brown carbon, Chem. Rev., 115(10), 4335-4382, doi:10.1021/cr5006167, 2015.

Le, G. E., Breysse, P. N., McDermott, A., Eftim, S. E., Geyh, A., Berman, J. D., and Curriero, F. C: Canadian forest fires and the effects of long-range transboundary air pollution on hospitalizations among the elderly. ISPRS International Journal of Geo-Information, 3(2), 713-731, doi: 10.3390/ijgi30207213, 2014.

Lee, H. J., P. K. Aiona, A. Laskin, J. Laskin, and S. A. Nizkorodov: Effect of solar radiation on the optical properties and molecular composition of laboratory proxies of atmospheric brown carbon, Environ. Sci. Technol., 48, 10,217–10,226, doi:10.1021/es502515r, 2014.

Lee, J. D., Moller, S. J., Read, K. A., Lewis, A. C., Mendes, L., and Carpenter L. J: Year-round measurements of nitrogen oxides and ozone in the tropical North Atlantic marine boundary layer, J. Geophys. Res., 114, D21302, doi:10.1029/2009JD011878, 2009.

Lewis, K., Arnott, W. P., Moosmuller, H., and Wold, C. E.: Strong spectral variation of biomass smoke light absorption and single scattering albedo observed with a novel dual-wavelength photoacoustic instrument, J. Geophys. Res., 113, D16203, doi:10.1029/2007JD009699, 2008.

Li, H., Lamb, K., Schwarz., J. P., Selimovic, V., Yokelson, R. J., McMeeking, G. R., and May, A. A.: A systematic inter-comparison of black carbon measurement techniques using biomass burning smoke, Atmos. Environ. 206, 156—169, https://doi.org/10.1016/j.atmosenv.2019.03.010, 2019.

Li, Y. and Shiraiwa, M.: Timescales of secondary organic aerosols to reach equilibrium at various temperatures and relative humidities, Atmos. Chem. Phys., 19, 5959–5971, https://doi.org/10.5194/acp-19-5959-2019, 2019.

Lim, C. Y., Hagan, D. H., Coggon, M. M., Koss, A. R., Sekimoto, K., de Gouw, J., Warneke, C., Cappa, C. D., and Kroll, J. H.: Secondary organic aerosol formation from the laboratory oxidation of biomass burning emissions, Atmos. Chem. Phys., 19, 12797–12809, https://doi.org/10.5194/acp-19-12797-2019, 2019.

Lin, P., Liu, J., Shilling, J. E., Kathmann, S. M., Laskin, J., and Laskin, A.: Molecular characterization of brown carbon (BrC) chromophores in secondary organic aerosol generated from photo-oxidation of toluene, Phys. Chem. Chem. Phys., 17(36), 23312-23325, https://doi.org/10.1039/C5CP02563J, 2015.

Lindaas, J., Farmer, D. K., Pollack, I. B., Abeleira, A., Flocke, F., Roscioli, R., Herndon, S., and Fischer, E. V.: Changes in ozone and precursors during two aged wildfire smoke events in the Colorado Front Range in summer 2015, Atmos. Chem. Phys., 17, 10691-10707, https://doi.org/10.5194/acp-17-10691-2017, 2017.

Liu J., Scheuer, E., Dibb, J., Ziemba, L. D., Thornhill, K. L., Anderson, B. E., Wisthaler, A., Mikoviny, T., Devi, J. J., Bergin, M., and Weber, R. J.: Brown carbon in the continental troposphere, Geophys. Res. Lett., 41(6), 2191—2195, https://doi.org/10.1002/2013GL058976, 2014.

Liu, C., Chung, C. E., Yin, Y., and Schnaiter, M.: The absorption Ångström exponent of black carbon: from numerical aspects, Atmos. Chem. Phys., 18, 6259–6273, https://doi.org/10.5194/acp-18-6259-2018, 2018.

Liu, J. C., Pereira, G., Uhl, S. A., Bravo, M. A., and Bell, M. L: A systematic review of the physical health impacts from non-occupational exposure to wildfire smoke, Environmental Research, 136, 120-132, doi: 10.1016/j.envres.2014.10.015, 2015.

Liu, S., Aiken, A. C., Arata, C., Dubey, M. K., Stockwell, C. E., Yokelson, R. J., Stone, E. A., Jayarathne, T., Robinson, A. L., DeMott, P. J., and Kreidenweis, S. M.: Aerosol single scattering albedo dependence on biomass combustion efficiency: Laboratory and field studies, Geophys. Res. Lett., 41, 742–748, doi:10.1002/2013GL058392, 2014.

Liu, X. X., Zhang, Y., Huey, L. G., Yokelson, R. J., Wang, Y., Jimenez, J. L., Campuzano-Jost, P., Beyersdorf, A. J., Blake, D. R., Choi, Y., St Clair, J. M., Crounse, J. D., Day, D. A., Diskin, G. S., Fried, A., Hall, S. R., Hanisco, T. F., King, L. E., Meinardi, S., Mikoviny, T., Palm, B. B., Peischl, J., Perring, A. E., Pollack, I. B., Ryerson, T. B., Sachse, G., Schwarz, J. P., Simpson, I. J., Tanner, D. J., Thornhill, K. L., Ullmann, K., Weber, R. J., Wennberg, P. O., Wisthaler, A., Wolfe, G. M., and Ziemba, L. D.: Agricultural fires in the southeastern US during SEAC4RS: Emissions of trace gases and particles and evolution of ozone, reactive nitrogen, and organic aerosol, J. Geophys. Res.-Atmos., 121, 7383–7414, https://doi.org/10.1002/2016jd025040, 2016.

Liu, X., Huey, G. L., Yokelson, R. J., Selimovic, V., Simpson, I. J., Müller, M., Jimenez. J. L., Campuzano-Jost, P., Beyersdorf. A. J., Blake, D. R., Butterfield, Z., Choi, Y., Crounse, J. D., Day, D. A., Diskin, G. S., Dubey, M. K., Fortner, E., Hanisco, T. F., Hu, W., King, L. E., Kleinman, L., Meinardi, S., Mikoviny, T., Onasch, T. B., Palm, B. B., Peischl, J., Pollack, I. B., Ryerson, T. B., Sachse, G. W., Sedlacek, A. J., Shilling, J. E., Springston, S., St. Clair, J. M., Tanner, D. J, Peng, A. P., Wennberg, P. O., Wisthaler, A., and Wolfe, G. M.: Airborne measurements of western U.S wildfire emissions: Comparison with prescribed burning and air quality implications, J. Geophys. Res. Atmos., 122, 6108-6129, doi:10.1002/2016JD026315, 2017.

Lobert, J. M., D. H. Scharffe, W. M. Hao, T. A. Kuhlbusch, R. Seuwen, P. Warneck, and P. J. Crutzen.: Experimental evaluation of biomass burning emissions: Nitrogen and carbon containing

compounds, in Global Biomass Burning: Atmospheric, Climatic, and Biospheric Implications, edited by J. S. Levine, MIT Press, Cambridge, Mass., 1991.

Lobert, J. M., Keene, W. C., Logan, J. A., and Yevich, R.: Global chlorine emissions from biomass burning: Reactive Chlorine Emissions Inventory, J. Geophys. Res., 104, 8373–8389, doi:10.1029/1998jd100077, 1999.

Manfred, K. M., Washenfelder, R. A., Wagner, N. L., Adler, G., Erdesz, F., Womack, C. C., Lamb, K. D., Schwarz, J. P., Franchin, A., Selimovic, V., Yokelson, R. J., and Murphy, D. M.: Investigating biomass burning aerosol morphology using a laser imaging nephelometer, Atmos. Chem. Phys., 18, 1879–1894, https://doi.org/10.5194/acp-18-1879-2018, 2018.

Mao, Y. H., Li, Q. B., Henze, D. K., Jiang, Z., Jones, D. B. A., Kopacz, M., He, C., Qi, L., Gao, M., Hao, W.-M., and Liou, K.-N.: Estimates of black carbon emissions in the western United States using the GEOS-Chem adjoint model, Atmos. Chem. Phys., 15, 7685-7702, https://doi.org/10.5194/acp-15-7685-2015, 2015.

Mardi, A. H., Dadashazar, H., MacDonald, A. B., Braun, R. A., Crosbie, E., Xian, P., et al. Biomass burning plumes in the vicinity of the California coast: airborne characterization of physiochemical properties, heating rates, and spatiotemporal features. *J. Geophys. Res. Atmos*., 123(23), 13560—13582. doi:10.1029/2018jd029134, 2018.

Marlon, J. R., Bartlein, P. J., Gavin, D. G., Long, C. J., Anderson, R. S., Briles, C. E., Brown, K. J., Colombaroli, D., Hallett, D. J., Power, M. J., Scharf, E. A., and Walsh, M. K: Long-term perspective on wildfires in the western USA, P. Natl. Acad. Sci. USA, 109(9), E535—E543, https://doi.org/10.1073/pnas.1112839109, 2012.

Maudlin, L.C., Wang, Z., Jonsson, H. H., & Sorooshian A.: Impact of wildfires on size-resolved aerosol composition at a coastal California site. *Atmos. Environ.*, 119, 59-68, doi:10.1016/j.atmosenv.2015.08.039, 2015.

May, A. A., E. J. T. Levin, C. J. Hennigan, I. Riipinen, T. Lee, J. L. Collett Jr., J. L. Jimenez, S. M. Kreidenweis, and A. L. Robinson: Gas-particle partitioning of primary organic aerosol emissions: 3. Biomass burning, J. Geophys. Res. Atmos., 118, 11,327–11,338, doi:10.1002/jgrd.50828, 2013.

May, A. A., McMeeking., G. R., Lee, T., Taylor, J. W., Craven, J. S., Burling, I., Sullivan, A. P., Akagi, S., Collett Jr., J. L., Flynn, M., Coe, H., Urbanski, S. P., Seinfeld, J. H., Yokelson, R. J., and Kreidenweis, S. M.: Aerosol emissions from prescribed fires in the United States: A synthesis of laboratory and aircraft measurements, J. Geophys. Res. Atmos., 119, 11826-11849, doi:10.1002/2014JD021848, 2014.

May, A. A., Lee, T., McMeeking, G. R., Akagi, S., Sullivan, A. P., Urbanski, S., Yokelson, R. J., and Kreidenweis, S. M.: Observations and analysis of organic aerosol evolution in some prescribed fire smoke plumes, Atmos. Chem. Phys., 15, 6323-6335, doi:10.5194/acp-15-6323-2015, 2015.

McClure, C. D., and Jaffe, D. A: Investigation of high ozone events due to wildfire smoke in an urban area, *Atmos. Environ.*, 194, 146-157, doi:10.1016/j.atmosenv.2018.09.021, 2018.

McClure, C. D., and Jaffe, D. A: US particulate matter air quality improves except in wildfire-prone areas, P. Natl. Acad. Sci. USA., https://doi.org/10.1073/pnas.1804353115, 2018.

McComiskey, A., Schwartz, S. E., Schmid, B., Guan, H., Lewis, E. R., Ricchiazzi, P., and Ogren, J. A.: Direct aerosol forcing: calculation from observables and sensitivities to inputs, J. Geophys. Res. Atmos., 113(D9), https://doi.org/10.1029.2007JD009170, 2008.

McMeeking, G. R., Kreidenweis, S. M., Carrico, C. M., Collett, J. L., Day, D. E., and Malm, W. C.: Observations of smoke influenced aerosol during the Yosemite Aerosol Characterization Study: Size distributions and chemical composition J. Geophys. Res., 110, D18209, doi:10.1029/2004JD005389, 2005a.

McMeeking, G. R., Kreidenweis, S. M., Carrico, C. M., Collett, J. L., Day, D. E., and Malm, W. C.: Observations of smokeinfluenced aerosol during the Yosemite Aerosol Characterization Study:

2. Aerosol scattering and absorbing properties, J. Geophys. Res., 110, D18209, doi:10.1029/2004JD005624, 2005b.

McMeeking, G. R., Kreidenweis, S. M., Baker, S., Carrico, C. M., Chow, J. C., Collet Jr., J. L., Hao, W. M., Holden, A. S., Kirchstetter, T. W., Malm, W. C., Moosmüller, H., Sullivan, A. P., and Wold, C. E.: Emissions of trace gases and aerosols during the open combustion of biomass in the laboratory, J. Geophys. Res., 114, D19210, doi:10.1029/2009JD011836, 2009.

Miyakawa, T., Oshima, N., Taketani, F., Komazaki, Y., Yoshino, A., Takami, A., Kondo, Y., and Kanaya, Y.: Alteration of the size distributions and mixing states of black carbon through transport in the boundary layer in east Asia, Atmos. Chem. Phys., 17, 5851-5864, https://doi.org/10.5194/acp-17-5851-2017, 2017.

Mohr, C., Lopez-Hilfiker, F., Zotter, P., Prévôt, A. S. H., Xu, L., Ng, N. L., Herndon, S. C., Williams, L. R., Franklin, J. P., Zahniser, M. S., Worsnop, D. R., Knighton, W. B., Aiken, A. C., Gorkowski, K. J., Dubey, M. K., Allan, J. D., and Thornton, J. A.: Contribution of nitrated phenols to wood burning brown carbon light absorption in Detling, United Kingdom during winter time, Environ. Sci. Technol., 47, 6316–6324, https://doi.org/10.1021/es400683v, 2013.

Morgan, W. T., Allan, J. D., Bauguitte, S., Darbyshire, E., Flynn, M. J., Lee, J., Liu, D., Johnson, B., Haywood, J., Longo, K. M., Artaxo, P. E., and Coe, H.: Transformation and aging of biomass burning carbonaceous aerosol over tropical South America from aircraft in-situ measurements during SAMBBA, Atmos. Chem. Phys. Discuss., https://doi.org/10.5194/acp-2019-157, in review, 2019.

Morris, G. A., Hersey, S., Thompson, A. M., Paweson, S., Nielsen, J. E., Colarco, P. R., McMillian, W. W., Stohl, A., Turquety, S., Warner, J., Johnson, B. J., Kucsera, T. L., Larko, D. E., Oltmans, S. J., and Witte, J. C: Alaskan and Canadian forest fires exacerbate ozone pollution over Houston, Texas, on 19 and 20 July 2004, J. Geophys. Res., 111, D24S03, doi:10.1029/2006JD007090, 2006.

Müller, M., Anderson, B. E., Beyersdorf, A. J., Crawford, J. H., Diskin, G. S., Eichler, P., Fried, A., Keutsch, F. N., Mikoviny, T., Thornhill, K. L., Walega, J. G., Weinheimer, A. J., Yang, M., Yokelson, R. J., and Wisthaler, A.: In situ measurements and modeling of reactive trace gases in

a small biomass burning plume, Atmos. Chem. Phys., 16, 3813–3824, doi:10.5194/acp- 16-3813-2016, 2016.

Nakayama, T. Suzuki, H., Kagamitani, S., and Ikeda, Y.: Characterization of a three wavelength Photoacoustic Soot Spectrometer (PASS-3) and a Photoacoustic Extinctiometer (PAX), J. Meteorol. Soc. Japan, 93(2), 285–308, doi:10.2151/jmsj.2015-016, 2015.

Nergui, T., Lee, Y., Chung, S. H., Lamb, B. K., Yokelson, R. J., and Barsanti, K: Integrating Measurement Based New Knowledge on Wildland Fire Emissions and Chemistry into the AIRPACT Air Quality Forecasting for the Pacific Northwest, American Geophysical Union Fall Meeting, New Orleans, LA, Abstract# A41L-06, 2017.

Palm, B. B., Campuzano-Jost, P., Day, D. A., Ortega, A. M., Fry, J. L., Brown, S. S., Zarzana, K. J., Dube, W., Wagner, N. L., Draper, D. C., Kaser, L., Jud, W., Karl, T., Hansel, A., Gutiérrez-Montes, C., and Jimenez, J. L.: Secondary organic aerosol formation from in situ OH, O_3, and NO_3 oxidation of ambient forest air in an oxidation flow reactor, Atmos. Chem. Phys., 17, 5331–5354, https://doi.org/10.5194/acp-17-5331-2017, 2017.

Park, R. J., Jacob, D. J., and Logan, J. A.: Fire and biofuel contributions to annual mean aerosol mass concentrations in the United States, Atmos. Environ., 41(35), 7389-7400, doi:10.1016/j.atmosenv.2007.05.061, 2007.

Peterson, D., Fromm, M. D., Solbrig, J. E., Hyer, E. J., Surratt, M. L., and Campbell, J. R: Detection and Inventory of Intense Pyroconvection in Western North America using *GOES-1*5 Daytime Infrared Data, American Meteorological Society, https://doi.org/10.1175/JAMC-D-16-0226.1, 2017.

Pokhrel, R. P., Beamesderfer, E. R., Wagner, N. L., Langridge, J. M., Lack, D. A., Jayarathne, T., Stone, E. A., Stockwell, C. E., Yokelson, R. J., and Murphy, S. M.: Relative importance of black carbon, brown carbon, and absorption enhancement from clear coatings in biomass burning emissions, Atmos. Chem. Phys., 17, 5063-5078, https://doi.org/10.5194/acp-17-5063-2017, 2017.

Pokhrel, R. P., Wagner, N. L., Langridge, J. M., Lack, D. A., Jayarathne, T., Stone, E. A., Stockwell, C. E., Yokelson, R. J., and Murphy, S. M.: Parameterization of single-scattering albedo (SSA) and absorption Ångström exponent (AAE) with EC / OC for aerosol emissions from

biomass burning, Atmos. Chem. Phys., 16, 9549-9561, https://doi.org/10.5194/acp-16-9549-2016, 2016.

Pokhrel, R. P., Beamesderfer, E. R., Wagner, N. L., Langridge, J. M., Lack, D. A., Jayarathne, T., Stone, E. A., Stockwell, C. E., Yokelson, R. J., and Murphy, S. M.: Relative importance of black carbon, brown carbon, and absorption enhancement from clear coatings in biomass burning emissions, Atmos. Chem. Phys., 17, 5063-5078, https://doi.org/10.5194/acp-17-5063-2017, 2017.

Praveen, P. S., Ahmed, T., Kar, A., Rehman, I. H., and Ramanathan, V.: Link between local scale BC emissions in the Indo-Gangetic Plains and large scale atmospheric solar absorption, Atmos. Chem. Phys., 12, 1173-1187, doi:10.5194/acp-12-1173-2012, 2012.

Radke, L. F., Hegg, D. A., Hobbs, P. V., Nance, J. D., Lyons, J. H., Laursen, K. K., Weiss, R. E., Riggan, P. J., and Ward, D. E.: Particulate and trace gas emissions from large biomass fires in North America, in: Global biomass burning – Atmospheric, climatic, and biospheric implications, MIT Press, Cambridge, MA, 209–224, 1991.

Ramanathan, V., Crutzen, P. J., Kiehl, J. T., and Rosenfeld, D: Aerosols, climate, and the hydrological cycle, Science, 294(5549), 2219-2124, https://doi.org/10.1126/science.1064034, 2001.

Reid, C. E., Brauer, M., Johnson, F. H., Jerrett, J., Balmes, J. R., and Elliot, C. T.: Critical review of health impacts of wildfire smoke exposure. Environ. Health Perspect., 124, 1334-1343, doi:10.1289/ehp.1409277, 2016.

Reid, J. S., Koppmann, R., Eck, T. F., and Eleuterio, D. P.: A review of biomass burning emissions part II: intensive physical properties of biomass burning particles, Atmos. Chem. Phys., 5, 799–825, doi:10.5194/acp-5-799-2005, 2005a.

Reid, J. S., Eck, T. F., Christopher, S. A., Koppmann, R., Dubovik, O., Eleuterio, D. P., Holben, B. N., Reid, E. A., and Zhang, J.: A review of biomass burning emissions part III: intensive optical properties of biomass burning particles, Atmos. Chem. Phys., 5, 827-849, https://doi.org/10.5194/acp-5-827-2005, 2005b.

Reinhardt, E.D., Keane, R.E., and Brown, J.K.: First order fire effects model: FOFEM. USDA Forest Service, Rocky Mountain Research Station, Ogden, Utah, GTR-INT-344, 1997.

Reisen, F., Meyer, C. P., Weston, C. J., and Volkova, L: Ground-Based field measurements of $PM_{2.5}$ emission factors from flaming and smoldering combustion in eucalypt forests, J. Geophys. Res-Atmos., 123, 8301-8314, https://doi.org/10.1029/2018JD028488, 2018.

Roberts, J. M., Stockwell, C. E., Yokelson, R. J., de Gouw, J., Liu, Y., Selimovic, V., Koss, A. R., Sekimoto, K., Coggon, M. M., Yuan, B., Zarzana, K. J., Brown, S. S., Santin, C., Doerr, S. H., and Warneke, C.: The nitrogen budget of laboratory-simulated western U.S. wildfires during the FIREX 2016 FireLab study, Atmos. Chem. Phys. Discuss., https://doi.org/10.5194/acp-2020-66, in review, 2020.

Robinson, A. L., Donahue, N. M., Shirvastava, M. K, Weitkamp, E. A., Sage, A. M., Grieshop, A. P., Lane, T. E., Pierce, J. R., and Pandis, S. N: Rethinking organic aerosols: Semivolatile emissions and photochemical aging, Science, 315(5816), 1259—1262, doi:10.1126/science.1133061, 2007.

Rothman, L. S., Gordon, I. E., Barbe, A., Benner, D. C., Bernath, P. F., Birk, M., Boudon, V., Bornw, L. R., Campargue, A., Champion, J. P., Chance, K., Coudert, L. H., Dana, V., Devi, V. M., Fally, S., Flaud, J. M., Camache, R. R., Goldman, A., Jacquemart, D., Kleiner, I., Lacome, N., Lafferty, W. J., Mandin, J. Y., Massie, S. T., Mikhailenko, S. N., Miller, C. E., Moazzen-Ahmadi, N., Naumenko, O. V., Nikitin, A. V., Orphal, J., Perevalov, V. I., Perrin, A., Predoi-Cross, A., Rinsland, C. P., Motger, M., Simeckova. M., Smith, M. A. H., Sung, K., Tashkun, S. A., Tennyson, J., Toth, R. A., Vandaele, A. C.,and Auwera, J. V: The HITRAN 2008 molecular spectroscopic database, J Quant. Spectrosc. Ra., 110(9-10), 533—572, 2009.

Russell, P. B., Bergstrom, R. W., Shinozuka, Y., Clarke, A. D., DeCarlo, P. F., Jimenez, J. L., Livingston, J. M., Redemann, J., Dubovik, O., and Strawa, A.: Absorption Angstrom Exponent in AERONET and related data as an indicator of aerosol composition, Atmos. Chem. Phys., 10, 1155-1169, https://doi.org/10.5194/acp-10-1155-2010, 2010.

Sahu, L. K., Kondo, Y., Moteki, N., Takegawa, N., Zhao, Y., Cubison, M. J., Jimenez, J. L., Vay, S., Diskin, G. S., Wisthaler, A., Mikoviny, T., Huey, L. G., Weinheimer, A. J., and Knapp, D. J: Emission characteristics of black carbon in anthropogenic and biomass burning plumes over California during ARCTAS-CARB 2008, J. Geophys. Res-Atmos, 117(D16), doi:10.1029/2011JD017401, 2012.

Saide, P. E., Peterson, D. A., da Silva, A., Anderson, B., Ziemba, L. D., Diskin, G., Sachse, G., Hair, J., Butler, C., Fenn, M., Jimenez, J. L., Campuzano-Jost, P., Perring, A. E., Schwarz, J. P., Markovic, M. Z., Russell, P., Redemann, J., Shinozuka, Y., Streets, D. G., Yan, F., Dibb, J., Yokelson, R., Toon, O. B., Hyer, E. and Carmichael, G. R.: Revealing important nocturnal and day-to-day variations in fire smoke emissions through a multiplatform inversion, Geophysical Research Letters, 42(9), 2015GL063737, doi:10.1002/2015GL063737, 2015.

Saleh, R., Robinson E. S., Tkacik, D. S., Ahern, A. T., Liu, S., Aiken, A. C., Sullivan, R. C., Presto, A. A., Dubey, M. K., Yokelson, R. J., Donahue, N. M., and Robinson, A. L.: Brownness of organics in aerosols from biomass burning linked to their black carbon content. Nature Geoscience, 7, 647-650, doi:10.1038/ngeo2220, 2014.

Santin, C., Doerr, S. H., Kane, E. S., Masiello, C. A., Ohlson, M., Maria de la Rosa, J., Preston, C. M., and Dittmar, T.: Towards a global assessment of pyrogenic carbon from vegetation fires, Glob Change Biol, 22: 76-91, doi:10.1111/gcb.12985, 2015a.

Santin, C., Doerr, S. H., Preston, C. M., and Gonzalez-Rodriguez, G: Pyrogenic organic matter production from wildfires: a missing sink in the global carbon cycle, Glob. Chang Biol., 21(4), 1621—1633, https://doi.org/10.1111/gcb.12800, 2015b.

Sareen, N., Schwier, A. N, Shapiro, E. L., Mitroo, D., and McNeil, V. F: Secondary organic material formed by methylglyoxal in aqueous aerosol mimics, Atmos. Chem. Phys., 10, 997–1016, doi:10.5194/acp-10-997-2010, 2010.

Schlosser, J. S., Braun, R. A., Bradley, T., Dadashazar, H., MacDonald, A. B., Aldhaif, A. A.: Analysis of aerosol composition data for western United States wildfires between 2005 and 2015: Dust emissions, chloride depletion, and most enhanced aerosol constituents. *J. Geophys. Res. Atmos*.**,** 122(16), 8951-8966, doi:10.1002/2017jd026547, 2017.

Schoennagel, T., Balch, J. K., Brenkert-Smith, H., Dennison, P. E., Harvey, B. J., Krawchuk, M. A., Mietkiewicz, N., Morgan, P., Mortiz, M. A., Rasker, R., Turner, M. G., and Whitlock, C: Adap to more wildfire in western North American forests as climate changes, P. Natl. Acad. Sci. USA., 114(18), 4582—4590, https://doi.org/10.1073/pnas.1617464114, 2017.

Schuster, G. L., Dubovik, O., and Holben, B. N.: Angstrom exponent and bimodal aerosol size distributions, J. Geophys. Res., 111, D07207, doi :10.1029/2005JD006328, 2006.

Sedlacek III, A. J., Buseck, P. R., Adachi, K., Onasch, T. B., Springston, S. R., and Kleinman, L.: Formation and evolution of tar balls from northwestern US wildfires, Atmos. Chem. Phys., 18, 11289–11301, https://doi.org/10.5194/acp-18-11289-2018, 2018.

Sekimoto, K., Koss, A. R., Gilman, J. B., Selimovic, V., Coggon, M. M., Zarzana, K. J., Yuan, B., Lerner, B. M., Brown, S. S., Warneke, C., Yokelson, R. J., Roberts, J. M., and de Gouw, J.: High- and low-temperature pyrolysis profiles describe volatile organic compound emissions from western US wildfire fuels, Atmos. Chem. Phys., 18, 9263–9281, https://doi.org/10.5194/acp-18-9263-2018, 2018.

Selimovic, V., Yokelson, R. J., Warneke, C., Roberts, J. M., de Gouw, J., Reardon, J., and Griffith, D. W. T.: Aerosol optical properties and trace gas emissions by PAX and OP-FTIR for laboratory-simulated western US wildfires during FIREX, Atmos. Chem. Phys., 18, 2929-2948, https://doi.org/10.5194/acp-18-2929-2018, 2018.

Selimovic, V., Yokelson, R. J., McMeeking, G. R., and Coefield, S.: In situ measurements of trace gases, PM, and aerosol optical properties during the 2017 NW US wildfire smoke event, Atmos. Chem. Phys., 19, 3905–3926, https://doi.org/10.5194/acp-19-3905-2019, 2019.

Selimovic, V., Yokelson, R. J., McMeeking, G. R., and Coefield, S: Aerosol mass and optical properties, smoke influence on O_3 and high NO_3 production rates in a western US city impacted by wildfires, *J. Geophys. Atmos*., in prep, 2020.

Shaddix, C. R., Harrington, J. E., and Smyth, K. C: Quantitative measurements of enhanced soot production in a flickering methane/air diffusion flame, Combust. Flame., 99(3-4), 723-732, https://doi.org/10.1016/0010-2180(94)90067-1, 1994.

Shaddix, C. R., Harrington, J. E., and Smyth, K. C: Quantitative measurements of enhanced soot production in a flickering methane/air diffusion flame, Combust. Flame., 99(3-4), 723-732, https://doi.org/10.1016/0010-2180(94)90067-1, 1994.

Sharpe, S. W., Johnson, T. J., Sams, R. L., Chu, P. M., Rhoderick, G. C., and Johnson, P. A.: Gas-phase databases for quantitative infrared spectroscopy, Appl. Spectrosc., 58, 1452–1461, 2004.

Shingler, T., Crosbie, E., Ortega, A., Shiraiwa, M., Zuend, A., Beyersdorf, A.: Airborne characterization of subsaturated aerosol hygoscopicity and dry refractive index from the surface to 6.5 km during the SEAC4RS campaign. *J. Geophys. Res. Atmos.*, 121(8), 4188-4210, doi:10.1002/2015jd024498, 2016.

Shivdenko, A. Z., and Schepaschenko, D. G: Climate change and wildfires in Russia, Contemp. Probl. Eco., 6(7), 683—692, doi: https://doi.org/10.1134/S199542551307010X, 2013.

Shrivastava, M., Cappa, C. D., Jiwen, F., Goldsten, A. H., Guenther, A. B., Jimenez, J. L., Kuang, C., Laskin, A., Martin, S. T., Ng, N. L., Petaja, T., Pierce, J. R., Rasch, P. J., Roldin, P., Seinfeld, J. H., Shilling, J., Smith, J. N., Thornton, J. A., Volkamer, R., Wang, J., Worsnop, D. R., Zaveri, R. A., Zelenyuk, A., and Zhang. Q: Recent advances in understanding secondary organic aerosol: Implications for global climate forcing, *Revs. Of. Geophys.*, 55(2), 509—559, doi:10.1002/2016RG000540, 2017.

Singh, H.B., Anderson, B. E., Brune, W. H., Cai, C., Cohen, R. C., Crawford, J. H.: Pollution influences on atmospheric composition and chemistry at high northern latitudes: Boreal and California forest fire emissions, *Atmos. Environ.*, 44, 4553-4564, doi:10.1016/j.atmosenv.2010.08.026., 2010.

Stein, A.F., Draxler, R.R, Rolph, G.D., Stunder, B.J.B., Cohen, M.D., and Ngan, F.: NOAA's HYSPLIT atmospheric transport and dispersion modeling system, Bull. Amer. Meteor. Soc., 96, 2059-2077, http://dx.doi.org/10.1175/BAMS-D-14-00110.1, 2015.

Stevens, J. T., Safford, H. G., and Latimer, A. M: Wildfire-contigent effects of fuel treatments can promote ecological resilience in seasonally dry conifer forests, Can. J. Forest Res., 44(5), 843—854, https://doi.org/10.1139/cjfr-2013-0460, 2014.

Stocks, B. J., van Wilgen, B. W., Trollope, W. S. W., McRae, D. J., Mason, J. A., Weirich, F., and Potgieter, A. L. F: Fuels and fire behavior dynamics on large-scale savanna fires in Kruger National Park, South Africa, J. Geophys. Res. Atmos., 101(D19), 23541—23550, 1996.

Stockwell, C. E., Yokelson, R. J., Kreidenweis, S. M., Robinson, A. L., DeMott, P. J., Sullivan, R. C., Reardon, J., Ryan, K. C., Griffith, D. W. T., and Stevens, L.: Trace gas emissions from combustion of peat, crop residue, domestic biofuels, grasses, and other fuels: configuration and Fourier transform infrared (FTIR) component of the fourth Fire Lab at Missoula Experiment (FLAME-4), Atmos. Chem. Phys., 14, 9727-9754, https://doi.org/10.5194/acp-14-9727-2014, 2014.

Stockwell, C. E., Veres, P. R., Williams, J., and Yokelson, R. J.: Characterization of biomass burning emissions from cooking fires, peat, crop residue, and other fuels with high-resolution proton-transfer-reaction time-of-flight mass spectrometry, Atmos. Chem. Phys., 15, 845-865, https://doi.org/10.5194/acp-15-845-2015, 2015.

Stockwell, C. E., Jayarathne, T., Cochrane, M. A., Ryan, K. C., Putra, E. I., Saharjo, B. H., Nurhayati, A. D., Albar, I., Blake, D. R., Simpson, I. J., Stone, E. A., and Yokelson, R. J.: Field measurements of trace gases and aerosols emitted by peat fires in Central Kalimantan, Indonesia, during the 2015 El Niño, Atmos. Chem. Phys., 16, 11711-11732, https://doi.org/10.5194/acp-16-11711-2016, 2016a.

Stockwell, C. E., Christian, T. J., Goetz, J. D., Jayarathne, T., Bhave, P. V., Praveen, P. S., Adhikari, S., Maharjan, R., DeCarlo, P. F., Stone, E. A., Saikawa, E., Blake, D. R., Simpson, I. J., Yokelson, R. J., and Panday, A. K.: Nepal Ambient Monitoring and Source Testing Experiment (NAMaSTE): emissions of trace gases and light-absorbing carbon from wood and dung cooking fires, garbage and crop residue burning, brick kilns, and other sources, Atmos. Chem. Phys., 16, 11043-11081, https://doi.org/10.5194/acp-16-11043-2016, 2016b.

Subramanian, R., Roden, C. A., Boparai, P., and Bond, T. C: Yellow beads and missing particles: trouble ahead for filter-based absorption measurements, Aerosol. Sci. Tech., 41(6), 630-637, https://doi.org/10.1080/02786820701344589, 2007.

Thornhill, G. D., Ryder, C. L., Highwood, E. J., Shaffrey, L. C., and Johnson, B. T.: The effect of South American biomass burning aerosol emissions on the regional climate, Atmos. Chem. Phys., 18, 5321-5342, https://doi.org/10.5194/acp-18-5321-2018, 2018.

Tkacik, D. S., Robinson, E. S., Ahern, A., Saleh, R., Stockwell, C., Simpson, I. J., Meinardi, S., Blake, D. R., Yokelson, R. J., Presto, A. A., Sullivan, R. C., Donahue, N. M., and Robinson, A. L.: A dual-chamber enhancement method for quantifying effects of atmospheric perturbations on secondary organic aerosol formation from biomass burning emissions, J. Geophys. Res. Atmos., 122, doi:10.1002/2016JD025784, 2017.

Tomaz, S, Cui, T., Chen, Y., Sexton, K. G., Roberts, J. M., Warneke, C., Yokelson, R. J., Surratt, J. D., and Turpin, B. J: Photochemical cloud processing of primary wildfire emissions as a potential source of secondary organic aerosol, Environ. Sci. Technol., 52(19), 11027—11037, doi:10.1021/acs.est.8b03293, 2018.

Toon, O., Maring, H., Dibb, J., Ferrare, R., Jacob, D., Jensen, E., Luo, Z., Mace, G., Pan, L., Pfister, L., Rosenlof, K., Redemann, J., Reid, J. S., Singh, H., Thompson, A., Yokelson, R. J., Minnis, P., Chen, G. Jucks, K., and Pszenny, A.: Planning, implementation, and scientific goals of the Studies of Emissions and Atmospheric Composition, Clouds and Climate Coupling by Regional Surveys (SEAC^{4}RS) field mission, J. Geophys. Res., 121, 4967-5009, doi:10.1002/2015JD024297, 2016.

Turner, M. G., Braziunas, K. H., Hansen, W. D., and Harvey, B. J: Short-interval severe fire erodes the resilience of subalpine Lodgepole pine forest, 116 (23), 11319—11328, doi:10.1073/pnas.1902841116, 2019.

United States Department of Agriculture: The Rising Cost of Wildfire Operations: Effects on the Forest Service's Non-Fire Work, https://www.fs.fed.us/sites/default/files/2015-Fire-Budget-Report.pdf, 2015.

United States Environmental Protection Agency: "Climate Indicators: Wildfires", accessed October 8, 2018, from:

http://web.archive.org/web/20160512002554/https://www3.epa.gov/climatechange/science/indicators/ecosystems/wildfires.html.,

United States National Interagency Fire Center: Total Wildland Fires and Acres (1926-2017), accessed October 8, 2018, from: https://www.nifc.gov/fireInfo/fireInfo_stats_totalFires.html.

Urbanski, S. P., Hao, W. M., and Nordgren, B.: The wildland fire emission inventory: western United States emission estimates and an evaluation of uncertainty, Atmos. Chem. Phys., 11, 12973-13000, https://doi.org/10.5194/acp-11-12973-2011, 2011.

Vakkari, V., Kerminen, V., Beukes, J. P., Tiitta, P., van Zyl, P. G., Josipovic, M., Venter, A. D., Jaars, K., Worsnop, D. R., Kulmala, M., and Laasko, L: Rapid changes in biomass burning aerosols by atmospheric oxidation, 41(7), 2644-2651, https://doi.org/10.1002/2014GL059396, 2014.

Vakkari, V., Beukes, J. P., Dal Maso, M., Aurela, M., Josipovic, M. and van Zyl, P. G.: Major secondary aerosol formation in southern African open biomass burning plumes, Nature Geosci., 11, 580–583, doi:10.1038/s41561-018-0170-0, 2018.

Wagenbrenner, N. S., Forthofer, J. M., Lamb, B. K., Shannon, K. S., and Butler, B. W.: Downscaling surface wind predictions from numerical weather prediction models in complex terrain with WindNinja, Atmos. Chem. Phys., 16, 5229–5241, https://doi.org/10.5194/acp-16-5229-2016, 2016.

Wagner, N. L., Adler, G., Franchin, A., Lamb, K., Manfred, K. M., Middlebrook, A. M., Selimovic V., Schwarz, J. P., Washenfelder, R. A., Womack, C., and Yokelson, R. J: The absorption budget of fresh biomass burning aerosol from realistic laboratory fires, in preparation, 2017.

Wang, J., Geng, N. B., Xu, Y. F., Zhang, W. D., Tang, X. Y., and Zhang, R. Q: PAHs in PM2.5 in Zhengzhou: concentration, carcinogenic risk analysis and source apportionment, Environ. Monit. Assess., 186(11), 7461-7473, https://doi.org/10.1007/s10661-014-3940-1, 2014.

Wang, J., Yue, Y., Wang, Y., Ichoku, C., Ellison, L., and Zeng, J: Mitigating satellite-bassed fire sampling limitations in deriving biomass burning emission rates: application to WRF-Chem model over the northern sub-saharan African region, J. Geophys. Res.-Atmos, 123(1), 507-528, https://doi.org/10.1002/2017JD026840, 2017.

Ward, D. E. and Radke, L. F.: Emissions measurements from vegetation fires: A Comparative evaluation of methods and results, in: Fire in the Environment: The Ecological, Atmospheric and Climatic Importance of Vegetation Fires, edited by: Crutzen, P. J. and Goldammer, J. G., John Wiley, New York, 53–76, 1993.

Westerling, A. L., Hidalgo, H. G., Cayan, D. R., and Swetnam, T. W.: warming and earlier spring increase western U.S forest wildfire activity, Science, 313 (5789), 940-943, doi:10.1126/science.1128834, 2006.

Westerling, A.L. 2016. Increasing western US forest wildfire activity: sensitivity to changes in the timing of spring. *Philos Trans R Soc Lond B Biol Sci* 371:e20150178.

Wigder, N. L., Jaffe, D. A., and Saketa, F. A.: Ozone and particulate matter enhancements from regional wildfires observed at Mount Bachelor during 2004—2011, Atmos. Environ., 75, 24—31, doi:10.1016/j.atmosenv.2013.04.026, 2013.

Wiggins, E. B., Andrews, A., Sweeney, C., Miller, J. B., Miller, C. E., Veraverbeke, S., Commane, R., Wofsy, S., Henderson, J. M., and Randerson, J. T.: Evidence for a larger contribution of smoldering combustion to boreal forest fire emissions from tower observations in Alaska, Atmos. Chem. Phys. Discuss., https://doi.org/10.5194/acp-2019-1067, in review, 2020.

Wilkins, J. L., Pouliot, G., Foley, K., Appel., W., and Pierce, T.: The impact of US wildland fires on ozone and particulate matter a comparison of measurements and CMAQ model predictions from 2008 to 2012, Int. J. Wildland Fire., https://doi.org/10.1071/WF18053, 2018.

Wu, H., Taylor, J. W., Szpek, K., Langridge, J., Williams, P. I., Flynn, M., Allan, J. D., Abel, S. J., Pitt, J., Cotterell, M. I., Fox, C., Davies, N. W., Haywood, J., and Coe, H.: Vertical variability of the properties of highly aged biomass burning aerosol transported over the southeast Atlantic during CLARIFY-2017, Atmos. Chem. Phys. Discuss., https://doi.org/10.5194/acp-2020-197, in review, 2020.

Yates, E.L., Iraci, L. T., Singh, H. B., Tanaka, T., Roby, M. C., Hamill, P., Clements, C. B., Lareau, N., Contezac, J., Blake, D. R., Simpson, I. J., Wisthaler, A., Mikoviny, T., Diskin, G. S., Beyersdorf, A. J., Choi, Y., Ryerson, T. B., Jimenez, J. L., and Gore, W: Airborne measurements

and emissions estimates of greenhouse gases and other trace constituents form the 2013 California Yosemite Rim wildfire, 127, 293-302, https://doi.org/10.1016/j.atmosenv.2015.12.038, 2016.

Yokelson, R. J., Griffith, D. W. T., and Ward, D. E.: Open path Fourier transform infrared studies of large-scale laboratory biomass fires, J. Geophys. Res., 101, 21067–21080, doi:10.1029/96JD01800, 1996.

Yokelson, R. J., Susott, R., Ward, D. E., Reardon, J., and Griffith, D. W. T.: Emissions from smoldering combustion of biomass burning measured by open-path Fourier transform infrared spectroscopy, J. Geophys. Res. Atmos., 102(D15), 18865-18877, https://doi.org/10.1029/97JD00852, 1997.

Yokelson, R. J., Goode, J. G., Ward, D. E., Susott, R. A., Babbitt, R. E., Wade, D. D., Bertschi, I., Griffith, D. W. T., and Hao, W. M.: Emissions of formaldehyde, acetic acid, methanol, and other trace gases from biomass fires in North Carolina measured by airborne Fourier transform infrared spectroscopy, J. Geophys. Res., 104, 30109–30125, doi:10.1029/1999jd900817, 1999.

Yokelson, R.J., T.J. Christian, I.T. Bertschi, and W.M. Hao, Evaluation of adsorption effects on measurements of ammonia, acetic acid, and methanol, J. Geophys. Res. 108, 4649, doi:10.1029/2003JD003549, 2003.

Yokelson, R. J., Karl, T., Artaxo, P., Blake, D. R., Christian, T. J., Griffith, D. W. T., Guenther, A., and Hao, W. M.: The Tropical Forest and Fire Emissions Experiment: overview and airborne fire emission factor measurements, Atmos. Chem. Phys., 7, 5175–5196, doi:10.5194/acp-7-5175-2007, 2007.

Yokelson, R. J., Christian, T. J., Karl, T. G., and Guenther, A.: The tropical forest and fire emissions experiment: laboratory fire measurements and synthesis of campaign data, Atmos. Chem. Phys., 8, 3509-3527, doi:10.5194/acp-8-3509-2008, 2008.

Yokelson, R. J., Crounse, J. D., DeCarlo, P. F., Karl, T., Urbanski, S., Atlas, E., Campos, T., Shinozuka, Y., Kapustin, V., Clarke, A. D., Weinheimer, A., Knapp, D. J., Montzka, D. D., Holloway, J., Weibring, P., Flocke, F., Zheng, W., Toohey, D., Wennberg, P. O., Wiedinmyer, C., Mauldin, L., Fried, A., Richter, D., Walega, J., Jimenez, J. L., Adachi, K., Buseck, P. R., Hall, S.

R., and Shetter, R.: Emissions from biomass burning in the Yucatan, Atmos. Chem. Phys., 9, 5785-5812, https://doi.org/10.5194/acp-9-5785-2009, 2009.

Yokelson, R. J., Burling, I. R., Gilman, J. B., Warneke, C., Stockwell, C. E., de Gouw, J., Akagi, S. K., Urbanski, S. P., Veres, P., Roberts, J. M., Kuster, W. C., Reardon, J., Griffith, D. W. T., Johnson, T. J., Hosseini, S., Miller, J.W., Cocker III, D. R., Jung, H., and Weise, D. R.: Coupling field and laboratory measurements to estimate the emission factors of identified and unidentified trace gases for prescribed fires, Atmos. Chem. Phys., 13, 89–116, doi:10.5194/acp-13-89-2013, 2013a.

Yokelson, R. J., Andreae, M. O., and Akagi, S. K.: Pitfalls with the use of enhancement ratios or normalized excess mixing ratios measured in plumes to characterize pollution sources and aging, Atmos. Meas. Tech., 6, 2155-2158, doi:10.5194/amt-6-2155-2013, 2013b.

Yue, C., Ciais, P., Cadule, P., Thonicke, K., and van Leeuwen, T. T.: Modelling the role of fires in the terrestrial carbon balance by incorporating SPITFIRE into the global vegetation model ORCHIDEE – Part 2: Carbon emissions and the role of fires in the global carbon balance, Geosci. Model Dev., 8, 1321-1338, doi:10.5194/gmd-8-1321-2015, 2015.

Zhang, A., Wang, Y., Zhang, Y., Weber, R. J., Song, Y., Ke, Z., & Zou, Y. (2020) Modeling the global radiative effect of brown carbon: a potentially larger heating source in the tropical free troposphere than black carbon, *Atmos. Chem. Phys.*, 20, 1901-1920, doi: 10.5194/acp-20-1901-2020.

Zhao, R., Lee, A. K. Y., Huang, L., Li, X., Yang, F., and Abbatt, J. P. D: Photochemical processing of aqueous atmospheric brown carbon, Atmos. Chem. Phys., 15, 6087-6100, https://doi.org/10.5194/acp-15-6087-2015, 2015.

Zhong, M., and Jang, M: Dynamic light absorption of biomass burning organic carbon photochemically aged under natural sunlight, Atmos. Chem. Phys., 14, 1517–1525, doi:10.5194/acp-14-1517-2014, 2014.

Zhou, S., Collier, S., Jaffe, D. A., Briggs, N. L., Hee, J., Sedlacek III, A. J., Kleinman, L., Onasch, T. B., and Zhang, Q.: Regional influence of wildfires on aerosol chemistry in the

western US and insights into atmospheric aging of biomass burning organic aerosol, Atmos. Chem. Phys., 17, 2477-2493, doi:10.5194/acp-17-2477-2017, 2017.

Zhou, L., Baker, K. R., Napelenok., S. L., Pouliot, G., Elleman, R., O'Neill, S. M., Urbanski, S. P., and Wong, D. C: Modeling crop residual burning experiments to evaluate smoke emissions and plume transport. Sci. Total Environ., 627, 523-533, https://doi.org/10.1016/j.sciototenv.2018.01.237, 2018.

1. APPENDIX Supplementary Tables

Table S1. *FIREX (lab) fire and fuel details.*

Fire "name"	Stack/Room[1]	Date	Ignition time	Fuel type	Relative Humidity	%C	%H	%N	%S	Cl (mg/kg)	MCE
	SC = smog chamber fill	2016 mm/dd	MST hh:mm:ss	Sampling location = Lubrecht unless otherwise noted	%	best estimate fuel avg					Flaming/Smoldering
Fire01	Stack/SC	10/4	15:05:00	ponderosa pine	30.0	50.42	6.51	0.52	0.06	83.87	0.9373
Fire02	Stack/SC	10/5	10:30:55	ponderosa pine	33.0	51.01	6.55	0.93	0.07	113.72	0.9310
Fire03	Stack/SC	10/5	14:02:00	ponderosa pine	31.0	51.06	6.52	0.96	0.06	108.60	0.9356
Fire04	Stack/SC	10/6	8:48:25	ponderosa pine	33.0	50.65	6.62	0.82	0.07	118.28	0.9297
Fire05	Stack	10/6	10:33:31	lodgepole pine	34.0	50.01	6.31	0.73	0.08	224.95	0.9311
Fire06	Stack	10/7	8:10:45	lodgepole pine	30.0	50.02	6.36	0.71	0.07	198.64	0.9410
Fire07	Stack/SC	10/7	10:07:11	lodgepole pine	28.0	50.09	6.36	0.75	0.07	228.53	0.9431
Fire08	Stack	10/7	13:13:45	Engelmann spruce	30.0	48.49	5.85	0.96	0.08	157.86	0.9200
Fire09	Stack	10/7	14:44:49	Engelmann spruce	35.0	48.10	5.80	0.76	0.08	224.40	0.9259
Fire10	Stack	10/8	8:16:03	Douglas fir	45.0	49.81	6.24	1.06	0.05	46.57	0.9435
Fire11	Stack/SC	10/8	10:05:56	Douglas fir	46.0	49.57	6.29	0.90	0.06	42.83	0.9481
Fire12	Stack	10/8	12:10:04	Engelmann spruce, duff	44.0	41.91	4.47	0.94	0.11	210.11	0.8681
Fire13	Stack	10/8	13:48:57	ponderosa pine, rotten log	37.0	50.14	5.86	0.37	<0.03	54.89	0.9569
Fire14	Stack	10/8	15:02:30	Douglas fir	34.0	49.65	6.26	0.85	0.05	41.59	0.9260
Fire15	Stack	10/10	8:18:20	subalpine fir, Fish Lake[2], canopy	35.0	51.46	6.46	0.54	0.05	303.14	0.8856
Fire16	Stack/SC	10/10	10:05:15	ponderosa pine, litter	31.0	50.31	6.72	0.55	0.08	136.21	0.9544
Fire17	Stack	10/10	12:10:34	Engelmann spuce, Fish Lake, canopy	29.0	50.04	6.29	0.76	0.08	372.23	0.8903
Fire18	Stack	10/10	13:00:49	Douglas fir, canopy	28.0	49.84	6.72	1.01	0.08	37.51	0.9279
Fire19	Stack	10/10	14:00:20	ponderosa pine, canopy	27.0	50.29	6.85	1.23	0.12	163.30	0.9345
Fire20	Stack	10/10	15:01:00	lodgepole pine, canopy	28.0	50.77	6.48	1.01	0.09	149.03	0.9355
Fire21	Stack	10/11	8:32:49	lodgepole pine, litter	28.0	48.14	6.22	0.95	0.08	60.27	0.9255
Fire22	Stack/SC	10/11	10:05:43	Douglas fir, litter	25.0	47.29	5.74	1.04	0.10	67.01	0.9454
Fire23	Stack	10/11	12:04:09	subalpine fir, Fish Lake, canopy	25.0	51.46	6.46	0.54	0.05	303.14	0.9471
Fire24	Stack	10/11	12:46:35	chaparral (chamise), San Dimas[3], canopy	26.0	50.72	6.42	0.86	0.06	89.75	0.9480
Fire25	Stack	10/11	13:31:33	Engelmann spruce, canopy	26.0	50.04	6.29	0.76	0.08	372.23	0.9499
Fire26	Stack	10/11	14:45:30	Engelmann spruce, duff	25.0	41.91	4.47	0.94	0.11	210.11	0.8171
Fire27	Stack	10/12	8:01:04	chaparral (chamise), North Mountain[4], canopy	25.0	49.65	6.75	0.81	0.08	290.00	0.9459
Fire28	Stack/SC	10/12	9:41:08	chaparral (manzanita, NM), canopy	26.0	48.67	6.32	0.56	0.08	76.62	0.9631
Fire29	Stack	10/12	12:04:09	chaparral (chamise, SD), canopy	23.0	50.72	6.42	0.86	0.06	89.75	0.9593
Fire30	Stack	10/12	13:31:19	chaparral (manzanita, SD) canopy	23.0	47.20	6.01	0.66	0.05	37.30	0.9630
Fire31	Stack	10/12	15:00:01	Douglas fir, rotten log	27.0	56.49	5.56	0.25	0.03	43.51	0.7805
Fire32	Stack	10/13	8:02:22	chaparral (chamise, NM), canopy	24.0	49.65	6.75	0.81	0.08	290.00	0.9539
Fire33	Stack/SC	10/13	9:31:28	chaparral (manzanita, SD), canopy	27.0	47.20	6.01	0.66	0.05	37.30	0.9622
Fire34	Stack	10/13	12:02:06	chaparral (manzanita, NM), canopy	24.0	48.67	6.32	0.56	0.08	76.62	0.9644
Fire35	Stack	10/13	13:37:30	loblolly pine[5], litter	27.0	49.77	6.47	0.36	0.06	347.71	0.9223

Table S1. Continued

Fire "name"	Fuel mixture components by mass as grams dry weight (red entry is wet weight due to missing fuel moisture data)										Total fuel mass	Total Residual
	Duff	Litter	Dead and down woody debris diameter (cm)[8]				Shrub	Herbaceous	Canopy (needle+branch)	Other fuels	italic number > fuel added during fire	grams ash plus unburned fuel
			0-0.64 (1h)	0.64-2.5 (10h)	2.5-7.6 (100h)	>7.6 (1000h)						
Fire01	0.0	330.0	17.0	141.0	179.0	0.0	89.0	0.0	0.0	0.0	756.0	nm
Fire02	276.3	538.9	11.1	124.6	179.0	0.0	60.6	0.0	307.4	0.0	1497.9	381.0
Fire03	229.1	306.2	12.6	121.8	174.1	0.0	59.5	0.0	279.3	0.0	1182.6	447.0
Fire04	190.7	980.5	44.8	262.6	142.8	0.0	96.0	0.0	557.8	0.0	*2275.1*	535.0
Fire05	311.4	159.4	37.7	13.9	114.1	0.0	95.2	82.7	291.1	0.0	1105.5	359.0
Fire06	273.6	161.1	37.8	144.2	111.5	0.0	88.5	75.1	322.2	0.0	1214.0	389.0
Fire07	640.9	466.2	105.5	430.3	129.1	0.0	349.7	247.9	1014.1	0.0	*3383.7*	305.0
Fire08	400.3	257.7	44.3	167.2	129.6	0.0	82.7	576.0	341.5	0.0	1999.4	385.0
Fire09	205.3	229.9	46.0	163.1	162.6	0.0	88.8	0.0	342.1	0.0	1237.8	541.4
Fire10	356.3	130.1	50.1	139.3	203.6	0.0	0.0	0.0	378.1	0.0	1257.5	517.0
Fire11	276.3	382.9	151.9	414.7	164.6	0.0	0.0	0.0	831.6	0.0	*2222.0*	235.0
Fire12	687.3	0.0	0.0	0.0	0.0	0.0	0.0	0.0	0.0	0.0	687.3	318.0
Fire13	0.0	0.0	0.0	222.0	223.0	242.6	0.0	0.0	0.0	0.0	687.6	88.0
Fire14	122.3	139.8	43.9	131.3	199.2	0.0	0.0	0.0	276.0	0.0	912.5	145.0
Fire15	0.0	0.0	0.0	0.0	0.0	0.0	0.0	0.0	370.8	0.0	370.8	168.0
Fire16	0.0	4434.6	0.0	0.0	0.0	0.0	0.0	0.0	0.0	0.0	*4434.6*	438.0
Fire17	0.0	0.0	0.0	0.0	0.0	0.0	0.0	0.0	428.8	0.0	428.8	430.0
Fire18	0.0	0.0	0.0	0.0	0.0	0.0	0.0	0.0	374.6	0.0	374.6	187.0
Fire19	0.0	0.0	0.0	`	0.0	0.0	0.0	0.0	588.9	0.0	588.9	211.0
Fire20	0.0	0.0	0.0	0.0	0.0	0.0	0.0	0.0	806.8	0.0	806.8	498.0
Fire21	0.0	682.1	0.0	0.0	0.0	0.0	0.0	0.0	0.0	0.0	682.1	193.0
Fire22	0.0	279.4	0.0	0.0	0.0	0.0	0.0	0.0	0.0	0.0	*279.4*	125.0
Fire23	0.0	0.0	0.0	0.0	0.0	0.0	0.0	0.0	815.3	0.0	815.3	329.0
Fire24	0.0	0.0	0.0	0.0	0.0	0.0	0.0	0.0	767.8	0.0	767.8	89.0
Fire25	0.0	0.0	0.0	0.0	0.0	0.0	0.0	0.0	553.6	0.0	553.6	342.0
Fire26	797.5	0.0	0.0	0.0	0.0	0.0	0.0	0.0	0.0	0.0	797.5	647.0
Fire27	0.0	0.0	0.0	0.0	0.0	0.0	0.0	0.0	2485.7	0.0	2485.7	166.0
Fire28	0.0	0.0	0.0	0.0	0.0	0.0	0.0	0.0	4428.4	0.0	*4428.4*	260.0
Fire29	0.0	0.0	0.0	0.0	0.0	0.0	0.0	0.0	2667.1	0.0	2667.1	345.0
Fire30	0.0	0.0	0.0	0.0	0.0	0.0	0.0	0.0	4603.5	0.0	4603.5	220.0
Fire31	0.0	0.0	0.0	297.5	0.0	0.0	0.0	0.0	0.0	0.0	297.5	211.0
Fire32	0.0	0.0	0.0	0.0	0.0	0.0	0.0	0.0	2822.0	0.0	2822.0	550.0
Fire33	0.0	0.0	0.0	0.0	0.0	0.0	0.0	0.0	3291.4	0.0	*3291.4*	191.0
Fire34	0.0	0.0	0.0	0.0	0.0	0.0	0.0	0.0	3540.1	0.0	3540.1	150.0
Fire35	0.0	1211.3	0.0	0.0	0.0	0.0	0.0	0.0	0.0	0.0	1211.3	120.0

Table S1. Continued

Fire "name"	Stack/Room[1]	Date	Ignition time	Fuel type	Relative Humidity	%C	%H	%N	%S	Cl (mg/kg)	MCE
	SC = smog chamber fill	2016 mm/dd	MST hh:mm:ss	Sampling location = Lubrecht unless otherwise noted	%	best estimate fuel avg					Flaming/Smoldering
Fire36	Stack	10/13	15:10:37	Englmann spruce, duff	27.0	41.91	4.47	0.94	0.11	210.11	0.8713
Fire37	Stack/SC	10/14	9:47:29	ponderosa pine	35.0	50.73	6.60	0.95	0.08	120.39	0.9396
Fire38	Stack	10/14	12:04:48	ponderosa pine, litter	39.0	50.31	6.72	0.55	0.08	136.21	0.9448
Fire39	Stack	10/14	13:30:20	ponderosa pine, canopy	35.0	50.29	6.85	1.23	0.12	163.30	0.9041
Fire40	Stack	10/14	15:00:00	lodgepole pine, canopy	35.0	50.77	6.48	1.01	0.09	149.03	0.9240
Fire41	Stack	10/16	7:59:55	lodgepole pine, litter	33.0	48.14	6.22	0.95	0.08	60.27	0.9377
Fire42	Stack/SC	10/16	9:36:02	lodgepole pine	32.0	50.15	6.46	0.80	0.07	196.07	0.9513
Fire43	Stack	10/16	12:01:05	Douglas fir, litter	33.0	47.29	5.74	1.04	0.10	67.01	0.9507
Fire44	Stack	10/16	13:48:52	Engelmann spruce, canopy	32.0	50.04	6.29	0.76	0.08	372.23	0.9549
Fire45	Stack	10/16	15:03:07	Douglas fir, canopy	32.0	49.84	6.72	1.01	0.08	37.51	0.9185
Fire46	Stack	10/17	8:18:44	chaparral (chamise, SD), canopy	31.0	50.72	6.42	0.86	0.06	89.75	0.9563
Fire47	Stack/SC	10/17	10:16:08	subalpine fir, Fish Lake	34.0	49.45	6.32	0.64	0.07	249.81	0.9323
Fire48	Stack	10/17	12:11:16	chaparral (chamise, NM), canopy	30.0	49.65	6.75	0.81	0.08	290.00	0.9539
Fire49	Stack	10/17	13:30:28	Excelsior (poplar)	31.0	48.40	6.30	0.23	0.05	<25	0.9710
Fire50	Stack	10/17	15:00:28	yak dung, MT	31.0	37.42	5.45	1.90	0.19	500.00	0.8993
Fire51	Stack	10/18	8:03:35	subalpine fir, Fish Lake, litter	29.0	49.82	6.68	0.97	0.11	446.36	0.9063
Fire52	Stack/SC	10/18	9:51:25	Engelmann spruce	30.0	49.14	6.02	0.69	0.07	214.72	0.9573
Fire53	Stack	10/18	12:03:00	loblolly pine, litter	30.0	52.54	6.40	0.57	0.06	123.17	0.9294
Fire54	Stack/SC	10/18	13:49:33	Engelmann spruce	32.0	49.02	6.00	0.70	0.07	235.34	0.9469
Fire55	Stack	10/18	15:06:10	Peat, Kalimantan[6], mixed sites	34.0	56.97	5.57	1.53	0.25	182.02	0.8314
Fire56	Stack	10/19	8:03:14	subalpine fir, Fish Lake, duff	33.0	42.15	5.25	1.19	0.11	94.52	0.8863
Fire57	Stack	10/19	9:44:02	Douglas fir	35.0	49.46	6.24	0.89	0.06	45.76	0.9511
Fire58	Stack/SC	10/19	12:04:04	lodgepole pine	33.0	50.05	6.44	0.75	0.13	156.25	0.9275
Fire59	Stack	10/19	13:31:40	ponderosa pine	32.0	50.80	6.59	0.97	0.08	118.27	0.9126
Fire60	Stack	10/19	15:07:30	rice straw, Arkansas	31.0	39.53	5.09	0.52	0.10	6100.00	0.9527
Fire61	Stack	10/20	8:04:47	Excelsior	26.0	48.40	6.30	0.23	0.05	<25	0.9451
Fire62	Stack	10/20	9:16:47	bear grass	26.0	45.83	5.50	0.93	NM	nm	0.8971
Fire63	Stack/SC	10/20	10:36:00	lodgepole pine	27.0	50.04	6.41	0.76	0.16	155.69	0.9364
Fire64	Stack	10/20	12:40:33	Douglas fir, canopy	27.0	49.84	6.72	1.01	0.08	37.51	0.9255
Fire65	Stack	10/20	14:12:55	jeffrey Pine, ?< duff	27.0	48.75	5.56	1.16	0.09	85.95	0.8771
Fire66	Stack	10/21	8:15:59	sagebrush, Clearwater, MT	36.0	46.39	6.22	0.78	0.07	1135.58	0.9192
Fire67	Stack/SC	10/21	9:46:48	subalpine fir, MT (remainder)	43.0	49.42	6.21	0.61	0.06	151.68	0.9421
Fire68	Stack	10/21	12:08:26	juniper, canopy	45.0	50.54	6.44	0.53	0.05	188.12	0.9284
Fire69	Stack	10/21	13:30:25	ceanothus	44.0	50.30	6.03	1.28	0.06	87.54	0.9422
Fire70	Stack	10/21	15:01:18	untreated lumber	43.0	46.70	5.75	BDL	BDL	40.31	0.9508

Table S1. Continued.

Fire "name"	Fuel mixture components by mass as grams dry weight (red entry is wet weight due to missing fuel moisture data)										Total fuel mass	Total Residual
	Duff	Litter	Dead and down woody debris diameter (cm)[8]				Shrub	Herbaceous	Canopy (needle+branch)	Other fuels	italic number > fuel added during fire	grams ash plus unburned fuel
			0-0.64 (1h)	*0.64-2.5 (10h)*	*2.5-7.6 (100h)*	*>7.6 (1000h)*						
Fire36	868.2	0.0	0.0	0.0	0.0	0.0	0.0	0.0	0.0	0.0	868.2	717.0
Fire37	239.6	579.9	30.7	243.3	158.3	0.0	133.7	0.0	829.9	0.0	*2215.4*	1943.0
Fire38	0.0	617.2	0.0	0.0	0.0	0.0	0.0	0.0	0.0	0.0	617.2	187.0
Fire39	0.0	0.0	0.0	0.0	0.0	0.0	0.0	0.0	796.1	0.0	796.1	390.0
Fire40	0.0	0.0	0.0	0.0	0.0	0.0	0.0	0.0	759.8	0.0	759.8	170.0
Fire41	0.0	330.3	0.0	0.0	0.0	0.0	0.0	0.0	0.0	0.0	330.3	107.0
Fire42	0.0	398.9	53.7	417.6	178.2	0.0	263.3	115.4	919.4	0.0	*2346.4*	308.0
Fire43	0.0	265.7	0.0	0.0	0.0	0.0	0.0	0.0	0.0	0.0	265.7	87.0
Fire44	0.0	0.0	0.0	0.0	0.0	0.0	0.0	0.0	907.5	0.0	907.5	535.0
Fire45	0.0	0.0	0.0	0.0	0.0	0.0	0.0	0.0	857.2	0.0	857.2	456.0
Fire46	0.0	0.0	0.0	0.0	0.0	0.0	0.0	0.0	2678.1	0.0	2678.1	250.0
Fire47	103.9	389.8	138.3	259.5	213.6	74.2	0.0	0.0	376.2	0.0	*1555.5*	415.0
Fire48	0.0	0.0	0.0	0.0	0.0	0.0	0.0	0.0	2661.3	0.0	2661.3	441.0
Fire49										1007.4	1007.4	44.0
Fire50										251.4	251.4	187.0
Fire51	0.0	276.4	0.0	0.0	0.0	0.0	0.0	0.0	0.0	0.0	276.4	127.0
Fire52	115.2	422.4	135.3	404.2	215.8	0.0	69.8	0.0	957.5	0.0	*2320.1*	662.0
Fire53	0.0	1372.0	0.0	0.0	0.0	0.0	0.0	0.0	0.0	0.0	1372.0	538.0
Fire54	210.0	372.3	144.4	427.7	216.9	0.0	115.7	0.0	1110.5	0.0	*2597.4*	766.0
Fire55	534.4	0.0	0.0	0.0	0.0	0.0	0.0	0.0	0.0	0.0	534.4	349.0
Fire56	258.6	0.0	0.0	0.0	0.0	0.0	0.0	0.0	0.0	0.0	258.6	107.0
Fire57	212.3	458.2	138.9	423.5	147.8	0.0	68.7	0.0	643.8	0.0	*2093.1*	481.0
Fire58	70.7	171.9	15.0	134.8	172.5	0.0	80.7	34.4	329.1	0.0	1009.2	397.0
Fire59	173.6	310.5	14.3	126.2	151.9	0.0	77.6	0.0	512.3	0.0	1366.3	568.0
Fire60	0.0	0.0	0.0	0.0	0.0	0.0	0.0	0.0	0.0	530.0	530.0	179.0
Fire61	0.0	0.0	0.0	0.0	0.0	0.0	0.0	0.0	0.0	1028.5	1028.5	25.0
Fire62	0.0	0.0	0.0	0.0	0.0	0.0	0.0	480.7	0.0	0.0	480.7	69.0
Fire63	239.0	447.4	39.9	389.5	161.6	0.0	244.6	72.9	684.7	0.0	*2279.5*	456.0
Fire64	0.0	0.0	0.0	0.0	0.0	0.0	0.0	0.0	1830.1	0.0	1830.1	nm
Fire65	528.5	0.0	0.0	0.0	0.0	0.0	0.0	0.0	0.0	0.0	528.5	150.0
Fire66	0.0	0.0	0.0	0.0	0.0	0.0	842.4	0.0	0.0	0.0	842.4	314.0
Fire67	333.0	0.0	129.8	397.6	171.0	0.0	222.3	37.7	971.1	0.0	*2262.5*	473.0
Fire68	0.0	0.0	0.0	0.0	0.0	0.0	0.0	0.0	918.5	0.0	918.5	354.0
Fire69	0.0	0.0	0.0	0.0	0.0	0.0	690.8	0.0	0.0	0.0	690.8	364.0
Fire70	0.0	0.0	0.0	0.0	0.0	0.0	0.0	0.0	0.0	1955.2	1955.2	250.0

Table S1. Continued

Fire "name"	Stack/Room[1]	Date	Ignition time	Fuel type	Relative Humidity	%C	%H	%N	%S	Cl (mg/kg)	MCE
	SC = smog chamber fill	2016 mm/dd	MST hh:mm:ss	Sampling location = Lubrecht unless otherwise noted	%	best estimate fuel avg					Flaming/Smoldering
Fire71	Stack	10/22	8:01:05	sagebrush, Clearwater, MT	36.0	46.39	6.22	0.78	0.07	1135.58	0.9225
Fire72	Stack/SC	10/22	9:45:00	ponderosa pine	37.0	50.65	6.63	0.89	0.08	120.97	0.9401
Fire73	Stack	10/22	11:10:32	ponderosa pine, rotten log	34.0	50.14	5.86	0.37	<0.03	54.89	0.9319
Fire74	Stack	10/22	13:02:48	ceanothus	33.0	50.30	6.03	1.28	0.06	87.54	0.9468
Fire75	Stack	10/22	14:04:32	juniper, canopy	31.0	50.54	6.44	0.53	0.05	188.12	0.9394
Fire76	Room/SC	10/25	9:57:00	chaparral (manzanita, NM), canopy	35.0	48.67	6.32	0.56	0.08	76.62	0.9453
Fire77	Room/SC	10/25	14:03:03	chaparral (chamise, NM), canopy	57.0	49.65	6.75	0.81	0.08	290.00	0.9446
Fire78	Room	10/26	8:01:27	ponderosa pine	37.0	51.00	6.52	0.96	0.07	109.33	0.9334
Fire79	Room/SC	10/26	12:08:30	lodgepole pine	56.0	50.02	6.37	0.74	0.24	133.29	0.9452
Fire80	Room	10/27	8:26:29	Douglas fir	44.0	49.72	6.31	0.97	0.06	47.63	0.9319
Fire81	Room/SC	10/27	12:34:22	subalpine fir	39.0	50.22	6.46	0.65	0.07	nm	0.9260
Fire82	Room	10/29	8:05:59	Excelsior	29.0	48.40	6.30	0.23	0.05	<25	0.9607
Fire83	Room/SC	10/29	12:29:00	Engelmann spruce	32.0	41.91	4.47	0.94	0.11	210.11	0.8213
Fire84	Room	10/31	8:02:34	chaparral (chamise, SD), canopy	36.0	50.72	6.42	0.86	0.06	89.75	0.9527
Fire85	Room/SC	10/31	12:30:48	sagebrush, Clearwater, MT	37.0	46.39	6.22	0.78	0.07	1135.58	0.9384
Fire86	Room	11/1	8:04:32	lodgepole pine	34.0	50.11	6.37	0.71	0.29	89.97	0.9490
Fire87	Room/SC	11/1	12:45:06	lodgepole pine, canopy	31.0	50.77	6.48	1.01	0.09	149.03	0.9281
Fire88	Room	11/2	8:16:29	juniper, canopy	28.0	50.54	6.44	0.53	0.05	188.12	0.9465
Fire89	Room/SC	11/2	12:45:24	ceanothus	30.0	50.30	6.03	1.28	0.06	87.54	0.9506
Fire90	Room	11/3	8:23:00	subalpine fir, duff	27.0	39.69	5.52	1.19	0.11	125.27	0.9238
Fire91	Room/SC	11/3	12:37:22	chaparral (manzanita, SD), canopy	28.0	47.20	6.01	0.66	0.05	37.30	0.9453
Fire92	Room	11/4	8:19:28	Engelmann spruce, duff	28.0	41.91	4.47	0.94	0.11	210.11	0.9114
Fire93	Room/SC	11/4	12:40:15	Peat, Kalimantan[6], site 2	30.0	56.97	5.57	1.53	0.25	182.02	0.8384
Fire94	Room	11/5	8:00:25	chaparral (chamise, NM), canopy	27.0	49.65	6.75	0.81	0.08	290.00	0.9584
Fire95	Room/SC	11/5	12:32:24	ponderosa pine, litter	28.0	50.31	6.72	0.55	0.08	136.21	0.9448
Fire96	Room	11/6	9:12:22	longleaf pine, Fort Stewart[7]	28.0	49.23	6.04	0.53	0.06	nm	0.9379
Fire97	Room/SC	11/6	13:36:20	longleaf pine, Fort Stewart	28.0	49.17	6.03	0.53	0.06	nm	0.9337
Fire98	Room	11/8	9:00:21	ponderosa pine, canopy	29.0	50.29	6.85	1.23	0.12	163.30	0.9246
Fire99	Room/SC	11/8	13:35:26	cow dung, MT	29.0	40.92	5.09	1.74	0.27	77.15	0.8390
Fire100	Room	11/9	10:00:01	Excelsior	29.0	48.40	6.30	0.23	0.05	<25	0.9607
Fire101	Room/SC	11/9	14:16:02	ponderosa pine, rotten log	28.0	50.14	5.86	0.37	<0.03	54.89	0.9156
Fire102	Room	11/10	9:07:53	Engelmann spruce, duff	28.0	41.91	4.47	0.94	0.11	210.11	0.9215
Fire103	Room/SC	11/10	13:40:34	cow dung, MT	30.0	40.92	5.09	1.74	0.27	77.15	0.9254
Fire104	Room	11/11	9:19:23	subalpine fir, duff	28.0	42.15	5.25	1.42	0.13	125.27	0.8881
Fire105	Room/SC	11/11	13:03:01	ponderosa pine, rotten log	25.0	50.14	5.86	0.37	<0.03	54.89	0.9177

Table S1. Continued

Fire "name"	Fuel mixture components by mass as grams dry weight (red entry is wet weight due to missing fuel moisture data)										Total fuel mass	Total Residual
	Duff	Litter	Dead and down woody debris diameter (cm)[8]				Shrub	Herbaceous	Canopy (needle+branch)	Other fuels	italic number > fuel added during fire	grams ash plus unburned fuel
			0-0.64 (1h)	0.64-2.5 (10h)	2.5-7.6 (100h)	>7.6 (1000h)						
Fire71	0.0	0.0	0.0	0.0	0.0	0.0	730.1	0.0	0.0	0.0	730.1	31.0
Fire72	247.9	930.2	43.5	379.8	159.8	0.0	124.2	0.0	1032.3	0.0	2917.7	885.0
Fire73	0.0	0.0	0.0	0.0	0.0	535.7	0.0	0.0	0.0	0.0	535.7	32.0
Fire74	0.0	0.0	0.0	0.0	0.0	0.0	1926.3	0.0	0.0	0.0	1926.3	842.0
Fire75	0.0	0.0	0.0	0.0	0.0	0.0	0.0	0.0	852.8	0.0	852.8	499.0
Fire76	0.0	0.0	0.0	0.0	0.0	0.0	0.0	0.0	2946.1	0.0	2946.1	2039.0
Fire77	0.0	0.0	0.0	0.0	0.0	0.0	0.0	0.0	2023.4	0.0	2023.4	nm
Fire78	215.8	318.7	14.8	127.9	153.5	0.0	83.1	0.0	288.0	0.0	1201.7	565.0
Fire79	196.2	196.8	12.6	137.0	90.8	0.0	88.7	23.3	316.5	0.0	1062.0	583.0
Fire80	165.8	145.5	47.7	135.1	164.9	0.0	85.0	0.0	460.4	0.0	1204.4	594.0
Fire81	0.0	410.6	47.1	133.0	189.0	0.0	51.5	13.9	368.0	0.0	1213.1	959.0
Fire82	0.0	0.0	0.0	0.0	0.0	0.0	0.0	0.0	0.0	2601.8	2601.8	196.0
Fire83	543.5	0.0	0.0	0.0	0.0	0.0	0.0	0.0	0.0	0.0	543.5	17.0
Fire84	0.0	0.0	0.0	0.0	0.0	0.0	0.0	0.0	3545.3	0.0	3545.3	348.0
Fire85	0.0	0.0	0.0	0.0	0.0	0.0	2571.2	0.0	0.0	0.0	2571.2	817.0
Fire86	289.9	162.5	13.0	129.2	182.0	0.0	75.5	0.0	376.6	0.0	1228.9	464.0
Fire87	0.0	0.0	0.0	0.0	0.0	0.0	0.0	0.0	377.5	0.0	377.5	1326.0
Fire88	0.0	0.0	0.0	0.0	0.0	0.0	0.0	0.0	1950.9	0.0	1950.9	642.0
Fire89	0.0	0.0	0.0	0.0	0.0	0.0	2310.6	0.0	0.0	0.0	2310.6	750.0
Fire90	591.3	0.0	0.0	0.0	0.0	0.0	0.0	0.0	0.0	0.0	591.3	3455.0
Fire91	0.0	0.0	0.0	0.0	0.0	0.0	0.0	0.0	4365.7	0.0	4365.7	372.0
Fire92	658.4	0.0	0.0	0.0	0.0	0.0	0.0	0.0	0.0	0.0	658.4	296.0
Fire93	420.4	0.0	0.0	0.0	0.0	0.0	0.0	0.0	0.0	0.0	420.4	96.0
Fire94	0.0	0.0	0.0	0.0	0.0	0.0	0.0	0.0	3390.3	0.0	3390.3	388.0
Fire95	0.0	1903.8	0.0	0.0	0.0	0.0	0.0	0.0	0.0	0.0	1903.8	170.8
Fire96	358.3	278.6	31.0	277.5	175.7	0.0	128.8	313.4	209.8	0.0	1773.1	653.0
Fire97	362.1	292.1	31.0	257.8	175.3	0.0	122.9	330.7	189.0	0.0	1761.0	577.0
Fire98	0.0	0.0	0.0	0.0	0.0	0.0	0.0	0.0	3125.0	0.0	3125.0	1492.0
Fire99	nm	nm	nm	nm	nm	nm	nm	nm	nm	658.0	658.0	87.0
Fire100	nm	nm	nm	nm	nm	nm	nm	nm	nm	3077.3	3077.3	75.0
Fire101	nm	nm	nm	nm	nm	nm	nm	nm	nm	618.0	618.0	12.0
Fire102	237.0	0.0	0.0	0.0	0.0	0.0	0.0	0.0	0.0	0.0	237.0	167.0
Fire103	nm	nm	nm	nm	nm	nm	nm	nm	nm	724.2	724.2	176.0
Fire104	352.3	0.0	0.0	0.0	0.0	0.0	0.0	0.0	0.0	0.0	352.3	103.0
Fire105	nm	nm	nm	nm	nm	nm	nm	nm	nm	674.6	674.6	15.0

Table S1. Continued

Fire "name"	Stack/Room[1]	Date	Ignition time	Fuel type	Relative Humidity	%C	%H	%N	%S	Cl (mg/kg)	MCE
	SC = smog chamber fill	2016 mm/dd	MST hh:mm:ss	Sampling location = Lubrecht unless otherwise noted	%	*best estimate fuel avg*					Flaming/Smoldering
Fire106	Room	11/12	9:00:00	ponderosa pine, littter and duff	27.0	50.30	6.77	0.83	0.10	147.23	0.9465
Fire107	Room/SC	11/12	13:01:50	chaparral (chamise, SD and NM), canopy	26.0	49.65	6.75	0.81	0.08	290.00	0.9612

Fire "name"	Fuel mixture components by mass as grams dry weight (red entry is wet weight due to missing fuel moisture data)										Total fuel mass	Total Residual
			Dead and down woody debris diameter (cm)[8]									
	Duff	Litter	0-0.64 (1h)	0.64-2.5 (10h)	2.5-7.6 (100h)	>7.6 (1000h)	Shrub	Herbaceous	Canopy (needle+branch)	Other fuels	italic number > fuel added during fire	grams ash plus unburned fuel
Fire106	0.0	1160.3	0.0	0.0	0.0	0.0	0.0	0.0	795.7	0.0	1956.1	nm
Fire107	0.0	0.0	0.0	0.0	0.0	0.0	0.0	0.0	4145.0	0.0	4145.0	242.0

1 - Stack/room detailed fire configuration descriptions in Stockwell et al., (2014)
2 - Fish Lake National Forest, UT, site of planned FASMEE burns
3 - San Dimas, CA is a heavily polluted chaparral site
4 - North Mountain, CA is a clean chaparral site
5 - Loblolly pine collected in
Kinston, NC
6 - Kalimantan peat collection sites described in Stockwell et al., (2016)
7 - Fort Stewart, Georgia, site of planned FASMEE burns
8 - Fuel "time-lag class" () in parentheses.

Table S2. *Emission Factors (g kg^{-1}) and optical properties by fire number for the 75 stack burns. OA is qualitative.*

	Fire #	Fire01	Fire02	Fire03	Fire04	Fire05	Fire06	Fire07	Fire08
Compound	**Fuel Type**	ponderosa pine	ponderosa pine	ponderosa pine	ponderosa pine	lodgepole pine	lodgepole pine	lodgepole pine	Engelmann spruce
CO_2		1695.9113	1713.4616	1714.8806	1681.2558	1665.2200	1694.9464	1694.3357	1598.5001
CO		72.1669	80.8134	75.1730	80.8872	78.3686	67.6560	65.1013	88.0729
CH_4		2.5792	2.4661	2.4302	2.8213	2.9104	2.3372	2.5794	4.5571
Methanol		0.6499	0.9895	1.2737	1.0600	1.0368	0.5678	0.7992	1.9027
Formaldehyde		1.4010	1.4333	1.8628	1.6405	1.9117	1.1785	1.1781	1.6181
HCl									
Acetylene		0.5836	0.2307	0.3792	0.4539	0.6000	0.4363	0.4595	0.2815
Ethylene		1.5569	0.9280	1.4336	1.6316	1.9478	1.5461	1.6162	1.2803
Propene		0.3995	0.4426	0.4690	0.5224	0.6299	0.2762	1.5003	0.6474
NH_3		0.4384	0.6061	0.6712	0.7001	0.7219	0.4902	0.6186	1.9641
1,3-Butadiene		0.0730			0.0230	0.0774	0.0000		
Acetic Acid		0.8311	0.6692	1.7072	1.4747	1.2691	0.3352	1.0065	1.8529
Formic Acid		0.2437	0.1969	0.2622	0.2090	0.2129	0.1579	0.1719	0.2068
Furan		0.4357		0.2271	0.3032	0.2359	0.1867	0.1772	0.3101
Hydroxyacetone		0.9186		0.9172	1.3873	0.9689	0.2031	0.6186	0.8498
Phenol					1.0411				
Furaldehyde					1.2927				
NO		1.0286	1.5204	1.4605	0.4413	1.8009	1.6729	1.9796	1.7242
NO_2		1.3357	2.9479	1.3735	1.1416	0.7526	0.7651	1.4987	2.5949
HONO		0.5441	0.2103	0.6038	0.7677	0.6920	0.6147	0.6537	0.4635
Glycolaldehyde					0.5787	0.5768	0.7148	0.5513	
HCN		0.2176	0.2658	0.3013	0.2156	0.2058	0.2190	0.1843	
SO_2		1.1558	0.7564	1.4473	2.0165	1.3439	1.1381	1.3621	1.3093
BC		0.7563	0.7157	0.5017	0.5530	0.4539	0.5018	0.3315	0.1439
OA		5.9642	4.5175	8.3624	6.1368	6.7473	5.2060	5.7593	4.7004
EFBabs870		3.5847	3.3924	2.3781	2.6212	2.1515	2.3785	1.5713	0.6821
XS_401/XS_870		3.8005	3.4750	4.6804	4.4645	5.2435	4.3151	5.7615	8.9240
EFBabs401		13.6237	11.7887	11.1303	11.7024	11.2813	10.2636	9.0531	6.0869
EFBabs401 (BrC)		5.8449	4.4271	5.9699	6.0144	6.6126	5.1022	5.6434	4.6068
EFBscat870		5.2448	4.2035	6.7004	4.7116	4.5809	3.2407	3.3307	5.9173
EFBscat401		46.1858	41.1330	64.2105	49.5879	52.0441	38.4156	42.2409	67.7987
SSA_405		0.7722	0.7772	0.8523	0.8091	0.8219	0.7892	0.8235	0.9176
SSA_870		0.5940	0.5534	0.7381	0.6425	0.6804	0.5767	0.6795	0.8966
AAE		1.7462	1.6291	2.0185	1.9568	2.1671	1.9123	2.2903	2.8626
MCE		0.9373	0.9310	0.9356	0.9297	0.9311	0.9410	0.9431	0.9200

Table S2. Continued

	Fire #	Fire09	Fire10	Fire11	Fire12	Fire13	Fire14	Fire15	Fire16
Compound	**Fuel Type**	Engelmann spruce	Douglas fir	Douglas fir	Engelmann spruce, duff	ponderosa pine, rotten log	Douglas fir	subalpine fir, Fish Lake, canopy	ponderosa pine, litter
CO_2		1596.3367	1696.9571	1689.0768	1276.7245	1732.8710	1651.9923	1529.9285	1726.5972
CO		81.3478	64.7321	58.8635	123.4135	49.7213	84.0332	123.2850	52.4116
CH_4		3.5568	2.1384	2.2998	11.1260	3.0453	2.8609	7.4825	1.4778
Methanol		1.9884	0.8248	0.7872	3.6520	0.7118	0.5275	2.9480	0.4703
Formaldehyde		1.8537	1.2558	1.5345	1.3608	1.3138	2.0929	4.7639	0.5233
HCl						0.0661			0.0361
Acetylene		0.2842	0.3579	0.5131	0.0737	0.1510	0.4656	2.1034	0.0976
Ethylene		1.2719	1.1905	1.5493	1.3749	0.5555	1.6318	7.8599	0.5036
Propene		0.5631	0.3491	0.3746	1.3022	0.1930	0.3956	2.4209	0.2566
NH_3		1.4761	0.5078	0.3613	4.8216	0.1417	0.5299	1.6808	0.4875
1,3-Butadiene				0.0133				0.7057	
Acetic Acid		2.2881	1.0578	1.0191	3.1999	0.5927	1.4470	4.1491	0.7854
Formic Acid		0.2200	0.1860	0.2457	0.2353	0.2623	0.3386	0.7894	0.0856
Furan		0.1017		0.1807	0.5300	0.1912		0.4773	0.1380
Hydroxyacetone		0.9081		0.6307	1.1357	0.6274		2.2802	0.3688
Phenol				0.7502		0.5756		0.9532	0.4496
Furaldehyde					0.9943	0.6756		0.6777	0.3986
NO		1.7700	1.9022	1.5318	0.6779	0.5056	2.1017	1.3773	1.8797
NO_2		2.1909	1.7703	1.1300	0.8181	1.1489	1.8492	0.5998	1.1000
HONO		0.1824	0.4821	0.6259	0.4179	0.2269	0.9059	1.2830	0.3271
Glycolaldehyde		0.6496		0.5775	0.2724	0.6909	0.4610	2.5411	0.2381
HCN		0.3098	0.1997	0.1746	0.9270	0.0695	0.2154	0.7889	0.1322
SO_2		1.3894	1.0985	1.1911	0.8237	0.5566	1.2462	2.2099	1.4066
BC		0.2071	0.2140	0.3014	0.0036	0.3204	0.2378	0.4342	1.1750
OA		4.3063	4.3382	5.6684	4.1557	3.6144	5.4545	29.1833	7.9619
EFBabs870		0.9817	1.0144	1.4286	0.0171	1.5187	1.1272	2.0581	5.5695
XS_401/XS_870		6.4694	6.3607	6.0578	240.4600	4.5020	6.9108	16.0663	3.5710
EFBabs401		6.3507	6.4520	8.6544	4.1032	6.8372	7.7897	33.0654	19.8887
EFBabs401 (BrC)		4.2205	4.2509	5.5543	4.0662	3.5416	5.3437	28.5994	7.8029
EFBscat870		5.4027	3.0055	3.7833	10.6772	3.3771	4.1336	36.8531	2.2757
EFBscat401		57.3247	40.3698	50.4058	94.8699	31.0894	54.4887	324.9041	29.4631
SSA_405		0.9003	0.8621	0.8535	0.9585	0.8197	0.8749	0.9076	0.5970
SSA_870		0.8462	0.7477	0.7259	0.9984	0.6898	0.7857	0.9471	0.2900
AAE		2.4419	2.4197	2.3559	7.1704	1.9677	2.5282	3.6316	1.6647
MCE		0.9259	0.9435	0.9481	0.8681	0.9569	0.9260	0.8856	0.9544

Table S2. Continued

	Fire #	Fire17	Fire18	Fire19	Fire20	Fire21	Fire22	Fire23	Fire24
Compound	**Fuel Type**	Engelmann spuce, Fish Lake, canopy	Douglas fir, canopy	ponderosa pine, canopy	lodgepole pine, canopy	lodgepole pine, litter	Douglas fir, litter	subalpine fir, Fish Lake, canopy	chaparral (chamise), San Dimas[3], canopy
CO_2		1515.9696	1633.3231	1664.7051	1696.9501	1614.4018	1609.3346	1760.2706	1746.3285
CO		115.0781	79.4561	73.2235	74.4584	80.2194	58.6066	61.4575	59.2124
CH_4		6.9558	3.1366	3.5586	2.3725	2.0874	1.4574	1.3326	0.9603
Methanol		3.8440	1.2229	1.6742	0.5802	0.8771	0.4516	0.2980	0.2349
Formaldehyde		4.1051	2.5902	1.8722	1.5896	1.0909	0.7152	0.6660	0.4892
HCl								0.0307	0.0588
Acetylene		1.7194	1.3718	0.4282	0.6556	0.1437	0.0990	0.3267	0.3168
Ethylene		5.5106	3.2809	1.9338	2.5885	0.8498	0.4411	0.8345	0.5294
Propene		1.9725	0.6901	0.7512	0.7282	0.4658	0.1945	0.1937	0.0817
NH_3		1.6937	0.7069	1.2922	0.7151	0.8249	0.3929	0.2897	0.3700
1,3-Butadiene		0.7398			0.1597				
Acetic Acid		8.3122	1.7092	1.9737	0.5938	1.6113	0.6068	0.3342	0.5994
Formic Acid		1.1746	0.4078	0.2120	0.1515	0.2013	0.0892	0.0699	0.0719
Furan		0.3586	0.1818	0.2767	0.0741		0.1186	0.0890	0.1041
Hydroxyacetone		2.6294	0.8627	0.8107	0.3626		0.2981	0.4749	0.2895
Phenol		1.1198	0.7503	0.8749	0.5227				0.5165
Furaldehyde				0.5970	0.3063				0.1631
NO		0.6167	1.7359	2.1513	2.4035	1.9955	1.6950	2.7710	2.6314
NO_2		0.6394	0.9806	0.6460	1.7461	3.3747	1.0753	0.4596	0.0636
HONO		1.1344	0.9785	0.5353	0.6329	0.2180	0.2322	0.3202	0.3428
Glycolaldehyde		2.9525	1.1480	0.5426	0.3421				0.2201
HCN		0.5790	0.4831	0.2356	0.2337	0.4614	0.1156	0.0802	0.0415
SO_2		2.8751	1.9231	1.5581	1.1715	1.3144	1.0540	0.6856	1.0538
BC		0.1405	0.2558	0.5487	0.3190	0.2472	0.8832	0.6283	0.3005
OA		20.9203	12.0578	11.8680	8.1676	3.1815	8.4154	7.2276	3.7669
EFBabs870		0.6660	1.2125	2.6008	1.5121	1.1717	4.1864	2.9782	1.4244
XS_401/XS_870		32.9646	11.9175	6.6418	7.4636	4.8314	4.1401	4.5483	4.7611
EFBabs401		21.9534	14.4499	17.2742	11.2854	5.6611	17.3320	13.5457	6.7816
EFBabs401 (BrC)		20.5083	11.8188	11.6304	8.0042	3.1184	8.2476	7.0830	3.6907
EFBscat870		18.0559	5.1005	5.1104	1.9968	2.8343	1.7231	0.8923	0.4471
EFBscat401		327.9097	92.0211	92.6141	43.3879	48.2483	28.4730	16.9850	10.0835
SSA_405		0.9373	0.8643	0.8428	0.7936	0.8950	0.6216	0.5563	0.5979
SSA_870		0.9644	0.8079	0.6627	0.5691	0.7075	0.2916	0.2306	0.2389
AAE		4.5715	3.2409	2.4763	2.6289	2.0601	1.8581	1.9811	2.0409
MCE		0.8903	0.9279	0.9345	0.9355	0.9255	0.9454	0.9471	0.9480

Table S2. Continued

	Fire #	Fire25	Fire26	Fire27	Fire28	Fire29	Fire30	Fire31	Fire32
Compound	**Fuel Type**	Engelmann spruce, canopy	Engelmann spruce, duff	chaparral (chamise), North Mountain[4], canopy	chaparral (manzanita, NM), canopy	chaparral (chamise, SD), canopy	chaparral (manzanita, SD) canopy	Douglas fir, rotten log	chaparral (chamise, NM), canopy
CO_2		1717.7540	1183.2180	1697.6269	1687.2951	1759.3670	1647.2996	1533.2036	1723.2381
CO		56.1512	168.5182	61.7639	41.1260	47.5444	37.8283	274.3201	53.0535
CH_4		1.8445	14.7900	1.3725	1.1906	0.8031	1.3116	12.7943	1.1792
Methanol		0.4790	4.3690	0.3620	0.5818	0.2466	0.3972	7.1173	0.4482
Formaldehyde		0.7426	1.6388		0.5620	0.3915	0.1692	9.2378	0.5441
HCl		0.0364					0.1467		
Acetylene		0.1098		0.3926	0.2769	0.2343	0.2876	0.1264	0.2287
Ethylene		0.6098	2.2291	0.5237	0.6903	0.3395	0.7216	1.3110	0.428
Propene		0.2202	1.9299	0.1003	0.2008	0.0720	0.2004	0.4351	0.1204
NH_3		0.5295	9.3719	0.5332	0.5463	0.2988	0.5570	0.6427	0.5596
1,3-Butadiene									
Acetic Acid		0.7524	5.1397	0.6836	2.7341	0.4850	0.3013	2.6999	0.7624
Formic Acid		0.1096	0.3478	0.0516	0.2988	0.0444	0.0650	1.3835	0.055
Furan		0.1402	1.2142	0.0923	0.8814	0.0754	0.0327	0.9193	0.044
Hydroxyacetone		0.4985	2.1128	0.3116	0.2513	0.3044	0.2716		0.3166
Phenol					0.2414	0.1697	0.1358		0.4435
Furaldehyde				0.2394	0.7989	0.2744	0.2251	4.4250	0.6601
NO		2.4985		2.4261	1.8953	2.5889	2.0038		2.3325
NO_2		0.9228		0.4695	0.8770	0.4929	0.6201		0.6148
HONO		0.3621		0.3565	0.4398	0.3517	0.3814		0.517
Glycolaldehyde		0.4657		0.1224	0.1835		0.1241	2.1704	
HCN		0.1134	1.4756	0.0781	0.0688	0.0594	0.0918	0.4897	0.0985
SO_2		1.3648	0.8169	0.8693	0.8969	0.7814	0.8130	2.6776	0.8249
BC		0.2309	0.0038	0.4694	0.3013	0.6175	0.2888	0.0075	0.5371
OA		6.4726	4.0635	5.6877	5.6679	6.7580	5.3626	9.0657	
EFBabs870		1.0945	0.0180	2.2250	1.4282	2.9270	1.3689	0.0356	2.5459
XS_401/XS_870		5.7960	226.0753	4.6751	6.0595	4.4325	6.0087	253.6029	
EFBabs401		6.3435	4.0721	10.4019	8.6539	12.9737	8.2254	9.0156	
EFBabs401 (BrC)		3.9685	4.0330	5.5737	5.5548	6.6222	5.2548	8.9384	
EFBscat870		1.0332	4.0441	0.5311	1.2591	0.5037	1.0270	18.3070	0.6741
EFBscat401		24.5184	93.8722	12.0256	23.7568	10.5736	21.3432	251.2057	
SSA_405		0.7945	0.9584	0.5362	0.7330	0.4490	0.7218	0.9653	
SSA_870		0.4856	0.9956	0.1927	0.4685	0.1469	0.4286	0.9981	0.2094
AAE		2.2981	7.0898	2.0171	2.3563	1.9474	2.3453	7.2400	
MCE		0.9499	0.8171	0.9459	0.9631	0.9593	0.9630	0.7805	0.9539

Table S2. Continued

Compound	Fire # / Fuel Type	Fire33 chaparral (manzanita, SD), canopy	Fire34 chaparral (manzanita, NM), canopy	Fire35 loblolly pine5, litter	Fire36 Englmann spruce, duff	Fire37 ponderosa pine	Fire38 ponderosa pine, litter	Fire39 ponderosa pine, canopy
CO_2		1652.2903	1709.6214	1663.9798	1298.5634	1716.8109	1721.3985	1605.4892
CO		41.2936	40.1127	89.2196	122.0426	70.2155	64.0137	108.4253
CH_4		0.9978	1.088	2.0799	6.873	2.4898	1.4926	5.4583
Methanol		0.4837	0.4759	0.9887	4.2425	1.9127	0.8926	2.7867
Formaldehyde		0.5535	0.3659	0.997	3.5455	1.7931	1.2283	3.8207
HCl								
Acetylene		0.2258	0.1533	0.0747	0.0944	0.5381	0.1073	1.3109
Ethylene		0.5394	0.4397	0.5759	1.2577	1.6804	0.5227	4.6978
Propene		0.142	0.1339	0.2513	1.1326	0.4828	0.2938	1.6404
NH_3		0.6075	0.5005	0.3512	4.437	0.6596	0.3672	1.9878
1,3-Butadiene						0.0252		0.3432
Acetic Acid		1.0682	0.7625	1.9739	3.9215	1.6832	1.6803	3.8524
Formic Acid		0.1099	0.0648	0.0826	0.5398	0.2876	0.1813	0.6447
Furan		0.0551	0.0435	0.1763		0.1566	0.2468	0.3571
Hydroxyacetone		0.2714	0.3641	0.4896		0.7429	1.1122	1.5499
Phenol		0.3886	0.3734	0.4918		1.0623	1.1587	1.2841
Furaldehyde		0.6635	0.6444	0.8678	0.1357	1.0051	1.1344	0.2553
NO		2.0009	1.8823	1.5495		1.5375	1.4935	1.3736
NO_2		0.9453	0.74	1.0769		1.6281	1.3498	1.4131
HONO		0.6291	0.4469	0.3225		0.7595	0.5526	0.7271
Glycolaldehyde						0.6555		1.5255
HCN		0.1191		0.2402	1.2338	0.3642	0.2395	0.7724
SO_2		1.0163		1.0095		1.4535	0.9717	2.1902
BC		0.3424	0.2561	0.3434	0.0019	0.2252	0.3113	0.1446
OA								
EFBabs870		1.623	1.2139	1.6277	0.009	1.0674	1.4756	0.6854
XS_401/XS_870								
EFBabs401								
EFBabs401 (BrC)								
EFBscat870		0.8727	0.533	1.9485	9.4277	2.1095	1.5375	7.036
EFBscat401								
SSA_405								
SSA_870		0.3497	0.3051	0.5449	0.999	0.664	0.5102	0.9112
AAE								
MCE		0.9622	0.9644	0.9223	0.8713	0.9396	0.9448	0.9041

Table S2. Continued

	Fire #	Fire40	Fire41	Fire42	Fire43	Fire44	Fire45
Compound	**Fuel Type**	lodgepole pine, canopy	lodgepole pine, litter	lodgepole pine	Douglas fir, litter	Engelmann spruce, canopy	Douglas fir, canopy
CO_2		1673.2418	1634.6638	1726.8346	1639.3637	1731.3458	1628.8629
CO		87.5965	69.0667	56.2422	54.089	52.0505	92.0059
CH_4		3.4809	2.1075	2.1669	1.9481	1.8707	3.2399
Methanol		1.4789	1.1645	0.7033	0.2751	0.5028	1.8644
Formaldehyde		2.9727	1.0076	1.367	0.4901	1.2227	3.4284
HCl		0.0271					0.0562
Acetylene		0.826	0.1203	0.4435	0.1056	0.6077	1.2363
Ethylene		3.9389	0.8586	1.5174	0.3468	1.5268	4.3047
Propene		1.222	0.4304	0.4505		0.3678	1.071
NH_3		0.9875	0.7928	0.4497	0.2921	0.413	0.9236
1,3-Butadiene		0.3768		0.0631		0.0594	0.3858
Acetic Acid		2.4746	2.3743	1.0045		0.8804	2.6194
Formic Acid		0.568	0.1644	0.1985	0.0759	0.1875	0.5501
Furan		0.1759	0.1106	0.1032			0.2055
Hydroxyacetone		1.3216	0.5889	0.3972		0.538	1.4191
Phenol		1.3099	0.2871	0.2455		0.2233	1.0046
Furaldehyde		0.9609	0.6629	0.701		0.866	0.8122
NO		1.5746	2.2944	2.0223	1.2223	1.87	1.5019
NO_2		1.3816	1.4191	1.2092	1.2525	1.5326	2.22
HONO		0.9582	0.3157	0.6668	0.2255	0.6555	1.0547
Glycolaldehyde		0.3506	0.4604	0.5275			1.2905
HCN		0.4427	0.2331	0.2155		0.305	0.6145
SO_2		2.6842	1.836	1.4162		1.2671	1.4399
BC		0.0987	0.0672	0.2009	0.445	0.0784	0.0483
OA							
EFBabs870		0.4678	0.3185	0.9523	2.1093	0.3716	0.2289
XS_401/XS_870							
EFBabs401							
EFBabs401 (BrC)							
EFBscat870		2.9361	1.9453	1.0292	0.6364	0.7165	3.7841
EFBscat401							
SSA_405							
SSA_870		0.8626	0.8593	0.5194	0.2318	0.6585	0.943
AAE							
MCE		0.924	0.9377	0.9513	0.9507	0.9549	0.9185

Table S2. Continued

Compound	Fire #	Fire46	Fire47	Fire48	Fire49	Fire50	Fire51	Fire52
	Fuel Type	chaparral (chamise, SD), canopy	subalpine fir, Fish Lake	chaparral (chamise, NM), canopy	Excelsior (poplar)	yak dung, MT	subalpine fir, Fish Lake, litter	Engelmann spruce
CO_2		1767.1597	1652.0785	1723.2332	1709.8545	1182.3088	1597.3364	1706.5052
CO		51.4354	76.3892	52.9731	32.4443	84.2355	105.1323	48.399
CH_4		0.9239	4.808	1.2309	0.824	6.6348	6.5274	1.2782
Methanol		0.2891	1.6721	0.3944	0.4161	2.4762	2.4289	0.6157
Formaldehyde		0.3501	2.1479	0.5475	0.6519	1.7133	0.9803	1.2309
HCl								0.0505
Acetylene		0.2326	0.4671	0.3106	0.0706	0.2486	0.2592	0.2993
Ethylene		0.3192	2.2355	0.4867	0.267	1.8491	2.7907	0.8622
Propene			0.9386	0.1031	0.0667	1.2105	1.4005	0.1946
NH_3		0.3554	1.2591	0.5793	0.1212	4.452	2.3838	0.524
1,3-Butadiene			0.1168					
Acetic Acid		0.6148	2.9439	0.769	0.838	6.3562	5.993	1.2418
Formic Acid		0.0329	0.2991	0.0528	0.0648	0.3367	0.3965	0.2368
Furan		0.0376	0.1833	0.056	0.065	0.5804		0.0596
Hydroxyacetone		0.4357	0.7805	0.4394	0.6125	1.4098	1.5986	0.6771
Phenol		0.4831	0.4218	0.5409	0.7216	0.5416	1.1571	0.6863
Furaldehyde		0.7846	0.3209	0.6912	0.7193	1.4733	1.7183	0.8414
NO		2.6271	1.9374	2.4211	0.7069	1.4176	3.5303	1.8078
NO_2		0.2863	1.4975	0.3987	0.0845	1.8723	3.6248	1.6164
HONO		0.4567	0.742	0.5663	0.3011	0.324	0.2712	0.5298
Glycolaldehyde			0.8632		0.571	0.66	1.2347	0.5549
HCN			0.2885	0.1309	0.0579	1.9583	0.4971	0.2206
SO_2		0.7248	2.0063	0.7634	0.447	2.8807	3.0728	1.0722
BC		0.4205	0.0853	0.2631	0.433	0.0134	1.5226	0.0815
OA								
EFBabs870		1.9932	0.4043	1.2471	2.0524	0.0635	7.2171	0.3863
XS_401/XS_870								
EFBabs401								
EFBabs401 (BrC)								
EFBscat870		0.3763	2.5387	0.359	0.5492	5.2283	4.1188	0.8758
EFBscat401								
SSA_405								
SSA_870		0.1588	0.8626	0.2235	0.2112	0.988	0.3633	0.6939
AAE								
MCE		0.9563	0.9323	0.9539	0.971	0.8993	0.9063	0.9573

Table S2. Continued

	Fire #	Fire53	Fire54	Fire55	Fire56	Fire57	Fire58	Fire59
Compound	**Fuel Type**	loblolly pine, litter	Engelmann spruce	Peat, Kalimantan6, mixed sites	subalpine fir, Fish Lake, duff	Douglas fir	lodgepole pine	ponderosa pine
CO_2		1770.0784	1677.1149	1687.9702	1300.6036	1705.9212	1671.6176	1656.0287
CO		85.598	59.8527	217.8979	106.1839	55.8495	83.1809	100.8904
CH_4		1.9379	2.703	10.3854	10.98	1.9573	2.6591	4.5848
Methanol		0.9013	0.8686	2.9293	4.1583	0.7711	0.9569	2.301
Formaldehyde		0.8218	1.5362	1.2231	0.8065	1.2246	2.3023	2.77
HCl		0.0451			0.2761			
Acetylene		0.0965	0.4335	0.123	0.0768	0.2707	0.6993	0.6807
Ethylene		0.5918	1.3138	1.6891	2.2942	0.9585	2.3244	2.5157
Propene		0.2874	0.4164	1.6038	2.3438	0.2882	0.7222	0.8312
NH_3		0.4977	0.5789	1.6517	8.4968	0.4761	0.6894	1.1406
1,3-Butadiene			0.02				0.0926	0.0334
Acetic Acid		1.77	1.4519	4.4491	7.9532	1.0442	1.5466	3.799
Formic Acid		0.091	0.2629	0.3685	0.2765	0.2219	0.2425	0.4704
Furan		0.1562	0.1426		0.6005	0.1085	0.1818	0.3897
Hydroxyacetone		0.7944	0.5686		2.1713	0.5386	0.2769	1.2525
Phenol		0.8423	0.5604		1.1833	0.1713	0.4006	0.6561
Furaldehyde		0.9783	0.6058		1.0504	0.6832	0.7992	0.7315
NO		2.0276	1.5627		0.5604	1.7997	1.8839	1.2876
NO_2		0.6563	1.7435		1.2962	1.5377	1.4316	0.6833
HONO		0.4395	0.4997		0.1459	0.5899	0.6711	0.6244
Glycolaldehyde		0.3233	0.6727			0.5618	0.6442	0.9327
HCN		0.246	0.2832	3.9791	1.8396	0.222	0.3139	0.42
SO_2		1.1356	1.5255	3.4152	0.5878	1.1752	1.1111	2.2332
BC		0.28	0.0559	0.0026	0.0052	0.1522	0.1937	0.1347
OA								
EFBabs870		1.3272	0.265	0.0123	0.0246	0.7214	0.9181	0.6385
XS_401/XS_870								
EFBabs401								
EFBabs401 (BrC)								
EFBscat870		1.6238	1.2614	3.1416	5.4284	1.1219	1.7748	4.3558
EFBscat401								
SSA_405								
SSA_870		0.5503	0.8264	0.9961	0.9955	0.6086	0.659	0.8722
AAE								
MCE		0.9294	0.9469	0.8314	0.8863	0.9511	0.9275	0.9126

Table S2. Continued

Compound	Fire #	Fire60	Fire61	Fire62	Fire63	Fire64	Fire65	Fire66	Fire67
	Fuel Type	rice straw, Arkansas	Excelsior	bear grass	lodgepole pine	Douglas fir, canopy	jeffrey Pine, ?< duff	sagebrush, Clearwater, MT	subalpine fir, MT (remainder)
CO_2		1361.3952	1624.5126	1427.7928	1678.1934	1644.41	1511.8498	1525.779	1667.5011
CO		42.9901	60.0084	104.1998	72.5694	84.2187	134.8154	85.3119	69.2174
CH_4		1.0027	1.8279	5.3916	3.0044	3.663	6.906	3.755	2.9105
Methanol		0.9497	1.6891	3.9426	1.0809	1.2754	2.416	1.1943	0.8922
Formaldehyde		1.4846	1.8691	3.6504	2.1067	2.9882	2.1721	2.2487	1.7011
HCl		0.6455		0.0844		0.0655			
Acetylene		0.0651	0.1264	0.9436	0.6363	1.0937	0.1255	0.806	0.537
Ethylene		0.4055	0.5509	3.1891	2.1679	3.5443	1.4135	2.5038	1.4877
Propene		0.1843	0.191	1.0924	0.6563	1.0155	0.5778	0.649	0.4296
NH_3		0.3646	0.2036	1.3543	0.7783	0.6909	1.3213	1.0313	0.4479
1,3-Butadiene				0.157	0.048	0.3989		0.0904	0.0639
Acetic Acid		2.4937	2.945	12.8011	1.5653	1.8323	3.6253	1.7692	1.0276
Formic Acid		0.2483	0.177	0.9153	0.2811	0.4037	0.5556	0.1788	0.2134
Furan		0.0746	0.1774	0.2773	0.1781	0.1565	0.5902	0.1151	0.1378
Hydroxyacetone		1.7122	1.0816	2.6176	0.6892	0.7361	1.2986	0.4436	0.6524
Phenol		0.6381	1.1534	1.3128	0.6063	1.3522	3.0921	0.478	0.8042
Furaldehyde		0.6717	1.1355	1.3765	0.7038	0.6591	2.6961	0.3226	0.8458
NO		1.7006	0.6102	1.3717	1.7075	1.383	0.929	1.8319	1.7706
NO_2		0.7479	0.0477	1.4565	1.1311	1.0116	0.7664	0.6227	1.2347
HONO		0.2312	0.2974	0.8502	0.7635	0.806	0.389	0.4001	0.6716
Glycolaldehyde		0.8989	0.7623	2.7169	0.7777	0.9945	0.1719	0.6908	0.6616
HCN		0.1568	0.0854	0.4053	0.3034	0.5746	0.8051	0.3912	0.2174
SO_2		1.4554	1.0336	2.9839	1.477	1.7901	2.7305	0.9557	1.3304
BC		0.0327	7.9172	2.6211	2.5471	0.73	1.4989	1.4567	1.8667
OA									
EFBabs870		0.155	37.5275	12.424	12.0733	3.4602	7.1048	6.9048	8.8482
XS_401/XS_870									
EFBabs401									
EFBabs401 (BrC)									
EFBscat870		3.3683	24.8507	135.7734	27.8325	40.8397	131.1579	22.2609	15.1259
EFBscat401									
SSA_405									
SSA_870		0.956	0.3984	0.9162	0.6975	0.9219	0.9486	0.7633	0.6309
AAE									
MCE		0.9527	0.9451	0.8971	0.9364	0.9255	0.8771	0.9192	0.9421

Table S2. Continued

	Fire #	Fire68	Fire69	Fire70	Fire71	Fire72	Fire73	Fire74	Fire75
Compound	**Fuel Type**	juniper, canopy	ceanothus	untreated lumber	sagebrush, Clearwater, MT	ponderosa pine	ponderosa pine, rotten log	ceanothus	juniper, canopy
CO_2		1681.2609	1710.3072	1607.9523	1537.9962	1715.0254	1680.9777	1727.3992	1713.6804
CO		82.5343	66.8188	52.9236	82.2548	69.5291	78.163	61.8059	70.3324
CH_4		2.7883	1.8429	0.795	2.9817	1.9493	3.9898	1.7506	2.0459
Methanol		0.9246	0.9043	0.2313	1.057	0.9769	1.5525	0.5622	0.7313
Formaldehyde		2.1235	1.1228	0.426	1.2883	1.6337	2.7301	0.6319	1.6387
HCl							0.6661	0.0176	0.0408
Acetylene		1.0323	0.4174	0.1432	0.475	0.4624	0.1187	0.1967	0.5944
Ethylene		3.0526	1.1154	0.2797	1.148	1.526	0.5784	0.646	2.1587
Propene		0.7188	0.2819	0.0471	0.3874	0.4574		0.1671	0.5325
NH_3		0.558	1.4232	0.1768	0.7484	0.5921		0.8632	0.7568
1,3-Butadiene		0.2921				0.0325			0.1108
Acetic Acid		1.2395	2.199	0.5451	1.8809	1.2895	1.805	1.2095	0.8215
Formic Acid		0.0812	0.2352	0.1617	0.1211	0.2707	0.8749	0.0748	0.1906
Furan		0.12	0.113		0.0752	0.2724		0.0827	0.0768
Hydroxyacetone		0.9066	0.9069	0.5261	0.4707	0.6294	1.5305	0.5	0.5315
Phenol		0.2676	1.0586	0.4727	0.1114	0.7943		0.6476	0.3527
Furaldehyde		0.7522	1.0479	0.5685	0.5339	0.7768	0.8173	0.7728	0.5067
NO		2.0906	3.0184	1.1318	2.3749	1.4708	0.4831	3.4446	2.4968
NO_2		0.6679	0.6675	0.0941	0.8024	1.5964	0.7139	0.6792	1.6176
HONO		0.9809	0.8826	0.3521	0.4297	0.7112	0.2587	0.5273	0.7412
Glycolaldehyde		1.0381	0.1679	0.0969	0.325	0.586	1.4719	0.0789	0.4516
HCN		0.365	0.3646	0.0574	0.1994	0.2596			0.3138
SO_2		1.4708	1.4217		1.1187	1.3735		1.0183	1.4465
BC		1.4746	1.0058	3.2223	2.5884	1.8016	1.3868	0.9324	0.8741
OA									
EFBabs870		6.9896	4.7675	15.2737	12.269	8.5396	6.5734	4.4196	4.1432
XS_401/XS_870									
EFBabs401									
EFBabs401 (BrC)									
EFBscat870		19.9889	14.7258	2.9616	7.2473	14.2432	49.3191	3.0243	10.3436
EFBscat401									
SSA_405									
SSA_870		0.7409	0.7554	0.1625	0.3713	0.6252	0.8824	0.4063	0.714
AAE									
MCE		0.9284	0.9422	0.9508	0.9225	0.9401	0.9319	0.9468	0.9394

Table S3. *Emission factors (g kg^{-1}) from Table S2, showing averages for individual fuel types. Values in brackets represent 1σ.*

Compound	Fuel Type	Bear Grass	Ceanothus	Chaparral - Chamise, North Mountain Canopy	Chaparral - Chamise, San Dimas Canopy	Chaparral - Manzanita, North Mountain Canopy
CO_2		1427.7928	1718.8532 (12.09)	1714.6994 (14.7853)	1757.6184 (10.5251)	1698.4582 (15.787)
CO		104.1998	64.3124 (3.54)	55.9301 (5.04523)	52.7307 (5.9408)	40.6194 (0.7166)
CH_4		5.3916	1.7967 (0.0652)	1.2609 (0.1001)	0.8958 (0.0823)	1.1393 (0.0725)
Methanol		3.9426	0.7332 (0.242)	0.4015 (0.0435)	0.2569 (0.0285)	0.5288 (0.0749)
Formaldehyde		3.6504	0.8774 (0.3472)	0.5458 (0.0024)	0.4102 (0.0714)	0.464 (0.1387)
HCl		0.0844	0.0176		0.0588	
Acetylene		0.9436	0.307 (0.1561)	0.3106 (0.082)	0.2612 (0.0481)	0.2151 (0.0874)
Ethylene		3.1891	0.8807 (0.3319)	0.4794 (0.0483)	0.3961 (0.1159)	0.565 (0.1772)
Propene		1.0924	0.2245 (0.0812)	0.108 (0.0109)	0.0768 (0.0069)	0.1673 (0.0473)
NH_3		1.3543	1.1432 (0.396)	0.5574 (0.0231)	0.3414 (0.0376)	0.5234 (0.0324)
1,3-Butadiene		0.157				
Acetic Acid		12.8011	1.7042 (0.6996)	0.7383 (0.0475)	0.5664 (0.0709)	1.7483 (1.3941)
Formic Acid		0.9153	0.155 (0.1134)	0.0531 (0.0018)	0.0497 (0.02)	0.1818 (0.1655)
Furan		0.2773	0.0978 (0.0214)	0.0641 (0.0252)	0.0723 (0.0333)	0.4625 (0.5925)
Hydroxyacetone		2.6176	0.7034 (0.2877)	0.3559 (0.0724)	0.3432 (0.0804)	0.3077 (0.0797)
Phenol		1.3128	0.8531 (0.2906)	0.4922 (0.0688)	0.3898 (0.1913)	0.3074 (0.0933)
Furaldehyde		1.3765	0.9104 (0.1945)	0.5302 (0.2523)	0.4074 (0.3314)	0.7216 (0.1092)
NO		1.3717	3.2315 (0.3014)	2.3932 (0.0527)	2.6158 (0.0234)	1.8888 (0.0092)
NO_2		1.4565	0.6733 (0.0083)	0.4943 (0.1102)	0.2809 (0.2147)	0.8085 (0.0969)
HONO		0.8502	0.7049 (0.2512)	0.48 (0.1097)	0.3837 (0.0633)	0.4434 (0.0051)
Glycolaldehyde		2.7169	0.1234 (0.0629)	0.1224	0.2201	0.1835
HCN		0.4053	0.3646	0.1025 (0.0266)	0.0504 (0.0126)	0.0688
SO_2		2.9839	1.22 (0.2852)	0.8192 (0.0532)	0.8533 (0.1759)	0.8969
BC		2.6211	0.9691 (0.0519)	0.4232 (0.1427)	0.4462 (0.1601)	0.2787 (0.032)
OA				5.6877	5.2625 (2.115)	5.6679
EFBabs870			4.5935 (0.246)	2.006 (0.6765)	2.1148 (0.7586)	1.321 (0.1515)
XS_401/XS_870				4.6751	4.5968 (0.2324)	6.0595
EFBabs401				10.4019	9.8776 (4.3785)	8.6539
EFBabs401 (BrC)				5.5737	5.1565 (2.0729)	5.5548
EFBscat870			8.8751 (8.2742)	0.5214 (0.1578)	0.4424 (0.0638)	0.896 (0.5134)
EFBscat401				12.0256	10.3285 (0.3465)	23.7568
SSA_405				0.5362	0.5235 (0.1053)	0.733
SSA_870				0.2085	0.1815 (0.05)	0.3868
AAE				2.0171	1.9942 (0.0661)	2.3563
MCE		0.8971	0.9445 (0.00330	0.9512 (0.0046)	0.9545 (0.0058)	0.9638 (0.0009)

Table S3. Continued

Compound	Fuel Type	Douglas Fir	Douglas Fir, Canopy	Douglas Fir, Litter	Douglas Fir, Rotten Log	Engelmann Spruce	Engelmann Spruce Canopy
CO_2		1685.9868 (23.684)	1635.532 (8.0055)	1624.3491 (21.2338)	1527.4888	1644.6142 (55.81)	1724.5499 (9.6108)
CO		65.8696 (0.6583)	85.2269 (6.3354)	56.3478 (3.1944)	273.2977	69.4181 (18.47)	54.1009 (2.8996)
CH_4		2.3141 (0.3905)	3.3465 (0.2789)	1.7027 (0.347)	12.7466	3.0238 (1.3887)	1.8576 (0.0185)
Methanol		0.7277 (0.1353)	1.4542 (0.3562)	0.3633 (0.1248)	7.0908	1.3438 (0.7033)	0.4909 (0.0168)
Formaldehyde		1.527 (0.4022)	3.0022 (0.4193)	0.6026 (0.1592)	9.2034	1.5597 (0.2572)	0.9827 (0.3394)
HCl			0.0609 (0.0066)			0.0505	0.0364
Acetylene		0.4018 (0.1089)	1.2339 (0.1391)	0.1023 (0.0047)	0.126	0.3246 (0.073)	0.3588 (0.3521)
Ethylene		1.3325 (0.3145)	3.71 (0.5316)	0.394 (0.0667)	1.3061	1.1821 (0.214)	1.0683 (0.6484)
Propene		0.3519 (0.0465)	0.9255 (0.2058)	0.1945	0.4335	0.4554 (0.1983)	0.294 (0.1044)
NH_3		0.4688 (0.075)	0.7738 (0.13)	0.3425 (0.0713)	0.6403	1.1358 (0.7039)	0.4712 (0.0824)
1,3-Butadiene		0.0133	0.3923 (0.0093)			0.02	0.0594
Acetic Acid		1.142 (0.2039)	2.0537 (0.4938)	0.6068	2.6898	1.7087 (0.463)	0.8164 (0.0905)
Formic Acid		0.248 (0.0652)	0.4539 (0.0833)	0.0826 (0.0094)	1.3783	0.2316 (0.0242)	0.1486 (0.055)
Furan		0.1446 (0.0511)	0.1812 (0.0245)	0.1186	0.9159	0.1535 (0.1098)	0.1402
Hydroxyacetone		0.5846 (0.0651)	1.006 (0.3634)	0.2981		0.7509 (0.1562)	0.5182 (0.0279)
Phenol		0.4608 (0.4094)	1.0357 (0.3022)			0.6234 (0.089)	0.2233
Furaldehyde		0.6832	0.7356 (0.1083)		4.4085	0.7236 (0.1666)	0.866
NO		1.8338 (0.2372)	1.5402 (0.1796)	1.4587 (0.3343)		1.7162 (0.1079)	2.1842 (0.4444)
NO_2		1.5718 (0.3229)	1.4041 (0.7068)	1.1639 (0.1253)		2.0364 (0.4465)	1.2277 (0.4312)
HONO		0.6509 (0.1806)	0.9464 (0.1274)	0.2288 (0.0047)		0.4188 (0.16)	0.5088 (0.2075)
Glycolaldehyde		0.5334 (0.0633)	1.1443 (0.1481)		2.1623	0.6258 (0.0624)	0.4657
HCN		0.2029 (0.021)	0.5574 (0.0674)	0.1156	0.4878	0.2712 (0.0458)	0.2092 (0.1355)
SO_2		1.1778 (0.061)	1.7177 (0.2496)	1.054	2.6676	1.3241 (0.1902)	1.316 (0.069)
BC		0.2264 (0.0617)	0.3447 (0.3494)	0.6641 (0.3099)	0.0074	0.1221 (0.0677)	0.1547 (0.1078)
OA		5.1537 (0.7143)	12.0578	8.4154	14.4008	4.5034 (0.2787)	6.4726
EFBabs870		1.0729 (0.2924)	1.6339 (1.6563)	3.1478 (1.4687)	0.0351	0.5788 (0.3207)	0.733 (0.5111)
XS_401/XS_870		6.4431 (0.4324)	11.9175	4.1401	253.6029	7.6967 (1.7357)	5.796
EFBabs401		7.632 (1.1096)	14.4499	17.332	8.8954	6.2188 (0.1865)	6.3435
EFBabs401 (BrC)		5.0496 (0.6997)	11.8188	8.2476	8.8193	4.4137 (0.2731)	3.9685
EFBscat870		3.0111 (13448)	16.5747 (21.0244)	1.1797 (0.7684)	18.0629	3.3643 (2.6638)	0.8748 (0.2239)
EFBscat401		48.4214 (7.2656)	92.0211	28.473	247.8563	62.5617 (7.4062)	24.5184
SSA_405		0.8635 (0.0108)	0.8643	0.6216	0.9653	0.909 (0.0122)	0.7945
SSA_870		0.717 (0.0764)	0.8909	0.2617	0.9981	0.8158 (0.0865)	0.5721
AAE		2.4346 (0.0871)	3.2409	1.8581	7.24	2.6523 (0.2975)	2.2981
MCE		0.9421 (0.0112)	0.924 (0.0049)	0.9481 (0.0037)	0.7805	0.9375 (0.0175)	0.9524 (0.0035)

Table S3. Continued

Compound	Fuel Type	Engelmann Spruce Duff	Excelsior	Jeffrey Pine Duff	Juniper, Canopy	Loblolly Pine - Litter	Lodgepole Pine
CO_2		1252.8353 (61.2712)	1667.1835 (60.3458)	1511.8498	1697.4707 (22.924)	1717.0291 (75.023)	1688.5246 (22.2637)
CO		137.9914 (26.4459)	46.2263 (19.4908)	134.8154	76.4334 (8.628)	87.4088 (2.5609)	70.5197 (9.6698)
CH_4		10.9297 (3.9622)	1.326 (0.7099)	6.906	2.4171 (0.5249)	2.0089 (0.1004)	2.6095 (0.3225)
Methanol		4.0878 (0.3827)	1.0526 (0.9001)	2.416	0.828 (0.1367)	0.945 (0.0618)	0.8575 (0.2015)
Formaldehyde		2.1817 (1.1892)	1.2605 (0.8607)	2.1721	1.8811 (0.3429)	0.9094 (0.1239)	1.6741 (0.4948)
HCl					0.0408	0.0451	
Acetylene		0.084 (0.0147)	0.0985 (0.0395)	0.1255	0.8134 (0.3096)	0.0856 (0.0155)	0.5458 (0.1136)
Ethylene		1.6206 (0.5302)	0.4089 (0.2007)	1.4135	2.6057 (0.6321)	0.5839 (0.0113)	1.8533 (0.3445)
Propene		1.4549 (0.42)	0.1288 (0.0879)	0.5778	0.6256 (0.1318)	0.2694 (0.0256)	0.7059 (0.4218)
NH_3		6.2102 (2.7449)	0.1624 (0.0583)	1.3213	0.6574 (0.1406)	0.4244 (0.1036)	0.6247 (0.1311)
1,3-Butadiene					0.2015 (0.1282)		0.0562 (0.0355)
Acetic Acid		4.087 (0.9805)	1.8915 (1.4898)	3.6253	1.0305 (0.2956)	1.872 (0.1441)	1.1212 (0.4571)
Formic Acid		0.3743 (0.154)	0.1209 (0.0794)	0.5556	0.1359 (0.0774)	0.0868 (0.0059)	0.2108 (0.0456)
Furan		0.8721 (0.4838)	0.1212 (0.0795)	0.5902	0.0984 (0.0306)	0.1662 (0.0142)	0.1771 (0.0425)
Hydroxyacetone		1.6242 (0.6909)	0.8471 (0.3317)	1.2986	0.7191 (0.2652)	0.642 (0.2155)	0.5256 (0.2878)
Phenol			0.9375 (0.3053)	3.0921	0.3102 (0.0602)	0.6671 (0.2478)	0.4175 (0.181)
Furaldehyde		0.565 (0.6071)	0.9274 (0.2943)	2.6961	0.6295 (0.1736)	0.923 (0.0781)	0.7346 (0.0559)
NO		0.6779	0.6585 (0.0684)	0.929	2.2937 (0.2872)	1.7885 (0.338)	1.8445 (0.1425)
NO_2		0.8181	0.0661 (0.0261)	0.7664	1.1427 (0.6715)	0.8666 (0.2974)	1.1314 (0.319)
HONO		0.4179	0.2993 (0.0026)	0.389	0.8611 (0.1695)	0.381 (0.0827)	0.677 (0.0495)
Glycolaldehyde		0.2724	0.6667 (0.1352)	0.1719	0.7448 (0.4147)	0.3233	0.632 (0.0987)
HCN		1.2121 (0.2749)	0.0717 (0.0194)	0.8051	0.3394 (0.0362)	0.2431 (0.0041)	0.2403 (0.0544)
SO_2		0.8203 (0.0048)	0.7403 (0.4148)	2.7305	1.4586 (0.0171)	1.0725 (0.0892)	1.3081 (0.1497)
BC		0.0031 (0.001)	4.1751 (5.2921)	1.4989	1.1744 (0.4246)	0.3117 (0.0448)	0.3364 (0.1413)
OA		4.1096 (0.0652)					5.9042 (0.7808)
EFBabs870		0.0147 (0.0049)	19.79 (25.0847)		5.5664 (2.0127)	1.4775 (0.2125)	1.5943 (0.67)
XS_401/XS_870		233.2677 (10.1715)					5.1067 (0.7328)
EFBabs401		4.0876 (0.022)					10.1993 (1.1155)
EFBabs401 (BrC)		4.0496 (0.0235)					5.786 (0.7652)
EFBscat870		8.0496 (3.5247)	12.7 (17.1838)		15.1662 (6.8202)	1.7862 (0.2296)	2.7913 (1.3995)
EFBscat401		94.371 (0.7055)					44.2335 (7.0293)
SSA_405		0.9585 (0.0001)					0.8115 (0.0194)
SSA_870		0.9977 (0.0018)					0.6354 (0.0711)
AAE		7.1301 (0.057)					2.1232 (0.1928)
MCE		0.8522 (0.0304)	0.9581 (0.0183)	0.8771	0.9339 (0.0078)	0.9258 (0.005)	0.9384 (0.0086)

Table S3. Continued

Compound	Fuel Type	Lodgepole Pine, Canopy	Lodgepole Pine, Litter	Longleaf Pine	Peat, Kalimantan (mixed sites)	Peat, Room Burn	Ponderosa Pine	Ponderosa Pine, Canopy
CO_2		1685.0959 (16.7643)	1624.5328 (14.3274)	1687.8552	1687.9702	1708.6217	1699.0535 (23.1167)	1635.0971 (41.8719)
CO		81.0275 (9.29)	74.6431 (7.8861)	76.2924	217.8979	207.6943	78.5251 (10.8985)	90.8244 (24.8914)
CH_4		2.9267 (0.7838)	2.0974 (0.0142)	2.0502	10.3854	7.3795	2.7601 (0.8458)	4.5085 (1.3433)
Methanol		1.0296 (0.6354)	1.0208 (0.2032)	0.7471	2.9293	3.3294	1.3091 (0.5857)	2.2305 (0.7867)
Formaldehyde		2.2812 (0.978)	1.0492 (0.0589)	0.8111	1.2231	2.3442	1.7906 (0.4639)	2.8464 (1.3778)
HCl		0.0271						
Acetylene		0.7408 (0.1204)	0.132 (0.0166)	0.5008	0.123	0.2994	0.4755 (0.1458)	0.8696 (0.6242)
Ethylene		3.2637 (0.9549)	0.8542 (0.0062)	1.3553	1.6891	0.907	1.6103 (0.4711)	3.3158 (1.9544)
Propene		0.9751 (0.3492)	0.4481 (0.0251)	0.324	1.6038	1.2208	0.515 (0.1444)	1.1958 (0.6288)
NH_3		0.8513 (0.1926)	0.8088 (0.0227)	0.1127	1.6517	1.2086	0.6869 (0.2177)	1.64 (0.4919)
1,3-Butadiene		0.2683 (0.1535)					0.0374 (0.0204)	0.3432
Acetic Acid		1.5342 (1.33)	1.9928 (0.5395)	1.2371	4.4491	3.592	1.6363 (1.034)	2.9131 (1.3284)
Formic Acid		0.3597 (0.2945)	0.1829 (0.0261)	0.1558	0.3685		0.2772 (0.0912)	0.4283 (0.306)
Furan		0.125 (0.072)	0.1106				0.2974 (0.103)	0.3169 (0.0568)
Hydroxyacetone		0.8421 (0.6781)	0.5889	0.4017			0.9747 (0.2922)	1.1803 (0.5227)
Phenol		0.9163 (0.5566)	0.2871	0.7626		0.7655	0.8885 (0.197)	1.0795 (0.2893)
Furaldehyde		0.6336 (0.4629)	0.6629	0.909			0.9516 (0.2571)	0.4262 (0.2416)
NO		1.9891 (0.5861)	2.1449 (0.2113)	1.3536		0.9206	1.2495 (0.3986)	1.7624 (0.5499)
NO_2		1.5638 (0.2578)	2.3969 (1.3829)	1.0635		7.0422	1.5295 (0.7017)	1.0295 (0.5424)
HONO		0.7956 (0.23)	0.2668 (0.0691)	0.5573			0.603 (0.1921)	0.6312 (0.1356)
Glycolaldehyde		0.3463 (0.006)	0.4604				0.6882 (0.1666)	1.034 (0.6951)
HCN		0.3382 (0.1478)	0.3473 (0.1615)	0.4301	3.9791	4.4658	0.292 (0.0761)	0.504 (0.3796)
SO_2		1.9279 (1.0696)	1.5752 (0.3688)	1.3653	3.4152	3.3073	1.4909 (0.4993)	1.8741 (0.447)
BC		0.2089 (0.1558)	0.1572 (0.1273)		0.0026		0.4811 (0.2537)	0.3467 (0.2857)
OA		8.1676	3.1815				6.2452 (1.5876)	11.868
EFBabs870		0.9899 (0.7384)	0.7451 (0.6033)				2.2804 (1.2026)	1.6431 (1.3544)
XS_401/XS_870		7.4636	4.8314				4.1051 (0.5627)	6.6418
EFBabs401		11.2854	5.6611				12.0613 (1.0818)	17.2742
EFBabs401 (BrC)		8.0042	3.1184				5.5641 (0.7614)	11.6304
EFBscat870		2.4664 (0.6641)	2.3898 (0.6286)				4.5543 (1.4998)	6.0732 (1.3616)
EFBscat401		43.3879	48.2483				50.2793 (9.9158)	92.6141
SSA_405		0.7936	0.895				0.8027 (0.0369)	0.8428
SSA_870		0.7159	0.7834				0.6699 (0.1062)	0.787
AAE		2.6289	2.0601				1.8377 (0.1814)	2.4763
MCE		0.9297 (0.0081)	0.9316 (0.0087)	0.9322	0.8314	0.832	0.9323 (0.0095)	0.9193 (0.0215)

Table S3. Continued

Compound	Fuel Type	Ponderosa Pine, Litter	Ponderosa Pine, Rotten Log	Rice Straw, Arkansas	Sagebrush	Subalpine Fir
CO_2		1723.9978 (3.676)	1706.9244 (36.6941)	1361.3952	1531.8876 (8.6389)	1659.7898 (10.9054)
CO		58.2126 (8.2039)	63.9421 (20.1113)	42.9901	83.7833 (2.1617)	72.8033 (5.0712)
CH_4		1.4852 (0.0105)	3.5175 (0.6679)	1.0027	3.3684 (0.5468)	3.8593 (1.3417)
Methanol		0.6814 (0.2986)	1.1322 (0.5945)	0.9497	1.1256 (0.0971)	1.2822 (0.5514)
Formaldehyde		0.8758 (0.4985)	2.0219 (1.0015)	1.4846	1.7685 (0.6791)	1.9245 (0.3159)
HCl		0.0361	0.3661 (0.4242)	0.6455		
Acetylene		0.1025 (0.0068)	0.1349 (0.0228)	0.0651	0.6405 (0.234)	0.502 (0.0494)
Ethylene		0.5132 (0.0135)	0.5669 (0.0162)	0.4055	1.8259 (0.9587)	1.8616 (0.5287)
Propene		0.2752 (0.0263)	0.193	0.1843	0.5182 (0.185)	0.6841 (0.36)
NH_3		0.4274 (0.085)	0.1417	0.3646	0.8898 (0.2001)	0.8535 (0.5736)
1,3-Butadiene					0.0904	0.0903 (0.0374)
Acetic Acid		1.2328 (0.6328)	1.1988 (0.8572)	2.4937	1.8251 (0.0789)	1.9857 (1.355)
Formic Acid		0.1334 (0.0677)	0.5686 (0.4332)	0.2483	0.1499 (0.0408)	0.2562 (0.0606)
Furan		0.1924 (0.0769)	0.1912	0.0746	0.0951 (0.0282)	0.1606 (0.0322)
Hydroxyacetone		0.7405 (0.5256)	1.079 (0.6385)	1.7122	0.4572 (0.0191)	0.7165 (0.0906)
Phenol		0.8041 (0.5014)	0.5756	0.6381	0.2947 (0.2592)	0.613 (0.2704)
Furaldehyde		0.7665 (0.5203)	0.7464 (0.1001)	0.6717	0.4282 (0.1494)	0.5833 (0.3711)
NO		1.6866 (0.2731)	0.4944 (0.0159)	1.7006	2.1034 (0.384)	1.854 (0.1179)
NO_2		1.2249 (0.1766)	0.9314 (0.3075)	0.7479	0.7126 (0.127)	1.3661 (0.1858)
HONO		0.4398 (0.1595)	0.2428 (0.0225)	0.2312	0.4149 (0.021)	0.7068 (0.0498)
Glycolaldehyde		0.2381	1.0814 (0.5523)	0.8989	0.5079 (0.2586)	0.7624 (0.1426)
HCN		0.1858 (0.0758)	0.0695	0.1568	0.2953 (0.1356)	0.253 (0.0503)
SO_2		1.1891 (0.3075)	0.5566	1.4554	1.0372 (0.1152)	1.6684 (0.478)
BC		0.7432 (0.6107)	0.8536 (0.7541)	0.0327	2.0226 (0.8002)	0.976 (1.2596)
OA		7.9619	3.6144			
EFBabs870		3.5225 (2.8949)	4.0461 (3.5742)		9.5869 (3.7931)	4.6262 (5.9707)
XS_401/XS_870		3.571	4.502			
EFBabs401		19.8887	6.8372			
EFBabs401 (BrC)		7.8029	3.5416			
EFBscat870		1.9066 (0.522)	26.3481 (32.4859)		14.7541 (10.6162)	8.8323 (8.9005)
EFBscat401		29.4631	31.0894			
SSA_405		0.597	0.8197			
SSA_870		0.4001	0.7861			
AAE		1.6647	1.9677			
MCE		0.9496 (0.0068)	0.9444 (0.0176)	0.9527	0.9209 (0.0023)	0.9372 (0.007)

Table S3. Continued

Compound	Fuel Type	Subalpine Fir, Canopy	Subalpine Fir, Duff	Subalpine Fir, Litter	Untreated Lumber	Yak Dung, MT
CO_2		1645.0996 (162.8764)	1300.6036	1597.3364	1607.9523	1182.3088
CO		92.3713 (43.7186)	106.1839	105.1323	52.9236	84.2355
CH_4		4.4075 (4.3487)	10.98	6.5274	0.795	6.6348
Methanol		1.623 (1.8738)	4.1583	2.4289	0.2313	2.4762
Formaldehyde		2.7149 (2.8977)	0.8065	0.9803	0.426	1.7133
HCl		0.0307	0.2761			
Acetylene		1.215 (1.2564)	0.0768	0.2592	0.1432	0.2486
Ethylene		4.3472 (4.9678)	2.2942	2.7907	0.2797	1.8491
Propene		1.3073 (1.5749)	2.3438	1.4005	0.0471	1.2105
NH_3		0.9853 (0.9836)	8.4968	2.3838	0.1768	4.452
1,3-Butadiene		0.7057				
Acetic Acid		2.2416 (2.6975)	7.9532	5.993	0.5451	6.3562
Formic Acid		0.4296 (0.5088)	0.2765	0.3965	0.1617	0.3367
Furan		0.2831 (0.2746)	0.6005			0.5804
Hydroxyacetone		1.3775 (1.2766)	2.1713	1.5986	0.5261	1.4098
Phenol		0.9532	1.1833	1.1571	0.4727	0.5416
Furaldehyde		0.6777	1.0504	1.7183	0.5685	1.4733
NO		2.0741 (0.9855)	0.5604	3.5303	1.1318	1.4176
NO_2		0.5297 (0.0992)	1.2962	3.6248	0.0941	1.8723
HONO		0.8016 (0.6808)	0.1459	0.2712	0.3521	0.324
Glycolaldehyde		2.5411		1.2347	0.0969	0.66
HCN		0.4345 (0.5011)	1.8396	0.4971	0.0574	1.9583
SO_2		1.4477 (1.0778)	0.5878	3.0728		2.8807
BC		0.5313 (0.1373)	0.0052	1.5226	3.2223	0.0134
OA		18.2055 (15.252)				
EFBabs870		2.5181 (0.6506)	0.0246	7.2171	3.2223	0.0134
XS_401/XS_870		10.3073 (8.1445)				
EFBabs401		23.3056 (13.8025)				
EFBabs401 (BrC)		17.8412 (15.2144)				
EFBscat870		18.8727 (25.4281)	5.4284	4.1188	3.2223	0.0134
EFBscat401		170.9445 (217.7317)				
SSA_405		0.732 (0.2484)				
SSA_870		0.5889 (0.5066)				
AAE		2.8064 (1.1671)				
MCE		0.9163 (0.0435)	0.8863	0.9063	0.9508	0.8993

Table S4. *Individual molar enhancement ratios (gases) and BC/CO (g/g) for each smoke event during the 2017 ambient monitoring period in Missoula.*

Peak	dd/mm, hh:mm (Local)	Source	CH_4/CO	C_2H_2/CO	C_2H_4/CO	MeOH/CO	NH_3/CO	BC/CO
A	08/12, 23:08--08/13, 02:17	MT+BC primary, WA secondary	0.0803	--	0.0198	0.0072	--	0.0019
B	08/13, 02:57--08/13, 13:46	MT+BC primary, WA secondary	0.2270	--	--	0.0280	--	0.0010
C	08/14, 15:59--08/15--05:17	Unknown, likely anthropogenic, not included in analysis	0.3202	--	--	0.0367	--	--
D	08/15, 06:51--08/15, 15:17	Lolo Peak fire	--	--	--	--	--	0.0005
E	08/15, 18:36--08/16, 18:29	Lolo Peak fire	0.2629	--	--	0.0317	--	0.0009
F	08/16, 20:18--18/16, 23:56	Unknown, likely anthropogenic, not included in analysis	--	0.0430	--	--	--	0.0003
G	08/17, 03:10--18/17, 20:02	Lolo Peak fire	0.1184	--	--	0.0098	--	0.0016
H	08/18, 04:33--08/18, 20:30	Lolo Peak fire	0.0754	--	--	0.0129	0.0167	0.0021
I	08/20, 05:00--08/20, 15:05	Lolo Peak fire	0.0505	--	--	0.0212	--	0.0015
J	08/20, 16:49--08/21, 04:23	Lolo Peak fire	0.0221	--	--	--	0.0196	0.0024
K	08/21, 06:32--08/21, 19:26	Lolo Peak fire	0.0296	--	--	0.0119	0.0105	0.0014
L	08/22, 03:33--08/24, 13:40	Lolo Peak fire primary, other regional (MT, OR, ID, CA) secondary	0.1155	--	--	0.0240	--	0.0014
M	08/24, 13:54--08/25, 16:56	Unknown, non-anthropogenic wildfire source, included in analysis	0.2624	--	--	--	--	0.0007
N	08/26, 18:43--08/27, 17:42	Lolo Peak fire	--	--	--	--	--	0.0008
O	08/27, 18:42--08/28, 17:42	Lolo Peak fire primary, other regional (MT, OR, ID, CA) secondary	0.2651	--	--	0.0118	--	0.0009
P	08/28, 22:24--08/30, 00:02	Regional	--	--	--	0.0062	--	0.0011
Q	08/30, 01:36--08/30, 23:10	Regional	0.0243	--	--	0.0216	--	0.0010
R	08/31, 01:05--08/31, 21:30	Lolo Peak fire	--	--	--	0.0503	--	0.0010
S	09/01, 00:08--09/02, 00:27	Unknown, non-anthropogenic wildfire source, included in analysis	0.1416	--	--	0.0401	0.0216	--
T	09/02, 01:56--09/02, 18:18	Lolo Peak fire primary, WA secondary	0.2358	--	--	--	--	0.0006
U	09/03, 00:25--09/04, 02:47	Lolo Peak fire primary, other regional (MT+WA+OR+ID+CA) secondary	0.1048	--	--	0.0043	0.0080	0.0013
V	09/04, 03:07--09/04, 17:25	Mostly Rice Ridge fire, small regional contribution (MT+WA+OR+ID+BC)	0.1137	0.0011	0.0117	0.0096	0.0097	0.0011
W	09/04, 17:30--09/05, 03:55	Mostly Rice Ridge fire, small regional contribution (MT+WA+OR+ID+BC)	0.1033	0.0017	0.0086	0.0130	0.0044	0.0010
X	09/05, 03:55--09/05, 16:39	MT fires, mixed	0.2100	--	--	--	--	0.0006
Y	09/05, 16:44--09/08, 19:28	Regional (MT+WA+OR+ID+BC)	0.2577	--	--	0.0181	--	0.0011

Table S5. *Individual optical properties for each smoke event during the 2017 ambient monitoring period in Missoula.*

Peak	dd/mm, hh:mm (Local)	Source	[a]Size parameter	AAE	ASE	SSA(401)	SSA(870)	%-401 Absorption by BrC
A	08/12, 23:08--08/13, 02:17	MT+BC primary, WA secondary	--	--	--	--	0.88	--
B	08/13, 02:57--08/13, 13:46	MT+BC primary, WA secondary	--	--	--	--	0.93	--
C	08/14, 15:59--08/15--05:17	Unknown, likely anthropogenic, not included in analysis	--	--	--	--		--
D	08/15, 06:51--08/15, 15:17	Lolo Peak fire	--	--	--	--	0.94	--
E	08/15, 18:36--08/16, 18:29	Lolo Peak fire	--	--	--	--	0.93	--
F	08/16, 20:18--18/16, 23:56	Unknown, likely anthropogenic, not included in analysis	--	--	--	--		--
G	08/17, 03:10--18/17, 20:02	Lolo Peak fire	--	--	--	--	0.90	--
H	08/18, 04:33--08/18, 20:30	Lolo Peak fire	--	--	--	--	0.93	--
I	08/20, 05:00--08/20, 15:05	Lolo Peak fire	--	--	--	--	0.94	--
J	08/20, 16:49--08/21, 04:23	Lolo Peak fire	--	--	--	--	0.92	--
K	08/21, 06:32--08/21, 19:26	Lolo Peak fire	--	--	--	--	0.95	--
L	08/22, 03:33--08/24, 13:40	Lolo Peak fire primary, other regional (MT, OR, ID, CA) secondary	--	--	--	--	0.94	--
M	08/24, 13:54--08/25, 16:56	Unknown, non-anthropogenic wildfire source, included in analysis	--	--	--	--	0.93	--
N	08/26, 18:43--08/27, 17:42	Lolo Peak fire	--	--	--	--	0.96	--
O	08/27, 18:42--08/28, 17:42	Lolo Peak fire primary, other regional (MT, OR, ID, CA) secondary	3.72	1.95	1.70	0.93	0.94	52.01
P	08/28, 22:24--08/30, 00:02	Regional	3.30	1.90	1.54	0.93	0.95	50.20
Q	08/30, 01:36--08/30, 23:10	Regional	2.87	1.60	1.36	0.93	0.94	37.18
R	08/31, 01:05--08/31, 21:30	Lolo Peak fire	3.30	1.85	1.54	0.94	0.95	48.42
S	09/01, 00:08--09/02, 00:27	Unknown, non-anthropogenic wildfire source, included in analysis	4.29	1.46	1.88	0.92	0.89	29.93
T	09/02, 01:56--09/02, 18:18	Lolo Peak fire primary, WA secondary	3.94	2.30	1.77	0.95	0.97	63.33
U	09/03, 00:25--09/04, 02:47	Lolo Peak fire primary, other regional (MT+WA+OR+ID+CA) secondary	3.81	1.65	1.73	0.93	0.92	39.64
V	09/04, 03:07--09/04, 17:25	Mostly Rice Ridge fire, small regional contribution (MT+WA+OR+ID+BC)	4.02	2.88	1.80	0.91	0.96	76.61
W	09/04, 17:30--09/05, 03:55	Mostly Rice Ridge fire, small regional contribution (MT+WA+OR+ID+BC)	2.65	2.00	1.26	0.92	0.96	53.76
X	09/05, 03:55--09/05, 16:39	MT fires, mixed	1.54	1.89	0.56	0.90	0.96	49.67
Y	09/05, 16:44--09/08, 19:28	Regional (MT+WA+OR+ID+BC)	2.75	2.10	1.31	0.94	0.97	57.19

Supplemental Table S7. Enhancement ratios (g/g) for each individual event.

Source	BC/CO	BC/$PM_{2.5}$	$PM_{2.5}$/CO
Central ID	0.0021	0.0183	0.1148
Northwest MT	0.0021	0.02	0.1050
British Columbia	0.0035	0.0225	0.1556
Pacific Northwest	0.0025	0.0242	0.1033
Prescribed Fire	0.0026	0.0157	0.1656

Table S8. *Critical aerosol enhancement (downwind) or emission (near source) ratios (g g^{-1}).*

Study	Fire Type	Source	BC/CO	BC/PM	PM/CO
MSO 2017[1]	Wildfire	MT+BC primary, WA secondary	0.0022	0.0158	0.1392
	Wildfire	MT+BC primary, WA secondary	0.0012	0.0082	0.1463
	Wildfire	Lolo Peak fire	0.0006	0.013	0.0462
	Wildfire	Lolo Peak fire	0.0011	0.0103	0.1068
	Wildfire	Lolo Peak fire	0.0018	0.0156	0.1154
	Wildfire	Lolo Peak fire	0.0024	0.0157	0.1529
	Wildfire	Lolo Peak fire	0.0017	0.0081	0.2099
	Wildfire	Lolo Peak fire	0.0027	0.015	0.1800
	Wildfire	Lolo Peak fire	0.0015	0.0104	0.1442
	Wildfire	Lolo Peak fire primary, other regional (MT, OR, ID, CA) secondary	0.0016	0.0154	0.1039
	Wildfire	Unknown, non-anthropogenic wildfire source, included in analysis	0.0007	0.0123	0.0569
	Wildfire	Lolo Peak fire	0.0009	0.0104	0.0865
	Wildfire	Lolo Peak fire primary, other regional (MT, OR, ID, CA) secondary	0.0010	0.0143	0.0699
	Wildfire	Regional	0.0013	0.015	0.0867
	Wildfire	Regional	0.0011	0.0137	0.0803
	Wildfire	Lolo Peak fire	0.0012	0.012	0.1000
	Wildfire	Lolo Peak fire primary, WA secondary	0.0006	0.01	0.0600
	Wildfire	Lolo Peak fire primary, other regional (MT+WA+OR+ID+CA) secondary	0.0015	0.0103	0.1456
	Wildfire	Mostly Rice Ridge fire, small regional contribution (MT+WA+OR+ID+BC)	0.0012	0.0086	0.1395
	Wildfire	Mostly Rice Ridge fire, small regional contribution (MT+WA+OR+ID+BC)	0.0011	0.0082	0.1341
	Wildfire	MT fires, mixed	0.0006	--	--
	Wildfire	Regional (MT+WA+OR+ID+BC)	0.0012	0.0178	0.0674
MSO 2018[1]	Wildfire	Central Idaho	0.0021	0.0183	0.1148
	Wildfire	Northwest Montana	0.0021	0.02	0.1050
	Wildfire	British Columbia (Aged)	0.0035	0.0225	0.1556
	Wildfire	Pacific Northwest	0.0025	0.0242	0.1033
	Prescribed Fire	Clearwater National Forest	0.0026	0.0157	0.1656
MSO 2019[1]	Prescribed Fire	TBD	0.0022	0.0179	0.1243
	Prescribed Fire	k	0.0022	0.0214	0.1005
SEAC4RS/BBOP: MBO[2]	Wildfire (MBO)	BB1			0.192
	Wildfire (MBO)	BB2			0.168
	Wildfire (MBO)	BB3			0.224
	Wildfire (MBO)	BB4			0.192
	Wildfire (MBO)	BB5			0.248
	Wildfire (MBO)	BB6			0.24
	Wildfire (MBO)	BB7			0.216
	Wildfire (MBO)	BB8			0.272
	Wildfire (MBO)	BB9			0.264
	Wildfire (MBO)	BB10			0.248
	Wildfire (MBO)	BB11			0.224
	Wildfire (MBO)	BB12			0.288
	Wildfire (MBO)	BB13			0.192
	Wildfire (MBO)	BB14			0.504
	Wildfire (MBO)	BB15			0.232
	Wildfire (MBO)	BB16			0.2
	Wildfire (MBO)	BB17			0.376

	Wildfire (MBO)	BB18			0.216
AERODYNE ML (2018) AMS & SP2[2]	Wildfire	Rattlesnake Fire	0.0012		
	Wildfire	Rabbit Foot Fire	0.0014		0.1308
	Wildfire	Cougar Fire	0.0017		0.1363
	Wildfire	Crescent Mtn/Twisp	0.0014		0.0866
AML 2019[2]	Wildfire	Plume 60	0.0008		0.11296
	Wildfire	Plume 168	0.00128		0.04936
	Wildfire	Plume 181			0.058
	Wildfire	Plume 205	0.0008		
	Wildfire	Plume 221	0.00168		
	Wildfire	Plume 225	0.00144		
	Wildfire	Plume 230	0.00136		
	Wildfire	Plume 250			0.1652
	Wildfire	Plume 253			0.13608
	Wildfire	Plume 255	0.00312		0.14176
	Wildfire	Plume 263	0.00296		0.11208
	Wildfire	Plume 265	0.00208		0.10232
	Wildfire	Plume 267	0.00248		0.09984
	Wildfire	Plume 272	0.00232		0.08536
	Wildfire	Plume 279	0.00144		0.10872
	Wildfire	Plume 280	0.00152		0.12816
	Wildfire	Plume 281			0.12528
	Wildfire	Plume 362	0.00136		0.14984
	Wildfire	Plume 363	0.00184		0.15304
	Wildfire	Plume 364	0.00192		0.14736
	Wildfire	Plume 379			0.21152
	Wildfire	Plume 381			0.18144
	Wildfire	Plume 384	0.0024		0.16176
	Wildfire	Plume 385			0.13688
	Wildfire	Plume 386			0.08488
	Wildfire	Plume 387	0.00184		0.14512
	Wildfire	Plume 388			0.1844
	Wildfire	Plume 414			0.06176
FIREX-AQ (2019)[2]	Wildfire	Sheep Fire	0.0017		0.1286
	Wildfire	Shady Fire	0.0054		0.2823
	Wildfire	Shady Fire	0.0019		0.3621
	Wildfire	North Hills Fire	0.0034		0.2637
	Wildfire	Tucker Fire	0.0036		0.2594
	Wildfire	Tucker Fire	0.0015		0.2423
	Wildfire	Lefthand Fire	0.0052		0.2894
	Wildfire	Ridgetop Fire	0.0097		0.2595
	Wildfire	Mica Fire	0.0019		0.2144
	Wildfire	Lick Creek Fire	0.0015		0.2358
	Wildfire	Williams Flats Fire	0.0042		0.3945
	Wildfire	Siberian Smoke	0.0043		0.3813
	Wildfire	Spokane Missed Approach	0.0028		0.1728
	Wildfire	Williams Flats Fire	0.0036		0.2769
	Wildfire	Horsefly Fire	0.0027		0.4998
	Wildfire	Williams Flats Fire	0.0031		0.3983
	Wildfire	Williams Flats Fire	0.0027		0.2321

	Wildfire	Castle Fire	0.0024		0.3411
	Wildfire	Castle Fire	0.0030		0.4078
	Wildfire	Sheridan Fire	0.0030		0.2533
WE-CAN 2018[2]	Wildfire	RF01 - Rattlesnake Creek			
	Wildfire	RF 02- Carr Fire	0.0030		0.224
	Wildfire	RF03 Taylor Creek Fire	0.0019		0.208
	Wildfire	RF 04 Sharps Fire	0.0028		0.176
	Wildfire	RF 05 Mendocino Complex Fire	0.0039		
	Wildfire	RF 06 Cougar Fire			
	Wildfire	RF 06 Kiwah Fire	0.0029		0.208
	Wildfire	RF 06 Rabbit Foot Fire	0.0033		0.24
	Wildfire	RF 07 Donnell Fire	0.0015		
	Wildfire	RF 07 Ferguson Fire			
	Wildfire	RF 08 Mendocino Complex Fire (Aged Central Valley)	0.0028		0.072
	Wildfire	RF 09 Dollar Ridge Fire			
	Wildfire	RF 09 Coal Hollow Fire			
	Wildfire	RF 09 Bear Trap Fire	0.0024		0.168
	Wildfire	RF 10 Nevada Dilute Smoke			
	Wildfire	RF 10 Goldstone Fire			0.248
	Wildfire	RF 10 Rabbit Foot Fire			0.248
	Wildfire	RF 10 Wigwam Fire			0.232
	Wildfire	RF 10 Monument Fire			0.232
	Wildfire	RF 11 Rabbit Foot Fire			0.2
	Wildfire	RF 11 Beaver Creek Fire			0.2
	Wildfire	RF 11 Shellrock Fire			
	Wildfire	RF 11 Goldstone Fire	0.0039		
	Wildfire	RF 12 Miriam Fire			
	Wildfire	RF 13 Sheep Creek	0.0042		
	Wildfire	RF 13 Mendocino Complex Fire	0.0028		
	Wildfire	RF 15 South Sugarloaf (1st)	0.0016		0.192
	Wildfire	RF 15 South Sugarloaf (2nd)			0.144
	Prescribed Fire	RF 18 Red Feather Lakes Rx Fire	0.0069		0.216
	Wildfire	RF 19 Silver Creek Fire	0.0038		0.224
SEAC4RS/BBOP[2]	Wildfire	Big Windy Complex	0.0011	0.004	0.2693
	Wildfire	Rim Fire Average	0.0024	0.0091	0.2614
SEAC4RS/BBOP (G-1)[2]	Wildfire (G1)	BB1			0.208
	Wildfire (G1)	BB2			0.248
	Wildfire (G1)	BB3			0.264
	Wildfire (G1)	BB4			0.312
	Wildfire (G1)	BB5			0.256
	Wildfire (G1)	BB6			0.192
	Wildfire (G1)	BB7			0.192
	Wildfire (G1)	BB8			0.216
	Wildfire (G1)	BB9			0.168
	Wildfire (G1)	BB10			0.136
	Wildfire (G1)	BB11			0.232
	Wildfire (G1)	BB12			0.296
	Wildfire (G1)	BB13			0.232
	Wildfire (G1)	BB14			0.2
Forrister et al., 2015[2]	Wildfire	Rim Fire (Fresh)	0.0025	0.00625	0.4

	Wildfire	Rim Fire (Aged)	0.0022	0.022	0.1
SLOBB (May et al., 2014)[2]	Prescribed Fire	Turtle Fire	0.0055	0.049	0.1
	Prescribed FIre	Shaver Fire	0.0058	0.048	0.11
ARCTAS (Sahu et al., 2012)[2]	Wildfire	P4 - BB	0.0019	--	--
	Wildfire	P6 - BB	0.001	--	--
	Wildfire	P10 - BB	0.0017	--	--
	Wildfire	P11 - BB	0.0008	--	--

[1] Denotes $PM_{2.5}$

[2] Denotes $PM_{1.0}$